Universidad Politécnica de Cartagena

Universidad Politécnica de Cartagena | Campus de Excelencia Internacional

CHARACTERIZATION AND NUMERICAL VERIFICATION OF SEEPAGE SCENARIOS IN ANISOTROPIC SOILS UNDER RETAINING STRUCTURES AND IN UNCONFINED AQUIFERS DUE TO PUMPING WELLS

PhD Program
Tecnología y Modelización en Ingeniería Civil, Minera y Ambiental

Author: María Encarnación Martínez Moreno

Director: Dr. Iván Alhama Manteca

Cartagena (2021)

Universidad Politécnica de Cartagena

Departamento de Ingeniería Minera y Civil

Characterization and Numerical Verification of Seepage Scenarios in Anisotropic Soils under Retaining Structures and in Unconfined Aquifers due to Pumping Wells

DOCTORAL THESIS

María Encarnación Martínez Moreno

Director: **Iván Alhama Manteca**

Cartagena (2021)

Acknowlegdments

To Séneca Foundation for Pre-doctoral Grant (Beca FPI) that I was awarded to carry out this Ph.D Thesis.

To my Thesis Director, Professor Iván Alhama, for giving me the chance to start my research career.

To Professor Francisco Alhama, for introducing me to nondimensionalization technique.

To Professor Gonzalo García, who has been an excellent guide during these pre-doctoral years, and to the rest of the members of 'Network Simulation' research group for their advice about programming.

To my family and partner, for being my support in the not few moments in which it seemed to me that I was not going to be able to go on with my research. Thanks for helping me to relax and to look for a new perspective.

And finally, to all my friends and mates that were always ready to come with me to have a coffee at the university cafeteria (or anywhere) when I needed to relax.

Acknowlegdments

Universidad Politécnica de Cartagena

DT-16

CONFORMIDAD DE SOLICITUD DE AUTORIZACIÓN DE DEPÓSITO DE TESIS DOCTORAL POR EL/LA DIRECTOR/A DE LA TESIS

D. Iván Alhama Manteca, Director de la Tesis doctoral "Characterization and numerical verification of seepage scenarios in anisotropic soils under retaining structures and in unconfined aquifers due to pumping wells"

INFORMAN:

Que la referida Tesis Doctoral, ha sido realizada por María Encarnación Martínez Moreno dentro del Programa de Doctorado Tecnología y Modelización en Ingeniería Civil, Minería y Ambiental, dando mi conformidad para que sea presentada ante el Comité de Dirección de la Escuela Internacional de Doctorado para ser autorizado su depósito.

Informe positivo sobre el plan de investigación y documento de actividades del doctorando/a emitido por el Director/Tutor (**RAPI**).

La rama de conocimiento en la que esta tesis ha sido desarrollada es Ciencias.

En Cartagena, a 1 de marzo de 2021

EL DIRECTOR DE LA TESIS

Fdo.: Iván Alhama Manteca

COMITÉ DE DIRECCIÓN ESCUELA INTERNACIONAL DE DOCTORADO

Universidad Politécnica de Cartagena

DT-17

CONFORMIDAD DE DEPÓSITO DE TESIS DOCTORAL POR LA COMISIÓN ACADÉMICA DEL PROGRAMA

Ángel Faz Cano, Presidente de la Comisión Académica del Programa Tecnología y Modelización en Ingeniería Civil, Minería y Ambiental,

INFORMA:

Que la Tesis Doctoral titulada, "Characterization and numerical verification of seepage scenarios in anisotropic soils under retaining structures and in unconfined aquifers due to pumping wells", ha sido realizada, dentro del mencionado Programa de Doctorado, por María Encarnación Martínez Moreno, bajo la dirección y supervisión del Director Iván Alhama Manteca

En reunión de la Comisión Académica, visto que en la misma se acreditan los indicios de calidad correspondientes y la autorización del Director de la misma, se acordó dar la conformidad, con la finalidad de que sea autorizado su depósito por el Comité de Dirección de la Escuela Internacional de Doctorado.

☑ Evaluación positiva del plan de investigación y documento de actividades por el Presidente de la Comisión Académica del programa (**RAPI**).

La Rama de conocimiento por la que esta tesis ha sido desarrollada es:

☑ Ciencias

En Cartagena, a 23 de febrero de 2021

EL PRESIDENTE DE LA COMISIÓN ACADÉMICA

ANGEL|FAZ|CANO

Firmado digitalmente por ANGEL|FAZ|CANO
Nombre de reconocimiento (DN): cn=ANGEL|FAZ|CANO, serialNumber=27459054K, givenName=ANGEL, sn=FAZ CANO, ou=CIUDADANOS, o=ACCV, c=ES
Fecha: 2021.02.23 23:11:32 +01'00'

Fdo: Ángel Faz Cano

COMITÉ DE DIRECCIÓN ESCUELA INTERNACIONAL DE DOCTORADO

INDEX

List of symbols

A: cross section in Darcy's law (m^2)

a: upstream horizontal length in dam scenarios (m)

a_1, a_2, …: constants in Muskat's flow experiment // constants in NMS definition

b: downstream horizontal length in dam scenarios (m)

Bat: battery

C: constant in Darcy's law (m/s)// capacity (F)// application point of the uplift force in dam scenarios (dimensionless)

c: application point of the uplift force in dam scenarios (m)

C_1, C_2…: constants in Muskat's experiments

c_1: capacity constant (F)

C_{DS}: application point of the force on the downstream side of the sheet pile (dimensionless)

c_{DS}: application point of force on the downstream side of the sheet pile (m)

C_o: constant in Darcy's law (m/kg/s)

c_s: location of the sheet pile under the dam in dam scenarios (m)

C_{US}: application point of the force on the upstream side of the sheet pile (dimensionless)

c_{US}: application point of the force on the upstream side of the sheet pile (m)

d: average grain size (m)// length of the dam foundation (m)

d: derivative

d_s: sheet pile length in dam scenarios (m)

e: void ratio (dimensionless)

F, F_1, F_2 …: unknown functions

F_{DS}: force on the downstream side of the sheet pile (N)

F_{ext}: external force (N)

F_{US}: force on the upstream side of the sheet pile (N)

g: gravity constant (m/s^2)

G: voltage controlled current source

H: stratum thickness in dam scenarios (m)// initial water head in well scenarios (m)

h: water head or hydraulic potential (m)

h_1: water head upstream the dam in dam scenarios (m)

h_2: water head downstream the dam in dam scenarios (m)

h_s: seepage surface (m)

h_w: water head in the well in well scenarios (m)

I: electric intensity (A)

i: hydraulic gradient (dimensionless)

i_e: exit gradient (dimensionless)

$I_{e,ave}$: average exit gradient (dimensionless)

J: electric current (A)

k: permeability (m^2)

l*: reference length (m)

l: length (m)

L: length of the medium in Darcy's law (m)// length dimension (m)// length of the medium in scenarios of dams in infinite medium

l_h: horizontal length for the calculation of $I_{e,ave}$ (m)

l_v: vertical length for the calculation of $I_{e,ave}$ (m)

L_{wc}: water head dimension (m)

$l_{x,95}$: horizontal characteristic length for 95% of flow (m)

$L_{x,95}$: horizontal characteristic length for 95% of flow (dimensionless)

$l_{x,90}$: horizontal characteristic length for 90% of flow (m)

$L_{x,90}$: horizontal characteristic length for 90% of flow (dimensionless)

$l_{y,95}$: vertical characteristic length for 95% of flow (m)

$L_{y,95}$: vertical characteristic length for 95% of flow (dimensionless)

$l_{y,90}$: vertical characteristic length for 90% of flow (m)

$L_{y,90}$: vertical characteristic length for 90% of flow (dimensionless)

M: mass dimension (kg)

m: constant in Network Simulation Method

n: orthogonal direction// constant in Network Simulation Method// power in of Muskat's flow experiments

p: pressure (N/m^2)

Q: water flow (m^3/s)

q: water flow in 2-D (m^2/s)

R: aquifer radius in well scenarios (m)// duct radius in porous media (m)

R: resistance value (Ω)

r: spatial direction (radial)

R_e: Reynolds number (dimensionless)

R_{inf}: influence radius in well scenarios

r_w: well radius in well scenarios (m)

s: length of the water column in Muskat's flow experiment (m)// studied direction

S: switch// surface (m^2)

Sw: switch

T: time dimension (s)

t: time variable (s)

u: pore pressure (kPa)

UF: uplift force (kN)

V: electric voltage (V)

v: velocity (m/s)

V_{ext}: potential energy (J)

w_d: dam width in dam scenarios (m)

w_s: sheet pile width in dam scenarios (m)

x: spatial direction (usually horizontal)

y: spatial direction (vertical in 2-D problems or horizontal in 3-D problems)

z: spatial direction (vertical in 3-D problems)

α: spatial direction (angular)

γ: water unit weight (N/m^3)

γ_f: unit weight of a fluid (N/m^3)

∂: partial derivative

Δ: variation

Θ: combination of ϕ and Ψ// dimension of g·h

κ: hydraulic conductivity (m/s)

μ: dynamic viscosity (P)

π: dimensionless group or monomial (dimensionless)

ρ: density (kg/m^3

ϕ: velocity potential (m^2/s)// Dimension of ρ·g·h

Ψ: stream function variable (m^2/s)

ξ: addend in a governing equation// water head dimensions (m)

ξ: statistic error in well inverse problem (%)

ζ: friction factor (dimensionless)

∇: gradient mathematical operator

∇^2: gradient mathematical operator

Γ_Q: deviation for water flow variable in well inverse problem

Γ_{hs}: deviation for seepage surface in well inverse problem

{}: denotes dimensional basis

{{}}: denotes list of relevant variables and parameters

Subscript and superscript

→: direction of the flow in porous media

vis: direction orthogonal to → in porous media

n: direction orthogonal to → and vis

average: average value of the variable

‘: dimensionless variable

pre-ine: related to pressure and inertial forces

pre-vis: related to pressure and viscous forces

ine-vis: related to inertial and viscous forces

x, y, z, r: related to spatial directions

i: related to horizontal direction

j, k: related to vertical direction

ref: related to a reference value of a variable

nondim: related to a dimensionless variable

sim: related to simulation values in well inverse problem with WaWSim

real: related to real values in well inverse problem

initial: related to initial values of hydraulic conductivity in well inverse problem

ξ: related to the statistic error in well inverse problem

cal: related to calculated values in well inverse problem with dimensionless abaci

Hall: related to Hall’s experiment

Harr: related to Harr’s theoretical results

Abstract

The main objective of this thesis is the search and verification of the dimensionless groups that govern the geotechnical problems of flow through porous media under gravity dams with or without a sheet pile at its base and groundwater flow in unconfined aquifers due to a pumping well. The aim is to find the groups which the dimensionless unknowns of interest depend on. These unknowns (groundwater flow, pore pressure, average exit gradient, seepage surface, etc) change according to the chosen scenario. The methodology to obtain these groups is the discriminated nondimensionalization of the governing equation. The solutions are displayed in universal abaci that depict values of monomial and dimensionless variables. The curves have been represented after carrying out a large number of simulations by models, also shown in the thesis, that have been specifically designed according to the network method. Chapter I thoroughly explains the objectives of the thesis.

Chapter II gathers the theoretical fundaments of the thesis. Firstly, references and different governing equations of flow through porous media are presented. It is basically focused on the scenarios studied throughout the thesis. In the following section, discriminated nondimensionalization is explained: different aspects, steps to apply the technique and examples in which it has been employed. Afterwards, a historical overview of electrical analogy is presented, with different application examples. In the following section, the bases of the network simulation method are presented, as well as examples of engineering problems in which this methodology has been successfully applied. The rest of the sections of the second chapter show the tools that have been used for the development of the compute programs employed for characterizing the problems researched in this thesis, Ngspice (software for

compilation) and Matlab (programming language for creating the models in text files and graphically processing the solutions).

Chapter III consists in a study of the dimensions of the soil parameters that are related to flow through porous media, that is permeability and hydraulic conductivity. The chapter starts revising the few references where the quantities involved in permeability are contemplated employing classical dimensional analysis, according to which quantities are measured in the same unit independently to the spatial direction in which they are measured. No satisfactory conclusion is reached, and the same happened when applying discriminated dimensional characterization, a methodology with which quantities are considered as distinct when measured in different directions or if they are of diverse nature. For this reason, the parameters are studied introducing quantities related to flow energy in the dimensional basis of the phenomenon, which does allow characterizing the units of hydraulic conductivity in terms of energy.

Chapter IV presents the application of dimensional nondimensionalization to different scenarios of flow through porous media: flow under gravity dams without a sheet pile, flow under gravity dams with a sheet pile located at its base, flow under dams in infinite media and flow in unconfined aquifers due to a pumping well. For each of these scenarios, governing equations, monomials ruling the phenomenon and groups involving unknowns are presented and universal abaci obtained from numerous simulations are depicted. Moreover, for the last problem there is a table where it is demonstrated that, for the same dimensionless scenario (although the values of the dimensional variables are different) the dimensionless unknowns remind the same.

Chapter V collects the models designed for the scenarios studied in this thesis: their boundary conditions, the cell structure, etc. The models, which are written as text files, include devices and routines that provide the unknown variables of interest for each of the scenarios as output information. Two codes have been developed: DamSim for flow under dams and WaWSim for flow due to a pumping well. Both simulation tools, in a Windows environment, are free, potent and reliable. Matlab codes have been employed for programming the model text files and the interfaces, and Ngspice for numerical simulation.

Chapter VI shows an inverse problem in which radial and vertical conductivities in a free aquifer are calculated from field's measurements in a pumping well. The problem is studied from two points of view: employing the universal abaci and the designed code. In both cases, the errors between real and estimated values are calculated. After this, a study has been carried out in

order to understand the effect of possible measure errors in the filed variables on the deviations of the estimated hydraulic conductivity values.

Chapter VII presents a set of applications: i) flow under gravity dams without a sheet pile; ii) flow under gravity dams with a sheet pile located at its base; and iii) flow in unconfined aquifers due to a pumping well. In addition, for each of the scenarios one of the variables have been compared with analytical or experimental results that can be found in references.

Resumen

El objetivo principal de esta tesis es la búsqueda y verificación de los grupos adimensionales que gobiernan los problemas geotécnicos de flujo a través de medios porosos bajo presas de gravedad con o sin tablaestaca en su base y flujo de agua en acuíferos libres debido a un pozo de bombeo. La finalidad es encontrar los grupos de los que dependen las incógnitas adimensionales de interés. Estas incógnitas (caudal, presión intersticial, gradiente medio a la salida, superficie de rezume, etc.) cambian de acuerdo con el escenario elegido. La metodología para obtener estos grupos es la adimensionalización discriminada de la ecuación de gobierno. Las soluciones se muestran en ábacos universales en los que se dibujan los valores de los monomios y las variables adimensionales. Las curvas se han representado después de llevar a cabo una gran cantidad de simulaciones mediante modelos, también presentados en esta tesis, que han sido diseñados específicamente de acuerdo con el método de redes. El Capítulo I explica los objetivos de la tesis en detalle.

El Capítulo II recoge los fundamentos teóricos de la tesis. Primero se presentan referencias y diferentes ecuaciones de gobierno para problemas de flujo en medios porosos. Básicamente se centra en los escenarios estudiados a lo largo de la tesis. En la siguiente sección se explica la adimensionalización discriminada: los diferentes aspectos, pasos para aplicar la técnica y ejemplos en los que se ha empleado. Después se presenta un repaso histórico de la analogía eléctrica, con diferentes ejemplos de aplicación. En la siguiente sección se muestra la base del método de simulación por redes, así como ejemplos de problemas de ingeniería en los que la metodología se ha aplicado satisfactoriamente. El resto de las secciones del segundo capítulo muestran las herramientas que se han usado para el desarrollo de los programas informáticos

empleados para caracterizar los problemas investigados en esta tesis, Ngspice (software para los cálculos) y Matlab (lenguaje de programación para crear los modelos en archivos de texto y graficar los resultados).

El Capítulo III consiste en el estudio de las dimensiones de parámetros del suelo relacionados con el flujo a través del medio porosos, que son la permeabilidad y la conductividad hidráulica. El capítulo comienza revisando las escasas referencias en las que se contemplan las magnitudes que participan en la permeabilidad empleando el análisis dimensional clásico, de acuerdo al cual las magnitudes se miden en la misma unidad independientemente de la dirección espacial en la que se midan. No se llegan a conclusiones satisfactorias, y lo mismo ocurre cuando se aplica la caracterización adimensional discriminada, una metodología en la que las magnitudes se consideran distintas cuando se miden en diferentes direcciones o tienen diferente naturaleza. Por esta razón, los parámetros se estudian introduciendo en la base dimensional del fenómeno magnitudes relacionadas con la energía del flujo, lo que sí permite caracterizar las unidades de conductividad hidráulica en términos de energía.

El Capítulo IV presenta la aplicación de la adimensionalización dimensional en diferentes escenarios de flujo en medios porosos: flujo bajo presas de gravedad sin tablaestaca, flujo bajo presas de gravedad con una tablaestaca en su base, flujo bajo presas en medios infinitos y flujo en acuíferos libres debido a un pozo de bombeo. Para cada uno de estos escenarios, se presentan las ecuaciones de gobierno, los monomios que controlan el fenómeno y los grupos en los que aparecen las incógnitas, y se dibujan ábacos universales tras numerosas simulaciones. Además, para el último problema hay una tabla en la que se demuestra que, para el mismo escenario adimensional (aunque los valores de las variables dimensionales sean diferentes) las incógnitas permanecen constantes.

El Capítulo V recoge los modelos diseñados para los escenarios estudiados en esta tesis: sus condiciones de contorno, la estructura de la celda, etc. Los modelos, que se escriben como archivos de texto, incluyen componentes y rutinas que proporcionan las variables de interés para cada uno de los escenarios como información de salida. Se han desarrollado dos códigos: DamSim para flujo bajo presas y WaWSim para flujo debido a un pozo de bombeo. Ambas herramientas de simulación, en un entorno Windows, son libres, potentes y fiables. Los códigos de Matlab se han usado para programar el modelo en archivo de texto y las interfaces, y Ngpisce para la simulación numérica.

El Capítulo VI muestra un problema inverso en el que se calculan las conductividades radial y vertical en un acuífero libre a partir de las medidas de campo en un acuífero libre. El problema

se estudia desde dos puntos de vista: empleando los ábacos universales y el código diseñado. En ambos casos se calculan las desviaciones entre los valores reales y estimados. Tras esto, se ha llevado a cabo un estudio para entender el efecto de posibles errores de medida de las variables de campo en las desviaciones de los valores de conductividad hidráulico estimado.

El Capítulo VII presenta una serie de aplicaciones: i) flujo bajo presas de gravedad sin tablaestaca; ii) flujo bajo presas de gravedad con una tablaestaca en su base; y iii) flujo en acuíferos libres debido a un pozo de bombeo. Además, para cada uno de los escenarios una de las variables se ha comprado con resultados analíticos o experimentales que pueden encontrarse en referencias.

Chapter I. Introduction and objectives

I.1 Introduction

At the end of 2017, in my second year of the Master's degree in Civil Engineering (Máster de Ingeniería de Caminos, Canales y Puertos) that I was studying in University of Cartagena (Universidad Politécnica de Cartagena), professor I. Alhama told me about a grant I could apply for to carry out a doctoral research. This grant (beca de Formación de Personal Investigador) was awarded by Séneca Foundation (Fundación Séneca de la Region de Murcia) and the thesis would be an investigation about flow through porous media and its dimensionless characterization.

Therefore, in March 2018, once all the forms had been filled, the doctoral research could start. This overlapped with the last term of the master's degree and the investigation that corresponded to the Master dissertation (which I also developed with professor I. Alhama). Certainly thanks to the help of my thesis director and the rest of colleagues from the research group 'Network simulation' ('Simulación por redes') in University of Cartagena (especially, to professor G. García), I sent two communications to an international congress about mathematics applied to science and engineering and finished my Master dissertation before 2018 was over.

The research topic of my thesis was initially the dimensionless characterization of flow through anisotropic media, which, of course, encompasses a large number of possible scenarios.

Particularly, the chosen problems were those of flow under gravity dams and flow through earth dams. For this aim, some network models and numerical codes based on the electrical analogy through the network method were going to be developed. Nevertheless, although the study of flow under gravity dams was kept as an objective, it was finally decided that the second part of the thesis would be about problems of flow in unconfined aquifers due to a pumping well.

During the first year of research, a reference review was carried out about the different problems finally approached. The two important references, whose content is still useful in spite of being old, are those texts of Harr [2012 its last version] and Muskat [1937] because both present useful graphics based on the classical dimensional characterization of these scenarios, especially for the calculation of flow under gravity dams. However, these authors only focused on isotropic soils. This widely justifies the contribution of this thesis, which is the dimensionless characterization of flow through anisotropic media (more realistic than isotropic soils) by procedures known as discriminated (more accurate than the classical approach). Moreover, during this first year, the development of a software for the simulation of flow under gravity dams was started.

Flow under retaining structures exclusively consisting of a gravity dam leads to a lower number of boundary conditions than those of more complex structures. This allows simplifying the numerical code and narrowing down the number of dimensionless monomials that rule the solution of the problem. Modifying the software, problems of flow under dams with a sheet pile have been studied, a scenario that presents more boundary conditions and dimensionless groups that characterize it.

The most complex problem that has been approached, from the point of view of dimensionless characterization and numerical simulation, has undoubtedly been that of flow in unconfined aquifers due to a pumping well. Modelling this problem employing the network method has required the use of modern (and almost ideal) circuit devices, as well as new configurations that do not appear in scientific literature yet. Aspects such as the introduction of cylindrical 2-D coordinates, the address seepage surface borders, the use of switches, etc, have been important challenges in the first versions of the code. However, once they have been overcome, we believe that it opens the door to more complex simulations (earth dams, use of more than one pumping well, optimization problems, lowering the piezometric level in excavations, etc). Once these models have been designed, the verification of the dimensionless groups derived from characterization has been relatively easy, allowing representing solutions by new universal curves or abaci after numerous simulations.

Due to the experience of the 'Network simulation' research group in designing codes that are useful for engineers and future researches, it was also initially thought to collect the models and codes created in this investigation in two open software that allow future users to apply them in practical problems. The new software, DamSim and WaWSim, which present all the advantage of a modern computer software (communication environment with windows, parameters introduced by the user, a graphic environment for the solutions, etc), are the result of this work.

Alongside this research, whose final aim has been to obtain universal solutions as abaci, a theoretical study about the dimensional character of permeability and hydraulic conductivity parameters has been carried out. This study justifies how non-classical groups with these parameters emerge in anisotropic media. Undoubtedly, we believe that it is one of the new results that allows reducing the number of monomials in these scenarios and, in this way, also reduces the number of curves or abaci which present the universal solutions.

All in all, we can summarize the investigation lines of this thesis in the following:

i) Dimensionless characterization and nondimensionalization of governing equations (Laplace-type equations with different boundary conditions), including spatial and general discrimination concepts, which allows deducing the dimensionless groups that rule the solution of the studied problems, all this supported by Pi theorem.

ii) Design of a numerical model based on the network method as an accurate simulation tool.

iii) Deepening in the dimensional character of anisotropic soil parameters in order to justify their correct use in the dimensionless groups obtained by characterization.

Figure 1.1 is a conceptual scheme of the thesis content.

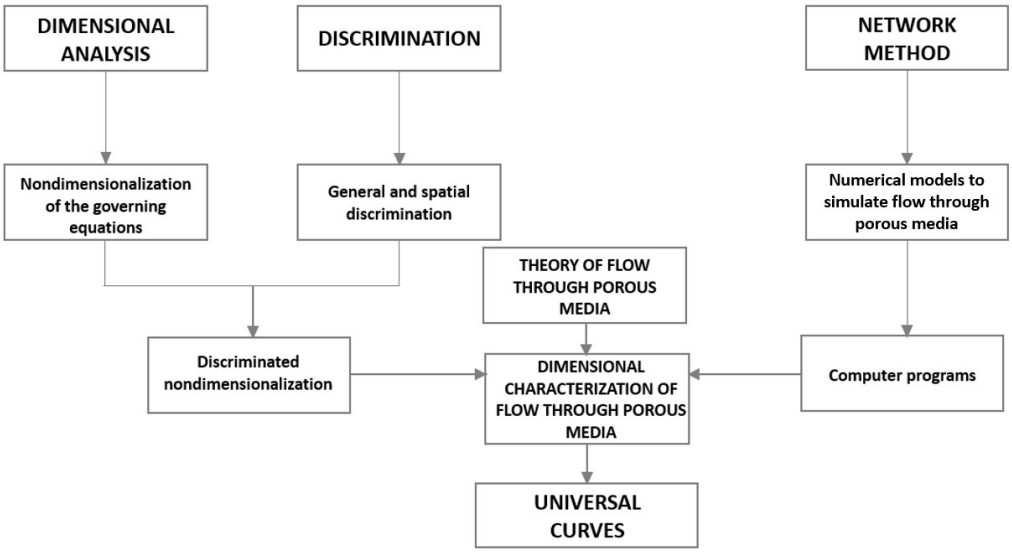

Figure 1.1. Research context of this Ph. D. thesis

I.2 Objectives

The objective of this thesis can be summarized in the following points:

i) Revising reference texts about problems of flow in porous media, especially scenarios of flow under gravity dams and flow to pumping wells in unconfined aquifers. Since these problems are different, the studied variables in each of them are different too. This revision should be aimed to find universal solutions.

ii) Applying the discriminated nondimensionalization in problems of flow through porous media to obtain the groups that govern the solution of these scenarios. For both problems, flow under dams with or without a sheet pile in 2-D rectangular coordinates and problems of flow in unconfined aquifers due to a pumping well in 2-D cylindrical coordinates.

iii) Designing models for all the studied scenarios applying the network method. These, verified when possible, are run in free software for solving circuits (Ngspice) that include modern computational algorithms for giving almost exact solution of the circuit (the errors would only depend on the discretization).

iv) Developing of software to simulate flow under concrete dams or sheet piles and flow to a pump well in unconfined aquifers

v) Deepening in the dimensional character of permeability and hydraulic conductivity parameters, focusing on anisotropic soils.

vi) Developing the inverse problem for scenarios of flow in unconfined aquifers using either a classic protocol which runs successive simulations until getting a convergent solution or the universal curves.

The previous objectives will be illustrated with the following applications:

- Rectangular scenario of flow under gravity dams without a sheet pile located in its base.
- Rectangular scenario of flow under dams with a sheet pile located in its base.
- Rectangular scenario of flow under dams in infinite media.
- Cylindrical scenario of flow in unconfined aquifers due to a pumping well .

I.3 Perspectives

The work presented in this thesis is not closed. Considering the geometry, either from the point of view of the numerical simulation or that of the characterization, the scenarios of flow under dams can increase by locating a larger number of sheet piles. Moreover, in scenarios of dams with a sheet pile, it is also interesting to plot curves where the overall resulting force on the pile and application point is presented, instead of using two different sets of abaci, one for the values for the upstream side of the pile and other for the downstream side. In the case of pumping wells in unconfined aquifers, transient-state scenarios could be studied, in order to search universal solutions and applications of inverse problems. These tasks would require more sophisticated models. Another interesting phenomenon to characterize and simulate is that known as re-wetting. Moreover, related to earth dams, it would also be interesting to approach the design of a code which allows representing the seepage surface for any kind of scenario in an accurate way.

I.4 Methodology

The methodology that describes each of the steps to must be taken to achieve the objectives proposed in the thesis are thoroughly presented in the corresponding sections (Chapters II, IV, V and VI). However, it is convenient to provide of a specific section in which the procedures are summarized. In this way, the reader can come back to the scheme at any moment and clarify the coherence of the document. The general methodological scheme is shown in Figure 1.2.

When designing a network model, the first step involves searching for the equivalence between the governing equation of the scenario to be simulated and that of the electric phenomenon. In case of modelling problems of flow through porous media, the equivalence between the variables is stated between hydraulic potential, h, and voltage, V, and between the electric current, I, and groundwater flow, Q. According to this analogy, and applying Ohm's law, the resistance expressions for resistors are obtained. Resistors are the basic devices that allow simulating the simplest phenomena. Other devices, such as switches and sources, are employed when trying to model more complex processes.

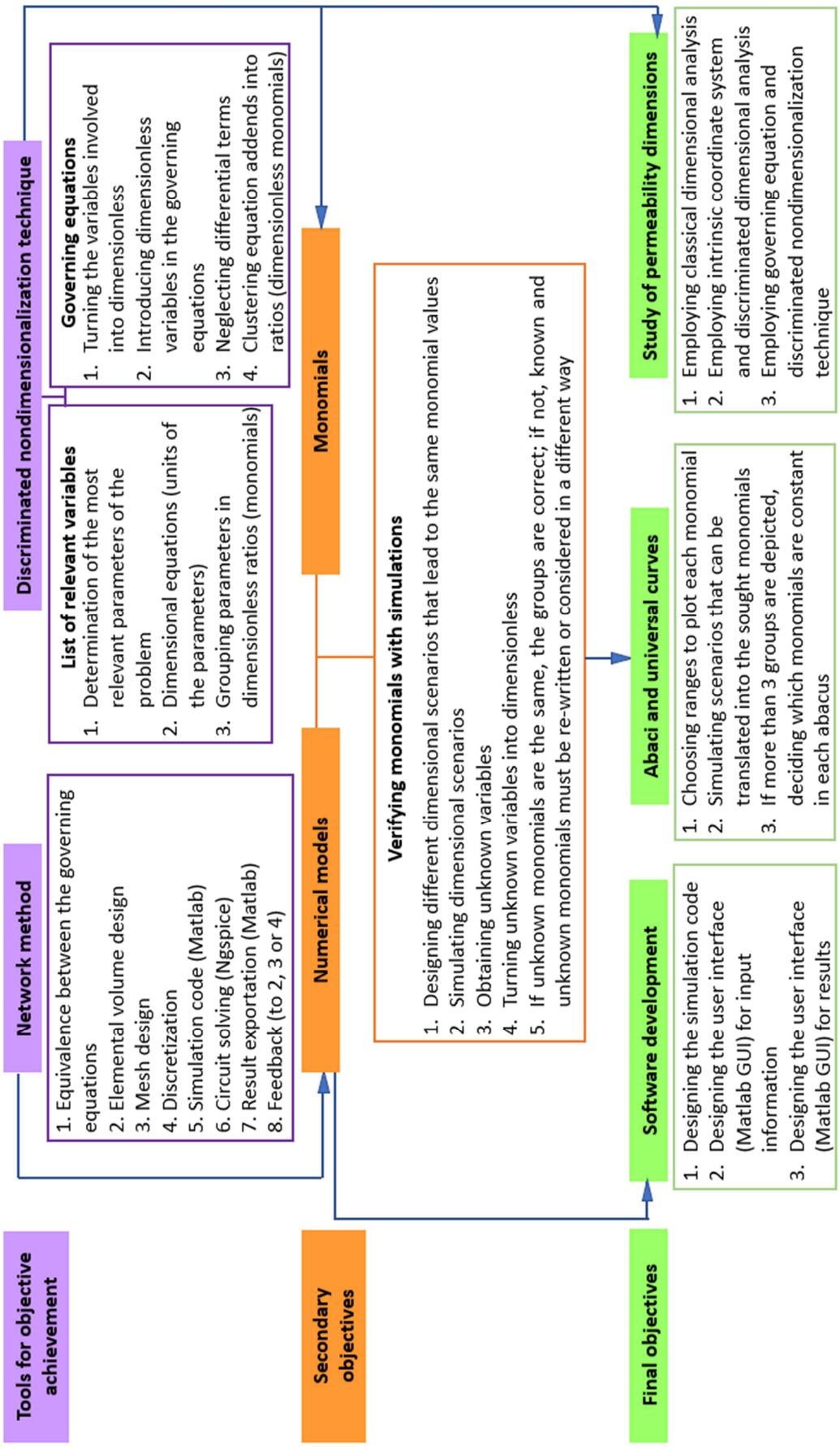

Figure 1.2. Methodology of the thesis

In order to carry out a simulation, the physical scenario must be discretized in cells, so each elemental volume of the medium is simulated with two resistors in each direction. The resistor expressions involve information about the cell size and the hydraulic conductivities. In this way, each cell is transformed into a circuit that is connected to the adjacent elemental volumes with ideal connexions. This information, together with the boundary conditions, is written in a text file, which is the input data for the software that carries out the calculations of the electric circuits. For this thesis, the chosen software for solving circuits is Ngspice.

The solution of the circuits is the voltage in all the nodes of the cells and the electric current in each branch. Voltage values can be directly read using the correct command, while for obtaining intensity values, batteries of zero voltage are connected in those branches where the designer may consider that this information is important (for example, the battery can be placed in one of the branches in each direction).

Voltage and electric current values, which are the output data provided by Ngspice are written in text files that are the input information for another software chosen for the calculation of the sought variables. In this way, and applying functions that already exist in the selected software, the solutions are presented as numerical information (for example, groundwater flow) and as graphical information (for instance, flow nets).

To generate the input file for Ngspice and read its output files, a tool is programmed employing Matlab. This tool, where geometrical and hydrogeological parameters are introduced, builds the discretized scenario and, afterwards, the circuits that are introduced in Ngspice. The text file written by Matlab includes the commands that are necessary to run Ngspice, as well as those that allow deciding which of the variable calculated by this software are exported back to Matlab. Using data that Matlab imports from Ngspice, the developed tool allows calculating the solutions with previously existing functions (graphical solutions, such as flow net and pore pressure distribution) or with functions programmed by the designer to obtain the sought numerical solutions.

In addition, Matlab allows designing interfaces, so the created tools are user-friendly in order to help future researchers to employ them without needing to understand the code. These interfaces, generated with GUI toolbox in Matlab, can be used for introducing the parameters of the problem as well as deciding which of the variables are drawn or calculated.

As regards the discriminated dimensional characterization of scenarios of flow through porous media, other important issue of research in this thesis, the methodology appears by the conjunction of the nondimensionalization of the governing equations which rule the problem

and the study of the list of relevant parameters, both methods approached by applying spatial and general discrimination techniques.

On the one hand, the variables involved in the governing equations are turned into dimensionless using parameters from the list, so the equations are also dimensionless once the dimensionless variables are introduced in them. The number of monomials that are obtained from one of the equations is the same as addends the equation has minus one, since a group is formed as the ratio of two of the addends of the equation.

On the other hand, from the list of relevant parameters, groups can also be obtained as ratio of these parameters. These groups are usually employed to relate and consider geometrical aspects of the scenarios.

The unknown variables of the problem must also be turned into dimensionless. Occasionally, obtaining the dimensionless expression of an unknown is simply done by dividing it by one of the parameters of the list of relevant parameters. In other cases, the unknowns are turned into dimensionless by generating a reference variable with mathematical manipulation of some of the reference parameters.

Once data and unknown monomials have been deduced with the different techniques, they must be checked by simulations of scenarios that, despite having different values for the dimensional parameters, can be reduced to the same values of the dimensionless groups. If the numerically simulated solution patterns are identical for different cases in which, with different combinations of the variables that make up the monomials, the value of the monomials is maintained, then the monomials have been correctly deduced and the technique has been correctly applied. If this does not happen, an error when choosing the references or when considering the discriminated dimensions of the parameters might have occurred.

When data and unknown monomials have been checked and verified, dimensionless curves and abaci can be depicted, relating both sets of groups. To this aim, numerous simulations are run so the results cover the higher range of possible scenarios.

As a last step, when graphically representing dimensionless curves, the importance of the monomials they relate must be considered. Following this recommendation, if the dimensionless unknown had to be presented in a set of abaci, they would be simple and easy to use. In order to depict the abaci shown in this thesis, a big number of simulations have been run. Depending on the scenario and variable, the number of simulations goes from 150 to 3000, taking each of the simulations from 10 minutes to 6 hours.

I.5 Thesis organization

Chapter II collects the state of art of problems of flow through porous media in general and focuses on the scenarios studied in the following chapters. First, a summary of the formulation traditionally employed in the study of these problems is presented (Darcy's law). After showing the formulation, which the rest of the thesis is based on, the following section is a summary of the discriminated nondimensionalization technique, presenting previous works in which this methodology has been successfully applied. The next section is a historical overview about electrical analogy as a simulation method in engineering problems, particularly those related with flow in porous media. The fourth section of Chapter II explains the bases of the network method and its use to model engineering problems in general, and geotechnics problems in particular. Finally, the last two sections show the computer tools (Ngspice and Matlab) used for the development of this thesis.

Chapter III is an investigation of the dimensional character of permeability and hydraulic conductivity, characteristics that define the soil behaviour in flow scenarios. Firstly, the problem is approached with the classical methodology presented in those texts of Muskat [1937] and Taylor [1948], and then, the concept of discrimination is applied, so lengths in different directions are considered with different units. With this second methodology, although incomplete, we get to some conclusions that confirm the dimensionless groups for anisotropic media applied in the following chapter of this document.

Chapter IV shows, for each of the studied scenarios, different aspects of discriminated nondimensionalization technique. Those problems are: flow under a gravity dam without a sheet pile in its base, flow under a gravity dam with a sheet pile in its base, flow under gravity dams in infinite media and pumping well in unconfined aquifers. For each of these scenarios, its mathematical model (governing equation and boundary conditions), nondimensionalization of the governing equation, deduction of the dimensionless groups and universal curves for determining the unknowns of interest are presented. In the case of flow in unconfined aquifers due to a pumping well, the last section presents the verification of the groups.

Network models are described in Chapter V. The text files for these models, written with Matlab, are run by free software of circuit simulation, Ngspice. Its solutions are processed back in Matlab for displaying them in tables or graphs. For the scenarios of flow under gravity dams with or without a sheet pile, 2-D rectangular coordinates are employed, while for those of flow in unconfined aquifer, the chosen coordinates are 2-D cylindrical because of its axial symmetry.

Based on the results from the previous Chapters (IV and V), Chapter VI presents the inverse problem for determining the value of the physical parameters (permeability or hydraulic conductivity) for flow to a pumping well in anisotropic unconfined aquifers. The inverse problem is approached employing the dimensionless curves shown in Chapter IV and a common protocol of successive numerical simulations. For both methodologies, the effect of statistic errors in is studied in a shallow way. The errors are applied to the real values of water flow and seepage surface, and then the influence on the estimation of the conductivities is calculated.

Chapter VII illustrates the results of this thesis through examples of application and comments about their solutions.

Contributions and conclusions of the research are summarized in a specific section at the end of this document.

Chapter II. Theoretical fundamentals

In this chapter, the first aspect that is introduced is the theoretical basis of the problems of water flow in soils. This section includes an approach to Darcy's law, after which the governing equations of the problem and its boundary conditions are presented. The last part of the section is a summary of the different problems that are studied throughout this thesis. The second section clusters the fundamentals of discriminated dimensional characterization, while the third section does the same for the electrical analogy. Section II.4 presents the Network Simulation Method (NSM), based on the electrical analogy, as the numerical tool to simulate solutions of flow through porous media. This fourth section first presents the concept, followed by the electrical devices available for modelling scenarios, and closes with a slight explanation of how the NSM is used as a numerical tool. Finally, the fifth and sixth sections briefly present the two codes that have been employed to simulate the scenarios, Matlab and Ngspice.

II.1 The flow of water in soils

II.1.1 Darcy´s law

As for flow of viscous fluids through hollow tubes, the physical principles which determine the behaviour of fluid flow through porous media should be deduced from the balance or forces (2nd Newton's law). Nevertheless, the intricate and complex duct network in porous media makes this task complex. In this way, when Darcy [1856] became interested in characterizing flow through sand filters, he had to resort to experiments. By employing them, he discovered the fundamentals of the quantitative law which describes the dynamical behaviour of these flows.

His experiments led to a simple result (known as Darcy's law): '*the amount of water (m^3/s) flowing through a porous medium is directly proportional to the filter's cross section, A (m^2), and the pressure difference between the inlet and the outlet, Δp (N/m^2), and inversely proportional to the length of the medium, L (m)*'. The analytical expression (which was originally stated as $\mathrm{Q} = \mathrm{C}\frac{\mathrm{A}}{\mathrm{L}}(\Delta\mathrm{h})$, where Δh is the piezometric or hydraulic potential difference between the inlet and the outlet of the medium) is

$$\mathrm{Q} = \mathrm{C_o}\frac{\mathrm{A}}{\mathrm{L}}(\Delta\mathrm{p}) \qquad \text{(II-1)}$$

with C_0 a dimensional constant whose physical meaning is complex if approaching it from its dimensional equation, $[\mathrm{C_o}] = \mathrm{LM^{-1}T^{-1}}$, or its units, $m \cdot kg^{-1} \cdot s^{-1}$. However, its definition is immediate for a sample inside an impervious cylindrical container: 'C_0 is the amount of water flowing through a cross section of unit area and length, to which a unit pressure difference between its bases is applied'. Evidently, C_0 is a constant that depends on the physical properties of the fluid (viscosity and density) and the geometrical properties of the porous network (grain size, porosity, connectivity and tortuosity). The dimensional character of both the law and the constant C_0, as well as its dependence on the cited properties, is thoroughly presented in Chapter III. The first attempts of deriving Darcy's law from classical hydrodynamical equations were those of Muskat [1937] and Bose ([1929] and [1930]), and none of them reached to a correct solution.

The validity of Equation (II-1), due to its fundamental character and the simple relation, has been subject of much research in order to verify it, from theoretical attempts based on Pi theorem (Muskat [1937]) to myriad of experiments in different types of media under a broad range of pressures. The most reliable results conclude that

- low average velocities $\frac{\Delta p}{\Delta s} = a_1 v$ (equivalent to Darcy's law) (II-2a)
  'laminar viscous flux'
- higher velocities $\frac{\Delta p}{\Delta s} = a_1 v + a_2 v^n$ ($\frac{\Delta p}{\Delta s}$ increases faster than v) (II-2b)
  'partially or totally turbulent flux'

Case (II-2a) is known as viscous flow, as an analogy to hydrodynamics in hollow ducts. Indeed, experimental logarithmical charts developed by Fancher et al. [1933] relating friction factor, $\zeta = \frac{(\Delta p)d}{2L\rho v^2}$, to Reynolds number, $R_e = \frac{v\rho d}{\mu}$ (where d is the average grain size), confirm that for Re<1, $\zeta \cdot R_e =$ constant. This is

$$\frac{\Delta p}{L} \propto \frac{\mu}{d^2} v, \qquad \text{or} \qquad \frac{\Delta p}{L} = C_3 \cdot v \qquad \text{(II-3)}$$

where C_3 is a dimensional constant that includes parameters related to the fluid and the medium. This result is coherent with Darcy's law. Later in this document (Chapter III), Muskat [1937] strongly stated that parameter d has to be the average grain size: '*Physically, of course, the parameter d should represent the average pore rather than the grain diameter. However, as the former can be directly measured only by microscopic examination of the cross section of the porous medium itself, all attends to define or use a value of d to enter into the Reynolds number have referred to the averages of the actual grains diameter*'.

This law lacks validity when the flow becomes partially or completely turbulent, having to apply in these scenarios expression (II-2b) with a value of n around 2, according to all the experimental results in different kinds of media. The strongest example that corroborates expression (II-2b) is that from Lindquist's experiment [1933], who studied water flow through uniform-size bullet columns where n=2. The chart where his results were collected, presenting $\zeta \cdot R_e$ vs R_e, displays two lines, one horizontal (for 0<R_e<4, approximately) followed by the second with constant positive slope (for R_e>4, approximately) which adjust to line equation $\zeta R_e = C_4 + C_5 R_e$, where C_4 and C_5 are dimensional constants, as $\zeta \cdot R_e = \frac{1}{2}\frac{(\Delta p)}{L}\left(\frac{d^2}{\mu}\right)\left(\frac{1}{v}\right)$. The equation can be written in the form $\frac{1}{2}\frac{(\Delta p)}{L}\left(\frac{d^2}{\mu}\right)\left(\frac{1}{v}\right) = C_4 + C_5\frac{v\gamma d}{\mu}$ or, finally,

$$\frac{(\Delta p)}{L} = \left(\frac{2\mu C_4}{d^2}\right) v + \left(2C_5\frac{\rho}{d}\right) v^2 = C_6 v + C_7 v^2 \qquad \text{(II-4)}$$

Equation (II-4) is equivalent to expression (II-2b). Perhaps, capillary and irregular nature of the porous media is the reason why the transition from laminar viscous to turbulent regimen is not as sharp as in the case of hollow ducts.

Different experiments (for example those of Lindquist [1933] with homogeneous bullets and Ehrenberger [1928] with heterogeneous sands) stablished that the limit of application of Darcy's

law in values of Reynolds number would oscillate between 12 and 1; from these data it can be deduced that R_e value is reduced as heterogeneity increases due to the wide variations of pore size, although neither the shape nor grain angularity nor cementation degree (physical aspects that determine porosity, connectivity and tortuosity) are clustered in d expression. Nevertheless, we accept $R_e = 1$ as the lower limit to ensure viscous or Darcy's regimen, where d can take any reasonable definition of the average grain size.

In ground engineering, there are many problems in which the most influent potential agent causing pressure difference (and, therefore, water filtration in soil) is gravity. For this reason, Darcy' s law is frequently written in terms of hydraulic gradient, $\frac{d\mathrm{h}}{d\mathrm{x}}$. The relation between the changes in pressure (p) and variation of fluid head or fluid hydraulic potential (h), for the same geometric vertical position z (height from a specific reference), is:

$$d\mathrm{p} = \rho \mathrm{g}(d\mathrm{h}) \tag{II-5}$$

where $\rho \mathrm{gh}$ is the energy per unit of fluid volume due to the weight of a fluid column of density, ρ, and height, h. The column would communicate this point to the atmosphere. gh is this same energy per unit of mass, and h the energy per unit of weight. According to Bernoulli's equation, neglecting velocity loads, variables h and p are related by

$$\mathrm{h} = \frac{\mathrm{p}}{\rho \mathrm{g}} \pm \mathrm{z} \tag{II-6}$$

where ± sign depends on the sense in which z grows, + if the variable grows upwards and – if the variable grows downwards.

The variable *d*p presents the work of the pressure forces per unit of volume (with negative sign), when the pressure is caused by gravitational forces or potentials. This work modifies the gravitational potential energy of the fluid in the same value (the potential energy decreases if the work is positive, *d*p<0, and increases when the work is positive, *d*p>0). Employing this hypothesis, Darcy's law can be written as

$$\mathrm{v} = \frac{\mathrm{k}\rho \mathrm{g}}{\mu}\left(\frac{\mathrm{dh}}{\mathrm{dx}}\right) = \frac{\mathrm{k}\,\gamma_{\mathrm{f}}}{\mu}\left(\frac{\mathrm{dh}}{\mathrm{dx}}\right) = \kappa \frac{\mathrm{dh}}{\mathrm{dx}} \tag{II-7}$$

where

$$\kappa = \frac{\mathrm{k}\rho \mathrm{g}}{\mu} \tag{II-8}$$

This new parameter κ is known as hydraulic conductivity, and it depends on the porous media and the fluid. The other parameter, k, is known as permeability, and only clusters physical properties of the media. Since the hydraulic gradient has null dimension (which lacks physical

meaning), κ (m/s) has that of a velocity, $[\kappa] = LT^{-1}$, leading to a certain degree of confusion. Hydraulic conductivity does not present the same nature as velocity, which is kinematic physical quantity. However, it is commonly measured in Darcy (1 cm/s= 1040 darcys, so it is a velocity unit). Finally, k (m^2) has the same units of a surface, $[k]=L^2$.

All in all, Darcy's law defines the macroscopic behaviour of a fluid that flows through a porous medium, relating concepts involved in dynamics. Macroscopically, it means that the fluid volume elements to which it refers have many pores, so velocity and pressure variables are averaged values in these pores. Local values of the variables (in each pore) can vary sharply and, in order to know this information, Navier-Stokes equation must be solved. Therefore, Darcy's law can be considered as the statistical result of averaging the results of Navier-Strokes solution in a big number of individual pores, being this the reason of its importance.

Although Darcy's experiments were carried out in 1-D scenario, the translation to 3-D scenarios is immediate. In rectangular cartesian coordinates

$$v_x = -\frac{k_x}{\mu}\frac{\partial p}{\partial x} \tag{II-9a}$$

$$v_y = -\frac{k_y}{\mu}\frac{\partial p}{\partial y} \tag{II-9b}$$

$$v_z = -\frac{k_z}{\mu}\frac{\partial p}{\partial z} \tag{II-9c}$$

where μ is the dynamic viscosity of the fluid and k the permeability, that can vary from one point to another as well as in each spatial direction in the same point. In isotropic soils, $k_x=k_y=k_z=k$, so

$$v_x = -\frac{k}{\mu}\frac{\partial p}{\partial x}, \quad v_y = -\frac{k}{\mu}\frac{\partial p}{\partial y}, \quad v_z = -\frac{k}{\mu}\frac{\partial p}{\partial z} \tag{II-10}$$

As external forces exist (gravitational forces, for example), this must be added to the pressure gradient as forces per unit of volume. Darcy's law has then the following form

$$v_x = -\frac{k_x}{\mu}\left(\frac{\partial p}{\partial x} - F_{ext,x}\right) \tag{II-11a}$$

$$v_y = -\frac{k_y}{\mu}\left(\frac{\partial p}{\partial y} - F_{ext,y}\right) \tag{II-11b}$$

$$v_z = -\frac{k_z}{\mu}\left(\frac{\partial p}{\partial z} - F_{ext,z}\right) \tag{II-11c}$$

If external forces are conservative (as happens to gravitational), there is an associated potential energy from which they derive as

$$F_{ext,x} = \frac{\partial V_{ext}}{\partial x}i + \frac{\partial V_{ext}}{\partial y}j + \frac{\partial V_{ext}}{\partial k}k = -\nabla V_{ext} \tag{II-12}$$

Therefore, the previous Darcy's law expression is written as

$$v_x = -\frac{k_x}{\mu}\left(\frac{\partial p}{\partial x} + \frac{\partial V_{ext}}{\partial x}\right) = -\frac{k_x}{\mu}\left[\frac{\partial}{\partial x}(p + V_{ext})\right] \quad \text{(II-13a)}$$

$$v_y = -\frac{k_y}{\mu}\left(\frac{\partial p}{\partial y} + \frac{\partial V_{ext}}{\partial y}\right) = -\frac{k_y}{\mu}\left[\frac{\partial}{\partial y}(p + V_{ext})\right] \quad \text{(II-13b)}$$

$$v_z = -\frac{k_z}{\mu}\left(\frac{\partial p}{\partial z} + \frac{\partial V_{ext}}{\partial y}\right) = -\frac{k_z}{\mu}\left[\frac{\partial}{\partial z}(p + V_{ext})\right] \quad \text{(II-13c)}$$

If the medium is now assumed to be homogeneous (k and μ independent of position) and isotropic (independent of spatial direction), a new potential function is defined (although, as show later, it does not have meaning of energy per unit of volume) in the form

$$\Phi = \frac{k}{\mu}(p + V_{ext}) \quad \text{(II-14)}$$

The new variable Φ can be given the meaning of a velocity potential, a potential function from which velocity is derived in the same way as conservative forces are derived from its associated potential function,

$$v_x = -\frac{\partial \Phi}{\partial x}, \qquad v_y = -\frac{\partial \Phi}{\partial y}, \qquad v_z = -\frac{\partial \Phi}{\partial z} \quad \text{(II-15)}$$

or

$$v = -\nabla\Phi = -\nabla\left[\frac{k}{\mu}(p + V_{ext})\right] \quad \text{(II-16)}$$

It is important to keep k and μ as separated parameters in Equation (II-14) instead of defining a new parameter with the ratio of both, even if it is only to separate the fluid properties (μ) and the soil characteristics (k). Expressions (II-16), together with the definition of Φ (II-14) can be considered as the generalization of Darcy's law, the dynamic equation that substitutes Navier-Stokes equation as its equivalent macroscopic expression for homogeneous isotropic fluids and soils.

The physical meaning of quantities involved in Darcy's law can be written as:

p (pressure, N/m^2 o P)	→ force per unit of surface or energy associated to pressure (pressure energy) per unit of volume. Assuming p as energy per unit of volume gives this variable the meaning of an energetic potential from which pressure forces per unit of volume are derived.
$\boldsymbol{\nabla}p$ (N/m^3 o P/m)	→ force per unit of volume or spatial variation of pressure energy per unit of volume
$\mathbf{F}_{ext,x}$	→ force per unit of volume or spatial variation of the potential energy V_{ex} per unit of volume
V_{ext}	→ potential energy (associated to force $\mathbf{F}_{ext,x}$ per unit of volume

$p + V_{ext}$ → total potential energy per unit of volume (associate to external force)

$\boldsymbol{\nabla}(p + V_{ext})$ → total force per unit of volume associate to the spatial changes of the pressure energies and potential energy

$\Phi = \frac{k}{\mu}(p + V_{ext})$ (**isotropic media**) → velocity potential (its gradient determines the **v** components)

II.1.2 Governing equations

The governing equation in terms of the potential variable, h or Φ, assuming an incompressible fluid and steady flow, is obtained by substituting expressions (II-13) in the continuity equation (or fluid mass conservation)

$$\frac{\partial v_x}{\partial x} + \frac{\partial v_y}{\partial y} + \frac{\partial v_z}{\partial z} = 0 \qquad \text{(II-17)}$$

which result is

$$\kappa_x \frac{\partial^2 h}{\partial x^2} + \kappa_y \frac{\partial^2 h}{\partial y^2} + \kappa_z \frac{\partial^2 h}{\partial z^2} = 0 \qquad \text{(II-18)}$$

In isotropic soils, it can be reduced to $\frac{\partial^2 h}{\partial x^2} + \frac{\partial^2 h}{\partial y^2} + \frac{\partial^2 h}{\partial z^2} = 0$

or $\nabla^2 h = 0$, where ∇^2 is the Laplace mathematical operator, $\nabla^2 = \frac{\partial^2}{\partial x^2} + \frac{\partial^2}{\partial y^2} + \frac{\partial^2}{\partial z^2}$. In terms of velocity potential, it is easy to deduce the governing equation

$$\nabla^2 \Phi = \frac{\partial^2 \Phi}{\partial x^2} + \frac{\partial^2 \Phi}{\partial y^2} + \frac{\partial^2 \Phi}{\partial z^2} = 0 \qquad \text{(II-19)}$$

In bidimensional irrotational flow, in isotropic soils of any geometry, where the flow is the same in parallel planes (as it occurs in most ground engineering problems), the governing equation is $\nabla^2 \Phi = \frac{\partial^2 \Phi}{\partial x^2} + \frac{\partial^2 \Phi}{\partial y^2} = 0$, where $v_x = -\frac{\partial \Phi}{\partial x}$ and $v_y = -\frac{\partial \Phi}{\partial y}$. Among the harmonic functions (solutions of Laplace-type expressions) there is a solution, Ψ, known as the conjugated function of Φ, that is defined as

$$v_x = \frac{\partial \Psi}{\partial y} \text{ and } v_y = -\frac{\partial \Psi}{\partial x} \qquad \text{(II-20)}$$

Substituting this definition in continuity equation two different solutions are obtained: on the one hand, Cauchy-Riemann condition, $\frac{\partial^2 \Psi}{\partial x \partial y} - \frac{\partial^2 \Psi}{\partial y \partial x} = 0$; on the other hand, employing the velocity expression and the relation between Φ and Ψ ($-\frac{\partial \Phi}{\partial x} = \frac{\partial \Psi}{\partial y}$, and $-\frac{\partial \Phi}{\partial y} = -\frac{\partial \Psi}{\partial x}$), the conjugated function Ψ (stream function) that also meets Laplace expression.

$$\nabla^2 \Psi = \frac{\partial^2 \Psi}{\partial x^2} + \frac{\partial^2 \Psi}{\partial y^2} = 0 \qquad \text{(II-21)}$$

In steady state, any point of a particle path meets $\frac{v_y}{v_x} = \frac{dy}{dx}$, or $v_y dx = v_x dy$. Introducing velocity expressions (II-21) in this equation, we obtain $\frac{\partial \Psi}{\partial x} dx + \frac{\partial \Psi}{\partial y} dy = 0$, so $d\Psi = 0$. This means that in a streamline, Ψ= constant. Another property of Ψ is that water flow per unit of length in the z direction (q m^2/s) between two lines is always the difference between the value of Ψ of both lines. Indeed,

$$q = \int_{\Psi_1}^{\Psi_2} v_x \, dy = \int_{\Psi_1}^{\Psi_2} d\Psi = \Psi_2 - \Psi_1 \qquad \text{(II-22)}$$

The set of graphics Φ=constant and Ψ= constant, are perpendicular between them, so ones can be easily obtained if the others are known. Their graphical solution is the flow net, a very useful tool in problems involving groundwater flow. Analytically, the relation between both harmonic functions can be easily found

$$\Psi = \int \left(\frac{\partial \Phi}{\partial x} dy - \frac{\partial \Phi}{\partial y} dx \right), \qquad \Phi = \int \left(\frac{\partial \Psi}{\partial y} dx - \frac{\partial \Psi}{\partial x} dy \right) \qquad \text{(II-23)}$$

The combination of Φ and Ψ in the form $\Theta = \Phi + i\Psi$ (complex potential) has an especial interest, since $\nabla^2 \Theta = \nabla^2 \Phi + i\nabla^2 \Psi$ meets the continuity equation and the governing equations $\nabla^2 \Phi = 0$ and $\nabla^2 \Psi = 0$. In this way, the flow is continuous and irrotational.

The main disadvantage of employing the variable Φ instead of h is that the information about the anisotropy of the soil is lost, because the isotropic permeability or hydraulic conductivity is involved. Therefore, in order to obtain more realistic flow nets, it is a better option to introduce the hydraulic potential (or water head) variable, h. For this purpose, variables h and Ψ are related by

$$v_x = -\kappa_x \frac{\partial h}{\partial x} = \frac{\partial \Psi}{\partial y} \qquad v_y = -\kappa_y \frac{\partial h}{\partial y} = -\frac{\partial \Psi}{\partial x} \qquad \text{(II-24)}$$

With this formulation, similar conclusions to those obtained for isotropic soils are reached but, in this last case, isopotential lines and streamlines do not have to be necessary perpendicular to each other. In order to plot the stream function variable, two different approaches can be used. On the one hand, the variable can be solved by itself, considering its own boundary conditions. On the other hand, it can be solved from the results of the hydraulic potential by numerical integration. For this second option, Equation (II-24) must be translated into spatial derivatives

$$v_x = -\kappa_x \frac{\Delta h}{\Delta x} = \frac{\Delta \Psi}{\Delta y} \qquad v_y = -\kappa_y \frac{\Delta h}{\Delta y} = -\frac{\Delta \Psi}{\Delta x} \qquad \text{(II-25)}$$

According to this, the stream function variable can be integrated following two different paths

$$\Psi_{i,j} - \Psi_{i,j-1} = -\kappa_x \frac{\Delta h \, \Delta y}{\Delta x} \quad \text{or} \quad \Psi_{i,j} - \Psi_{i-1,j} = -\kappa_y \frac{\Delta h \, \Delta x}{\Delta y} \qquad \text{(II-26)}$$

Both expressions derive in the same solution of the stream function, and for the development of the calculations presented later in this work, the first option is employed This has an advantage, since only one boundary or initial condition must be known.

II.1.3 Boundary conditions

They complete the mathematical model and are classified as:

- First class or Dirichlet. This is the most common one and imposes a constant value of the dependent variable at the border. Since the governing equation can be stablished in terms of any of the potential variables, hydraulic potential (h) or stream function (Ψ), this condition can be set in both models. For variable h, the flow in the border adjusts along it to be coherent with the imposed potential, while for variable Ψ (which implies an impervious border) is the piezometric potential the one that adjusts along the border to be coherent with the constant value of Ψ. Their expressions are

  h = constant (1^{st} class in h) $\Rightarrow$ isopotential border

  Ψ = constant (1^{st} class in Ψ) $\Rightarrow$ impervious border

  Moreover, in the border with isopotential lines, the hydraulic gradient along the line ($\frac{\partial h}{\partial s}$) is null, which means that the component of the velocity is perpendicular to the border line or surface. In the same way, at border lines with constant value of Ψ, the gradient of Ψ along the line ($\frac{\partial \Psi}{\partial s}$) is also null, so the velocity in the perpendicular direction to this line (proportional to $\frac{\partial \Psi}{\partial s}$) is null. This all is independent of the isotropic or anisotropic character of the medium. First class condition can also be applied to the mathematical model with the velocity potential variable, $\Phi = \frac{k}{\mu}(p \pm \rho g z) = \rho g h$. Its expression is Φ = constant and has the same physical meaning as h=constant, since ρ and g are constant.
- Second class of Neumann. For the potential variable it defines a constant inlet or outlet water flow through a border (perpendicular to the studied contour). Its equation is

  $\frac{\partial h}{\partial n}$ = constant (2^{nd} class in h)

  If $\frac{\partial h}{\partial n} = 0$, it is a homogeneous second-class condition and defines an impervious border in terms of h. In both cases, the potential h in the border must adjust to meet this condition. For variable Ψ, second class condition is written as

  $\frac{\partial \Psi}{\partial n}$ = constant (2^{nd} class inΨ)

This means that the water flow is constant in the direction of the border (eventually null if it is a homogeneous condition, $\frac{\partial \Psi}{\partial n} = 0$). In both cases, Ψ automatically adjusts to meet the condition.

- Free surface. It is a special condition without analogy in problems of flow of other nature. It is related to the streamlines located in those borders that generally are not defined a priori in the problem (if no capillary flow is considered). Those streamlines have constant pressure (p), usually atmospheric. Therefore, in this border there is no flow perpendicular to it. It is expressed in terms of two equations that must be simultaneously met

  p = constant and $\frac{\partial h}{\partial s}$ = constant (free surface condition)

  $\frac{\partial h}{\partial s}$= constant means that Δh for the same values of Δs along the free surface are the same.

- Seepage surface condition. It is a special condition that is related to constant pressure lines that emerge in wells, ditches, vertical walls and earth dams, and can be vertical or horizontal. They are not streamlines, since there is a flow component perpendicular to these lines. They are defined surfaces which present one unknown limit. This limit is considered as a problem unknown, although it is located in the same place as one of the limits of the free surface. It can be expressed as

  p = constant

  It is a known border except for one limit (free surface condition)

Free and seepage conditions make the design of analogical models based on the network method very complex due to the lack of definition of these borders. Their resolution is cumbersome and can be considered as inverse problems, for which new data must be introduced. For example, determining these lines in a well could be obtained by successive approximations if the pumping rate is given. Lines move successively for each solution until the final water flow is reached. The introduction of specific electrical devices in the model, as presented in Chapter V, or other input information (such as piezometry in a point of the free surface, experimentally measured) can also lead to the solution of the problem.

II.1.4 Scenarios of dams and wells

Along this thesis, two different problems of flow through porous media are studied: ground water flow under impervious dams, and water flow in unconfined aquifers due to a pumping well. Although both phenomena occur due to a difference of hydraulic potential, for each of them, the employed coordinate system differs. Flow under dams is modelled in rectangular 2-D coordinates (x, y), while in pumping well scenarios, the flow is simulated with 2-D cylindrical coordinates (r, z) because the problem can be simplified as axisymmetric. Dam scenarios can present some differences among them: the structure may have a foundation or not, and it can present a sheep pile under it, located in different points at its base. All these options (Figure 2.1) alter the values of the studied variables. In problems of flow in unconfined aquifers due to pumping wells (Figure 2.2), two specific variables appear: free surface, which is the area of the saturated soil under atmospheric pressure, and seepage surface, which is the area above the well where the water head values are the same as the vertical position and there is flow outside the aquifer.

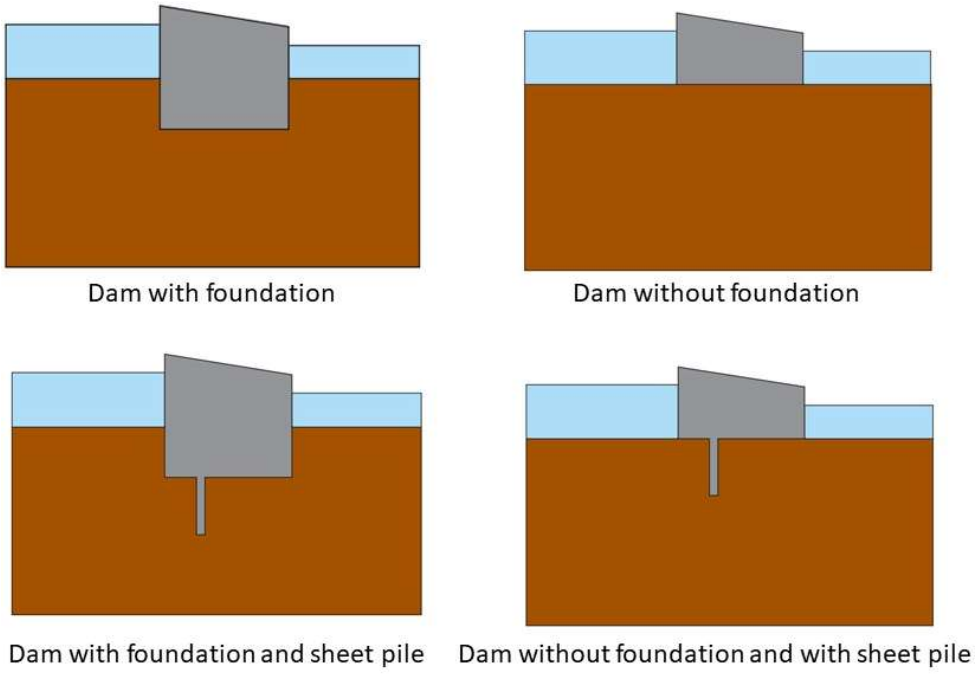

Figure 2.1. Different scenarios of flow under dams

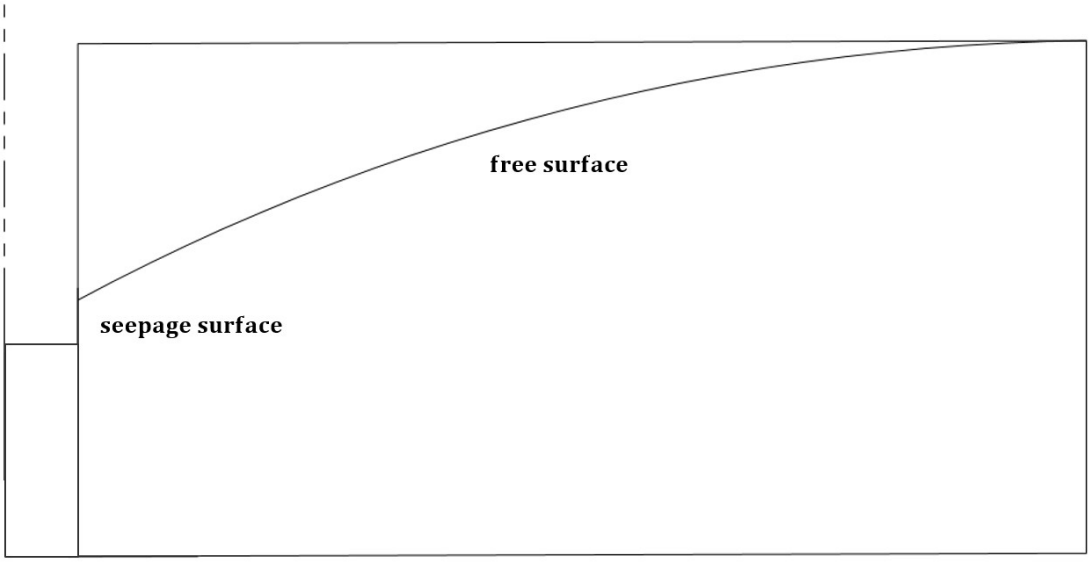

Figure 2.2. Scenario of flow in unconfined aquifers due to a pumping well

II.1.4.1 Dams with or without foundation

This kind of problems can be modelled according to the boundary conditions and the parameters shown in Figure 2.3. As anisotropic soils, two hydraulic conductivities are considered, one for each direction that is considered, κ_x and κ_y.

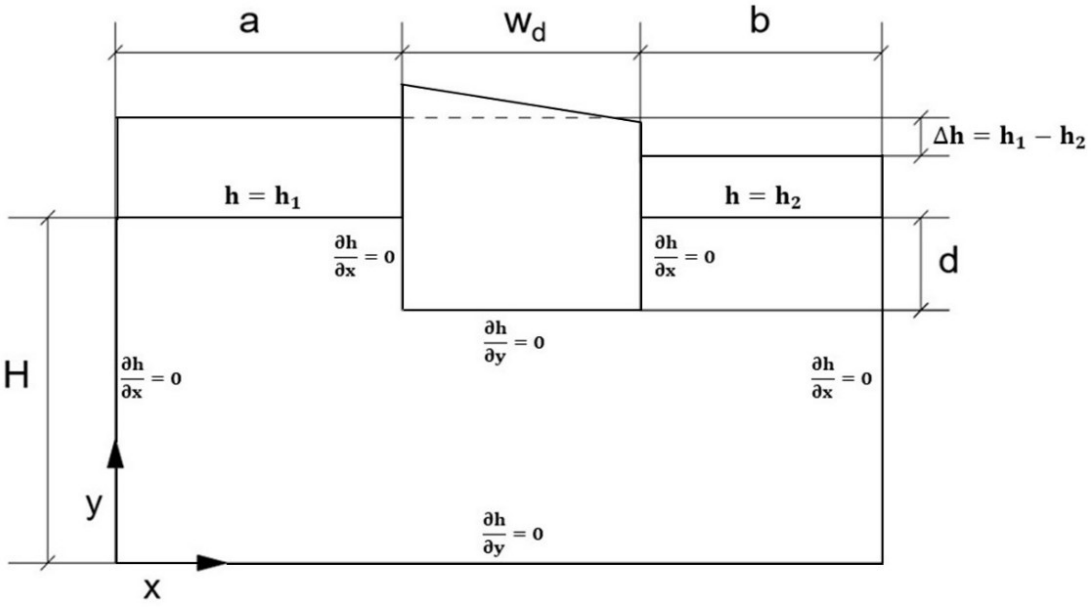

Figure 2.3. Parameters and boundary conditions of flow under dams

The governing equation for these problems is a Laplace-type expression that has been previously shown in this section.

$$\kappa_x \frac{\partial^2 h}{\partial x^2} + \kappa_y \frac{\partial^2 h}{\partial y^2} = 0 \qquad \text{(II-27)}$$

In these problems, to the horizonal upstream and downstream contours are applied constant values of hydraulic potential, while the rest of the contours are considered as impervious. The vertical external contours, which represent the connections with the river, can be modelled with other conditions, $h=h_1$ and $h=h_2$ for the left and right borders respectively, as in other research papers (Mateo-Lázaro et al. [2016]). However, this option is not employed in this thesis.

If a dam without a foundation is considered, d=0, so the vertical boundary conditions which modelled this part of the structure disappear.

II.1.4.2 Dams with sheet pile

In this case, the parameters and boundary conditions are similar to those of the previous scenarios, and then the ones related to the length and position of the sheet pile are added. All this is displayed in Figure 2.4.

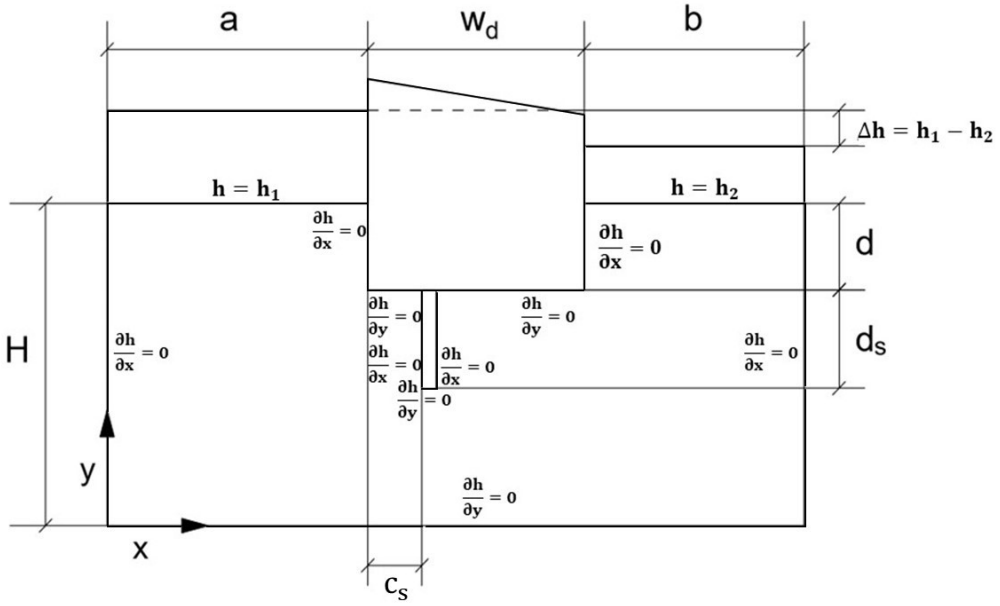

Figure 2.4. Parameters and boundary conditions of flow under dams with sheet pile

The governing equation in these scenarios is the same as in II.1.4.1, because the existence of the sheet pile does not alter the expression. Nevertheless, it affects the boundary conditions, as it adds two vertical and one horizontal impervious contour.

Although the sheet pile width is considered as negligible for this research, when modelling it a small value must be given. This means that this width must be represented as a horizontal

impervious border, so it becomes a boundary condition too. If a dam without a foundation is considered, d=0, so the vertical boundary conditions which modelled this part of the structure disappear.

II.1.4.3 Pumping wells in unconfined aquifers

Among the various fields of hydrogeology and ground engineering, water flow through porous media due to the presence of a pumping well has been widely reviewed in several publications and manuals (Barlow & Leake [2012], Ayvaz & Karahan [2008]). Not only water supply (Massuel et al. [2017]), but also oil and gas production (Davies et al. [2014]) as well as investigation about pollution (Bakis & Tuncan [2011]), are topics related to this research area. Nevertheless, these issues involve other elements, such as solutes or other fluids, which increases the difficulty of its study.

As in any other processes of water flowing through soil particles, when studied from a macroscopic point of view, it is based on Darcy's law. Moreover, specific formulation based on Darcy's law to characterize the flow due to pumping wells have been developed. These expressions, which involve geometrical and hydrogeological parameters, allow achieving results in a rather simple manner. The expressions and procedures to reach results vary according to the nature of the aquifers. According to the water level position, aquifers can be considered confined, semiconfined or unconfined. In addition, another way to classify aquifers is conforming to time: when the phenomenon is stabilised, then it is known as steady-state or stationary, while before this moment it is considered as transient-state.

Confined aquifers are those whose piezometric level is above the upper border along the whole horizontal length that is being considered. When pumping is happening, none of the new values of water level generated by the extraction or injection of water can be below the upper border of the aquifer. When steady state is studied, Thiem approximate formulation (Thiem [1906]) is employed. It states that the volume of pumped water depends on the variation of hydraulic potential or drawdown in a linear way. If the problem is studied before the phenomenon has stabilised, the problem is time-dependent, and the solutions are affected by this new variable. Theis [1935] developed a methodology to study this phenomenon. The equations and graphics he presented came from the solution of heat flow from an instant source in a 2-D medium (Carslaw [1921]). However, simplifications have been elaborated in order to avoid the use of Theis graph, although they are subjected to restrictions. The most-known simplification is that of Jacob [1963], which is valid for values of u lower than 0.03, being u an auxiliary function in

Theis expression (inherited from the heat flow formulation). It involves some of the variables of the scenario, such as the well radius, the storage coefficient, the transmissivity of the aquifer (which is the product of the hydraulic conductivity and the aquifer thickness) and the moment (time) when the test is being carried out. If the restriction is met, then Jacob formula is very easy to use, as its independent variable is time.

Semiconfined aquifers are a second kind of aquifers, and they are also known as leaky. These appear when the aquifer is recharged by an aquitard (layer of lower permeability) that is commonly placed above it (although it is also possible to find the aquitard underneath the studied aquifer). Therefore, while the aquitard is supposed to keep a constant piezometric level (so the hydraulic potential is assumed not to vary in any point of it), it does vary inside the aquifer. In the same way that occurs for confined aquifers, semiconfined aquifers are studied in a different manner if they are considered to have reached a balance (steady-state) or not (transient-state). De Glee [1930] developed his formulation for steady-state semiconfined aquifers. He modelled the combination of the aquifer and the aquitard introducing a new parameter, leakage factor (B), which clusters information about both structures, as it involves the transmissibility of the aquifer, the saturated thickness of the aquitard and its hydraulic conductivity. Moreover, an auxiliary variable K_o (in which B takes part) is employed in order to reach the solution of the problem. For transient-state semiconfined aquifers Hantush [1964] solution is similar to that presented by De Glee, as they both employed the parameter B. However, Hantush formulation is also based on the solution provided by Theis although, while Theis only presented one curve (W(u)), Hantush developed an abacus where each curve shows the function W(u) for different values of B.

The last type of aquifers are unconfined aquifers, which are also known as water table aquifers. They are given this name because the groundwater surface (phreatic level) is below the upper border of the permeable stratum, so the water is at atmospheric pressure. Whether steady or transient state scenarios are considered, the same restrictions are applied when employing the traditional formulations to study the flow due to a pumping well. Firstly, the aquifer is supposed to be of infinite extension, homogeneous and isotropic, with horizontal bottom and constant thickness. Moreover, the diameter of the pumping well is negligible, and the well is fully penetrating. Traditionally, only radial flow is considered, an assumption that is commonly known as 'Dupuit-Forcheimer hypothesis'. The last restriction is to consider only one pumping well in the area that works at a constant discharge rate.

If the steady state has been reached (a hypothesis only valid if pumped groundwater is compensated by other recharge source of water), the formulation that has been traditionally

employed is that developed by Dupuit [1863]. He stated that the water flow value depends on the difference of the squared values of hydraulic potential in two points of the water table. Some authors, however, explained that Thiem equation could be applied if the potential difference was lower that 10-15 % (González de Vallejo [2002]). If the potential difference is higher, Jacobs correction ([1963]) can be employed to work in terms of drawdowns, which is common when plotting curves.

Transient state in unconfined aquifers is difficult to study by traditional protocols. There is not a specific theoretical formulation accompanied by curves or abaci to obtain results, and the phenomenon must be approached with empirical methodology in which , for example, different pumping rates are employed to reach the sought parameters. To study transient state in these aquifers following a more traditional method, a graphical method is used, in which the curve is divided in three parts and Theis formulation is employed in the first and the last parts. Due to the complexity of this methodology, simplifications for long times have been developed (Custodio & Llamas [1976]).

Non-realistic results are obtained if the hypotheses previously presented are considered in problems of flow in unconfined aquifers due to pumping wells. Soils are commonly anisotropic, so instead of modelling the problem with a single hydraulic conductivity, at least two values (one in the radial direction and another in the vertical one, since we still consider the problem as axisymmetric) must be employed to simulate the phenomenon in a more realistic way. Moreover, only considering radial flow is also a strong restriction which affects the solution, since there must be a vertical component in the vicinity of the well whose importance depends on the variation of the hydraulic potential due to the pumping. Some authors have modelled anisotropic soil by assuming an equivalent isotropic soil (Childs et al. [1957], de Cazenove [1961]).

Not considering the vertical component of the vertical flow in the well surroundings has led to lay aside the analytical study of the seepage surfaces, which are the wet surface above the position of the water in the well (Castany [1971]). This area, as well as the free surface, is at atmospheric pressure. Some authors have presented research defending that the seepage surface is the variable that should be introduced in Dupuit formulation instead of the water head (or hydraulic potential) in the well (Boulton [1951]). Other investigations carried out empirical studied of the seepage surface with scale models (Simpson et al. [2003] and Hall [1955]). With these models, mathematical expressions were obtained. The conjunction of electrical analogy (Babbitt & Caldwell [1948]) and the finite difference (Stallman [1963]) is a different mean to approach a solution for the variable

This kind of problems, whose parameters and boundary conditions are displayed in Figure 2.5, have less boundary conditions than those in Sections II.1.4.1 and 2, although finding the free and seepage surfaces makes the resolution cumbersome because they are not initially known. In this case, the conductivities are κ_r and κ_z. Furthermore, as explained in Chapter IV, h_s is the length of the well wall where the hydraulic potential, h, takes a higher value than the vertical position, z, including this the well, h_w and the seepage surface. Authors, such as Hall, consider the variable h_s in their research, and the same has been used for this thesis, naming the variable 'seepage surface' in order to simplify the document.

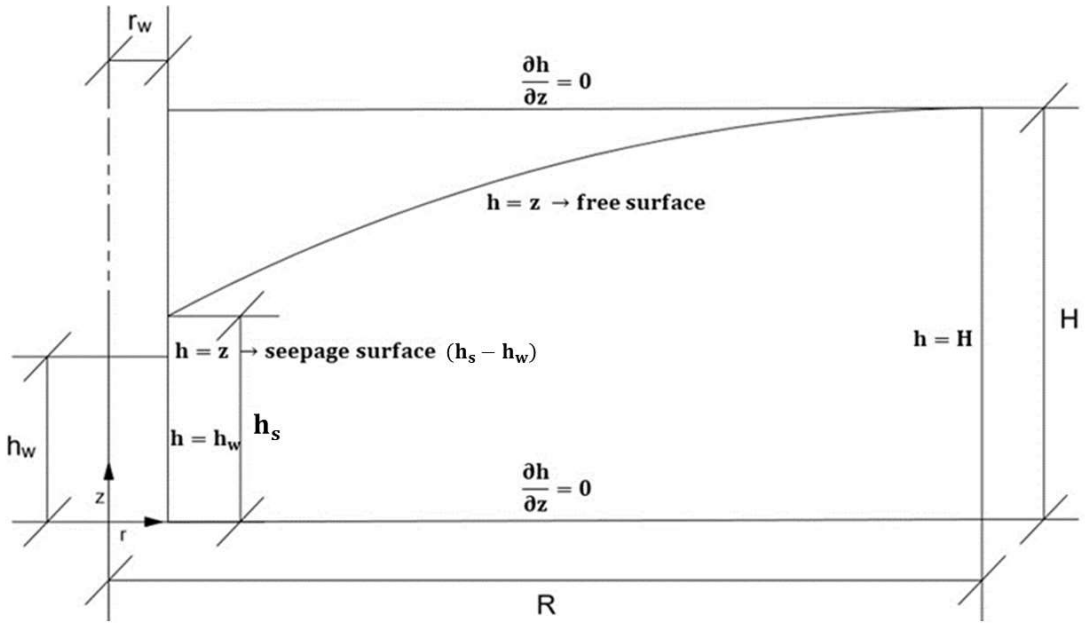

Figure 2.5. Parameters and boundary conditions of flow in unconfined aquifers due to a pumping well

The governing equation in these problems is also a Laplace-type expression, although in cylindrical coordinates, since well models are considered axisymmetric. This is

$$\kappa_r \frac{1}{r}\frac{\partial}{\partial r}\left(r\frac{\partial h}{\partial r}\right) + \kappa_z \frac{\partial^2 h}{\partial z^2} = 0 \qquad \text{(II-28)}$$

In these scenarios, the vertical borders present constant values of hydraulic potential. The further border has the initial potential in the aquifer, H, while the one next to the well is divided into two kind of values: constant value, h_w, along the well length, and the border above it in which the constant value varies with the vertical position, h=z.

II.2 Discriminated nondimensionalization. Dimensionless groups and universal curves

Without a thorough explanation, this section presents the concept of 'dimensional characterization', whose final subject is the setting of the correct and more precise independent dimensionless groups that govern the solution of a problem. Its application in this thesis has allowed, on the one hand, simplifying classical solutions expressed by their related groups and, on the other hand, presenting new universal curves in the fields of groundwater flow applied to ground engineering.

It is known that the reduction of the set of physical and geometrical parameters to the smallest number of dimensionless groups that rule a given problem and the deep understanding the relative weight of any parameter on the final solution, especially if it is a complex one, is generally the first step to simplify the analytical study. With this technique, which requires a certain level of knowledge about dimensional theory (or analysis), the use of an efficient and reliable protocol to obtain the groups and the application of Pi theorem lead to interesting results without much mathematical effort. The solutions of the problem, or its solution patterns, depend on the number of dimensionless groups that can be formed with the physical and geometrical parameters of the physical phenomenon and the scenario that is developed. The complexity of the solutions noticeably increases with the number of groups.

In this way, for instance, the simplest solutions are obtained when no dimensionless groups can be formed with the physical and geometrical parameters involved in the problem. In this case, the solution of any global unknown (independent of space and time variables) is obtained associating a unity order of magnitude to the single dimensionless group that can be formed with the previously mentioned unknown. This group is the dimensionless expression of the studied unknown. If it is not a global unknown and, therefore, it is referred to a concrete position and/or a certain instant, the dimensionless expression of the unknown is function of the normalized position and/or instant dimensionless form, both obtained adopting well-chosen references for length and time. If there is a single dimensionless group, global unknowns can be displayed with simple universal curves (one for each unknown). These curves are generally obtained after a large number of numerical simulations. Non-global unknowns depend again on the normalized time and/or position dimensionless variables too. If two dimensionless groups emerge from the problem, the solution for each global unknown is an abacus, and if three groups appear, a set of abaci. The existence of more than three dimensionless groups increases the complexity of the construction of dimensionless curves for global unknown (and even more for

local unknown) and it is then convenient to reduce the range of values of these groups to those existing in real problems to obtain simple and useful abaci for engineers.

The compulsory dependence between unknowns, expressed in their dimensionless form, and the independent dimensionless groups are set by Pi theorem. This was stated more than one century ago by Buckingham [1914] and it is based on the 'dimensional homogeneity of the physical equation' or the almost evident fact that all the terms of an equation must have the same dimension (governing equations are simply balance of fluid, solute, energy, momentum…). According to Pi theorem, '*every physical law may be written in terms of some monomials of zero dimensional exponents called the numbers'*. Bridgman [1931] was the author who named Buckingham's theorem as Pi theorem, since π was the chosen symbol to make reference to those 'numbers'. Pi theorem also implies the invariability of the solution when the measurement units of the involved quantities change.

Currently, the search of dimensionless groups can be carried out employing three different procedures: i) dimensional analysis, ii) nondimensionalization of governing equations and iii) laboratory experiments. In the first, a list with the relevant physical and geometrical parameters and variables is written, and their dimensional equation is deduced by choosing a suitable dimensional basis. For its correct application, on the one hand, no variable or parameter influencing the solution can be forgotten, in the same way that variables and parameters that do not influence the solution should not be included in this list; on the other hand, the dimensional basis must be well defined. In this way, from the list of relevant variables and parameters and by means of simple mathematical manipulations (clustering two or more of the parameters in it), the independent dimensional groups are obtained. The second procedure, which is later explained, is the one followed in this thesis since it has proved its efficiency in numerous problems. The third procedure, more laborious and expensive, is only a resource when the governing equations or the essential physical phenomena involved in the problem are not known.

Going back to Pi theorem, its statement stablished that the solution (or pattern of solutions) of any mathematical or physical problem can be written as

$$\pi_i = f(\pi_1, \pi_2, \dots, \pi_n) \qquad \text{(II-29a)}$$

where π_i is the dimensionless group that can be formed with the global unknown i, f an arbitrary (unknown) mathematical function and π_1, π_2, …, π_n are the independent dimensionless groups or 'numbers' which involve the parameters of the problem. For a local and/or instantaneous unknown, Equation (II-29a) is written as

$$\pi_j = f(\pi_1, \pi_2, \dots, \pi_n, x', t') \quad \text{(II-29b)}$$

where π_j is the dimensionless group formed with the unknown j, and x' and t' are the normalized dimensionless position and time variables.

In his work, Buckingham, apart from a demonstration of the theorem, presented its application to a group of selected problem which can be classified as 'physical' (not 'engineering') problems. Previously, Fourier [1822] had referred (for the first time) to the dimension of a physical quantity, a nearly philosophical concept which the dimensional theory is based on and which is tightly related to the theorem.

When several parameters are involved in a dimensional group or monomial, the solution or patterns of solution do not vary for the same numerical value of this group, no matter the change done in two or more of the parameters included in the group. With this advantage, the theoretical and experimental researches could work with the dimensionless groups instead of the individual parameters of the problem, saving a large number of experiments, simulations and, therefore, saving time.

However, to which point is this theorem useful as an investigation tool in engineering? How are the groups obtained? And how do we ensure that the number of groups is the minimum? This last question is not trivial, since there are many examples in which the deduced dimensionless groups employing a classical dimensional basis- length (L), mass (M) and time (T), noted as {L,M,T} – do not behave as independent groups. A representative example that has been pointed out by many authors, including Muskat [1937], is Reynolds number, R_e. What is wrong? Why does this number behave as independent in some problems (for example, transversal flows through cylindrical pipes), but not in others (for instance, flow along a flat)? In short, which are the limitations or restrictions of Pi theorem?

Undoubtedly, these limitations are associated to the correct election or deduction of the dimensionless groups, for which the simple dimensional analysis theory that has been followed or applied in most texts and problems is not enough. One thing is accepting the veracity of Pi theorem (a non-discussible question in the scientific community), and another very different is applying it when the involved dimensionless groups have not been correctly deduced. Therefore, it seems that the determining factor for the correct election of groups in a problem is a reliable protocol for its deduction. This protocol, when following simple rules of classical dimensional analysis, usually fails, particularly if non-trivial problems are studied.

Reducing parameters to dimensionless groups, as well as individual unknowns to their dimensionless expressions, is a step that appears in almost every scientific text about any field,

although there are some exceptions. In this way, Kreith & Bohn [1993] stated: *"The most serious limitation of dimensional analysis is that it gives no information about the nature of the phenomenon. In fact, to apply dimensional analysis, it is necessary to know beforehand what variables influence the phenomenon and the success or failure of the method depending on the proper selection of these variables'.* Bejan [1995] went beyond and suggested that it was a useless technique. Indeed, this author developed his own technique, called scale analysis (a kind of spatial discrimination of the coordinates), to obtain accurate dimensionless groups and give new physical meaning to many of the classical groups (for example, Reynolds and Nusselt numbers). In his advance text about flow in porous media, Nield & Bejan [2006] did not allude to dimensional analysis, although Bejan dedicated an extensive chapter to this topic in a former text about heat transfer (Bejan & Krauss [2003]).

Dimensional analysis evolution (and, somehow, Pi theorem) has been slow, and no interesting results (in complex problems) have been obtained from a theoretical point of view until recently. Nevertheless, its limitations have been occasionally pointed out by some authors during the twentieth century. In this way, the efforts have been orientated to how the theory should be improved (Palacios [1964], Herranz & Arenas [2005], Sonin [1992], Szirtes [2007], Gibbings [2011] and Alhama & Madrid [2012]). In any case, there are still some fundamental questions many engineers wonder and that we can synthetize as follows:

- How can dimensionless groups be obtained in an accurate way: starting from the governing equation, from the list of relevant variables or by any other way?
- How can these groups be interpreted, referring to their physical meaning?
- What is their order of magnitude? What is the order of magnitude of the unknown functions set by Pi theorem?
- What is the role of individual parameters of null dimension (porosity, tortuosity, …)? Are these parameters independent dimensionless groups?
- How should non-lineal problems be treated?
- What is the criterion to choose the references to obtain dimensionless variables involved in the dimensionless form of the governing equations?
- What are the hidden quantities and how are they justified?
- How are standardized or normalized dimensionless equations obtained?
- How can we stablish the quantities of a dimensional basis?
- …

Without a doubt, these are interesting questions for the scientific community and this field is only started. Alhama & Madrid [2012] carried out a review of the historical evolution of dimensional analysis, its connection with the technique to obtain dimensionless groups and, principally, the concept of spatial and general discrimination. In their book, they present a large number of classical (non-trivial) problems of heat transmission and fluid dynamics in which they criticize many of the classical dimensionless groups which are generally accepted as so in engineering (Reynolds, Nusselt, Peclet, …), and they substituted by new ones (Madrid & Alhama [2005], [2006], [2008], and Alhama & Madrid [2007]). This leads to collect the previous questions in a unique, closed and coherent investigation line.

The advance in the research of these topics has appeared with the progressive and more general introduction of the concept of 'discrimination'. The history of its development can be read in Alhama & Madrid [2012]. It can be said that the first hints of discrimination are ascribed to Williams [1892], while deeper understanding was developed by Huntley [1952], Runge [1952], Palacios [1955, 1964], Arenas [1970], Herranz & Arenas [2005], Szirtes [2007], Prieto et al. [1994], Potter & Wiggert [1997], Martynenko & Khramtsov [2005], and Madrid & Alhama [2005, 2008].

The first important step in the theory of dimensional analysis is said to be given by Palacios [1964] with the introduction of the so called spatial discrimination, a tool that was later applied by Herranz & Arenas [2005], Alhama & Madrid [2012], Seco-Nicolás et al. [2018], Zimparov & Petkov [2009], Capobianchi & Aziz [2012], García-Ros et al. [2019 a], Manteca et al. [2014], Cánovas et al. [2016] and Sanchez-Perez & Alhama [2020]. Palacios and the other mentioned authors conveniently increased the dimensions of the basis with as many lengths as spatial directions the physical scenario has, solving a good number of coupled and complex engineering problems in the field of fluid dynamics with heat transfer or solute transport. For Palacios, vector quantities had different dimensional equations coherently with the spatial direction to which they refer.

Classical nondimensionalization technique states that any length has the same dimensional equation, whether they are vertical or horizontal. Moreover, velocities also present the same dimensional equation, being irrelevant their spatial direction. Generally, vector quantities are studied as scalar. This approach changes with the spatial discrimination, which gives the dimension $[L_x]$ for those lengths in the x direction and $[L_y]$ for those in the y direction. This means that dimensionless monomials cannot be obtained from the ratio of a horizontal and a vertical length. Something similar occurs with velocities, for which $v_x = [L_x]\cdot[T]^{-1}$ and $v_y = [L_y]\cdot[T]^{-1}$, as well as other quantities in which lengths are involved.

However, Palacios and the rest of the authors previously mentioned started from the same list of relevant variables and parameters of the problem (without considering the governing equations) and, after giving dimensions to all these, the dimensionless groups were obtained in a direct way. This technique, although correct, had severe drawbacks. For instance, dimensionless parameters such as porosity, angle and many others must be considered as independent dimensionless groups. This immediately increases in an unnecessary way the total number of groups to the point of making its application unworkable and useless. Another drawback is the difficulty of giving a physical meaning or order of magnitude to the groups.

Recently, following the spatial discrimination technique some authors have deduced the groups from the governing equations conveniently expressed in a dimensionless form (Cánovas et al. [2016], Manteca Jr et al. [2012], Manteca et al [2014] for problems of flow and transport in porous media, Madrid & Alhama [2008] for heat transfer, Conesa et al. [2016] for application in mechanical problems, and Manteca et al. [2018] and García-Ros et al. [2019 a] for non-lineal soil consolidation). This change in the protocol for obtaining the groups deletes the drawbacks previously mentioned and spatial discriminations is firmly stablished.

Nevertheless, apart from spatial discrimination, there is another discrimination that can be called 'general discrimination' that tries to approach other dares. How can we consider two quantities of different nature with the same dimensional equation (for example velocity and hydraulic conductivity)? Is it possible to assign to the variable angle its own dimension to dimensionally distinguish between angular velocity and frequency (or time)? Can we set the same quantity twice in a dimensional basis to approach, for example, problems with more than one vibration frequency? Is it possible to choose (for the dimensional basis) two lengths in the same direction, in order to differentiate two physical phenomena happening in a same direction (simultaneous heat and mass diffusion, with different diffusion coefficients)? Can we give different dimensions to the different forms of energy (mechanic and thermic, for example) in the same problem? These and other questions are answered by general discrimination, and an interesting example of its use is presented in Chapter III, where the dimensions of permeability and hydraulic conductivity are discussed. Some problems of general discrimination are studied in texts from Herranz & Arenas [2005] and Alhama & Madrid [2012], as well as other publications (Sanchez-Perez et al. [2020], Conesa et al. [2016]).

To sum up, we can state that the most accurate technique to obtain dimensionless groups is the one derived from the nondimensionalization of the governing equations, which involves a correct definition of the dimensionless variables together with the election of the most general

dimensional basis. In this thesis, discrimination is presented, but for each problem it is explained and justified. This has allowed studying anisotropic media as follows:

- establishing new groups and removing some of the classical ones
- choosing correct references for the problem variables
- introducing the concept of hidden quantities and determining their order of magnitude
- obtaining universal results among the new groups that can be displayed with an abacus or a group of abaci
- determining these universal solutions, parameters of the problems by simple experiments as an inverse problem

To finish this section, we present a summary of the formal steps that, after applying the process of discriminated nondimensionalization to the governing equation, lead to obtain the independent dimensionless groups that control the solutions of any unknown in the seepage problems studied in this thesis:

Step 1 → Choosing the references for the dependent and independent dimensionless variables involved in the problem.

According to spatial discrimination, these references are different for each direction in the problem if there is anisotropy and must be chosen (if possible) so the dimensionless variable is normalized, this is, its range of values is [0,1]. When no reference quantities can be found, these reference values are 'hidden' (unknown) quantities, and we proceed as if these were given as data. The monomials in which these unknowns are involved are treated as the dimensionless expression of such unknowns and depend, therefore and according to Pi theorem, on the rest of monomials without unknowns.

Step 2 → Introducing the dimensionless variables (through their definition) in the governing equations to obtain the governing equations in their dimensionless form.

If the derivatives of the dependent variables are considered as unity, which is justified by the normalization of these variables and by the fact that there are not strong non-linearities (acceptable in seepage problems), we can obtain the dimensional coefficients or factors that multiply the previous derivative terms.

Step 3 → Obtaining monomials by making ratios with independent pairs of dimensional coefficients from Step 2.

There are groups with unknowns and groups without them. The number of groups is (as much) the terms in the governing equation minus one.

Step 4 → Adding the rest of the groups derived from the boundary conditions or the geometry of the problem (employing spatial discrimination).

Step 5 →i) Solution for global unknowns contained in the groups from step 3. Their dimensionless form is function of the groups without unknowns.

ii) Solution of the other global unknowns (independent of position and time). Their dimensionless form (which must be determined) is also function of the groups without unknowns.

iii) Solution of the unknowns that depend on position and/or time. Their dimensionless form, which must also be determined, is function of the groups without unknowns as well as the dimensionless position and/or time.

II.3 The electrical analogy. Background and current development

Physical and engineering processes that are ruled by Laplace-type governing equations, which are the result of combing a linear constutive law (Darcy's, Ohm's, Hooke's or Fourier's) and a conservation equation, are easily studied by analogous models. Particularly, electrical models can be employed, due to its easy physical implementation and its direct and reliable lecture of the simulated results. Examples of these processes are heat conduction, electrostatics, normal displacements in elastic membranes, flexion and torsion in elasticity under certain conditions, groundwater flow, consolidation and electrical current in conductor media. Since the governing equation of steady-state flow of fluids in porous media is also a Laplace-type, both the method of handling and the own solutions may be taken over from those that have already been derived in the other branches, by simply translating them into their proper hydrodynamic equivalents.

Electric analogy has some advantages if comparing it to other analogies:

- devices and components to reproduce the physical properties of the material are available;
- any kind of geometry can be implemented (rectangular, radial, cylindrical and spherical), including irregular scenarios;
- common boundary conditions (first and second class) have an immediate implementation employing direct and simple electrical devices (resistors, batteries, capacitors);
- reliable measure equipments to easily read the results are available;

- in 2-D problems, electrical models present the advantage of providing both equipotential and streamlines by modelling conjugated scenarios where the potential borders are exchange with streamline borders and vice versa; another manner of obtaining streamline from equipotential values is numerical integration.

Undoubtedly, these advantages are the reason why this methodology has been widely used during the last century. According to Scott [1963]: '*The thermal analogy has not been used in practice mainly due to the difficulties of simulating the boundary conditions so that their use instructional functions. The same occurs with magnetic and membrane analogies whose development has rarely taken beyond an illustrative level. Conversely, electrical models, both on continuous and lumped-parameter versions, were spread used because of its convenience and availability and the easy and rapidity with which solutions can be obtained*'. In addition, electrical models have been used in merely mathematical problems (Bradfield et al. [1937]).

The first models based on the electric analogy are referred to steady-state problems and appeared in the second decade of the previous century; these were 2-D continuous models carried out in sheets of conductor paper, cut to reproduce the domain contours. Boundary conditions are applied in the contours employing batteries (first class condition) or resistors of infinite resistance value (second class). The measures of the potential variable (electrical voltage) allowed reproducing the patterns of this quantity while those of the flow and other variables were calculated in an indirect manner. An essential requirement for the reliability of these models is the equivalence, which is commonly referred as similarity between models. This equivalence is formulated from the well-defined dimensionless groups that rule the problem. Among the first investigations about general electric analogy, we can cite those of Pavlovsky [1933], Wyckoff & Reed [1935], Moore [1936], Paschkis & Baker [1942], Paschkis & Heisler [1946], and Kayan [1945]. Later, around 1930s, lumped-models were developed, which were initially physical model built from discrete element whose value was associated to the cell geometry and the physical properties of the medium. The values of the devices were obtained comparing the spatially discretized governing equation of the mathematical model to those of the electrical model. This technique allowed the implementation of very cumbersome problems (non-linear, transitory or complex boundary conditions) by connecting thousands of electrical devices. Bonilla [1965] employed this kind of models to study problems of heat transfer in nuclear reactors. Among the wide range of lumped models, we must highlight Kayan [1945], Oppenheim [1956], and Karplus [1958] as the oldest ones, and the most recent ones whose main objective was educational (Davies [1979 and 1994], Duffin & Knowles [1984], Baker & Shortt [1990], and Baughn & Rossi [1992]). In fact, discrete models used with educational aims

disappeared in 1960s with the emergence of digital computers which allowed solving problems with numerical techniques.

Nevertheless, the development of digital computers as well as their implemented computational algorithms has allowed the use of the electrical analogy again. Powerful circuit simulation codes, whose design was not focused on a numerical tool use, and its complex computational algorithm to manage analogical and digital signals of high frequency, together with powerful data processing, as well as the choice of devices of zero tolerance, are the reasons that have fostered the use of numerical simulation technique based on the electrical analogy. From 1960s so far, numerous works have been published. Among them, we chronologically highlight: Horno et al. [1990], Bello [1991], Hamill [1993], González-Fernández et al. [1995 and 1998], Alarcón et al. [2002], Madrid & Alhama [2005, 2006], Zueco & Alhama [2006, 2007], Soto et al. [2007 a and b], Anwar Bég et al. [2009], Luna-Abad et al. [2010, 2017], Moya [2011], Marín et al. [2012], Morales et al. [2012 a and b], Sánchez et al. [2012], Sánchez-Pérez et al. [2015], and García-Ros et al. [2018, 2019 b].

Related to the electrical analogy applied to the processes of water flow through porous media (particularly soils), the reference to manuals and works is wide, and we intend to be exhaustive. Former classical manuals (Muskat [1937], Harr [2012], and Scott [1963]), which were before the development of digital computation, have broad references to these analogies, thoroughly describing those experiments carried out in the first years. In the field electrical analogy applied to groundwater problems, pioneer works are those of Weaver [1932], Pavlovsky [1933], Harza [1935], Vreedenburgh & Stevens [1936], Wyckoff & Reed [1935], Vreedenburgh [1936], Rel'tov [1936], Selim [1947], Babbitt & Cadwell [1948], and Khosla et al. [1954]. Returning to classical works, later authors such as Azizi [1999] did not make any references to these analogies at all, while Lambe & Whitman [2005] (as the oldest version of Taylor [1948]) hardly introduced a comment about electrical analogy, emphasizing its utility for educational purposes and some complex flow net problems. However, Juárez & Rico [2010], presented almost a chapter about the electrical analogy, describing both continuous and grouped-formulation methods.

Nevertheless, flows through earth dams, ditches, wells and other ground engineering scenarios (the so-called gravity flows) present some difficulties that do not appear in the other physical problems and that the electrical analogy has not solved so far. In these scenarios there are special borders known as free and seepage surfaces whose length is not known a priori, so they cannot be directly implemented without applying some techniques, such as those applied by Schafferank [1917], Van Iterson [1916 and 1917], and Casagrande [1940]. Another manner of approaching these phenomena is including specific devices when designing the models, as

presented in Chapter V in which the models are explained. Continuing with the former studies, Muskat stated [1937]: '*There is no immediate electrical analogue of the effect of gravity in a flow system*' and *'the free surface in an electrical model must, therefore, be introduced artificially by varying the physical boundaries of the conducting model'.* Due to this circumstance, these borders must be initially supposed to solve the problem and suitably correct them until a convergent solution is reached.

Former continuous models can be classified as:

- Laboratory prototypes, formed by two glass plates with a small separation where more or less fine sand is introduced; on these plates the original model borders are reproduced (affected by a scale) and, if necessary, piezometers are installed. Streamlines are displayed with tints.
- Viscous flow models (tinted glycerines) between two plates slightly separated in which the hydraulic conductivity to model depends on the separation of the plates and the fluid properties (Helle-Shaw cell [1899], for horizontal flow).
- Electrolytic model, the most flexible type, in which the points of the potential distribution maps in 2-D and 3-D were read by probes over an electrolyte model that simulates the barriers of the porous media by a nonconducting body; it was successfully applied to the 2-D problem of water flooding and 3-D problem of the suppression of water coning in partially penetrating oil wells by shale lenses (Muskat [1946]).
- Plain sheet-conduction model, based on Pavlovsky´s prototype, in which impermeable borders were simulated by cutting out from the conducting sheet figures geometrically similar to the studied contour.

Referring to the inconvenient of the previous models we can state that: first, those models cannot simulate infinite domains, having to set upstream and downstream the principle area (dam, for example) and, therefore, producing an error that can be relevant; second, it is difficult to implement non-homogeneous and/or anisotropic conditions of the porous media due to the lack of papers with different conductivities; third, as previously commented, there are problems to implement free and seepage surfaces.

The first simulator of problems of confined flow, which was successful for classroom demonstration, was developed by Pavlovsky [1933]. As flow domain, he used high resistance material in sheets of metal or paper treated with colloidal graphite or even diluted copper sulphate solutions. Its inlet and outlet borders were painted with silver tint. The geometry corresponded to that of the physical scenario of the real problem. Batteries, high impedance

voltmeters and paper clips were also employed. The methodology consisted in obtaining the pattern of the equipotential lines, deducing from these the streamlines, as in isotropic soils both are perpendicular. Alternatively, streamlines could be directly obtained employing conjugated models (exchanging contour conditions). Layers with different permeability or hydraulic conductivity and non-homogeneous soils could be modelled by electrically equivalent regions or regions with proportional electrical conductivity, while isotropic soils were simply implemented transforming the dimensions of the studied flow regions. Finally, filters, drains, wells or other regions of 'infinite' permeability were implemented with high electrical conductivity materials. Pavlovsky's models, known in 1918 but published in 1933, was improved by later authors (Babbitt & Cadwell [1948], Harza [1935], Khosla et al. [1954], Rel'tov [1936], Selim [1947], Vreedenburgh [1936], Vreedenburgh & Stevens [1936], Weaver [1932], and Wyckoff & Reed [1935]).

Considering grouped models, they were formed by a set of permanent tables with electrical connections placed in a constant size cell where resistors of small power were connected. In the first models, Macneal [1953], errors were around 5% higher than those obtained by continuous models due to the production tolerance of the model components. The inconvenient of the implementation of free and seepage surfaces was not overcome by these models, which determined these lines by approximate methods and then corrected the values of the resistors in these contours (without changing the position of the table connections). Macneal [1953] and Landau [1957] indicated how the parameters of these models should be calculated, and this could be simply extended to 2-D and 3-D scenarios with a more complex elaboration of the table connections. In some institutions, permanent networks have been built employing resistors of variable resistance values. Moreover, it seems easy to extend the analogy with non-linear resistors (voltage-dependent resistors) to the study of water flow though soils with velocities above the range of validity of Darcy's law, since the equivalent law for turbulent flow is known (Forchheimer's law). Moreover, transient hydraulic flow can be simulated by connecting an electrical capacitor to each node of the net, while the other end of the device is connected to common ground.

II.4 The network simulation method (NSM) and the design of network models

II.4.1 Concept

Section II.4 must be written, since one of the main objectives of the thesis is to design tools based on the NMS. The theoretical fundamentals of this methodology are presented by Horno [2002]. This methodology has also been the basis for many other doctoral theses in which other engineering problems where studied (Alarcón [2001], Zueco [2003], Castro [2005], Soto [2007], Del Cerro [2009], Luna-Abad [2010], Morales [2012], Sánchez [2013], Marín [2013] and García-Ros [2016]), and these can be consulted for more thorough explanations of the applications described in Horno [2002].

The NSM essentially presents two steps. The first one is the design of a network model or electrical circuit which reproduces in an accurate way the behaviour or the phenomena involved in the studied physical problem. In the second step, the network model is simulated with a software for the resolution of electrical circuits and, then, the results (voltage and electric currents) are interpreted in terms of the physical variables of the problem. In order to build a correct network, it is enough to assure that: i) the finite-difference differential equations obtained from the spatial reticulation of the mathematical model (equations governing the physical problem) are formally equivalent to the equations of a network method for a volume element or cell of the physical domain (Laplace equation and Ohm's law); and ii) the cells are connected until the whole domain is complete and boundary conditions are added from discretized equations in the contours, together with initial conditions. If transient problems are modelled, time is kept as a variable, although in the numerical resolution with the chosen code the time variable is also discretized.

II.4.2 Electrical devices and model design

The analogy between the real model and the circuit can be stablished following two ways that lead to conjugated models. This procedure will be slightly explained referring to any of the local governing equations that are part of a mathematical model. The most general expression of this equation presents the form

$$\sum_1^n \xi_s = 0 \qquad \text{(II-30)}$$

where ξ_s is a term or addend ($1 \leq s \leq n$), and n is the number of terms. Of course, the equation is physically homogeneous, which means that it expresses a local balance of dimensionally equal

quantities. However, the expression of any of the addends can be either very simple or very complex (it may present more than one dependent variable, temporal or spatial derivatives of the variables, crossed derivatives, arbitrary functions of one or more dependent or independent variables, etc.). If the problem has more than one dependent variable, compatibility imposes the existence of as many governing equations as the number of this kind of variables. This allows stablishing a biunivocal relation (which is conveniently chosen) between the governing equations and dependent variables and separate circuits, independently of the existence of more than one of these variables in all or some of the equations.

In the mathematical models involving flow problems (as those that will be presented in this thesis), the variables that appear in their equations are potential variables, their first derivative are proportional to flows which cross the borders of a volume element according to constitutive laws, and its temporary derivatives represent net flow that goes inside or outside the volume. Second spatial derivatives represent changes in flow per unit of length in each spatial direction, and these kinds of interpretation can be done for each type of term, although their meaning can be very complex. In this models, fundamental equations present balances of quantities (mass, heat, momentum …), so it is logical to assume that in the electrical analogy each term of equation (II. 30) is associated to the electric current, as well as associating the potential deriving the currents to electric voltage. In this way, in the network model, each addend is considered as the current in an independent branch which converges with the currents in the other branches (whose sense is compatible with the sign of the addend) in a common node (different for each cell and equation) whose voltage is the solution of the problem (this is, the potential variable of that cell, Figure 2.6). Since Kirchhoff theorems are conditions that are already integrated in codes for solving circuits, it is not necessary to verify numerical rounding for assuring the correct balance of currents or of the equation. This task is accurately done by the computer code with a high degree of approximation (nearly null errors).

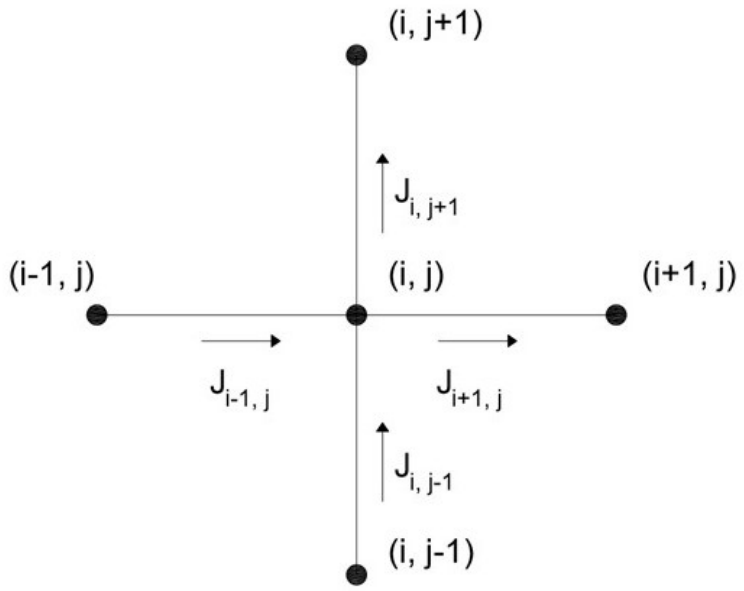

Figure 2.6. Currents converging in a common node, centre of (i, j) cell

How can we impose in each branch the current in every moment from the term associated to the equation? That is the second part of the analogy, and it only requires the knowledge of some rules. These are briefly described employing the nomenclature in Figure 2.7, and the terms of the equation are classified as: constant value terms, lineal terms in first and second derivatives of the potential variable, and non-lineal terms which includes coupled terms.

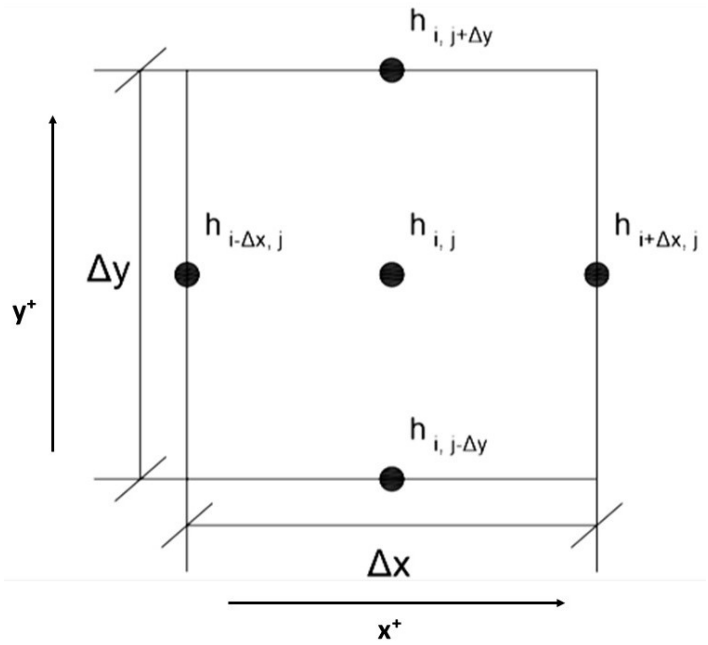

Figure 2.7. Nomenclature of a generic 2-D cell (i, j)

- Constant terms or time-dependent terms. They are directly implemented by a constant current generator or a time-dependent current generator. In the libraries of commercial codes there

is a wide variety of this generators with functional dependences that cover all the possible functions and special sources that can be used to reproduce any kind of term. These devices are connected to common ground or reference node and the central node. It is the device named as I constant for the constant current generator, and I (t) for the time dependent current generation in Figure 2.8.

- Terms in first order spatial finite differences. For spatial variable x, they have the form

$$a_1 \frac{\Delta \xi_s}{\Delta x} = \frac{\xi_s\left(i+\frac{\Delta x}{2},j\right) - \xi_s\left(i-\frac{\Delta x}{2},j\right)}{\left(\frac{\Delta x}{a_1}\right)}$$

where a_1 is a constant. They are implemented by an electric resistor, since the constitutive law that involves voltage and current in a resistor is $I_R = \frac{\Delta V}{R}$, where I_R is the current in the resistor, ΔV is the potential difference (V) between its ends, and R the resistance value in the resistor (Ω) that is obtained comparing the previous equations in the analogy, $R = \frac{\Delta x}{a_1}$. Its connection is done between nodes $i + \frac{\Delta x}{2}$, j and $i - \frac{\Delta x}{2}$, j. This device is shown in Figure 2.8 as R. In the vertical direction, $R_{y,a} = \frac{\Delta y}{a_2}$ represents the resistance value for the resistor for variable y, $a_2 \frac{\Delta \xi_s}{\Delta y} = \frac{\xi_s\left(i,j+\frac{\Delta x}{2}\right) - \xi_s\left(i,j-\frac{\Delta x}{2}\right)}{\left(\frac{\Delta y}{a_2}\right)}$.

- Terms in second order spatial finite differences. For the spatial variable x are of the form

$$a_3 \frac{\Delta^2 \xi_s}{\Delta x^2} = \frac{\frac{\xi_s\left(i+\frac{\Delta x}{2},j\right) - \xi_s(i,j)}{\frac{\Delta x}{a_3}} - \frac{\xi_s\left(1+\frac{\Delta x}{2}\right) - \xi_s\left(1-\frac{\Delta x}{2}\right)}{\frac{\Delta x}{a_3}}}{\left(\frac{\Delta x}{2}\right)} = \frac{\xi_s\left(i+\frac{\Delta x}{2},j\right) - \xi_s(i,j)}{\frac{(\Delta x)^2}{2\,a_3}} - \frac{\xi_s\left(1+\frac{\Delta x}{2}\right) - \xi_s\left(1-\frac{\Delta x}{2}\right)}{\frac{(\Delta x)^2}{2\,a_3}}$$

where a_3 is constant. This is implemented by two resistors, $R_{x,b}$ $R_{x,c}$. The implemented device is also a resistor R in Figure 2.8. The two resistors are of the same value, $R_{x,b} = R_{x,c} = \frac{(\Delta x)^2}{2\,a_3}$ for variable x, connected to the ends and the centre of the cell. $R_{y,b} = R_{y,c} = \frac{(\Delta y)^2}{2\,a_4}$ are the resistance values for variable y.

- First order temporal derivatives. Their form is $c_1 \frac{d\xi_s}{dt}$, where c_1 is a constant. They are implemented by a capacitor, since the law involving voltage and intensity is of the form $I_c = C\frac{dV}{dt}$, where I_c is the current in the capacitor, C is its capacity (F) and $\frac{dV}{dt}$ the variation rate in time of the voltage between its ends. It is immediate to see that $C = c_1$. Figure 2.8 shows a capacitor, named as C.
- Non-lineal terms, coupled terms (involving more than one dependent variable), crossed derivatives and others that can be implemented by special devices known as 'control current source'; the control function can only have either potential variables ('voltage controlled current source') or current variables ('current controlled current source'). When the source is

simultaneously controlled by the two variables, auxiliary circuits must be designed to transform one variable to the other. Generally, it is a device whose outlet current is an arbitrary function or product of arbitrary functions. These possible functions include dependent and independent variables, or the currents of other devices of the model. The versatility in the application of these devices is very wide, allowing the implementation of any kind of term thanks to auxiliary circuits to build intermediate variables or functions. In order to specify these sources in the text file of the network model, the expression of the term and the nodes or devices of the models in which the variables must be read is written. The devices are connected to the common node and the cell centre with an electric polarity according to the algebraic sign of the term in the equation. Figure 2.8 shows a voltage controlled current source, named as G.

- Boundary conditions, as well as the governing equation, must be spatially discretized, and its application to the contour cells do not imply the use of new devices. First class condition are simple batteries (displayed as V in Figure 2.8) of constant value while second class are modelled as constant current sources (I constant), or resistors of infinite resistance value if it is a homogeneous condition (R). For more complex conditions, those controlled sources previously mentioned are used.
- Finally, terms which present both third order and higher order spatial discretization, second order and higher order crossed derivatives are implemented following similar rules, but they are not presented in this thesis as they are not applicable in problems of flow through porous media. Morales et al. [2012 b], Perez et al. [2016], and Alhama et al. [2012] did employ models involving these terms.
- The implementation of any kind of conditions, which are necessary for modelling processes of wetting and drying in infiltration phenomenon, is done employing switches or programming. Ngspice, as other codes for the simulation of circuits, presents controlled switches in its library. Switches states, ON (active or closed) and OFF (deactivate or open), are actioned when certain values or voltage and/or current in some nodes or devices in the model are reached. When switch is on, its inner resistance is negligible, so the connection between the nodes is ideal; when it is off, the resistance value is considered as infinite, so the devices are electrically isolated. In Figure 2.8, a switch named S is symbolized.

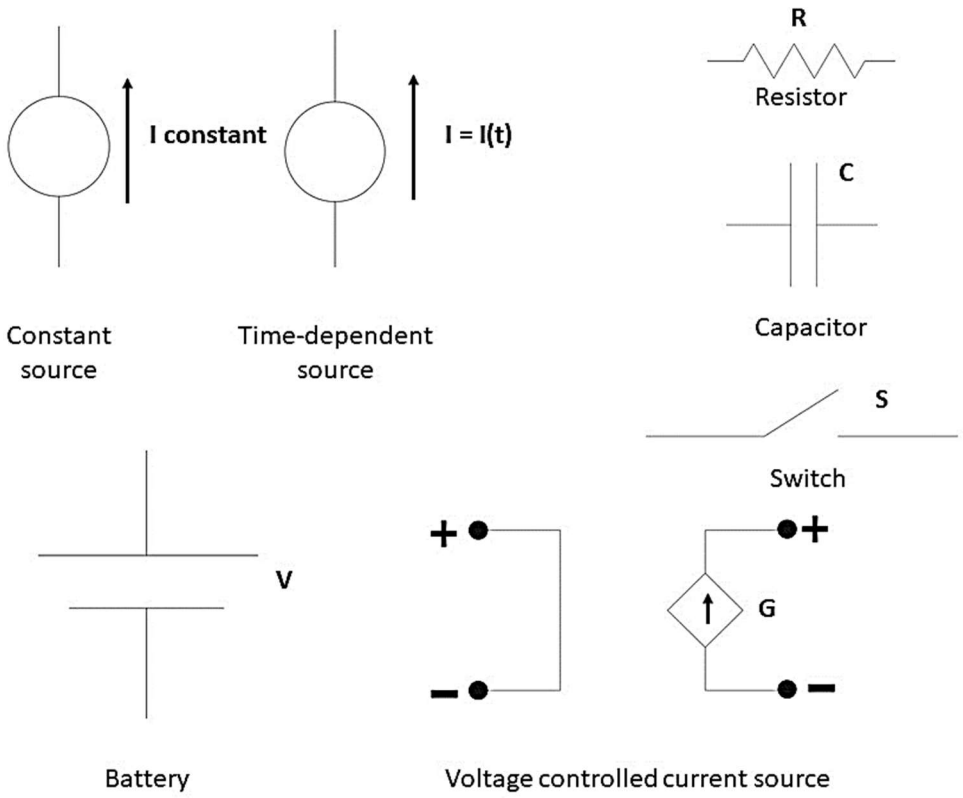

Figure 2.8. Devices implemented in Network Simulation Method

Once the design of the cell network model is complete, it must be connected to the adjacent cells to model the whole domain. This connection can be carried out by coding or by employing specific functions of the circuit software (if it has it). Contour cells are usually special, because sometimes the network model is not compatible with the imposed conditions, and approximate solutions must be used. Including contour and initial conditions (the last could be certain voltage or charges in the capacitors before starting the simulation) completes the network model.

In the dual model, the addends of the equation are considered voltages and its addition leads to a network model in which there is only one close branch containing as many elements as addends the equation has. The unknown variable that makes the solution compatible is the intensity, which must adjust to meet Kirchhoff's theorem of voltages. Horno [2002] presented some applications of dual models.

II.4.3 NSM as numerical tool

NSM is, indeed, a numerical tool, since it numerically solves the equations governing the network model of the problem. It leads to results of negligible errors whenever the number of volume elements is sufficient large. Moreover, initial and contour conditions, as well as the

physical characteristic of the medium, can be altered in order to reach solutions beyond those that can be obtained with real measures. The simulation is structured in the following basic subprograms (Figure 2.9):

- Data input. In this, devices and nodes in the model have been correctly stablished and verified, warning about any mistake in the elaboration. In addition, during this step it is also verified that the operational requirements in DC (direct current) are met (a test that removes errors which are difficult to find).
- Organization. It builds the data structures that are needed for the computational analysis subprogram, which is the essential core of the code, with complex algorithm which takes most of the computation time.
- Computational analysis (simulation). It is structured in different tasks: equation formulation, lineal equation solution and numerical integration when needed.
- Data output. It organizes and saves solutions in tables for its later graphical presentation with routines and auxiliary codes.

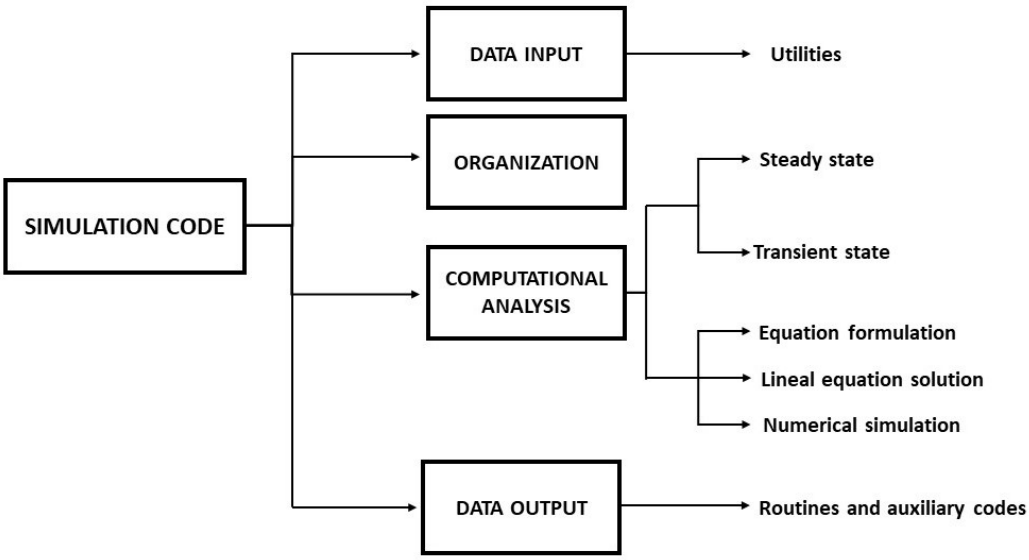

Figure 2.9. Blocks of Ngspice simulation software

Ngspice [2016] derives from Pspice, another software for the simulation of circuits. Pspice comes from a software family, SPICE2 (Nagel [1975]), which was developed from 1960s in University of California, Berkeley. Its powerful calculation algorithm and its extended use is a proof of its power for the treatment of a wide variety of problems. Among the investigation works that have employed these software, the following can be highlighted: Castro et al. [2005] in mechanical vibrations, Zueco & Alhama [2006, 2007], Zueco et al. [2005, 2006], and Alhama & Zueco [2007] in inverse problems of heat transfer, Benavent et al. [2010] in sound emission, Anwar Bég et al.

[2009] in magnetohydrodinamics, Soto [2007] and Soto et al. [2007 a and b] in problems of fluid flow and solute transport, Luna-Abad et al. [2010] in the optimization of heat dissipation fin, Morales et al. [2012 a and b] in elastostatics, Marín et al. [2012] in tribology, Sánchez et al. [2012] and Sánchez-Pérez et al. [2019] in corrosion, Moya [2011] in electrochemistry, Cánovas et al. [2015] in flow with heat transport, Perez et al. [2016] in mechanical problems, and García-Ros et al. [2018, 2019 b] in non-lineal soil consolidation. Moreover, different software in which NSM is employed as numerical calculation tool have been patented: PRODASIM [2005] and PROCCA-09 [2005] for problems of heat transfer and fin design; FATSIM-A [2010] and FAHET [2011] for the simulation of fluid flow with solute and heat transport, respectively; EPSNET_10 [2011] for elasticity problems; OXIPSIS-12 [2013] for corrosion problems; CODENS-13 [2014] for the simulation of coupled ordinary differential equations; SICOMED_3D [2017] and EDUCONSOL [2018] for the simulation of soil consolidation; CONCRELIFE [2019] for the calculation the service life of reinforced concrete structures in marine environments.

II.5 Programming with Matlab

MATLAB ® (Matlab [2015]) is a technical calculation high-level language as well as an interactive environment for developing algorithms, numerical calculation, data visualization and analysis and programming. It is currently used by millions of engineers and scientists as a tool to explore and display ideas. Moreover, it allows working in signal and image processing, communication, control systems and computational finances.

Coding with Matlab allows analysing data, developing algorithms and creating applications and models. This language and the tools and mathematical functions implemented in the software facilitate the exploration of the multiple possible approaches, reaching to a solution faster than employing spreadsheet (for example, Microsoft Excel ® files).

For the research presented in this thesis, Matlab has been used for both data importation and exportation, since it allows the interaction of the developed tool with other software, such as Ngspice. Moreover, Matlab has been employed to develop the code for the two numerical tools used to obtain the universal solutions, one for flow under dams (DamSim) and another for flow in unconfined aquifers due to a pumping well (WaWSim). For each of the software, Matlab was used for three different aspects:

i) It was the language for elaborating the text files for the network models of each problem.

ii) It was employed for developing the user interface (window environment).

iii) It was used to program the routines for the graphical representation of results.

As a powerful tool for the design and edition of graphical user interfaces, Matlab has allowed developing an interactive environment for the two developed software. In addition, it has been used for their design, providing the most common components, such as drop-down menus buttons, tool bars, list boxes, among others.

According to all these, the user interfaces that have been created are composed by different windows with controllers (components) that allow the user to interactively introduce the data and visualize the results once the simulation has been run. In this way, the user does not have to create, modify or understand the script or write command lines to carry out the corresponding tasks.

All in all, the user interfaces created with Matlab can carry out any kind of calculation, read and write data files, launch other software, communicate with other user interfaces and show results as tables, individual data and graphics.

II.6 Ngspice computer program

Ngspice is a circuit simulation software for non-lineal and lineal analysis with BDS license (free software). Circuits can involve resistors, capacitors, inductors, dependent or independent voltage or current sources, semiconductor devices, etc.

As commented before, it is an update Spice3f5, the last version of the free code simulator Spice3 developed by EECS Department of the University of California at Berkeley, in http://bwrcs.eecs.berkeley.edu/Classes/IcBook/SPICE/. It includes all its characteristics and most of the bugs have been fixed. This software is sustained by a great user community which, providing new characteristics, improvements and bug-fixing (Ngspice project). It is based on three free software packages:

- Spice3. Origin of all electronic circuit simulators. Its successors are widely employed by the electronic community.
- Xspice. Extension of Spice3 that provides additional code models in C language to support modelling the analogical behaviour and the co-simulation of digital devices employing a pushed algorithm of fast event.

- Cider. It adds a numerical device simulator to Ngspice, and coupled to the simulator, it provides a higher accuracy to the simulation (although higher computational time is needed).

Ngspice is a software in continuous evolution, since its great number of users contribute to its bug-fixing and improvements, which has led to additional characteristics and higher robustness.

Ngspice is implemented with three types of analysis: i) non-linear analysis; ii) transient non-linear analysis, which includes transient noise simulations; and iii) AC linear analysis, which includes small noise signal simulations and a function of pole-zero and transference analysis. Its Windows® version presents a simple user interface, Figure 2.10, a small console in which data input and command lines are introduced. It also provides text output.

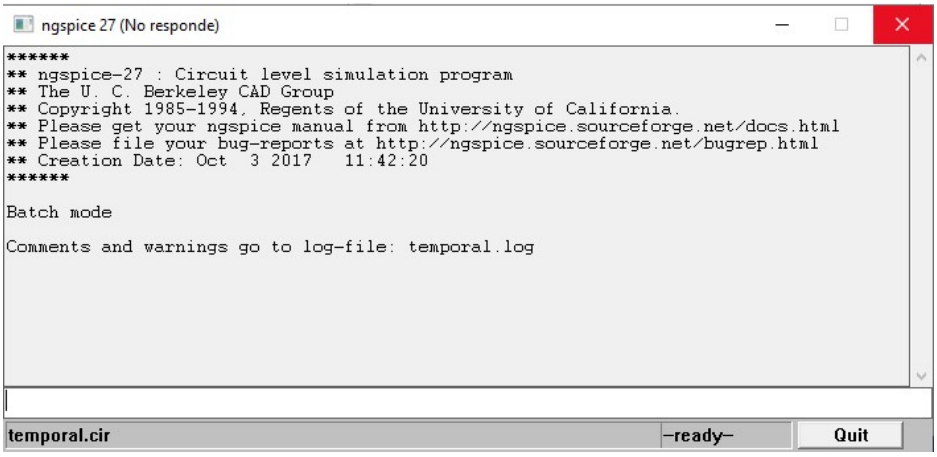

Figure 2.10. Command line input console of Ngspice 27 software

With these command lines, which can be included in the circuit file to analyse (text file with extension .cir), the result printing can be carried out by dumping Ngspice results into text files (.txt). The new text files can be exported to Matlab, as done in this thesis, or any other software of numerical calculation, so data can be processed and results displayed. In this way, as previously described, Ngspice can solve the chosen scenarios once they have been transformed into an electrical circuits.

Chapter III. Permeability and hydraulic conductivity units

The objectives of this chapter are explained firstly. Section III.2 shows a historical overview of the different methodologies that have been developed to calculate the value of permeability and hydraulic conductivity. In Section III.3 Darcy's and Forchheimer's expressions are studied employing Pi theorem in first place, and then the discrimination is introduced. Section III.4 includes the deduction of the dimensional character of permeability, and the lack of relevant results associated with these solutions leads to Section III.5, in which the fluid energetic potential is introduced as a new unit in the dimensional basis. In this way, a dimensionless group governing problems of water flow through anisotropic soil can be deduced, and the dimensional equations and units of the variable h, the hydraulic potential or water head (widely used in hydrogeology), are obtained. These procedure also allows assigning a physical meaning to the units of h.

III.1 Importance of permeability and hydraulic conductivity

The importance of permeability is reflected in the major effort of many authors in both empirical and theoretical field. In the last area, research has been focused on achieving more or less complex formulations. Nevertheless, this effort has not been applied on the investigation of the dimensional character of the parameter, which is a necessary information to find reliable dimensionless groups that involve this parameter and rule the solution patterns for the problems of flow through porous media, especially in anisotropic scenarios. There is almost no

dimensional study of Darcy's and Forchheimer's laws in the existing literature, further than the investigations carried out long time ago by Muskat [1937], based on Pi theorem (Buckingham [1914]) and later, to a lesser extent, by Taylor [1948]. Muskat, who was very knowledgeable of Pi theorem in its classical from, insisted on justifying these empirical laws as limit cases of a general dependences in which the effects of pressure, inertial and viscous forces are involved. However, his conclusions were of little use if intending to apply them in the deduction of the dimensionless groups we are interested in, and even less in anisotropic scenarios for which no useful solution was developed. Beside leading to the deduction of these two laws, the application of Pi theorem in its discriminated form allows:

i) Justifying the emergence of the product $\zeta \cdot Re$ (friction factor·Reynolds number) as a dimensionless group.
ii) Delving into the dimensional complexity of permeability.
iii) Deducing an inaccurate dimensional equation that cannot be employed for the characterization of the anisotropic media.

The spatial discrimination, together with the emergence of the energetic potential, h, as a substitute of the mass quantity in the classical basis (justifiably due to the lack of inertial forces in Darcy's law,) allows the definition of the new basis $\{L_x,L_y,L_z,T,\xi\}$, where ξ is the dimension of the potential variable, and it leads to surprising results. This new basis does not bring a concrete dimensional equation for permeability, although it does permit obtaining it for hydraulic conductivity. This research line is justified in the application of the discrimination (originally proposed formally by Palacios [1964]) to the dimensional theory, whose result is generally redefining the basis and obtaining more accurate groups and, in many cases, a lower number of them. This simplifies the solution and makes its graphical representation with universal curves easier.

Indeed, the introduction of the energetic potential in the basis has two effects:

i) Removing Newton's law of viscosity from the problem (because it is unnecessary), so viscosity is just a physical parameter involved in the hydraulic conductivity.
ii) As this energetic potential does not have spatial discrimination, the hydraulic conductivity emerges with its own dimensions and, therefore, new dimensionless groups in anisotropic domains can be deduced.

These groups degenerate in simpler ones, which are also new, when removing viscosity parameters, as its value does not depend on the spatial direction.

III.2 Permeability and its determination. A brief historical review

Physically, general porous media are formed by grain or particles of different sizes, packed in varying degrees of density, materializing its internal structure (skeleton). This structure presents numerous voids or pores of also different sizes (porosity), which are partially or totally connected among them, creating flow paths. The tortuosity of those pathways also depends on the grain shape (angularity), as well as on the chemical deterioration that may exist in their contacts. In this way, grain size, compaction, porosity, connectivity and tortuosity (this one linked to angularity), which are not independent, are the basic physical properties of the porous media. However, two of the properties are measurable without correlation between them: porosity and hydraulic conductivity. Heterogeneity in the shape and the size of particles in natural materials and their compaction and cementation degrees determine the broad ranges of porosity and permeability in these media (Muskat [1937]).

Darcy [1856] wrote his law as Q=Aκi, where Q is the water flow (m^3/s), A is the cross section transverse to flow direction (m^2), h is the hydraulic or piezometric potential (energy per unit of fluid weight, usually measured in m), and i is the hydraulic gradient, $\frac{dh}{dx}$, commonly assumed by most authors, texts and papers as dimensionless. κ is the hydraulic conductivity parameter and its units is m/s, according to this law. Muskat replaced variable h by pressure (p) and expressed the law as $v = \frac{k}{\mu}\frac{dp}{dx}$, introducing a new parameter, k (m^2), which is known as permeability and is related to hydraulic conductivity by

$$k = \frac{\kappa\mu}{\rho g} \qquad \text{(III-1)}$$

where g is gravitational acceleration and ρ is the fluid density. Permeability can be obtained with formulation in which geometrical properties of the studied soil are involved (Mavis & Wilsey [1936] and Anderson [1940]), or by laboratory tests in a more precise way (as long as the soil samples are kept unaltered). Developed formulas for the permeability calculation are, chronologically presented, those of: Hazen [1892]; Slichter [1899]; Terzaghi [1925], who introduced a variation of Slichter expression for sands with heterogeneous grains of different shapes; Kozeny [1927], who obtained an expression from Poiseuille equation for capillary tubes; Mavis & Wilsey [1936]; Carman [1938 and 1939], who verified Kozeny's expression; Anderson [1940] and Wyllie & Rose [1950]. The last expression, which was obtained by dimensional analysis, is applied to porous media with grains of constant diameter with a modification for soils with different grain sizes by introducing a shape factor.

A proof of the lack of accuracy of the different theoretical and even semi-empirical formulations for calculating hydraulic conductivity (κ) of porous media can be found in Kozeny's research [1927]. He compared three of the solutions (Hazen, Krüger and Kozeny) with experimental values, and obtained discrepancies that went from -36 to 180% (Hazen), from -50 to 84% (Krüger), and from -68.7 to 85.7% (Kozeny). Moreover, Fancher et al. [1933], among other results, obtained values for conductivity that were 45 time larger for grain differences of 2%. Referring to the cementation degree (which is hard to consider and measure), it has been concluded that small contents of cementing particles (from 5.6 to 22.7%) produce large changes in the porosity and, therefore, variations in conductivity higher than these percentages.

After these classical authors, hydraulic conductivity has been again studied in several investigations. Chronologically, Loudon [1952] checked the validity of the previous formulation with different experimental results for a broad range of sands. He concluded that Hazen's expression, although very useful due to its simplicity, does not lead to accurate results to the extent of ±2 times, while Kozeny's is more precise. Moreover, if empirical corrections are included in this Kozeny's expression in order to consider the specific surface, the angularity factor and the coefficient of rugosity of the grains (Robertson & Emödi [1943]), the hydraulic conductivity of sand can be computed to an accuracy of about ±20%. These authors also proved that sands with higher angularity or specific surface are more permeable than those with round sand of the same porosity.

Other authors, such as Wise [1952], Herdan [1960], Gray [1968] and Scheidegger [1974] tried to find a general theory, although their search was not very successful. By the end of 20th century, Åberg [1992 a and b] also investigated in this field, developing a simple stochastic model for soils and other granular materials based on its grain-size distribution, grain shape, degree of densification and other variables. Åberg defined the porous medium resistance in a viscous addend (proportional to the specific discharger, q) and an inertial addend (proportional to q^2). In each term a different representative grain side is involved. Later, Carrier [2003], in his technical note, recommended to simply retire Hazen's formulation [1892], based on D_{10} (particle size in cm, for which 10% of the soil is finer), and replaced it with Konezy-Carman (Konezy [1927] and Carman [1938, 1939]), which considers the entire particle size distribution, the particle shape and the void ratio. On the one hand, Carrier thoroughly described the limitations in Hazen's expression (0.01 cm < D_{10} < 0.3 cm) and gave a list of authors who assigned different ranges to the constant factor in this formulation (going from 1 to 1000 according to each author). He did the same with Kozeny-Carman's formulation, providing expressions for the specific surface in homogeneous and non-homogeneous isotropic soils, and in angular soils (with

limitations). Odong [2007] confirmed that Kozeny-Carman's formulation is the one which gives closer results to the experimental ones.

Recently, Shin [2017] introduced the tortuosity for the determination of Kozeny's hydraulic diameter of the porous media. The hydraulic diameter has been employed to date as the most accurate parameter for the calculation of the permeability coefficient with grains of the same size. The parameter already included fundamental geometrical features such as grain size, packing and grain shape. According to the author, the tortuous hydraulic diameter is the most important characteristic parameter governing porous flow aspect. Introducing the new parameter, the deviations with the experimental results are reduced from 12.8% to 1.67%, which is demonstrated by employing numerical computation (CFD).

III.3 Pi theorem, discrimination and Darcy's and Forchheimer's laws

In fluid mechanics, the dimensional basis commonly used is {M,L,T} (mass, length and time quantities, respectively). According to the common basis, the hydraulic or piezometric potential (gravitational and pressure potential energy per unit of fluid weight) has the dimension of [h]=L, which means that the hydraulic gradient, $\mathrm{i} = \frac{d\mathrm{h}}{d\mathrm{x}}$, is dimensionless. With all this and employing Darcy's law [1856] as $\mathrm{Q} = \mathrm{A}\kappa\mathrm{i}$, the dimensions of the hydraulic conductivity can be immediate deduced, $[\kappa] = \mathrm{LT}^{-1}$. As previously mentioned, it is widely accepted by the scientific community and it does not affect the experimental researches that are carried out in this field.

Not numerous comments can be found in scientific literature about the dimensional character of permeability. In this way, Loudon [1952] refined the definition for κ saying that 'permeability (he referred to hydraulic conductivity) is expressed in centimetres per second per unit of hydraulic gradient', which is practically saying that the unit of the hydraulic conductivity is m/s. Åberg [1992 b], as commented in the previous section, adopted dimensional concepts to justify the choice of different grain sizes in the inertial and viscous terms in the flow resistance. Finally, Shin [2017], based on the experimental evidences and perhaps on the results from the internal friction flow analysis (Fancher et al. [1933]), used the product of the friction factor and the Reynolds numbers ($\zeta \cdot R_e$) to characterize the flow through porous media, a non-coherent approach with the application of Pi theorem, since both Re and ζ, are dimensionless groups by their own. As far as we know, no other comment of interest appears in the literature related to the dimensional character of permeability or conductivity, apart from those thoroughly presented in the following section.

III.3.1 Darcy's law and Pi theorem

Muskat [1937] has been the only researcher who deeply reflected about the dimensions of the parameter related to Darcy's law [1856], originally expressed in the form $Q = C\frac{A}{L}(\Delta h)$, where Δh is the piezometric or hydraulic potential difference along the distance L in the porous sample. Muskat wrote this law in the way that has been previously mentioned

$$Q = C_o \frac{A}{L}(\Delta p) \quad \text{(III-2)}$$

where Q is the groundwater flow (m^3/s) through a porous medium of cross section A (m^2) and length L (m), caused by the pressure difference Δp (N/m^2). Using the classical basis {M,L,T}, the author deduced that C_o is a dimensional constant which involves the physical properties of the fluid (viscosity and density) and geometrical properties of the porous medium. The physical meaning of the constant is complex to find according to its dimensional equation ($[C_o]=M^{-1}LT^{-1}$) or its units ($m\cdot kg^{-1}s^{-1}$), although its experimental determination is immediate. To obtain this equation with dimensional considerations (Pi theorem, Buckingham [1914]), and citing Bridgman [1931], Muskat started from a list of six relevant variables, {{Δp,ρ,μ,d,v,Δs}}. In this list Δp is the pressure difference (N/m^2), ρ the density (kg/m^3), μ the fluid dynamic viscosity ($kg\cdot m^{-1}\cdot s^{-1}$), d a characteristic length (m) equivalent to the average pore or grain size because both of them are proportional, v the average fluid velocity (m/s), and Δs the length of the sample (m). The dimensional equations of these quantities are (involving the variable p in Muskat's deduction all the energetic effects but those of velocity, since they can be neglected in flow through porous media):

$$[\Delta p] = ML^{-1}T^{-2} \quad \text{(III-3)}$$

$$[\rho] = ML^{-3} \quad \text{(III-4)}$$

$$[d] = L \quad \text{(III-5)}$$

$$[v] = LT^{-1} \quad \text{(III-6)}$$

$$[\mu] = ML^{-1}T^{-1} \quad \text{(III-7)}$$

$$[\Delta s] = L \quad \text{(III-8)}$$

With these equations, Muskat determined the three dimensionless groups that characterize the problem, which are

$$\pi_1 = \frac{(\Delta p)\rho d^2}{\mu^2}, \quad \pi_2 = \frac{v\rho d}{\mu}, \quad \pi_3 = \frac{(\Delta s)}{d}, \quad \text{(III-9)}$$

According to Pi theorem, the solution is $\pi_1 = F(\pi_2, \pi_3)$, or

$$\frac{(\Delta p)\rho d^2}{\mu^2} = F\left\{\frac{v\rho d}{\mu}, \frac{(\Delta s)}{d}\right\} \quad \text{(III-10)}$$

where F is an unknown function. To qualify, Muskat wrote Equation (III-10) in the form

$$\frac{(\Delta p)\rho d^2}{\mu^2} = F_1\left\{\frac{v\rho d}{\mu}\right\} \cdot F_2\left\{\frac{(\Delta s)}{d}\right\} \quad \text{(III-11)}$$

an expression that does not strictly adjust to Pi theorem, which states there should be only one function. After the considerations based in the experimental results of other authors, and with the aim of refining his deduction, Muskat directly assumed that $\frac{(\Delta p)\rho}{\mu^2}$ is a lineal function of the monomial $\frac{(\Delta s)}{d}$. Therefore, the former expression is reduced to

$$\frac{\Delta p}{\Delta s} = \frac{\mu^2}{\rho d^3} F\left(\frac{v\rho d}{\mu}\right) \quad \text{(III-12)}$$

In order to support this simplification, it can be said that removing of one of the monomials (π_1 or π_3) is simply justified by the fact that Δp and Δs do not play independent physical roles in the solution, but a single role by the ratio $\Delta p/\Delta s$. This hypothesis reduces the list of relevant variables to five elements, {{$\Delta p/\Delta s$, ρ, μ, d, v}}.

The argument of F is the so-called Reynolds number, $R_e = \frac{v\rho d}{\mu}$, known in the fluid flow analysis in ducts. For Muskat, Equation (III-12) is simply a 'dimensional' equation to determine the character (either laminar or turbulent) of flow in pipes. For laminar flow in circular pipes, according to experimental results, Equation (III-12) approaches to the proportionality ratio

$$\frac{\Delta p}{\Delta s} = C_1\left(\frac{\mu v}{d^2}\right) \quad \text{(III-13)}$$

known as Poiseuille's law, where C_1 is a dimensionless constant. For turbulent regimen, Equation (III-12) becomes independent of viscosity and its proportional to the squared value of velocity:

$$\frac{\Delta p}{\Delta s} = C_2\left(\frac{\rho v^2}{d_o}\right) \quad \text{(III-14)}$$

where C_2 is a dimensional constant. According to these results, different authors have selected distinct expressions for the relation between $\frac{\Delta p}{\Delta s}$ and v for the porous media. For instance

$$\frac{\Delta p}{\Delta s} = a_1 v, \frac{\Delta p}{\Delta s} = a_1 v + a_2 v^n \text{ or } \frac{\Delta p}{\Delta s} = a_3 v^n \quad \text{(III-15)}$$

where a_1, a_2 and a_3 are dimensional constants, and n is a number between 0 and 1, so the most reliable results of Darcy law (Fancher et al. [1933]) concludes that:

(i) for low average velocities: $\frac{\Delta p}{\Delta s} = a_1 v$ (equivalent to Darcy's law) (III-16a)

'laminar viscous flow'

(ii) for higher velocities: $\frac{\Delta p}{\Delta s} = a_1 v + a_2 v^n$ ($\frac{\Delta p}{\Delta s}$ is increased faster than v) (III-16b)

'partially or totally turbulent flow'

Indeed, this occurs. Experimental logarithmical charts from these authors, which relate the friction factor, $\zeta = \frac{(\Delta p)d}{2L\rho v^2}$, with Reynolds number, $R_e = \frac{v\rho d}{\mu}$ (where d is the average grain diameter), confirm that for Re<1, $\zeta \cdot R_e$= constant (validating Equation (III-16a)). This is

$$\frac{\Delta p}{L} \propto \frac{\mu}{d^2} v, \qquad \text{or} \qquad \frac{\Delta p}{L} = C_3 \cdot v \tag{III-17}$$

where C_3 is a dimensional constant. Muskat, in a footnote, discussed the physical meaning of d, stating that: '*Physically, of course, the parameter d should represent the average pore rather than the grain diameter. However, as the former can be directly measured only by microscopic examination of the cross section of the porous medium itself, all attends to define or use a value of d to enter into the Reynolds number have referred to the averages of the actual grains diameter'*.

The strongest example to confirm Equation (III-16b) is Lindquist' experiment [1933], in which the water flow through a column of uniform pellets is studied. In this experiment, the value of n is 2. His results, presented in plots of $\zeta \cdot R_e$ versus R_e, separate this dependence in two straight lines: the first one, completely horizontal (for $0<R_e<4$, approximately); and the second one with positive slope (for $R_e>4$), which adjusts to the line equation $\zeta R_e = C_4 + C_5 R_e$, where C_4 and C_5 are dimensional constants. As $\zeta \cdot R_e = \frac{1}{2}\frac{(\Delta p)}{L}\left(\frac{d^2}{\mu}\right)\left(\frac{1}{v}\right)$, the expression can be written in the form $\frac{1}{2}\frac{(\Delta p)}{L}\left(\frac{d^2}{\mu}\right)\left(\frac{1}{v}\right) = C_4 + C_5\frac{v\gamma d}{\mu}$, or finally,

$$\frac{(\Delta p)}{L} = \left(\frac{2\mu C_4}{d^2}\right) v + \left(2C_5\frac{\rho}{d}\right) v^2 = C_6 v + C_7 v^2 \tag{III-18}$$

This formulation is similar to Equation (III-8b). The limit value in the graphic, $R_e \approx 4$, is a mere indication of the value of R_e which separates viscous flow, described by $\zeta \cdot R_e$ = constant or $\frac{\Delta p}{\Delta s} = a_1 v$ (Darcy's law or Equation (III-16a)) from partially or totally turbulent flow, described by $\frac{\Delta p}{\Delta s} = a_1 v + a_2 v^n$(Equation (III-16b)). The capillary and irregular nature of the porous media is without doubt the reason why the transition from viscous to turbulent regimen is not as sharp as in the case of empty tubes or ducts. In this case, it is a diffuse transition region.

All in all, Muskat summarized his conclusions about Darcy's law (exclusively referring to sandy soils), stating that it was a reliable approach to what he called 'law of flow' or Equation (III-12), $\frac{\Delta p}{\Delta s} = \frac{\mu^2}{\rho d^3} F\left[\frac{v\rho d}{\mu}\right]$, deduced by dimensional argumentation (Pi theorem). Its validity range, however, is difficult to stablish due to the lack of definition of the parameter of the porous media or characteristic length, d, which appears in R_e. Therefore, it would determine the laminar or turbulent nature of the flow. In this way, from the previous explanations, it can be deduced that the effects of porosity, connectivity, tortuosity, grain size, and compaction and cementation degrees are the cause of the lack of definition and knowledge of the characteristic length, d. This would be equivalent to admit that it is impossible to carry out a rigorous dimensional treatment which leads to an accurate dimensional equation for permeability.

III.3.2 Discrimination and Darcy's and Forchheimer's laws

Discrimination, in dimensional analysis theory (Palacios [1964], Alhama & Madrid [2012]) that includes Pi theorem as the most useful tool in the search of the dimensional groups that characterize a physical problem, assumes the existence of extended dimensional bases instead of the classical one {M,L,T}.

One manner of discrimination is spatial, which assumes different dimensional equations for each of the lengths that define the spatial directions as well as the derived quantities involving these lengths, such as velocity, acceleration and forces. In this way, rectangular geometries have a spatially discriminated basis involving five quantities, $\{L_x,L_y,L_z,M,T\}$, and its use generally leads to more accurate results than the classical Pi theorem (which does not consider discrimination), especially in anisotropic media. Because of its application, many of the classical numbers, such as Reynolds, Peclet and Rayleigh, have dimensions and do not express a balance of quantities that counteract in the system or the whole physical scenario, since its value is generally much higher or lower than unit). Nevertheless, discriminated dimensional groups do express balance of quantities and, consequently, are of the order of magnitude of the unit (Alhama & Madrid [2012]).

There are other kinds of discriminations which present a rather conceptual character. For example, including in the dimensional basis two different masses, one related to inertial effects and another one related to countable effects (water flow measure) or, as presented later in the chapter, potential quantities (for example the piezometric head).

Is it possible to derive Darcy's law from discrimination and Pi theorem? Theoretically it is, and that is what it is intended in this section. For this, a discriminated dimensional basis applicable to any geometry {M, $L_{\rightarrow}$, L_{vis}, L_n, T}, where $L_{\rightarrow}$ is the spatial dimension in the direction of the flow, L_{vis} is the spatial dimension in the direction perpendicular to the previous and that has been chosen so both directions define the plains of viscous surface, and L_n is the third spatial direction, normal to the other ones. In this way viscous surfaces S_{vis} have dimensions $[S_{vis}]=L_{\rightarrow}L_{vis}$.

In this basis, the dimensions of the different quantities involved in ζ and R_e, and what has been called previously in this chapter list of relevant variables of the problem {{$\Delta p/L$, d, v, ρ,μ}}, are:

$$[\Delta p/L] = [\frac{f}{S\,L}]= \frac{ML_{\rightarrow}T^{-2}}{L_{vis}L_nL_{\rightarrow}} = ML_{vis}^{-1}L_n^{-1}T^{-2} \quad \text{(III-19a)}$$

$$[d] = L_n \quad \text{(III-19b)}$$

$$[v] = L_{\rightarrow}T^{-1} \quad \text{(III-19c)}$$

$$[\mu]= [\frac{f_{vis}}{S_{vis}\left(\frac{\partial v}{\partial n}\right)}] = \frac{ML_{\rightarrow}T^{-2}}{L_{vis}L_{\rightarrow}\frac{L_{\rightarrow}T^{-1}}{L_n}} = ML_{\rightarrow}^{-1}L_{vis}^{-1}L_nT^{-1}= MS_{vis}^{-1}L_nT^{-1} \quad \text{(III-19d)}$$

$$[\rho]= [\frac{mass}{volumen}] = \frac{M}{L_{vis}L_{\rightarrow}L_n} = ML_{\rightarrow}^{-1}L_{vis}^{-1}L_n^{-1} = MS_{vis}^{-1}L_n^{-1} \quad \text{(III-19e)}$$

Intentionally, the direction for d has been chosen perpendicular to the viscous surface, so its value would be related to the average pore size. It is also important to highlight that the direction for the forces derived from pressure that has been chosen is the same as the one for velocity, as it is in this direction in which the pressure quantity produces effect. According to the previous expression, the dimensions for ζ and R_e are:

$$[\zeta] = [\frac{(\Delta p)d}{2L\rho v^2}]=\frac{(ML_{\rightarrow}L_{vis}^{-1}L_n^{-1}T^{-2})(L_n)}{(L_{\rightarrow})(ML_{\rightarrow}^{-1}L_{vis}^{-1}L_n^{-1})(L_{\rightarrow}^2T^{-2})} = \frac{L_n}{L_{\rightarrow}} \quad \text{(III-20)}$$

$$[R_e] = [\frac{v\rho d}{\mu}]= \frac{(L_{\rightarrow}T^{-1})(ML_{\rightarrow}^{-1}L_{vis}^{-1}L_n^{-1})(L_n)}{ML_{\rightarrow}^{-1}L_{vis}^{-1}L_nT^{-1}} = \frac{L_{\rightarrow}}{L_n} \quad \text{(III-21)}$$

so the product $\zeta\cdot R_e = \left(\frac{(\Delta p)d}{2L\rho v^2}\right)\left(\frac{v\rho d}{\mu}\right) = \frac{(\Delta p)d^2}{2Lv\mu}$ has null dimension. In order to make this monomial the only dimensionless group that characterizes the behaviour of the problem, it is necessary to remove ρ from the list of relevant variables, since it does not appear in the expression, but that would mean to neglect the inertial effects!.

Indeed, this happens because this parameter is directly linked to these effects, in the same way that μ is to viscous effects, and Δp is to those effects caused by pressure forces. However, v is directly connected to inertial effects and indirectly to viscous ones through its gradient, while L and d, as the contours of the domain in which the forces per unit of volume are balanced, can

appear involved in the three effects. For negligible inertial forces, if compared to viscous and pressure forces (or such low velocities that this hypothesis can be assumed), the only discriminated dimensionless group governing the problem is

$$\pi_{\mathrm{pre-vis}} = \zeta \cdot \mathrm{R_e} = \frac{(\Delta p)\mathrm{d}^2}{2\mathrm{L}\nu\mu} \sim 1 \qquad \text{(III-22)}$$

where the subscript 'pre-vis' means that it is a monomial in which the two forces, viscous and pressure, are balances. This is the reason why the monomial has the order of magnitude of unity, since it is assumed that both intervene and influence the process to the same degree. The fluid loses pressure (or pressure energy) as energy is dissipated by viscous friction. In this way, $\mathrm{v} \sim \frac{\Delta p \mathrm{d}^2}{\mathrm{L}\mu} = \left(\frac{\mathrm{d}^2}{\mu}\right)\frac{\Delta p}{\mathrm{L}}$, a coherent result with Darcy's law.

For the general case in which the three kinds of forces (pressure, inertial and viscous) exist, the independent dimensionless groups that can be obtained from the list of variables {{Δp/L,d,v,ρ,μ}} with the dimensional Equations (III-19 a to f) are two, and can be written in any of the following forms:

$$\pi_{\mathrm{pre-v}} = \frac{(\Delta p)\mathrm{d}^2}{2\mathrm{L}\nu\mu}, \qquad \pi_{\mathrm{pre-i}} = \frac{(\Delta p)}{\rho \mathrm{v}^2} \qquad \text{(III-23a)}$$

$$\pi_{\mathrm{pre-v}} = \frac{(\Delta p)\mathrm{d}^2}{2\mathrm{L}\nu\mu}, \qquad \pi_{\mathrm{ine-vis}} = \frac{\pi_{\mathrm{pre-i}}}{\pi_{\mathrm{pre-vis}}} = \frac{\rho \mathrm{v} \mathrm{d}^2}{2\mathrm{L}\mu} \qquad \text{(III-23b)}$$

$$\pi_{\mathrm{ine-vis}} = \frac{\pi_{\mathrm{pre-i}}}{\pi_{\mathrm{pre-vis}}} = \frac{\rho \mathrm{v} \mathrm{d}^2}{2\mathrm{L}\mu}, \qquad \pi_{\mathrm{pre-ine}} = \frac{(\Delta p)}{\rho \mathrm{v}^2} \qquad \text{(III-23c)}$$

Adopting any of these pairs and employing Pi theorem, for example the first one, the solution of the problem is $\pi_{\mathrm{pre-vis}} = \mathrm{F}(\pi_{\mathrm{pre-ine}})$, or

$$\frac{(\Delta p)\mathrm{d}^2}{2\mathrm{L}\nu\mu} = \mathrm{F}\left(\frac{\Delta p}{\rho \mathrm{v}^2}\right) \qquad \text{(III-24)}$$

where F is an arbitrary and unknown function of its argument. From this, Darcy's velocity can be written, in a more general way, as

$$\mathrm{v} = \frac{\mathrm{d}^2}{\mu}\left(\frac{\Delta p}{\mathrm{L}}\right)\mathrm{F}_3\left(\frac{\Delta p}{\rho \mathrm{v}^2}\right), \qquad \text{or} \qquad \mathrm{v} = \frac{\mathrm{d}^2}{\mu}\left(\frac{\Delta p}{\mathrm{L}}\right)\mathrm{F}_2\,\frac{\rho \mathrm{v} \mathrm{d}^2}{\mu \mathrm{L}} \qquad \text{(III-25)}$$

The limit cases of this results are:

(i) Negligible inertial effects if compared to viscous and pressure effects. This removes ρ from the list of variables, leading to the already reached solution, Equation (III-22), or

$$\mathrm{v} \propto \frac{\mathrm{d}^2}{\mu}\left(\frac{\Delta p}{\mathrm{L}}\right) \qquad \text{(negligible inertial effects, Darcy's law)} \qquad \text{(III-26a)}$$

(ii) Negligible viscous effects if compared to inertial and pressure effects. This hypothesis removes μ from the list and gives the solution $\pi_{\mathrm{pre-ine}} = \frac{(\Delta p)}{\rho v^2} \sim 1$ or

$$v^2 \propto \frac{L}{\rho}\left(\frac{\Delta p}{L}\right) \qquad \text{(negligible viscous effects, Forchheimer's law)} \qquad \text{(III-26b)}$$

(iii) Negligible effects of pressure force if compared to inertial and viscous ones. It is a type of problem of a different nature associated to the existence of a limit layer that should not be commented here since pressure forces are determinant in the problems of flow through porous media.

Combining the two solutions of the simplified cases, $v \sim \frac{d^2}{\mu}\left(\frac{\Delta p}{L}\right)$ and $v^2 \sim \frac{L}{\rho}\left(\frac{\Delta p}{L}\right)$, it would be reasonable to think of a general solution of the form

$$\left(\frac{\Delta p}{L}\right) = c_1 \frac{\mu}{d^2} v + c_2 \frac{\rho}{L} v^2 \qquad \text{(III-27)}$$

where c_1 and c_2 are dimensional constants which depend on the physical properties of the fluid and the geometrical characteristics of the porous media. These constants determine the relative influence among the pressure, viscous and inertial effects in the problems. Many authors have proposed an almost identical solution, $\left(\frac{\Delta p}{L}\right) = c_1 \frac{\mu}{d^2} v + c_2 \frac{\rho}{d} v^2$, since d and L are of the same order of magnitude in those porous media with regular grains (at this point it is important to remember that Åberg [1992 b] introduced different size grains for viscous and inertial resistance). Expressing it in terms of R_e and ζ, it is an equivalent equation to $R_e \zeta = c_4 + c_5 R_e$, where c_4 and c_5 are dimensional constants.

Those media with non-regular grains or whose grains are spatially orientated (leading this to spatially orientated voids too) present clearly different values for d and L. If supposing a media of flat grains with narrow and long ducts (low tortuosity, Figure 3.1.a, L>>d), fluid particles almost do not change direction, so inertial forces can be negligible compared to viscous one, which are high due to the large contact surface between the fluid and the grain surfaces. In this type of media, the most important term in Equation (III-27) is the first one, so $\left(\frac{\Delta p}{L}\right) = c_1 \frac{\mu}{d^2} v$. Nevertheless, in a medium as the one in Figure 3.1.b, particles frequently change direction, so inertial effects are high, comparing to the previous medium. If these effects are of a higher order of magnitude than that of viscous effects, Equation (III-27) is simplified to $\left(\frac{\Delta p}{L}\right) = c_2 \frac{\rho}{L} v^2$.

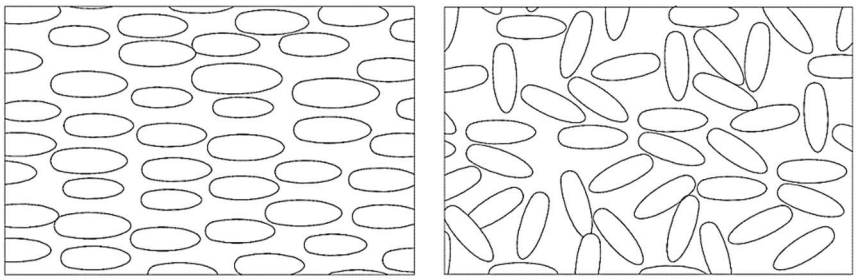

1 a) 1 b)

Figure 3.1. Porous media. a) flat long particles in the flow direction. b) flat long particles in random directions

To finish this section, interpreting the dimensionless groups (III-23 a to c) in terms of force balance, it is important to highlight that Muskat did not consider Reynolds number in porous media ($R_e=\frac{v\rho d}{\mu}$) as a ratio of inertial and viscous forces, which is coherent with the conclusions of this section. If he had done so, he would not have been able to justify that, for negligible inertial forces ($0<R_e<4$), the value of R_e could be of value unity, or slightly higher.

III.4 Approach to the dimensional character of permeability

In its original form, $v=\kappa\frac{\Delta h}{L}$ or $v=C_o\frac{\Delta p}{\Delta x}$, constants κ or C_o cluster the influence of the fluid and the porous medium, which is the reason why its dimensions cannot be related to a certain property. For this, Muskat went back to the dimensional considerations and commented that one should start from Equation (III-13), separating the influence of the fluid (μ) from the influence of the porous medium, which is summarized in a characteristic length d (grain effective diameter) and a constant C_1 (which involves the rest of the properties). Therefore, Darcy's law can be rewritten as $v=C_1\left(\frac{d^2}{\mu}\right)\left(\frac{dp}{dx}\right)$. Numerous experiments -from those carried out by Slichter [1899] with uniform ensembled spheres applying Poiseuille's law to the extensive ones developed by Fancher et al. [1933] to plot the typical charts of friction factor versus Reynolds number- have tried to directly determine constants C_o and C_1, stating that they depend on the squared value of certain average grain size. This corroborates the role of d in the law and its meaning.

It should be noted that with both classical dimensional analysis (where $[\frac{\Delta p}{\Delta x}]=ML^{-2}T^{-2}$, $[d]=L$, $[v]=LT^{-1}$ and $[\mu]=ML^{-1}T^{-1}$) and discriminated dimensional analysis (where $[\frac{\Delta p}{\Delta x}]=ML_{vis}^{-1}L_n^{-1}T^{-2}$, $[d]=L_n$, $[v]=L_{\rightarrow}T^{-1}$, and $[\mu]=MS_{vis}^{-1}L_nT^{-1}$), constant C_1 is dimensionless despite clustering the complex properties of the porous media not associated to the grain size. This could be the

reason of its broad range values. However, focusing on the discriminated analysis as a more accurate dimensionless technique, and admitting that properties such as tortuosity or angularity are linked to aspect ratios (for instance, L_n/L_{vis}), different conclusions can be reached:

i) all the properties involved in C_1 are conjugated in such a way that the constant is dimensionless;
ii) one of the dimensional equations is not correct, and the only possibility is the dimensional equation of d;
iii) the whole approach is incorrect.

In the light of the lack of coherent results necessary for presenting present some validity and generality for Equation (III-13), Muskat thought it was reasonable to cluster factors C_1 and d^2 in a single parameter (permeability, k) which involves the dynamic behaviour of the porous media as carrier of the viscous fluid, $k = C_1 d^2$. According to dimensional characterization, and following its classical technique, he gave k the dimensional equation L^2.

To finish this study, Taylor's contributions based on the classical dimensional analysis must be presented since he is the only author, together with Muskat, who researched in this field. In his analysis, Taylor stablished the following steps:

i) the study of flow through circular ducts (Poiseuille's law),
ii) the extension of the study to flow through ducts of sections with different sizes,
iii) the introduction of the concept of hydraulic radius,
iv) the effect of sinuosity of the path, and
v) the deduction of the permeability as function of the typical grain size, viscosity, fluid density and a factor that depends on the void ratio e

If the discrimination is included in Taylor's proposal, so L_{vis} has the direction of the perimeter of the duct cross section, the dimensions of the relevant variables are

$$[\nabla p]=ML_{vis}^{-1}L_n^{-1}T^{-2} \quad \text{(III-28)}$$

$$[R] = L_n \text{ (duct raduis)} \quad \text{(III-29)}$$

$$[v_{average}] = L_{\rightarrow}T^{-1} \quad \text{(III-30)}$$

$$[\mu]= MS_{vis}^{-1}L_nT^{-1} \quad \text{(III-31)}$$

Comparing both laws, Poiseuille's and Darcy's, $\mathbf{v}_{average} \propto \frac{R^2}{\mu}(\nabla p)$ and $v_{average} = \left(\frac{k}{\mu}\right)(\nabla p)$, respectively, it can be concluded that $[k] = L_n^2$. This result is the same as the one obtained by

Muskat. Assuming ducts of different sizes would only imply that an average value of the hydraulic radius that would not vary the dimensional equation of k.

Admittedly, insisting on discrimination, the previous result ($[k] = L_n^2$, whose physical meaning is not direct) could be conveniently separated in the product of the pore section ($L_{vis}L_n$) and a shape factor of this section ($\frac{L_n}{L_{vis}}$). This allows justifying the inclusion of at least one aspect ratio in the dependence of k. However, Taylor's definition of tortuosity is simply associated to a higher pressure drop per unit of particle longitudinal advance, so it is a direct and dimensionless coefficient which correct the velocity expression. All in all, Taylor admitted that *'possibly, there are other factors related to the effects of the pore section shape and 'other constants', which should be considered to extrapolate solutions of the capillary straight ducts that are employed in the real model of the porous media'*.

To sum up, Muskat (and his application of Pi theorem), Taylor (and his theory of circular ducts) and the discriminated dimensional analysis conclude that k dimension is $[k] = L_n^2$ and this coefficient clusters all the influence of the porous media. According to the relationship (even if partial) between this dimension and the squared of the average size of the grain, it seems to justify the proposed expressions in the scientific literature for determining the permeability from the grain size distribution.

Paradoxically, the historical approach to the dimensional character of permeability that has been presented previously in this section leads to mistaken conclusion when applying them to the search of dimensionless groups that characterize the anisotropic media. Indeed, if the problem is simplified to a 2-D medium, $[k_x] = L_y^2$ and $[k_y] = L_x^2$, so $[\frac{k_x}{k_y}] = \frac{L_y^2}{L_x^2}$. With this, the dimensionless group would be $\frac{k_x}{k_y}\frac{l_x^{*2}}{l_y^{*2}}$, where l_x^* and l_y^* are arbitrary geometrical quantities which define the problem in the indicated direction. As shown later in this chapter, the dimensional group that characterizes the problem is not $\frac{k_x}{k_y}\frac{l_x^{*2}}{l_y^{*2}}$, but $\frac{k_x}{k_y}\frac{l_y^{*2}}{l_x^{*2}}$. Perhaps, the problem is that two empirical laws (Newton's for viscosity and Darcy's) have been combined in the same dimensional analysis employing an inadequate basis.

III.5 Introduction of the fluid energetic potential in the dimensional basis

In this section, an alternative and direct procedure is proposed. This new way does not lead to accurate dimensions for permeability but gives remarkable results to find the dimensionless groups which rule the problems of flow through porous media. Moreover, the results obtained in the previous section are critically argued. Discrimination technique, in its wider and more general conception (Madrid & Alhama [2005]), allows introducing the dimension of the variable 'energetic potential of the fluid' (p or h) in the dimensional basis. This variable is responsible of the flow through porous media, and its dimension replaces the mass, since the inertial effects can be considered as negligible. Naming the potential dimension Φ, the basis becomes {Φ,L_x,L_y,L_z,T}, so Darcy's law, in the forms $v_{average} = \left(\frac{k}{\mu}\right)(\nabla p)$ or $v_{average} = C_o(\nabla p)$, allows assigning dimensional equations to $\left(\frac{k}{\mu}\right)$ or C_o, $\left[\frac{k}{\mu}\right] = [C_o] = L^2T^{-1}\Phi^{-1}$

III.5.1 Emergence of the group $\frac{k_x}{k_y}\frac{l_y^{*2}}{l_x^{*2}}$ in anisotropic media

According to the beginning of the section, $\left(\frac{k}{\mu}\right)$ and C_o components in x and y directions are:

$$\left[\frac{k}{\mu}\right]_x = \left[\frac{k_x}{\mu_x}\right] = [C_o]_x = \frac{L_x^2T^{-1}}{\Phi} \quad \text{(III-32)}$$

$$\left[\frac{k}{\mu}\right]_y = \left[\frac{k_y}{\mu_y}\right] = [C_o]_y = \frac{L_y^2T^{-1}}{\Phi} \quad \text{(III-33)}$$

which allows writing $\left[\frac{k_x}{\mu_x}\right] \Big/ \left[\frac{k_y}{\mu_y}\right] = \frac{L_x^2}{L_y^2}$, an essential result, as it implies that dimensionless groups can be obtained combining the ratio $\left[\frac{k_x}{\mu_x}\right] \Big/ \left[\frac{k_y}{\mu_y}\right]$ with ratios of lengths of the problem $\frac{k_x\mu_y}{k_y\mu_x}\frac{l_y^{*2}}{l_x^{*2}}$.

Numerically, $\mu_x = \mu_y$, so the groups can be simplified to

$$\pi = \frac{k_x}{l_x^{*2}}\frac{l_y^{*2}}{k_y}. \quad \text{(III-34)}$$

An alternative manner to obtain this group is to deduce it from the steady governing equation that rules the movement of fluid through anisotropic porous media. This Laplace type equation ($\frac{k_x}{\mu_x}\frac{\partial^2 p}{\partial x^2} + \frac{k_y}{\mu_y}\frac{\partial^2 p}{\partial y^2} = 0$), result of combining Darcy's law and continuity equation, must be turned into dimensionless, obtaining

$$\left[\frac{k_x\mu_y}{k_y\mu_x}\frac{l_y^{*2}}{l_x^{*2}}\right]\frac{\partial^2 p'}{\partial x'^2} + \frac{\partial^2 p'}{\partial y'^2} = 0 \quad \text{(III-35)}$$

Dimensionless variables p', x' and y' are calculated as

$$p' = \frac{p}{\Delta p_o},\ x' = \frac{x}{l_x^*},\ y' = \frac{y}{l_y^*} \qquad \text{(III-36)}$$

where Δp_o, l_x^* y l_y^* the chosen references to define them. The only dimensionless group that rules the solution of this equation (apart from aspect factors) is the coefficient multiplying $\frac{\partial^2 p'}{\partial x'^2}$, this is $\pi = \frac{k_x \mu_y}{k_y \mu_x} \frac{l_y^{*2}}{l_x^{*2}}$, since the differential average terms can be considered as unity.

This expression degenerates again in the Equation (III-34) by deleting the viscosity. Therefore, either employing Darcy's law and the correct discrimination or the dimensionless governing equation, the same governing group for anisotropic soils is obtained, a corrected permeability ratio. Although there is no possible manner to know the concrete dimensions of k, those of the ratio $\left[\frac{k_x}{\mu_x}\right] \Big/ \left[\frac{k_y}{\mu_y}\right]$ are achieved.

III.5.2 Energetic potential h. Physical meaning of the constants

Variables h and p are related by Bernoulli's expression, neglecting the velocity term, $h = \frac{p}{\rho g} \pm z$, with + sign for z increasing upwards, and – downwards. In this way, Muskat's expression becomes Darcy's original, $v = -\frac{k\rho g}{\mu}\left(\frac{dh}{dx}\right) = -\kappa \frac{dh}{dx}$. Previously in this chapter, according to classical dimensional analysis, the hydraulic gradient $\frac{dh}{dx}$ is a dimensionless variable, which means that hydraulic conductivity dimensions are those of a velocity, $[\kappa]=LT^{-1}$. This approach makes impossible to deduce the sought dimensionless group. Nevertheless, introducing the dimensions of the energetic potential associated to h in the dimensional basis, and following the steps presented in Section III.5.1, the correct solution is again reached. Table 3.1 collects the physical meaning and dimensional equations of the constants involved in the water flow through porous media for different dimensional basis according to the energetic potential chosen. ξ, Θ and Φ are dimensions of the total energetic potentials per unit of specific weight, per unit of mass or per unit of volume, respectively.

Table 3. 1. Dimensional equation and physical meaning of the constants involved in Darcy's law

Parameter	Energetic potential	Discriminated basis	Dimensional equation	Physical meaning
$\kappa = \frac{k\rho g}{\mu} = \frac{v}{\frac{dh}{dx}}$	h	$\{L_{\rightarrow}, L_{vis}, L_n, T, \xi\}$	$[\kappa]= L_{\rightarrow}^2 T^{-1}\xi^{-1}$	velocity that causes a unit gradient of the energetic potential h
$\frac{k\rho}{\mu} = \frac{\kappa}{g} = \frac{v}{\frac{d(gh)}{dx}}$	g·h	$\{L_{\rightarrow}, L_{vis}, L_n, T, \Theta\}$	$[\frac{k\rho}{\mu}]= L_{\rightarrow}^2 T^{-1}\Theta^{-1}$	velocity that causes a unit gradient of energetic potential g·h
$\frac{k}{\mu} = \frac{\kappa}{\rho g} = \frac{v}{\frac{d(\rho gh)}{dx}}$	ρ·g·h	$\{L_{\rightarrow}, L_{vis}, L_n, T, \Phi\}$	$[\frac{k}{\mu}]= L_{\rightarrow}^2 T^{-1}\Phi^{-1}$	velocity that causes a unit gradient of energetic potential ρ·g·h

In order to simplify the nomenclature in the following chapters, the parameter to be employed to obtain the dimensionless groups as well as carry out the numerical simulation is κ, the hydraulic permeability. Moreover, instead of using the symbol ξ for the dimension of h, we use the symbol L_{wc}, length of the water column. For 2-D rectangular scenarios, the dimensional equations and, therefore, units are the following:

$$[\kappa_x] = L_x{}^2 T^{-1} L_{wc}{}^{-1} = \frac{m_x{}^2}{s \cdot m_{wc}} \quad \text{(III-37)}$$

$$[\kappa_y] = L_y{}^2 T^{-1} L_{wc}{}^{-1} = \frac{m_y{}^2}{s \cdot m_{wc}} \quad \text{(III-38)}$$

These are the hydraulic conductivity components and dimensions that are going to be used in problems of flow under dams studied in the following chapters. If, instead of 2-D rectangular coordinates, the scenario can be simplified as axisymmetric, with coordinates radial (r) and vertical (z), conductivity presents the following dimensions and units:

$$[\kappa_r] = L_r{}^2 T^{-1} L_{wc}{}^{-1} = \frac{m_r{}^2}{s \cdot m_{wc}} \quad \text{(III-39)}$$

$$[\kappa_z] = L_z{}^2 T^{-1} L_{wc}{}^{-1} = \frac{m_z{}^2}{s \cdot m_{wc}} \quad \text{(III-40)}$$

When simulating and obtaining the universal curves for the problems of water flow in unconfined aquifers due to pumping wells, those are the hydraulic conductivity components that are going to be used in the following chapters.

III.6 Final comments

The initial objective was the search of a dimensional equation for permeability (k) that allowed obtaining the accurate dimensionless groups which govern the solution of problems of flow through porous media (particularly in anisotropic scenarios), although, along the chapter, this aim has varied and divided into two.

The first contribution was an attempt to deduce an accurate dimensional equation for permeability. In order to achieve this, the Pi theorem has been applied, together with the discrimination technique, to study Darcy's and Forchheimer's laws. This work had already been carried out by Muskat, and to a lesser extent by Taylor, for isotropic soils. The two authors do not employ spatial discrimination, and only focus on isotropic soils. Their research, as well as the one developed along this chapter, conclude a dimensional equation for permeability, whether isotropic or anisotropic media is considered. However, when this dimensional equation is used to obtain the emerging discriminated dimensionless group that rules the problem of flow through porous media, this monomial, which can be considered as a ratio of permeabilities corrected by an aspect factor, does not behave as so.

All the troublesome process that has been presented in this chapter shows the difficulty to achieve the correct dimensional equation. This is due to the complexity of the physical mechanism that is involved in this parameter: grain size, porosity, connectivity, tortuosity…). According to all this, it can be deduced that combining two empirical laws, in this case Newton's for viscosity and Darcy's for flow through soils, is not a correct approach for the analysis of the dimensional character of permeability. Instead, a complex dimensional basis must be chosen in order to adjust to the problem, as the classical basis {M,L,T}, whether discriminated or not, probably cannot be applied directly when mixing two mechanical constitutive laws.

In order to achieve the second contribution, the problem has been approached again, but in this case, with a spatial discriminated dimensional basis that also involved the dimension of a new quantity: energetic potential of the fluid, which appears due to the pressure difference. The dimensional equation for permeability cannot be found with this new dimensional basis, but that of ratio permeability/viscosity is obtained. With this information, an accurate dimensionless group is deduced. The new monomial is a permeability ratio corrected by an aspect factor too, but this time the aspect ratio is the inverse of that of the first approach. The correct group can also be derived from the dimensionless form of the governing equation, and it behaves as a monomial that rules the problem.

In the following chapters of this thesis, the monomial obtained through the previous sections is employed, together with the different aspect ratios involving the contours of the domain led to the universal curves to solve problems of flow through porous media. In this case, the studied scenarios are flow under dams and flow in unconfined aquifers due to pumping wells. Moreover, the permeability, or more specifically the conductivity ratio, is proved to control these scenarios by verifying that the dimensionless results are the same when the monomial is kept constant although that parameters involved vary their values. This aspect is of importance and justifies the analysis made in Chapter III.

On the other hand, with the second contribution, the problem has been approached with a geometrically discriminated dimensional basis that specifically contains the dimension of the quantity 'energetic potential of the fluid'. In this basis, although the dimensional equation for permeability is not found, the one for the ratio permeability/viscosity is obtained. This result allows deducing an accurate and new dimensionless group in these problems from which viscosity can be deleted due to its isotropic character, also giving rise to a permeability ratio corrected by the squared value of the domain aspect factor. This aspect factor is the inverse of the one obtained with the first approximation. The new group, which is also derived from the dimensionless form of the governing equation, does behave like a monomial that rules the problem.

Chapter IV. Nondimensionalization technique: discriminated characterization of scenarios of flow through porous media

After introducing the classical dimensional treatment that former authors give (from long ago) to the scenarios presented in this thesis and explaining its drawbacks, the application of the discriminated treatment in the deduction of the governing groups in problems of flow under gravity dams without a sheet pile, flow under gravity dams with a sheet pile, flow under gravity dams in infinite media and flow in unconfined aquifers due to a pumping well is shown in this chapter. For the first three types of scenarios, the problem is considered in rectangular 2-D coordinates, while the last is studied as an axisymmetric problem, employing radial coordinates. For these problems, universal abaci for the global and instantaneous and local unknowns of interest are obtained. To do this, a numerical model based on the network simulation method has been employed (described in Chapter V).

The universal representation of the principal unknowns of a problem as functions of the variables of the scenario is the main objective when applying the discriminated nondimensionalization technique. For this, we must reduce the number of groups governing the problem, in order to simplify its use by future researchers and/or engineers. Nevertheless, the geometrical parameters involved in real scenarios are many and this makes their simplification intractable. According to this, the scenarios presented in this chapter are rather ideal problems

in which the number of groups governing the solution is three. For each unknown, its representation as a universal curve or abaci depends on the number of dimensionless groups.

Section IV.2.1 presents the universal curves for the following variables of flow under gravity dams without sheet pile: groundwater flow, pore pressure under the dam (which can be summarized as uplift force due to the pressure under the dam and its application point) and average exit gradient. Section IV.2.2 shows the universal curves for scenarios of flow under gravity dams with a sheet pile: groundwater flow, pore pressure under the dam (summarized as uplift force due to the pressure under the dam and its application point), force on the sheet pile on the upstream side and on the downstream side, application point of these forces on the upstream and the downstream side and the average exit gradient. Section IV.2.3. is a study of the limit groundwater flow and the characteristic lengths in infinite scenarios (considering anisotropy). Finally, Section IV.2.4 presents the universal abaci the variables of interest in problems of flow in unconfined aquifers due to a pumping well: groundwater flow, seepage surface and influence radius.

IV.1 Revision of the dimensionless study of flow through porous media

Several authors (Harr [2012], Muskat [1937]) have presented universal solutions for problems of flow through porous media, especially scenarios with gravity dams. These abaci employ 'dimensionless' groups, derived from classical dimensionless reasoning, in order to summarize many possible scenarios in a few curves. Their groups, which are commonly ratios between a horizontal and a vertical length, for example dam width and stratum thickness (w_d/H in our nomenclature), have led to correct results when considering isotropic problems, where the vertical and the horizontal hydraulic conductivities present the same value. However, when trying to apply their results to anisotropic scenarios where the hydraulic conductivity varies in each direction with ratio frequently of the order of magnitude unity or more (Beckwith et al. [2003 a]), their curves are not accurate enough and correct results cannot be obtained. The reason why it occurs is that spatial discrimination is not considered. When so, this technique lead to a new group: 'the product of a permeability (or hydraulic conductivity) and an aspect ratio', the last being the group traditionally used. According to this, if an isotropic soil is studied, the group would degenerate to the aspect ratio, w_d/H, which clearly explains why the traditional group works correctly in isotropic scenarios. The application of the discriminated dimensionless technique follows the steps presented at the end of Section II.3.

IV.2. Characterization of scenarios of flow through porous media

IV.2.1 Flow under gravity dams without sheet pile. Universal curves

IV.2.1.1 Mathematical model

The governing equation of the flow is a Laplace-type expression. It can be obtained by the combination of the momentum and continuity equations. Darcy's law relates the velocity of the groundwater flow to the change in the potential head and is written as Equation (IV-1) for 2-D rectangular media. On the other hand, the continuity equation, assuming a steady-state scenario with no sources and sinks, can be represented as Equation (IV-2).

$$\mathbf{v} = -\kappa\boldsymbol{\nabla}\mathrm{h} \quad \text{or} \quad \mathrm{v_x} = -\kappa_\mathrm{x}\frac{\partial \mathrm{h}}{\partial \mathrm{x}} \quad \text{and} \quad \mathrm{v_y} = -\kappa_\mathrm{y}\frac{\partial \mathrm{h}}{\partial \mathrm{y}} \tag{IV-1}$$

$$\boldsymbol{\nabla} \times \mathbf{v} = 0 \quad \text{or} \quad \frac{\partial \mathrm{v_x}}{\partial \mathrm{x}} + \frac{\partial \mathrm{v_y}}{\partial \mathrm{y}} = 0 \tag{IV-2}$$

The Laplace equation is then obtained introducing Equation (IV-1) in Equation (IV-2), leading to the governing equation in anisotropic soils (Equation (IV-3)).

$$\kappa_\mathrm{x}\frac{\partial^2 \mathrm{h}}{\partial \mathrm{x}^2} + \kappa_\mathrm{y}\frac{\partial^2 \mathrm{h}}{\partial \mathrm{y}^2} = 0 \tag{IV-3}$$

For an isotropic soil ($\kappa_x=\kappa_y=\kappa$) Equation (IV-3) is simplified to

$$\frac{\partial^2 \mathrm{h}}{\partial \mathrm{x}^2} + \frac{\partial^2 \mathrm{h}}{\partial \mathrm{y}^2} = 0.$$

The boundary conditions of the scenario are now presented to complete the mathematical model. In this scenario, only first and second-class conditions are employed. First class condition (also known as Diritlech condition) is presented in Equation (IV-4) and reflects a constant value of water potential in a given boundary. Second class (homogeneous) condition, or Neumann condition, is applied in impervious borders (Equation (IV-5)). These equations, when second class condition is homogeneous, are written as

$$\mathrm{h} = \mathrm{h_{o,r}} \qquad \text{at boundary regions 1,2…r} \qquad \text{(first class)} \tag{IV-4}$$

$$\left.\frac{\partial \mathbf{v}}{\partial \mathrm{n}}\right|_\mathrm{s} = 0 \qquad \text{at boundary regions 1,2…s} \qquad \text{(second class)} \tag{IV-5}$$

where n is the direction perpendicular to the impermeable boundary.

As commented in Chapter II, these kind of flow problems can also be studied employing the stream function variable, Ψ. Relations between stream function and velocity components are given by Equation (IV-6).

$$v_x = \frac{\partial \Psi}{\partial y} = -\kappa_x \frac{\partial h}{\partial x}, \; v_y = -\frac{\partial \Psi}{\partial x} = -\kappa_y \frac{\partial h}{\partial y} \qquad \text{(IV-6)}$$

In this way, because $\frac{\partial^2 h}{\partial x \partial y} = \frac{\partial^2 h}{\partial y \partial x}$, a new Laplace-type expression for anisotropic soils can be expressed as a function of this variable, Equation (IV-7),

$$\frac{1}{\kappa_y}\frac{\partial^2 \Psi}{\partial x^2} + \frac{1}{\kappa_x}\frac{\partial^2 \Psi}{\partial y^2} = 0 \qquad \text{(IV-7)}$$

If Equation (IV-7) is multiplied by the factor $\kappa_x \kappa_y$, it is reduced to

$$\kappa_x \frac{\partial^2 \Psi}{\partial x^2} + \kappa_y \frac{\partial^2 \Psi}{\partial y^2} = 0$$

This is an expression quite like Equation (IV-3). When modelling isotropic soils, Equation (IV-7) is simplified to $\frac{\partial^2 \Psi}{\partial x^2} + \frac{\partial^2 \Psi}{\partial y^2} = 0$. Moreover, boundary conditions can be translated to these variables. Due to the relation Ψ-h (Equation (IV-6)), the physical meaning of these new conditions changes. Diritlech condition, Equation (IV-8), reflects a constant value of flow along the boundary while Neumann homogenous condition, Equation (IV-9), applies to boundary where the value of the flow crossing it does not vary.

$\Psi = \Psi_{o,p}$ at boundary regions 1,2…p (first class) (IV-8)

$\left.\frac{\partial \Psi}{\partial n}\right|_q = 0$ at boundary regions 1,2…q (second class) (IV-9)

Clearly, Equations (IV-8) and (IV-9) are related to Equations (IV-4) and (IV-5) because the stream function values can be easily obtained by numerical integration of Equation (IV-6), as commented in Chapter II. The nomenclature of the scenario is presented in Figure 4.1, while the boundary conditions can be seen in Figure 4.2.

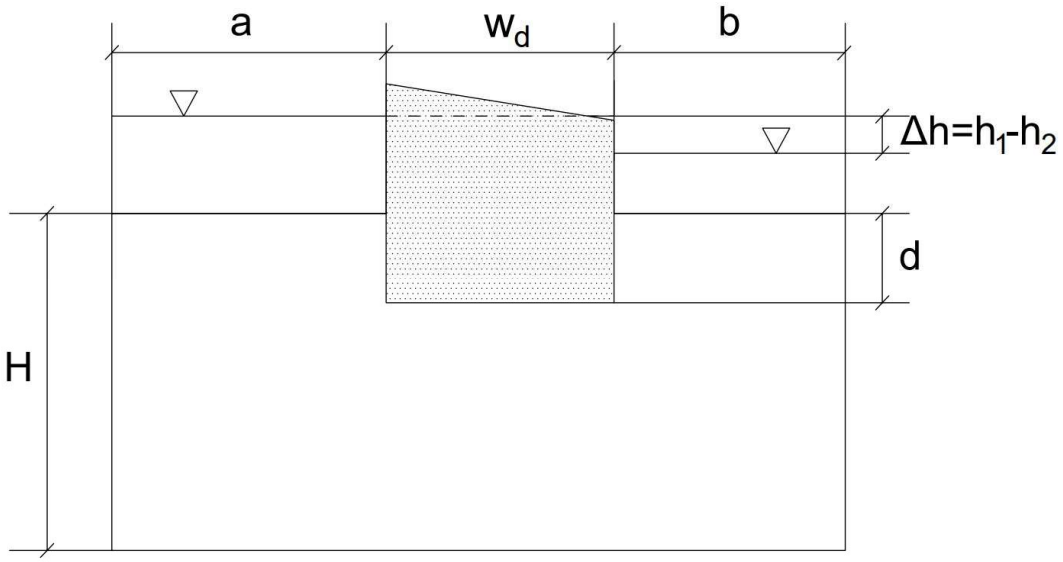

Figure 4.1. Nomenclature of the studied problem

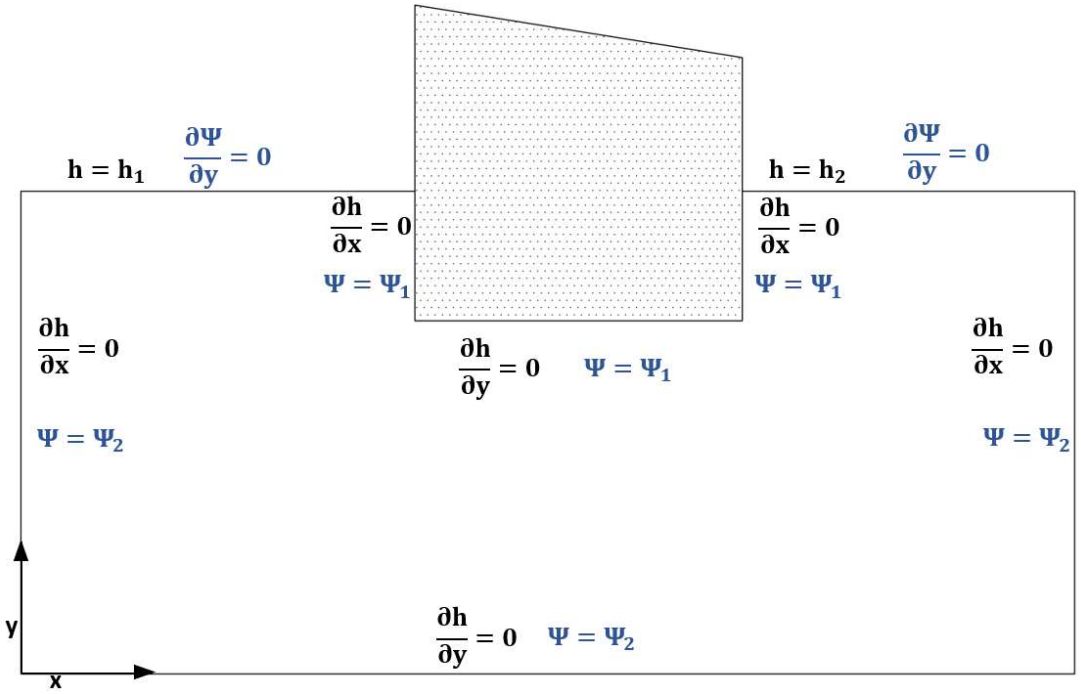

Figure 4.2. Boundary conditions of the studied problem

IV.2.1.2 Dimensionless governing equation and discriminated monomials

According to Figure 4.1 and choosing the following references for this scenario:

H: stratum thickness
w_d: dam width
Δh: water potential variation,

the dimensionless variables are

$$x' = \frac{x}{w_d}, y' = \frac{y}{H}, h' = \frac{h}{\Delta h} \quad \text{(IV-10)}$$

and the dimensionless governing equation turns to be

$$\frac{\kappa_x}{{w_d}^2}\frac{\partial^2 h'}{\partial x^{2}} + \frac{\kappa_y}{H^2}\frac{\partial^2 h'}{\partial y'^2} = 0 \quad \text{(IV-11)}$$

From Equation (IV-11) it can be deduced that the reference value Δh is not involved in the solution of h (x,y). Moreover, if the derivative factors $\frac{\partial^2 h'}{\partial x'^2}$ and $\frac{\partial^2 h'}{\partial y'^2}$ are of an order of magnitude unity due to the ranges chosen for the dimensionless variables h', x' and y', the coefficients $\frac{\kappa_x}{{w_d}^2}$ and $\frac{\kappa_y}{H^2}$ must be the same order of magnitude and the only dimensionless group that can be obtained from the governing equation

$$\pi_1 = \frac{\kappa_x H^2}{\kappa_y {w_d}^2}, \quad \text{(IV-12)}$$

has a value close to unity. Referring to the physical meaning of this coefficient and considering that the dimensions of the numerator and denominator are the inverse of time [T^{-1}], it is interesting to write π_1 as $\frac{(1/\kappa_y {w_d}^2)}{(1/\kappa_x H^2)}$. With this, the ratio can be interpreted as the quotient of the time a fluid takes to run a distance w_d in a medium of conductivity κ_y and the time the same fluid takes to run a distance H in a medium of conductivity κ_x. It is an interpretation which involves, for the same fluid, physical and geometrical properties in such a way that a value of π_1 higher than one does not necessary imply that the horizontal hydraulic conductivity is higher than the vertical conductivity, and vice versa. In any case, π_1 is the most relevant data group of these scenarios, considering 'data' groups those in which unknowns do not appear.

Note that this group was deduced in Chapter III by other dimensional reasoning. As presented in that chapter, monomial π_1 can be obtained thank to dimensional equation that is given to the anisotropic parameters permeability (k) or hydraulic conductivity (κ), in which the employed potential variable is given its own dimensions (in this case, $[h]=L_{wc}$). This dimensional equation is also used when deducing the dimensionless form of some of the unknown variables.

Nevertheless, other monomials rule these scenarios, which are connected to the geometry of the problem. In the case of a dam with or without foundation, the geometrical parameters are (see Figure 4.1):

a: upstream horizontal length of the medium,
b: downstream horizontal length of the medium,
d: depth of the dam foundation (when there is no foundation, it takes a value of zero).

The parameters w_d and H are also involved in the new dimensionless groups, which are:

$$\pi_2 = \frac{\mathrm{d}}{\mathrm{H}} \qquad \text{(IV-13)}$$

$$\pi_3 = \frac{\mathrm{a}}{\mathrm{w_d}} \qquad \text{(IV-14)}$$

$$\pi_4 = \frac{\mathrm{a}}{\mathrm{b}} \qquad \text{(IV-15)}$$

These groups can also be interpreted physically. π_2 expresses the importance of the depth of the foundations in front of the total depth of the scenario, a ratio that determines the aspect of the flow patterns for both head potential and stream function variables. If π_2 takes a value of 0, then the dam does not have foundation and this group is deleted. π_3 or its reverse, $\frac{\mathrm{w_d}}{\mathrm{a}}$, reflects the relevance of the region under dam (with impervious vertical boundaries) in relation with the upstream region with permeable upper boundary. Finally, π_4 determines the flow net asymmetry of the upstream and downstream regions.

Referring now to the global unknown dimensionless groups, let us begin with the groundwater flow, perhaps the unknown of most interest in porous media, in either dam or well scenarios. Groundwater flow in 2-D domains presents the following dimensional equation

$$Q = \frac{[L_x][L_y][L_z]}{[T][L_z]} = \frac{[L_x][L_y]}{[T]} \quad \text{(IV-16)}$$

Revising reference manuals, as Muskat [1937], several solutions for isotropic media presents dimensionless values of Q. In order to obtain it, the value is divided by the product of the water potential and the hydraulic conductivity. That is

$$Q_{nondim} = \frac{Q}{\Delta h \kappa} \quad \text{(IV-17)}$$

If a classical dimensional analysis is carried out and a former point of view of the dimension of h and κ, Q_{nondim} seems to have null dimensional equation. Nevertheless, once the discriminated nondimensional technique is applied and anisotropic media are considered (even in the values of κ_x and κ_y are the same), different conclusions are derived. Let us arrive to these conclusions employing the horizontal velocity from Darcy equation.

The average horizontal flow can be written $Q_{ref} = v_x S_x$, where v_x is the horizontal velocity and S_x is the cross-section under the dam. Now, substituting v_x with Equation (IV-2) and $S_x = L_y L_z$, the reference flow turns into $Q_{ref} = -\kappa_x \frac{\partial h}{\partial x} L_y L_z$. In this point, the variables can be replaced with parameters of the scenario providing that $Q_{ref} = -\kappa_x \frac{\Delta h}{w_d} H$, because this is a 2-D problem (L_z=1). According to Equation (IV-12), $\frac{H}{w_d} \sim \sqrt{\frac{\kappa_y}{\kappa_x}}$, the final equation for Q_{ref} can be written as

$$Q_{ref} = \sqrt{\kappa_x \kappa_y} \Delta h \quad \text{(IV-18)}$$

This expression has been employed by different authors (Castany [1971], de Cazenove [1961]) when considering anisotropic soils, but they did not set a formal demonstration of its use. Then, the value of the dimensionless groundwater group is finally written as

$$\pi_Q = \frac{Q}{\sqrt{\kappa_x \kappa_y} \Delta h} \quad \text{(IV-19)}$$

Another interesting variable is the pore pressure under the dam, one of the destabilising actions that can influences the safety of the structure. This is a local quantity whose value varies along the length of the dam base. Figure 4.3 shows a scheme of the components that determine this variable. It consists on a rectangular area (I), which is positional due to the depth of the foundation (d) and/or the value of the water head downstream the dam, and an energetic one

(II) that depends on the water head change generated by the dam-soil set. This last area can be considered as triangular.

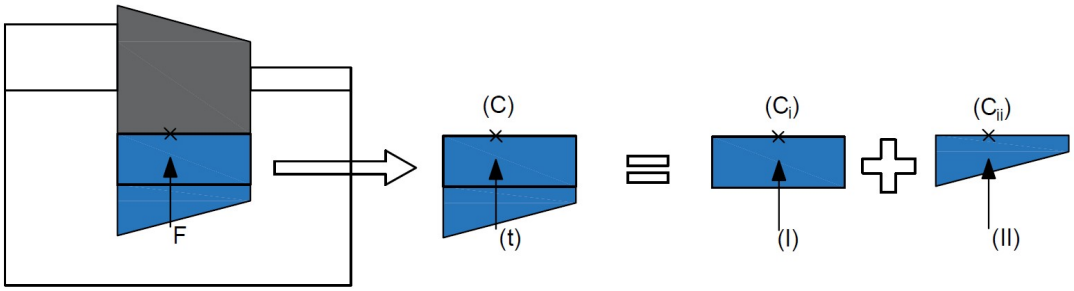

Figure 4.3. Scheme of the components of the pore pressure

Therefore, the dimensionless expression for the pore pressure variable is a manner to only study the energetic part.

$$u_{dimensionless} = \frac{u}{\Delta h \gamma_w} - \frac{h_2+d}{\Delta h} = \frac{\frac{u}{\gamma_w}-(h_2+d)}{\Delta h} = \pi_u \qquad \text{(IV-20)}$$

Other variables of interest are the uplift pressure and its application point under de dam. The first is a global quantity resulting from the integration of the pore pressure right under the dam along its base width. Considering the energetic part (II), since area (I) only appears due to geometry and not because of the flow itself, the dimensionless form of this variable writes as

$$UF_{nondim} = \frac{UF-\gamma_w w_d (d+h_2)}{\gamma_w w_d \Delta h} = \pi_{UF} \qquad \text{(IV-21)}$$

As regards the application point of the uplift force, the distance from this point to the dam heel is the ratio between the momentum due to the pore pressure (integrated along the width of the dam) and the uplift force. In order to obtain its dimensionless value, we must separately consider the application point of the rectangular area (C_i = 0.5·w_d) and that of the almost triangular one (C_{ii} between 0.33·w_d and 0.5·w_d). For the last, the dimensionless form is given by

$$C_{nondim} = \frac{\frac{c}{w_d} * UF-(d+h_2)*w_d*\gamma_w*0.5}{UF-(d+h_2)*w_d*\gamma_w} = \pi_C \qquad \text{(IV-22)}$$

Finally, we study the quantity 'average exit gradient', $I_{e,ave}$, which is also an important variable whose value is indicative to prevent piping and ensure the safety of the structure. Piping phenomenon appears in the flow exit zone and advances inside the medium It is explained by the iso potential lines concentration in the corners (speed increase) and soil mass decrease in favour of soil stability. This is the reason why the analysis is always carried out downstream the structure, next to it. There are standards, such as Eurocode-7 [2004], that propose methods to calculate exit gradients (I) only considering a zone of negligible thickness for its calculations (the

difference of water head between the highest and the lowest point of the dam foundation divided by this length). In this way, the only information contributing is that adjacent to the retaining structure.

Harr also studied this phenomenon, presenting graphics and formulation for obtaining the value of the exit gradient at the surface point right downstream the retaining structure (i_e), which means that, again, only information from the point right after the dam is used. Nevertheless, Harr also came up with a larger area, so more realistic calculations can be carried out, obtaining an average exit gradient, $I_{e,ave}$. The area Harr suggested was the buried length as its vertical length and half of the buried length as the horizonal length. This area, however, only works in isotropic soils. In this thesis, a different area is suggested: the vertical length would still be the buried length, and the horizontal length would be half of the vertical multiplied by an anisotropy ratio. Therefore, for problems of flow under dams without sheet piles, the vertical length, l_v, would be the dam foundation, d, while the horizontal length l_h, is $\frac{l_y}{2}\sqrt{\frac{\kappa_x}{\kappa_y}}$. The studied area is shown in Figure 4.4.

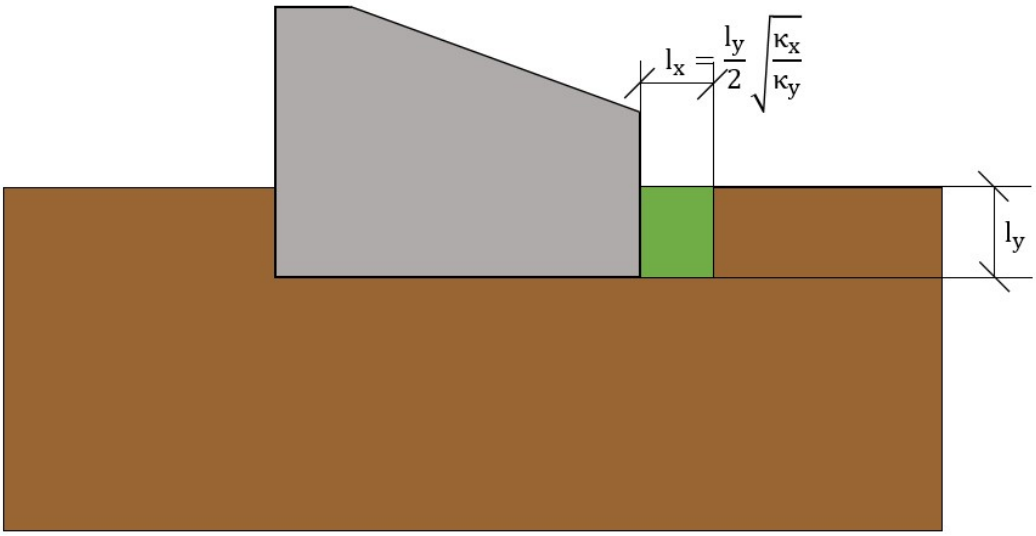

Figure 4.4. Area for the calculation of the average exit gradient ($I_{e,ave}$)

As any other gradient, the average exit gradient has been traditionally considered as dimensionless because it is the ratio of two lengths. However, considering discrimination it does have units, $\left[I_{e,ave}\right] = \frac{L_{wc}}{L_y}$. The discriminate dimensionless expression for this variable is then

$$\pi_{Ie,ave} = \frac{I_{e,ave} \cdot H}{\Delta h} \tag{IV-23}$$

In this way, summarizing and applying Pi theorem, unknown dimensionless groups are functions of these data monomial.

$$\pi_Q = f(\pi_1, \pi_2, \pi_3, \pi_4) \quad \text{(IV-24)}$$

$$\pi_{UF} = f(\pi_1, \pi_2, \pi_3, \pi_4) \quad \text{(IV-25)}$$

$$\pi_C = f(\pi_1, \pi_2, \pi_3, \pi_4) \quad \text{(IV-26)}$$

$$\pi_{Ie,ave} = f(\pi_1, \pi_2, \pi_3, \pi_4) \quad \text{(IV-27)}$$

The dimensionless pore pressure distribution is also function of the dimensionless position under the dam, $x' = \frac{x}{w_d}$.

$$\pi_u = f(x', \pi_1, \pi_2, \pi_3, \pi_4) \quad \text{(IV-28)}$$

IV.2.1.3 Universal abaci

Along this section, abaci and formulation for the unknowns described in the former section are presented as function of the data monomials, π_1, π_2, π_3 and the dimensionless location x'. π_4 has not been used because, after running a significance number of simulations, negligible relevance of this monomial was observed. In these abaci, the formulation is presented for each variable. The first curves presented in this section are those of groundwater flow (Figures 4.5 to 4.8).

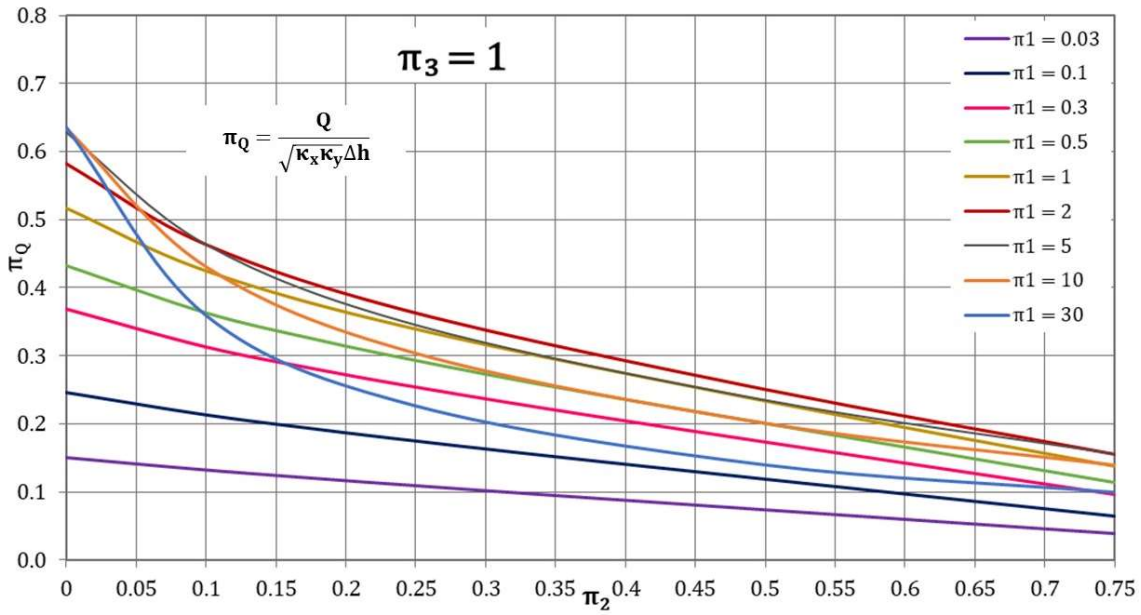

Figure 4.5. Dimensionless groundwater flow for $\pi_3 = 1$

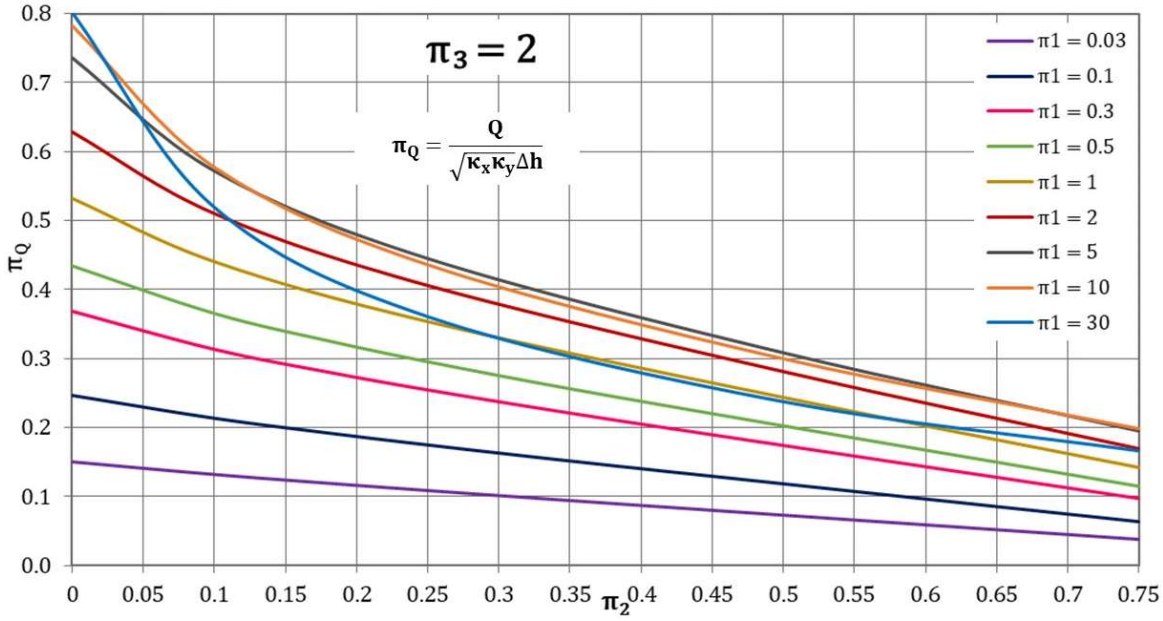

Figure 4.6. Dimensionless groundwater flow for $\pi_3 = 2$

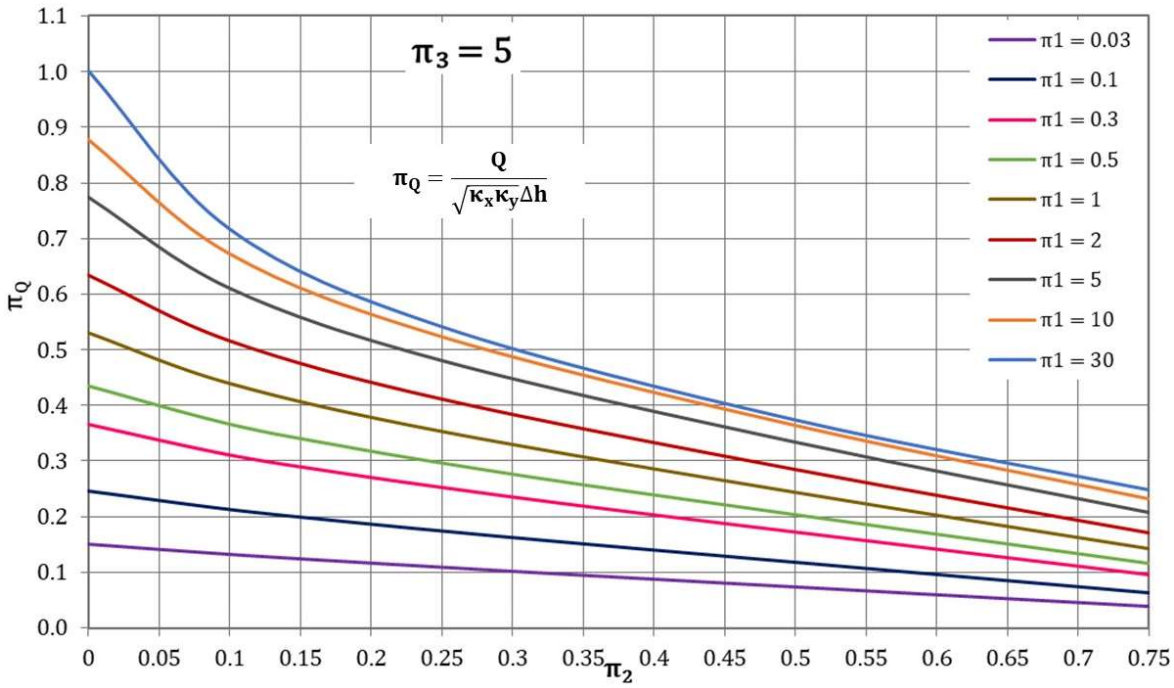

Figure 4.7. Dimensionless groundwater flow for $\pi_3 = 5$

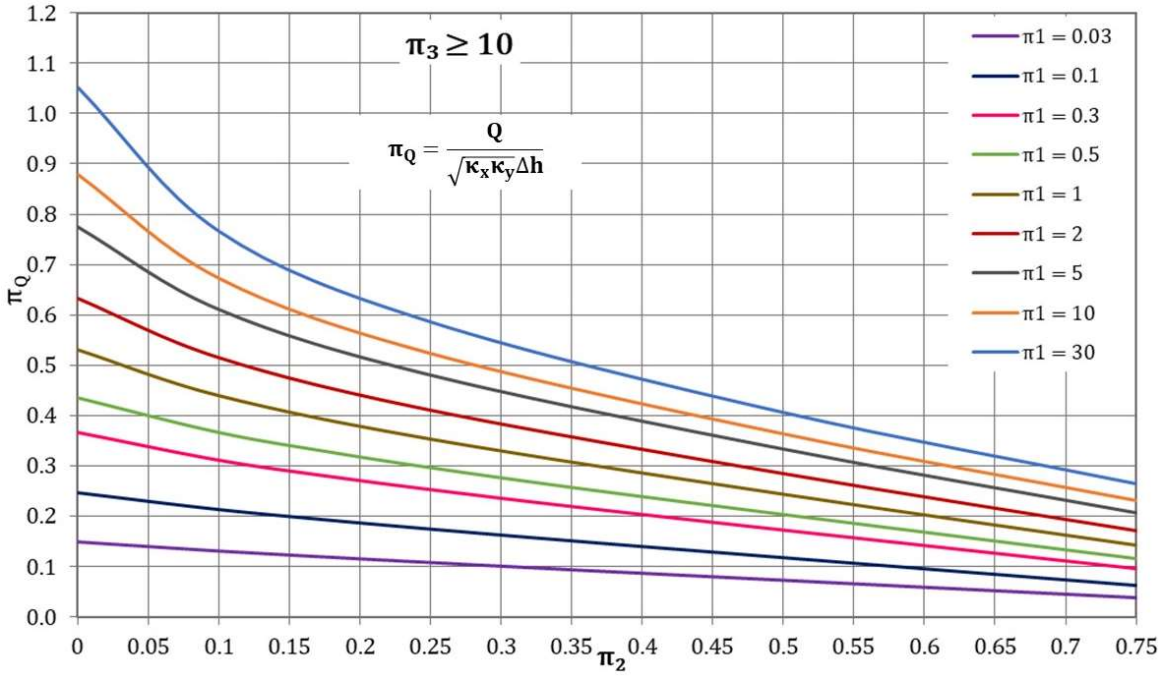

Figure 4.8. Dimensionless groundwater flow for $\pi_3 = 10$

According to Figures 4.5 to 4.8, the groundwater flow under the gravity dam increases with the value of π_1, which makes sense because this group (as mentioned before) is a comparison of the ease of the water to flow through porous media horizontally and vertically in the domain. In this way, as the nature of the flow under the dam is basically horizontal, the higher π_1, the easier it is for the flow to occur and the larger the value of the total flow is.

However, some exceptions appear for dams with foundations, that is, $\pi_2>0$. If focusing on π_Q for high values of π_1 (≥5) but low values of π_3 (1 and 2), the horizontal flow grows and is restricted at the same time, so in Figure 4.5 curves for π_1 = 5, 10 and 30 are below the curves corresponding to smaller values. Moreover, in Figure 4.6 the same occurs for π_1 = 10 and 30. In Figures 4.7 and 4.8, where the medium is horizontally large enough, the effect of π_1 on π_Q is the one expected. The monomial π_2 is also highly decisive in the groundwater flow under the dam. This group presents the depth of the structure foundation, so as it increases, the importance of the vertical flow rises. This is the reason why, as the value of π_2 increases, the dimensionless water flow does the opposite. The importance of π_3 seems to be reduced for low values of π_1, since for π_1=0.03-1, curves π_Q are basically the same for all π_3 studied. This occurs because, since the importance of π_1 is higher than that of π_3, low values of π_1 mean that the vertical flow grows, while large values of π_3 have the opposite meaning. In this way, the effects are somehow compensated.

Let us now show an example of how to use and obtain information from the previous abaci. The scenario to consider presents the following parameters:

w_d = 20 m
H = 20 m
d = 5 m
$\kappa_x = 10^{-6}$ m/s
$\kappa_y = 10^{-6}$ m/s
h_1 = 10 m
h_2 = 0 m
a = b → ∞.

Following Equations (IV-12) to (IV-15), the values of the data monomials (π_1, π_2, π_3 and π_4) are:

π_1 =1
π_2 =0.25
π_3 >10
π_4 =1

As π_3 has a value larger than 10, the abacus to use is that in Figure 4.8. In order to obtain the dimensionless value of the groundwater flow variable, the π_1 =1 curve is chosen (yellow curve) and from it, the value of π_2 =0.25 is read from the horizontal axis. π_Q has a value of 0.35, which, according to Equation (IV-19) leads to a dimensional result of the variable $3.5 \cdot 10^{-6}$ $m^3/s/m$.

The following abaci are those for the pore pressure distribution. These are presented in order to understand the behaviour of the other variables related to this one: uplift force and its application point. For this, as curves for each value of π_1 are very close among them, less values of the monomial have been plotted. Moreover, because a new data monomial is needed for plotting the dimensionless value of the pore pressure distribution (x'), the only value of π_3 that is presented is 10 (Figures 4.9 to 4.13).

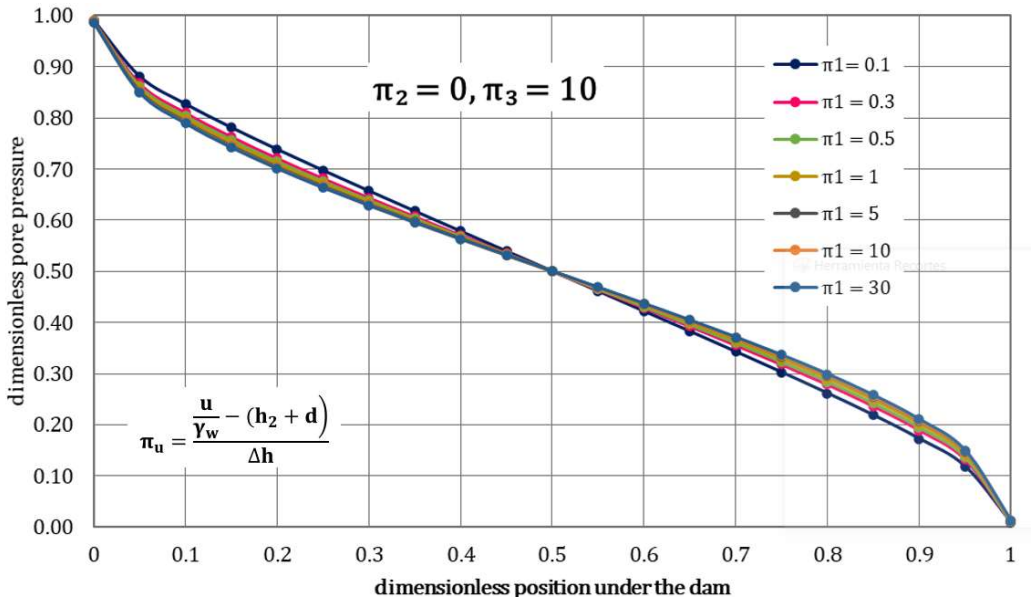

Figure 4.9. Dimensionless pore pressure distribution for π_2 = 0 and π_3 = 10

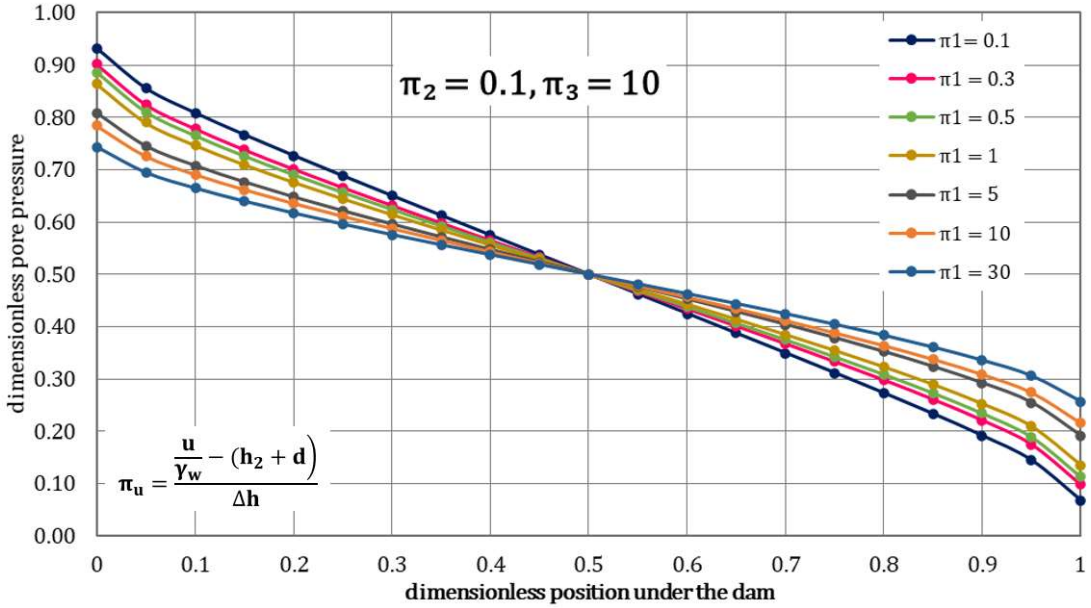

Figure 4.10. Dimensionless pore pressure distribution for $\pi_2 = 0.1$ and $\pi_3 = 10$

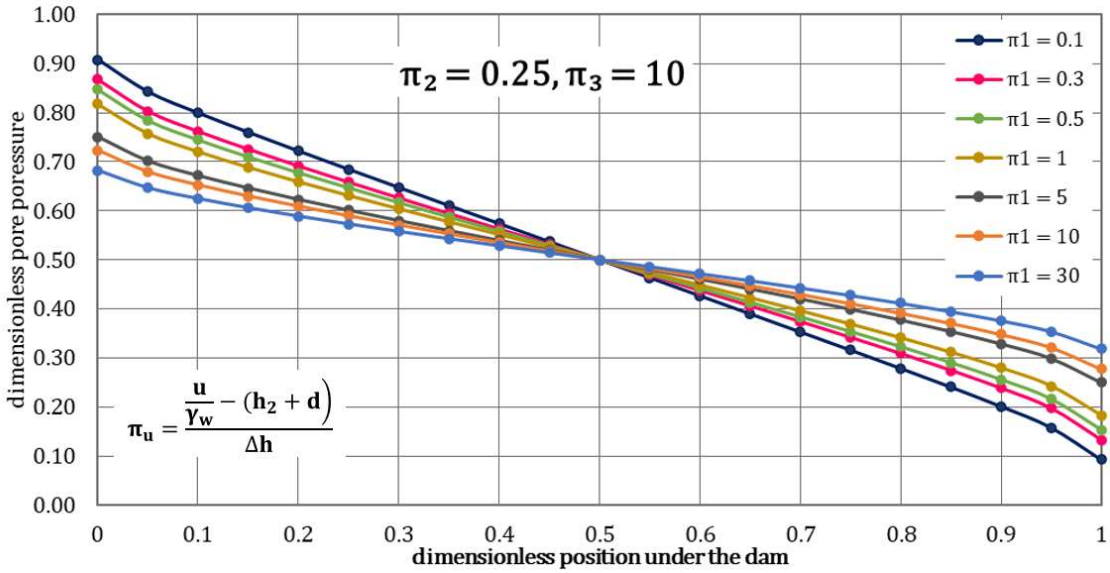

Figure 4.11. Dimensionless pore pressure distribution for $\pi_2 = 0.25$ and $\pi_3 = 10$

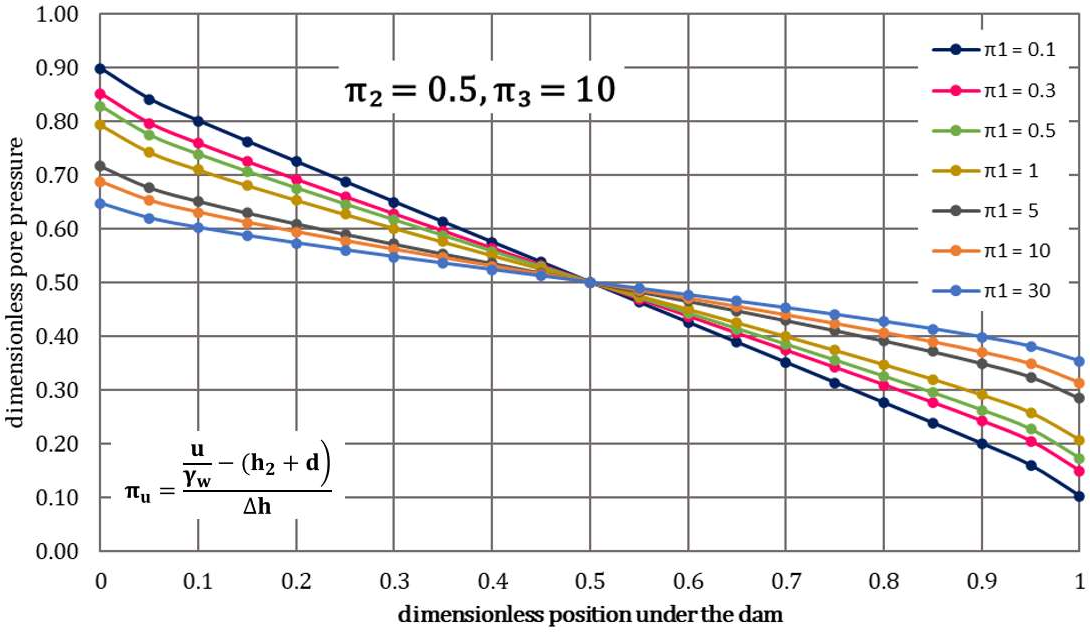

Figure 4.12. Dimensionless pore pressure distribution for $\pi_2 = 0.5$ and $\pi_3 = 10$

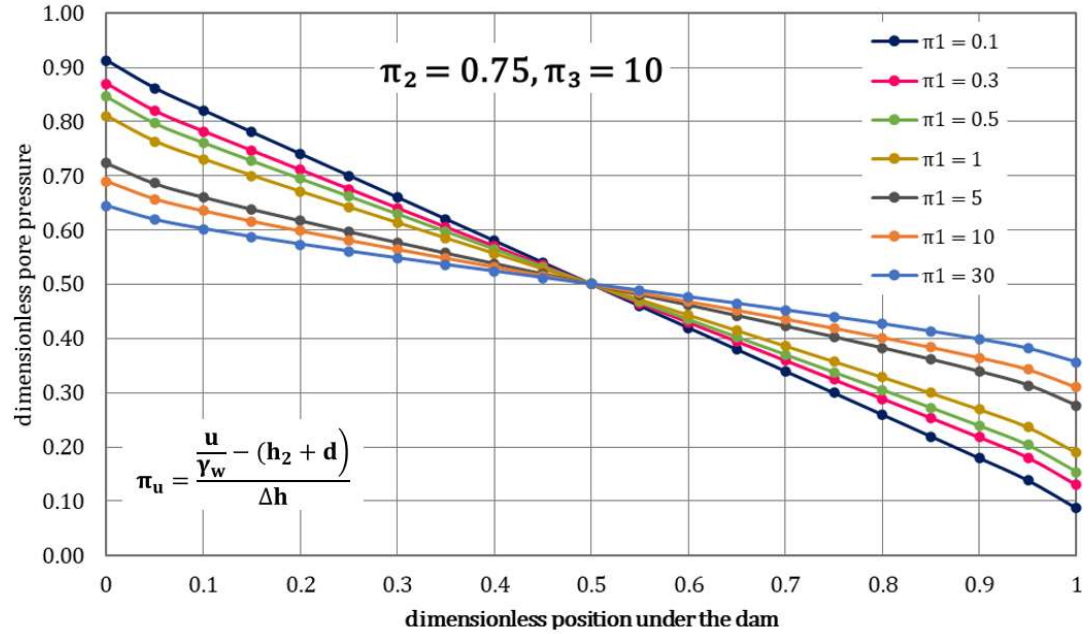

Figure 4.13. Dimensionless pore pressure distribution for $\pi_2 = 0.75$ and $\pi_3 = 10$

From Figures 4.9 to 4.13, the shape of the dimensionless pore pressure distribution is always quasi triangular, as commented before in this chapter. This leads to a dimensionless uplift value of 0.5 for all combinations of π_1, π_2 and π_3. This means that

$$\pi_{UF} = \frac{F - w_d \gamma_w (h_2 + d)}{w_d \gamma_w \Delta h} = 0.5 \qquad \text{(IV-29)}$$

In addition, these curves also help us to understand the behaviour of the other variable related to the pore pressure distribution: the application point of the uplift force, specifically the effect

of the little variation between the abaci for π_2 = 0.5 and 0.75. Referring to the effect of π_1 on π_u, it is almost negligible when studying dams without a foundation (all curves are very close to each other). If we now focus on the dams with foundations, we can see that the higher the value of π_1, the more different the curves are to those corresponding to a dam without a foundation.

As the formulation for the dimensionless uplift forces has already been shown and explained, the next dimensionless variable presented is the dimensionless application point, π_c. These abaci are depicted in Figures 4.14 to 4.17.

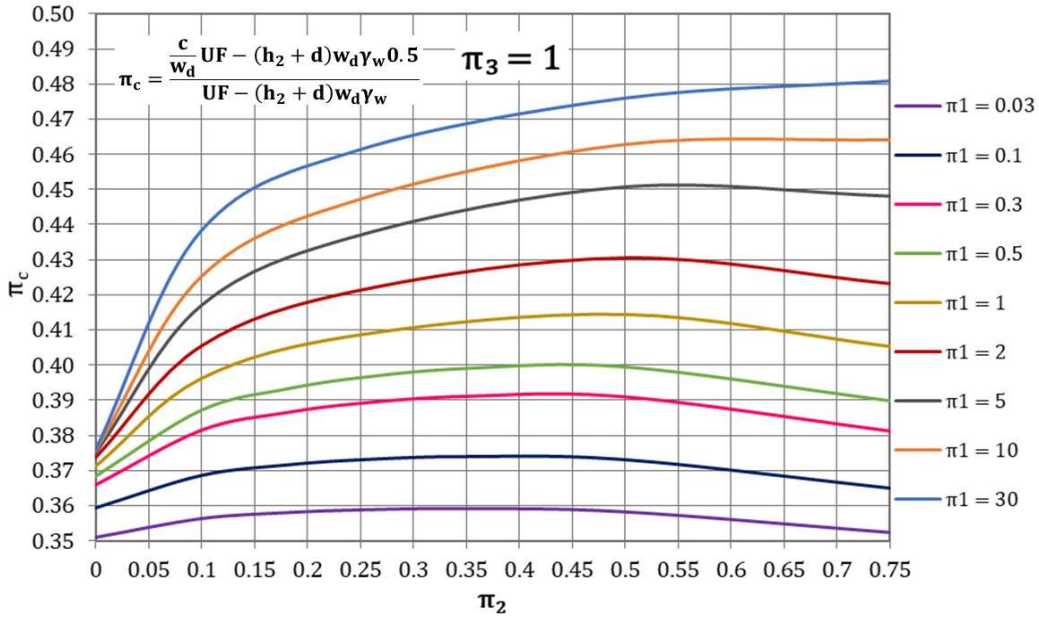

Figure 4.14. Dimensionless application point of the uplift force for π_3= 1

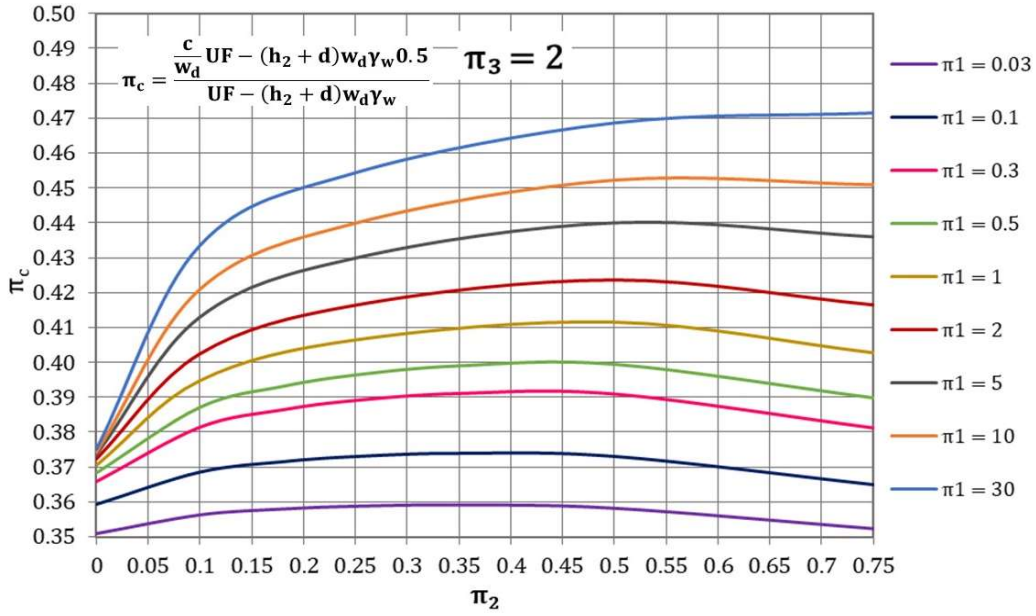

Figure 4.15. Dimensionless application point of the uplift force for π_3 = 2

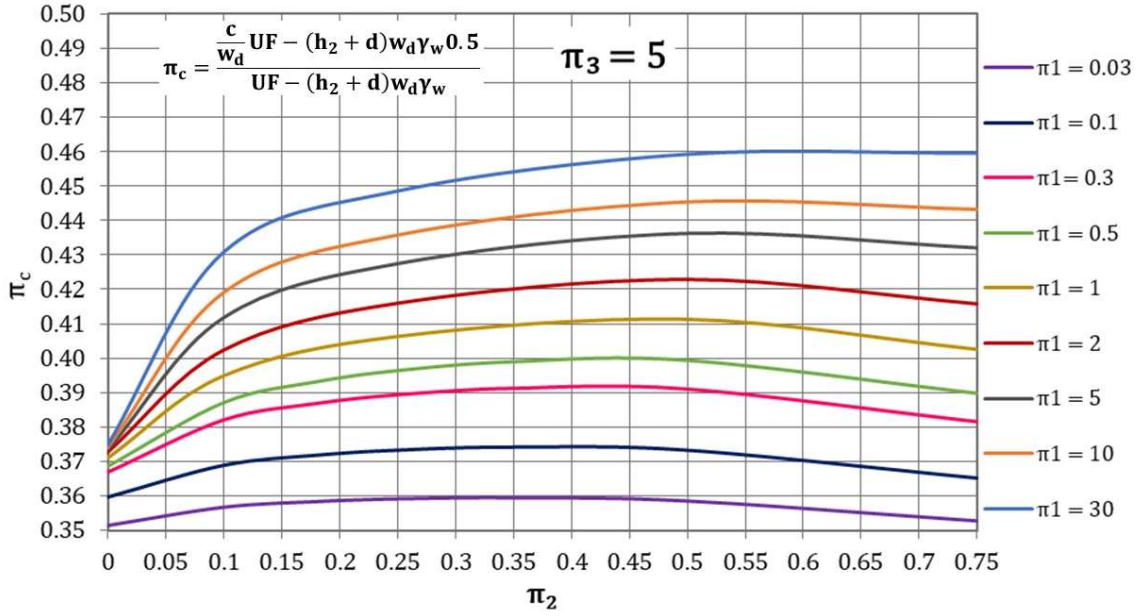

Figure 4.16. Dimensionless application point of the uplift force for $\pi_3 = 5$

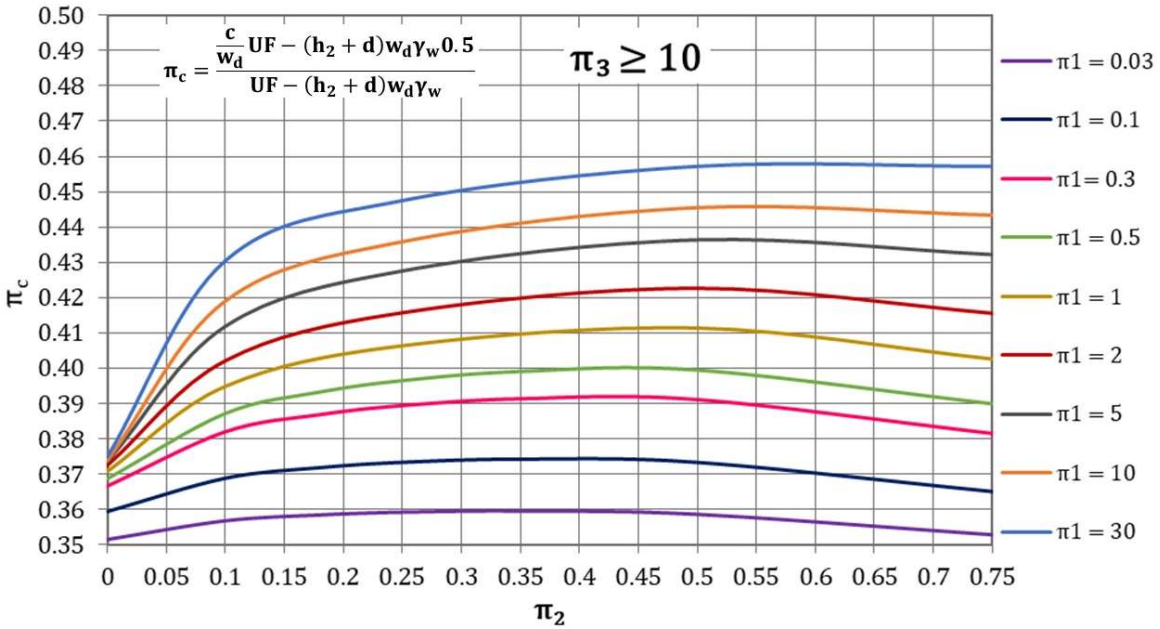

Figure 4.17. Dimensionless application point of the uplift force for $\pi_3 = 10$

Focusing on the effect of π_1 on the value of π_C, the higher the importance of the horizontal flow is, the bigger the value of the studied group. This happens because the increase of the horizontal flow means a decrease of the pore pressure in the upstream half of the dam base, occurring the opposite in the downstream side. In this way, the application point of the uplift force is shifted towards the geometrical centre of the dam base.

The monomial π_2 also affects the dimensionless application point of the uplift force. The study of the dimensional form of this variable shows that it moves towards the dam centre as the foundation is deeper, since the rectangular area of the dimensional pore pressure function becomes larger. However, as we have seen in Figures 4.12 and 4.13, for (approximately) $\pi_2 > 0.5$, the shape of the energetic area of the distribution hardly changes, while the rectangular area is increased. This is the reason why the value of π_C, which exclusively depends on the quasi-triangular area, decreases at the end of all the curves. Group π_3 affects π_C depending on the value of π_1. For the curves representing low values of π_1, π_C is hardly affected by π_3, although for larger values of the permeability monomial, the increase of π_3 leads to a decrease in π_C.

Finally, abaci related to the dimensionless form of the average exit gradient, $I_{e,ave}$, are shown in Figures 4.18 to 4.21. This variable is not presented for $\pi_2 = 0$ because there is not buried length in which it can be calculated, so the curves begin in $\pi_2 = 0.1$.

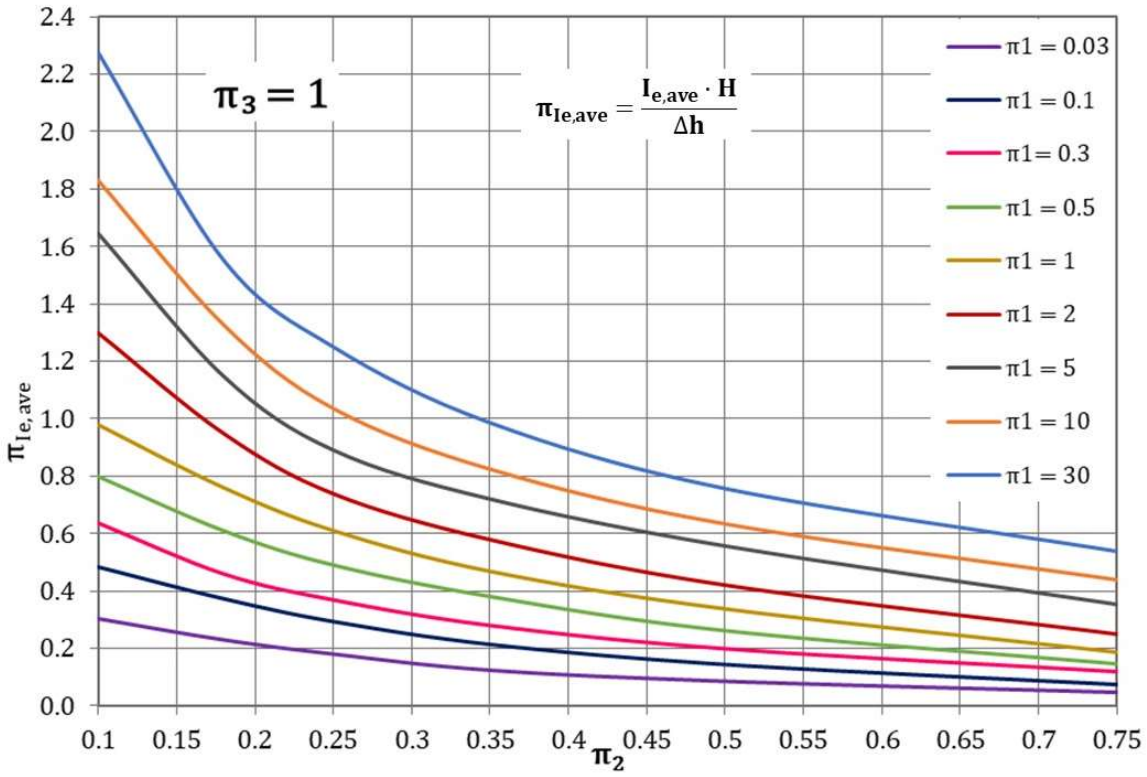

Figure 4.18. Dimensionless average exit gradient for $\pi_3 = 1$

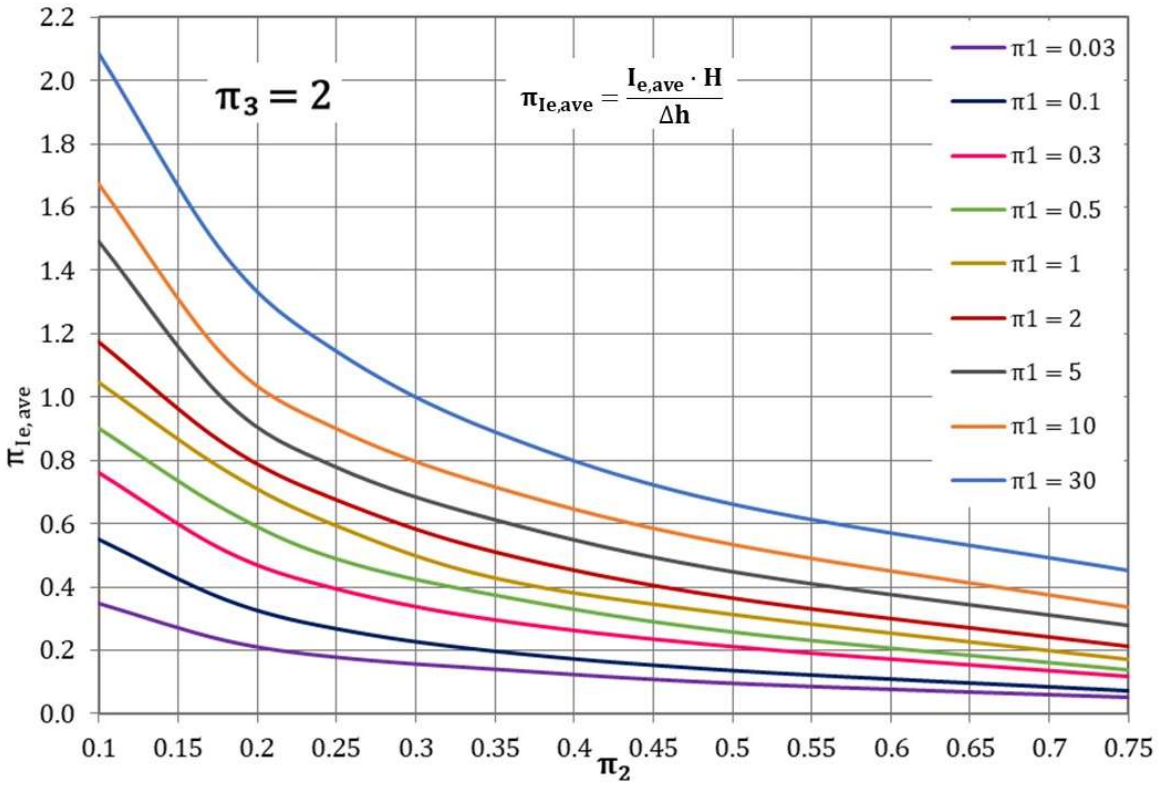

Figure 4.19. Dimensionless average exit gradient for $\pi_3 = 2$

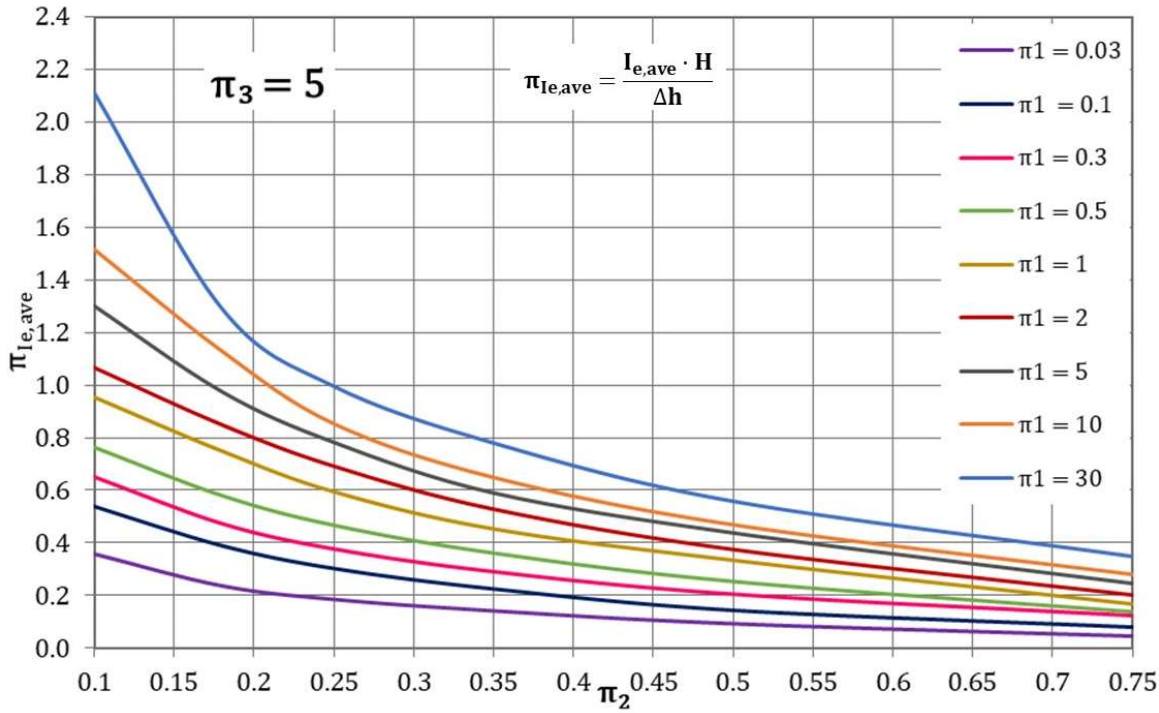

Figure 4.20. Dimensionless average exit gradient for $\pi_3 = 5$

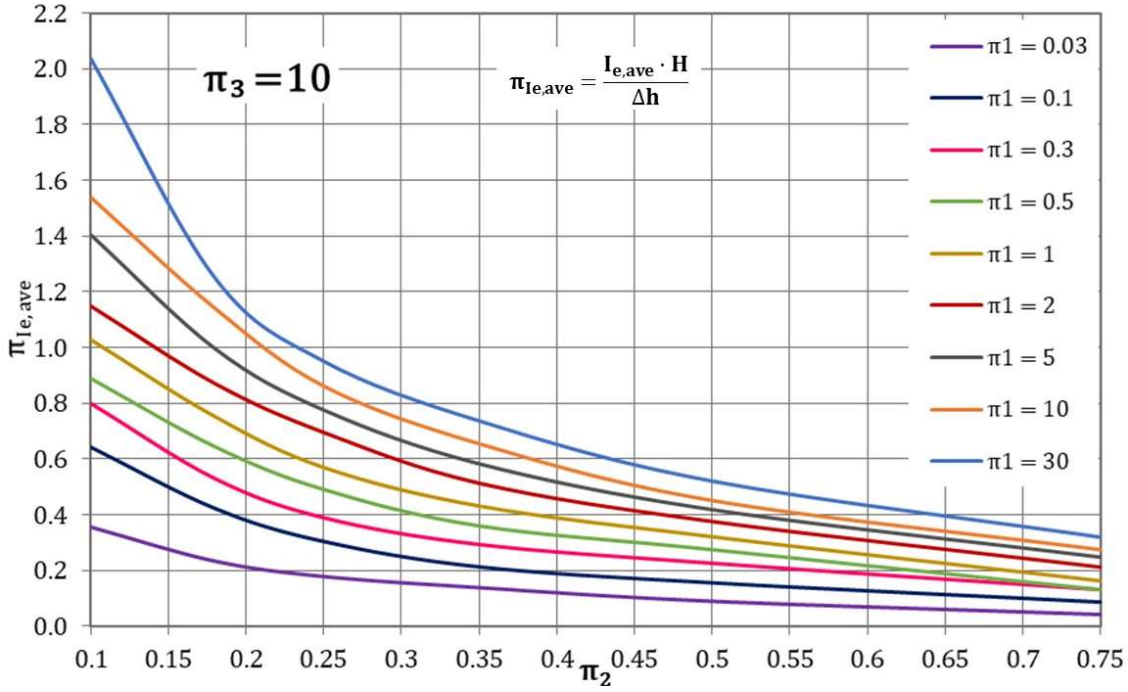

Figure 4.21. Dimensionless average exit gradient for $\pi_3 = 10$

When studying the effect of π_1 on the variable $\pi_{Ie,ave}$, it appears to be very similar to that on π_Q and π_C, because the increase of the importance of the horizontal flow means a higher variation of the water head on the lateral of the dam foundation instead of under it.

If we now focus on how π_2 affects $\pi_{Ie,ave}$, the effect is also evident, since the increase of the length of the dam foundation leads to a decrease of the average exit gradient. It occurs because, although the variation of the water head increases with the buried length, this increase is lower than that of the length.

The effect of π_3 is not as evident as those of π_1 and π_2 because it is somehow related to these two monomials. If comparing Figures 4.18 and 4.19 ($\pi_3 = 1$ and 2 respectively), they show that for $\pi_1 < 1$, values of $\pi_{Ie,ave}$ are lower for $\pi_3 = 1$, until certain values of π_2 (different for each π_1) from which curves for $\pi_3 = 1$ and 2 give almost the same values.

The $\pi_1 = 1$ curves for $\pi_{Ie,ave}$ in Figures 4.18 and 4.19 behave in a similar way, although for a certain value of π_2, instead of presenting the same values, they change their trend, and the values related to $\pi_3 = 1$ are higher than those of $\pi_3 = 2$. If $\pi_1 > 1$, then the curve $\pi_3 = 2$ is always lower than that of $\pi_3 = 1$.

Figures 4.20 and 4.21 show the curves for $\pi_3 = 5$ and 10 respectively, with a different behaviour than that of Figures 4.18 and 4.19. Curves for low values of π_1 (0.03-0.5) behave similarly than in the previous case: this is, the one of lower value of π_3 (5 in this pair) shows lower values than that of π_3 until a given value of π_2; from this point the values are almost the same for $\pi_3 = 5$ and

10. Curves for π_1=1-10 behave in the same way as those for π_1=1 in Figures 4.18 and 4.19, which means that the trend changes from a certain value of π_2. Finally, curves for π_1 = 30 in Figures 4.20 and 4.21 do not behave as in Figures 4.18 and 4.19, because for all values of π_2 (and, therefore, for all lengths of the dam foundations) $\pi_{le,ave}$ values are higher for π_3 = 5 than for π_3 = 10.

IV.2.2 Flow under gravity dams with sheet pile. Universal curves

IV.2.2.1 Mathematical model

Adding a new structure under the gravity dam increases the complexity of the studied problem, since the sheet pile means two new boundary conditions (or three if the pile thickness is not considered as negligible). However, introducing the new part of the structure does not alter the governing equation, which is still the Laplace expression presented in Equation (IV-3)

$$\kappa_x \frac{\partial^2 h}{\partial x^2} + \kappa_y \frac{\partial^2 h}{\partial y^2} = 0 \qquad \text{(IV-3)}$$

Moreover, the boundary conditions can also be expressed in the same way as they were presented for the scenario of flow under dams without sheet piles (Equations (IV-4) and (IV-5)):

$h = h_{o,r}$ at boundary regions 1,2…r (first class) (IV-4)

$\left.\frac{\partial v}{\partial n}\right|_s = 0$ at boundary regions 1,2…s (second class) (IV-5)

The Laplace expression employing the stream function variable does not change whether the dam scenario presents sheet piles or not, so Equation (IV-7) can also be used.

$$\frac{1}{\kappa_y}\frac{\partial^2 \Psi}{\partial x^2} + \frac{1}{\kappa_x}\frac{\partial^2 \Psi}{\partial y^2} = 0 \qquad \text{(IV-7)}$$

Finally, the boundary conditions for the scenario employing the stream function variable are not affected by the presence of a sheet pile, so Equations (IV-8) and (IV-9) can also be used

$\Psi = \Psi_{o,p}$ at boundary regions 1,2…p (first class) (IV-8)

$\left.\frac{\partial \Psi}{\partial n}\right|_q = 0$ at boundary regions 1,2…q (second class) (IV-9)

In this way, the mathematical model for problems of flow under gravity dams with a sheet pile is completely presented. Figure 4.22 shows the nomenclature of the scenario, while Figure 4.23 presents the boundary conditions of the problem.

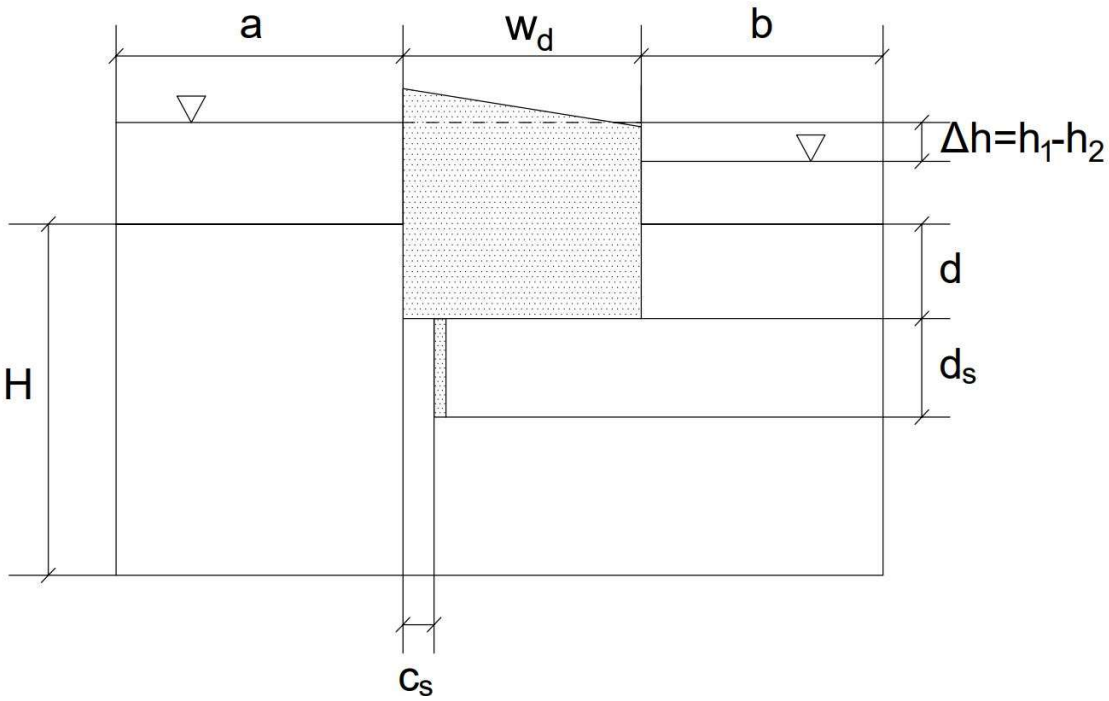

Figure 4.22. Nomenclature of the studied problem

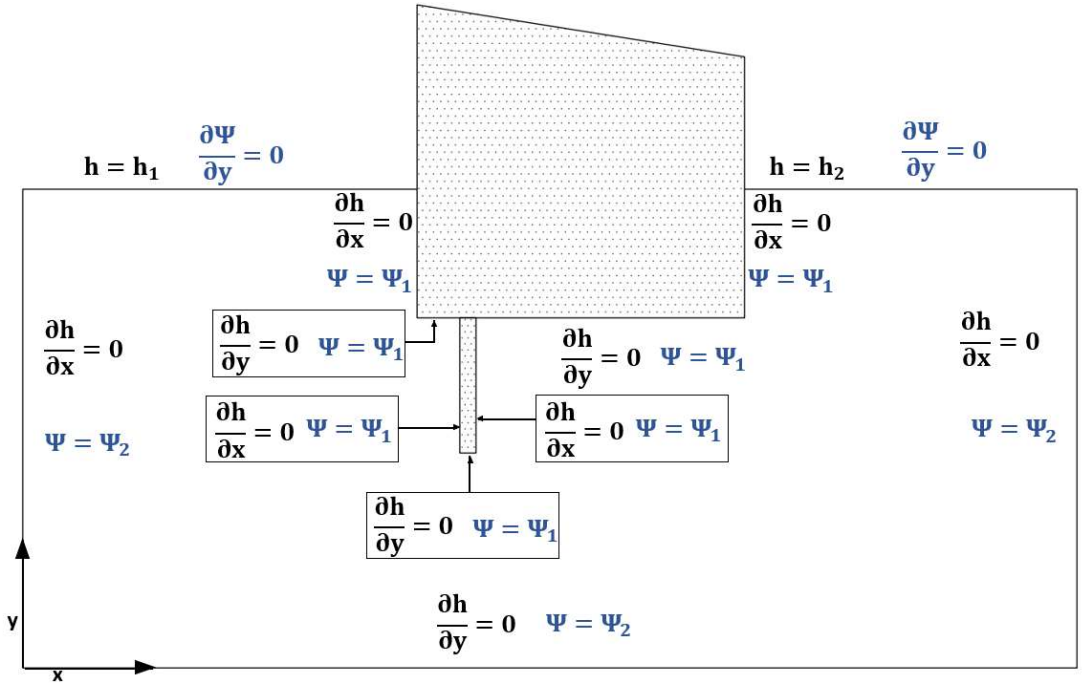

Figure 4.23. Boundary conditions of the studied problem

IV.2.2.2 Dimensionless governing equation and discriminated monomials

The first governing group of this kind of problem is the same as in the previous scenario, π_1, Equation (IV-14).

$$\pi_1 = \frac{\kappa_x H^2}{\kappa_y {w_d}^2} \quad \text{(IV-12)}$$

In addition, as presented in Figure 4.22, many of the geometric parameters in this scenario are also in the scenario of flow under dams without a sheet pile, as well as the boundary conditions (Figure 4.23). This means that monomials π_2, π_3 and π_4 are the same as in Section IV.2.2, shown in Equations (IV-13), (IV-14) and (IV-15).

$$\pi_2 = \frac{d}{H} \quad \text{(IV-13)}$$

$$\pi_3 = \frac{a}{w_d} \quad \text{(IV-14)}$$

$$\pi_4 = \frac{a}{b} \quad \text{(IV-15)}$$

The meaning of monomials π_1, π_2, π_3 and π_4 in this kind of scenarios is the same as in problems of flow under dams. Due to the sheet pile that now is placed under the dam base, two new monomials appear. These have two new parameters:

d_s: length of the sheet pile.
c_s: position of the sheet pile under the dam, measured from the dam heel.

Along the thesis, the sheet pile thickness (w_s) is assumed as negligible, so it is not involved in the modelling of the problem and, therefore, in the monomial definitions. Thus, the two new dimensionless groups governing the problems are

$$\pi_5 = \frac{c_s}{w_d} \quad \text{(IV-30)}$$

$$\pi_6 = \frac{d_s}{H} \quad \text{(IV-31)}$$

If, for some reason, the sheet pile thickness was not negligible, then an extra monomial would present a similar expression as presented in Equation (IV-32).

$$\pi_7 = \frac{w_s}{w_d} \quad \text{(IV-32)}$$

π_5 is linked to π_6 in the following way: if the last group presents a value of 0 (that is, there is a sheet pile of no length, so there is no sheet pile), then π_5 must no appear, since it loses its meaning. Nevertheless, the opposite does not happen; presenting a value of $\pi_5 = 0$ means that the sheet pile is located right at the heel of the dam (in the same way that a value of 1 means

that it has been placed at the toe of the structure). In a similar way, π_2 and π_6 are also connected, since both are related to the vertical direction of the scenario and, therefore, to the vertical water flow. If both values are defined as done in this thesis, where d and d_s are divided by H, then Equation (IV-33) must be met:

$$\pi_2 + \pi_6 = \frac{d}{H} + \frac{d_s}{H} < 1 \quad \text{(IV-33)}$$

Any other situation cannot be possible: if this addition is higher than one, it means that the vertical length of the whole retaining structure is larger than the stratum thickness, which, of course, is impossible; if this addition is exactly one, then there is an impervious contour along the whole stratum length, and no flow happens.

If the sheet pile thickness was not negligible, then another verification should be done, as shown in Equation (IV-34).

$$\pi_5 + \pi_7 = \frac{c_s}{w_d} + \frac{w_s}{w_d} < 1 \quad \text{(IV-34)}$$

Considering now the six dimensionless groups, the scenario presented in Section IV.1.2 can also be modelled and studied, as long as π_6 takes value 0 and, as explained previously, π_5 loses its meaning.

When a retaining structure is composed by a gravity dam and a sheet pile underneath it, new variables are studied apart from underground water flow, average exit gradient, uplift force and the application point of this force. The former monomials, however, are studied following the same expressions shown in Equations (IV-19), (IV-21), (IV-22) and (IV-23). Pore pressure distribution is only presented in this section in order to help to understand the data provided in abaci for uplift force and its application point.

$$\pi_Q = \frac{Q}{\sqrt{\kappa_x \kappa_y}\Delta h} \quad \text{(IV-19)}$$

$$UF_{nondim} = \frac{UF - \gamma_w w_d (d + h_2)}{\gamma_w w_d \Delta h} = \pi_{UF} \quad \text{(IV-21)}$$

$$C_{nondim} = \frac{\frac{c}{w_d} * UF - (d + h_2) * w_d * \gamma_w * 0.5}{UF - (d + h_2) * w_d * \gamma_w} = \pi_C \quad \text{(IV-22)}$$

$$\pi_{Ie,ave} = \frac{I_{e,ave} \cdot H}{\Delta h} \quad \text{(IV-23)}$$

The new variables are related to the pore pressure, although in this case, it is the one applied on the sheet pile: upstream and downstream side forces and their application points. The application point is always measured from the contact point of the dam and the sheet pile.

In order to obtain both forces, an integration of the pore pressure right on the surface of the sheet pile must be carried out, as shown in Figure 4.24. As it happened when calculating the uplift force under the dam (t), the foundation depth and the water potential downstream the dam generate a 'positional' pressure with rectangular shape (constant term) applied on both sides of the pile (I). Moreover, since the vertical position along the length of the pile varies, another 'positional' pore pressure appears, and in this case the shape is a triangle (II) because the value increases with depth.

Finally, the energetic part of the pore pressure is due to the hydraulic potential variation (III). Its shape is more arbitrary than the one of the energetic parts of the uplift force, although in some cases it can be considered an irregular triangle.

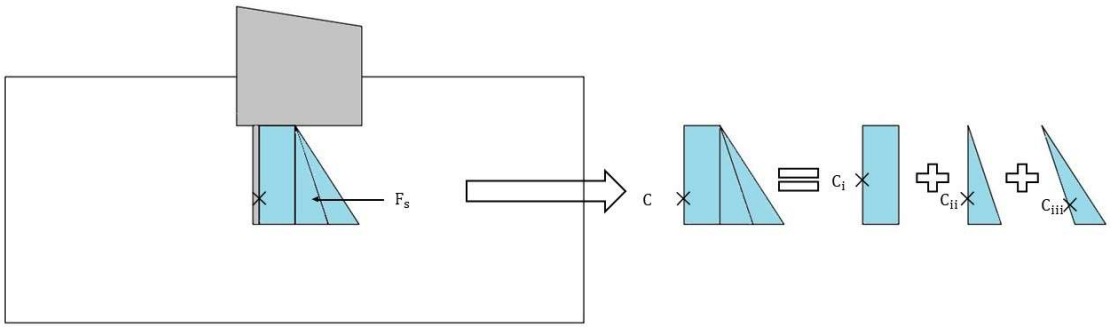

Figure 4.24. Pore pressure distribution along the sheet pile

Then, the procedure to obtain the dimensionless force due to the pore pressure is the same whether the upstream or the downstream side is being considered, Equation (IV-35).

$$F_{xS_{nondim}} = \frac{Force_{xS} - \gamma_w * d_s * (d+h_2) - \gamma_w * {d_s}^2/2}{d_s * \Delta h * \gamma_w} = \pi_{F_{xS}} \quad \text{(IV-35)}$$

Then, for each side of the sheet pile we obtain Equation (IV-36) and Equation (IV-37) for the upstream and downstream sides, respectively.

$$F_{US_{nondim}} = \frac{Force_{US} - \gamma_w * d_s * (d+h_2) - \gamma_w * {d_s}^2/2}{d_s * \Delta h * \gamma_w} = \pi_{F_{US}} \quad \text{(IV-36)}$$

$$F_{DS_{nondim}} = \frac{Force_{DS} - \gamma_w * d_s * (d+h_2) - \gamma_w * {d_s}^2/2}{d_s * \Delta h * \gamma_w} = \pi_{F_{DS}} \quad \text{(IV-37)}$$

This decomposition of the pore pressure into smaller shapes is also necessary in order to calculate the dimensionless value of the application points upstream and downstream the sheet pile (Figure 4.24). In a similar way as for the uplift force, the application point of the rectangular part of the pore pressure (I) is found at $0.5d_s$ (C_i), the one of the triangular part (II) is located at approximately $0.67d_s$ (C_{ii}). The energetic part (III) also has an application point (C_{iii}), whose dimensionless value is the unknown group to find.

As regards the force on the pile side, the formulation is the same to obtain this dimensionless group for both upstream and downstream the pileand is presented in Equation (IV-38).

$$C_{XS_{nondim}} = \frac{\frac{c_{XS}}{d_s} * Force_{XS} - (d+h_2) * d_s * \gamma_w * 0.5 - \frac{{d_s}^2}{2} * \gamma_w * \frac{2}{3}}{Force_{XS} - d_s * (d+h_2) * \gamma_w - \frac{{d_s}^2}{2} * \gamma_w} = \pi_{C_{XS}} \quad \text{(IV-38)}$$

For each side of the sheet pile the expressions are Equation (IV-39) for the upstream side and Equation (IV-40) for the downstream side.

$$C_{US_{nondim}} = \frac{\frac{c_{US}}{d_s} * Force_{US} - (d+h_2) * d_s * \gamma_w * 0.5 - \frac{{d_s}^2}{2} * \gamma_w * \frac{2}{3}}{Force_{US} - d_s * (d+h_2) * \gamma_w - \frac{{d_s}^2}{2} * \gamma_w} = \pi_{C_{US}} \quad \text{(IV-39)}$$

$$C_{DS_{nondim}} = \frac{\frac{c_{DS}}{d_s} * Force_{DS} - (d+h_2) * d_s * \gamma_w * 0.5 - \frac{{d_s}^2}{2} * \gamma_w * \frac{2}{3}}{Force_{DS} - d_s * (d+h_2) * \gamma_w - \frac{{d_s}^2}{2} * \gamma_w} = \pi_{C_{DS}} \quad \text{(IV-40)}$$

These new unknown monomials, together with those presented previously for the case without a sheet pile, are functions of the data monomial.

$$\pi_Q = f(\pi_1, \pi_2, \pi_3, \pi_4, \pi_5, \pi_6) \quad \text{(IV-41)}$$

$$\pi_{UF} = f(\pi_1, \pi_2, \pi_3, \pi_4, \pi_5, \pi_6) \quad \text{(IV-42)}$$

$$\pi_C = f(\pi_1, \pi_2, \pi_3, \pi_4, \pi_5, \pi_6) \quad \text{(IV-43)}$$

$$\pi_{F_{US}} = f(\pi_1, \pi_2, \pi_3, \pi_4, \pi_5, \pi_6) \quad \text{(IV-44)}$$

$$\pi_{F_{DS}} = f(\pi_1, \pi_2, \pi_3, \pi_4, \pi_5, \pi_6) \quad \text{(IV-45)}$$

$$\pi_{C_{US}} = f(\pi_1, \pi_2, \pi_3, \pi_4, \pi_5, \pi_6) \quad \text{(IV-46)}$$

$$\pi_{C_{DS}} = f(\pi_1, \pi_2, \pi_3, \pi_4, \pi_5, \pi_6) \quad \text{(IV-47)}$$

$$\pi_{Ie,ave} = f(\pi_1, \pi_2, \pi_3, \pi_4, \pi_5, \pi_6) \quad \text{(IV-48)}$$

IV.2.2.3 Universal abaci

In order to simplify the abaci presented and explained along this section, some of the monomials are considered with a single value, so the effect of the more relevant ones can be observed. In this way, monomial π_2 keeps a value of 0, so the effect of the dam foundation is not considered, monomial π_3 is given a value of 20, so large scenarios are modelled, and monomial π_4 is 1, since in large scenarios in the horizontal direction this group does not affect much.

The first unknown variable plotted is the dimensionless groundwater flow. For this, two abaci are shown, Figures 4.25 and 4.26. Figure 4.25 clusters the curves for $\pi_5 = 0$ and 1, since this variable has the same values in symmetrical positions. Figure 4.26 presents the values for $\pi_5 = 0.5$.

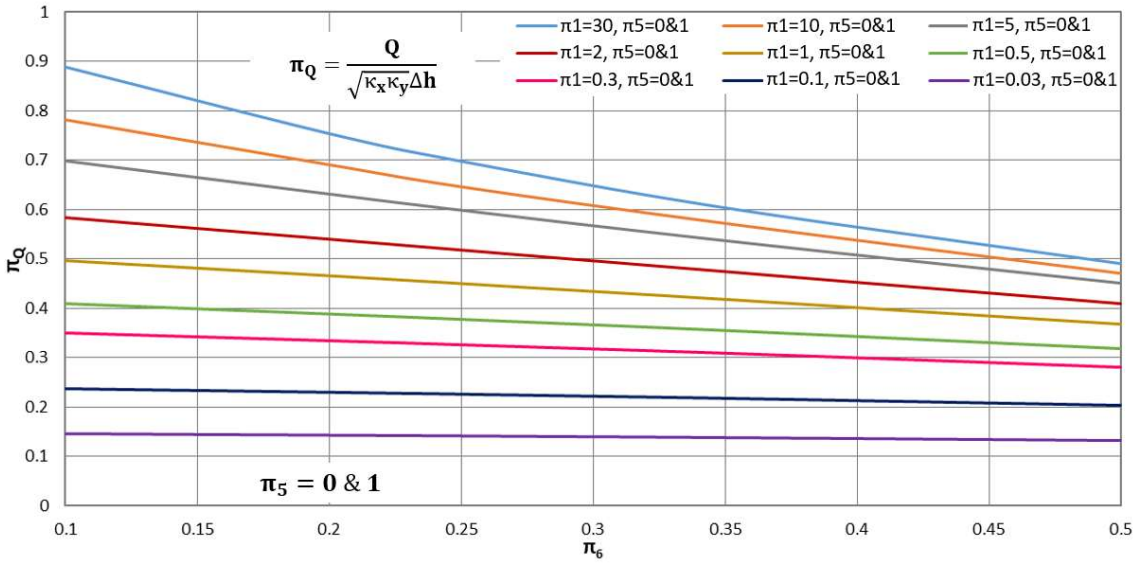

Figure 4.25. Dimensionless groundwater flow for $\pi_5 = 0$ and 1

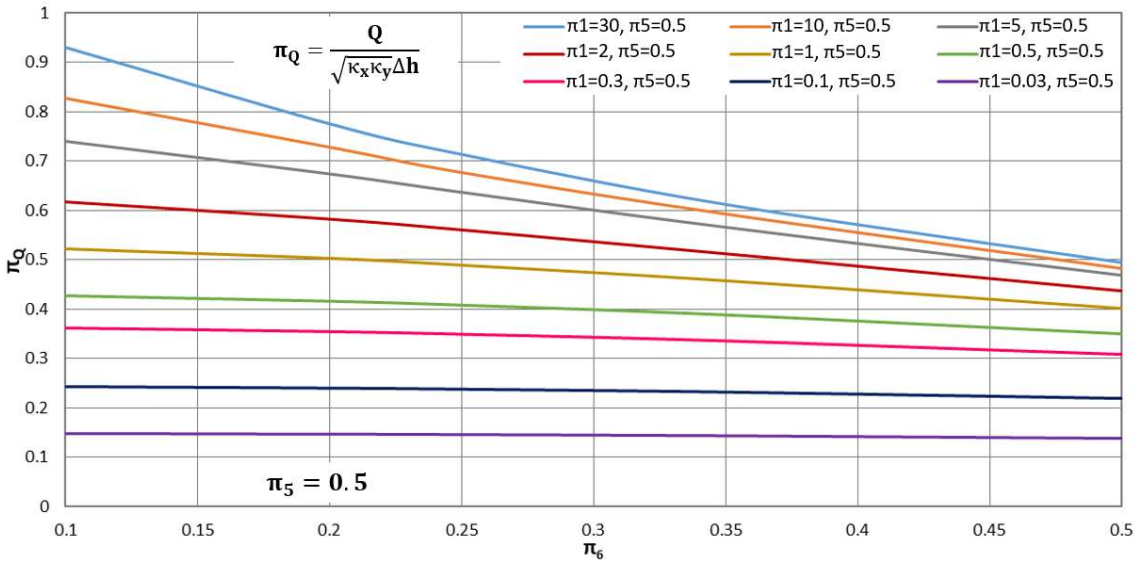

Figure 4.26. Dimensionless groundwater flow for $\pi_5 = 0.5$

Once the simulations that were necessary for plotting the curves in Figure 4.25 had been carried out, it was observed that, as studied in the different references for isotropic soils such as Harr [2012] and Muskat [1937], the value of the water flow is the same when locating the sheet pile at the heel and the toe of the dam. This means that the flow behaves symmetrically respect to the middle point of the dam base. Since the nondimensionalization expression of the

groundwater flow does not consider the position of the sheet pile, the equal values of dimensional water flow lead to the same values of dimensionless water flow. This is the reason why both configurations, $\pi_5 = 0$ and 1, have been plotted with the same curve for each value of π_1.

Moreover, if studying the position of the sheet pile, π_5, comparing Figures 4.25 and 4.26, it can be observed that, when placing the sheet pile at an end of the dam base, the amount of water flow is lower than if it is placed in the centre ($\pi_5 = 0.5$).The effect of monomial π_1 is foreseeable: as π_1 increases, π_Q does too, as the higher the horizontal permeability, the larger the amount of water running from upstream to downstream, in the same way that happened for flow under dam without a sheet pile. If the variable is studied as function of the sheet pile length, π_6, the effect is the same as Harr and Muskat presented in his works for isotropic soils: the dimensionless flow is lower as π_6 increases. If anisotropy is studied, then the effect of π_6 is more remarkable with π_1.

As regards the dimensionless uplift force, the solutions are presented in Figures 4.27 and 4.28 for $\pi_5 = 0$ and $\pi_5 = 1$, respectively. For $\pi_5 = 0.5$ it was observed that the dimensionless value of the uplift pressure takes the same value as if there was no sheet pile, that is, 0.5.

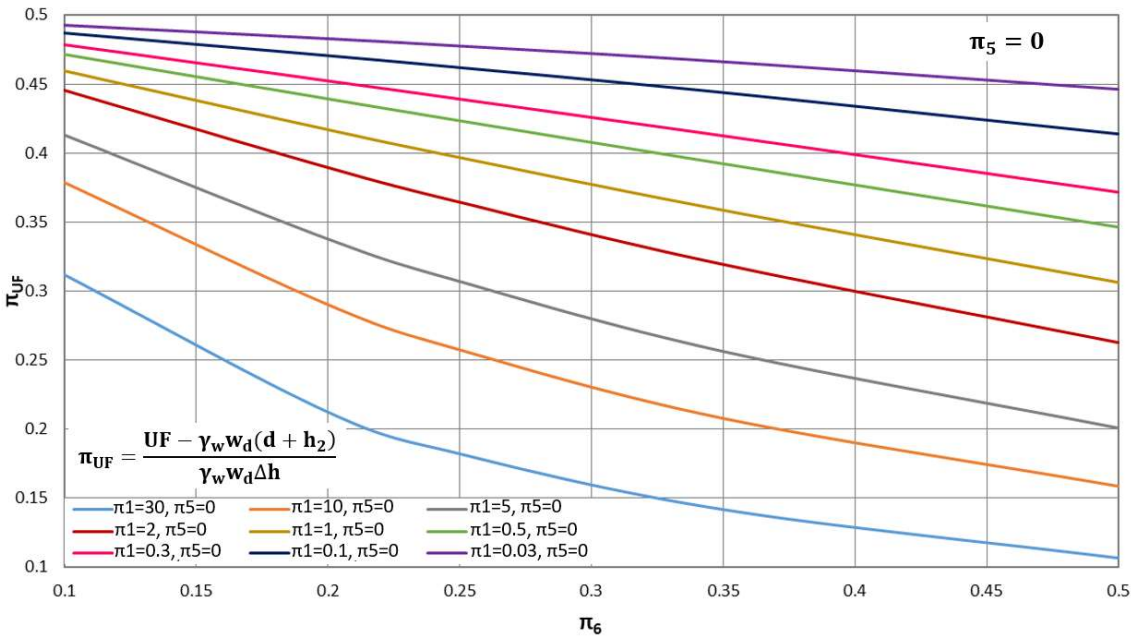

Figure 4.27. Dimensionless uplift force for $\pi_5 = 0$

As it occurred for the curves for the dimensionless groundwater flow (Figure 4.25), there is a relation between the values of π_{UF} when locating the sheet pile at the heel of the dam base (π_5=0) and at the toe of the dam base (π_5=1). After carrying out the different simulations for all $\pi_5 = 0.5$ casuistry, it was observed that, for all the sheet pile lengths (π_6) and all the possible permeability relations (π_1), the dimensionless values of the uplift force are always $\pi_{UF} = 0.5$. As

commented before, this is the same that occurred for the dimensionless value of the uplift force in dams without a sheet pile, where π_{UF} takes the value of 0.5 for the chosen values of π_1, π_2 and π_3. Moreover, manuals such as those of Muskat [1937] and Harr [2012] show that, when locating the sheet pile at the middle of the dam base, the uplift force value is the same as for dams without sheet pile, which would mean that the dimensionless values must be the same too.

For the case of $\pi_5 = 0$, Figure 4.27, the effect of π_6 on the behaviour of π_{UF} is due to the pressure drop caused downstream the pile, which increases with the length of the pile. For this reason, as the pore pressure decreases, the same happens with the uplift force.

Monomial π_1 plays a similar role than π_6, since its increase leads to a higher pressure drop downstream the sheet pile, decreasing the value of π_{UF}.

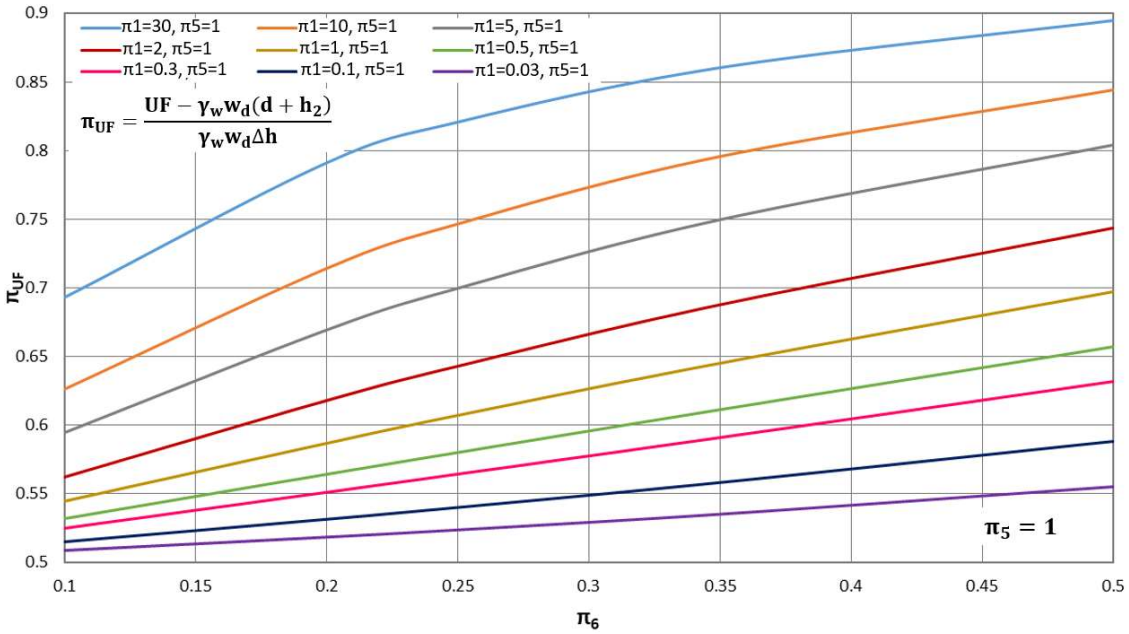

Figure 4.28. Dimensionless uplift force for $\pi_5 = 1$

For $\pi_5 = 1$, Figure 4.28, the behaviour of π_{UF} is the opposite of that in Figure 4.27 for both π_1 and π_6: if locating the sheet pile at the toe of the dam base, its length and a higher horizontal permeability mean a pore pressure increase along the dam base. For this reason, it can be said that the values of π_{UF} for $\pi_5 = 1$ are symmetrical to those for $\pi_5 = 0$ respect to a horizontal axis in $\pi_{UF} = 0.5$.

The next variable to discuss is the application point of the uplift force. In order to understand its behaviour, as commented before, some of the dimensionless pore pressure distribution abaci are also included. Figure 4.29 is the abacus of π_C for $\pi_5 = 0$.

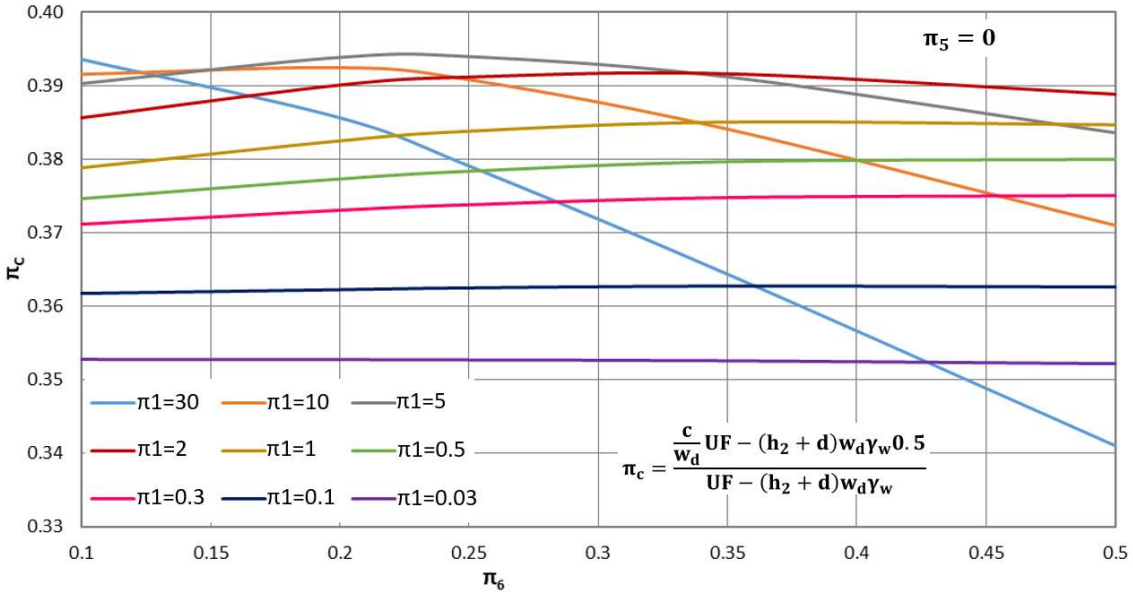

Figure 4.29. Dimensionless application point of the uplift force for $\pi_5 = 0$

Studying the application point when the sheet pile is located at the dam heel ($\pi_5 = 0$), three sets of curves can be distinguished according to π_1 values: low (0.03 and 0.1), medium (0.3-1), and high (2-30).

For low π_1 values, the dimensionless application points present little variation with the sheet pile length (π_6), because the pore pressure curves (presented in Figure 4.30 for $\pi_1 = 0.1$ and all values of π_6) are very close to each other. In this way, the application points are hardly affected.

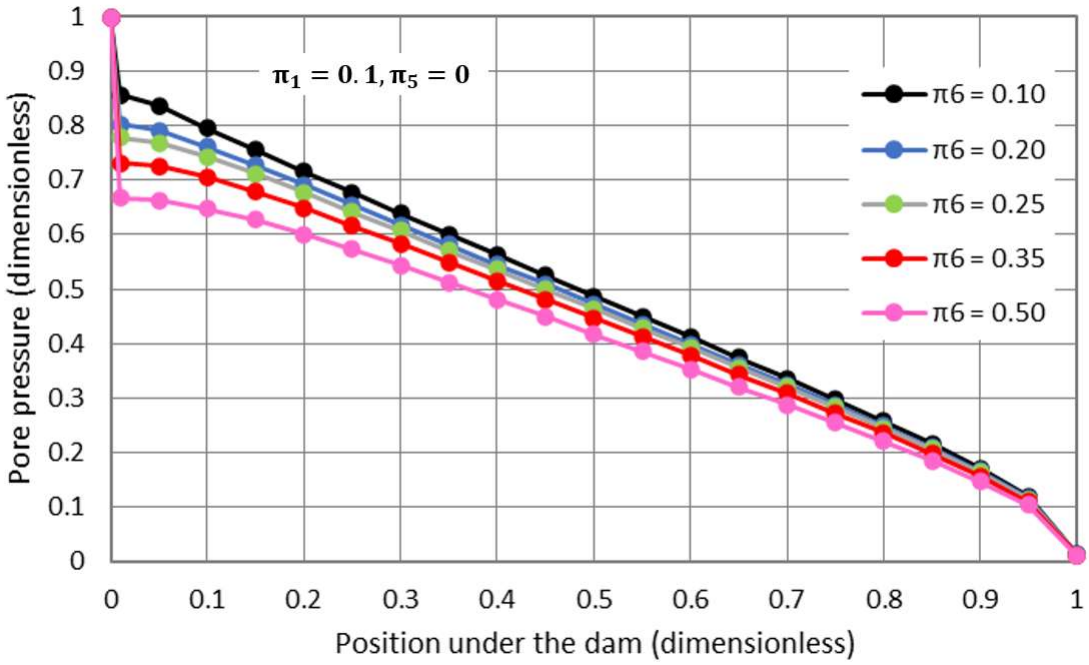

Figure 4.30. Dimensionless pore pressure distribution for $\pi_1 = 0.1$ and $\pi_5 = 0$

If the values of π_C are studied for medium values of π_1, these increase with the sheet pile length. The effect can be observed in Figure 4.31, which shows the pore pressure graphics for all values of π_6 and π_1=1. These curves have more disparate dimensionless pore pressure values on the left half of the dam base, getting lower values as π_6 is incremented. In the right half of the dam base, however, those differences are smaller. All these makes the application point move downstream, increasing the dimensionless value.

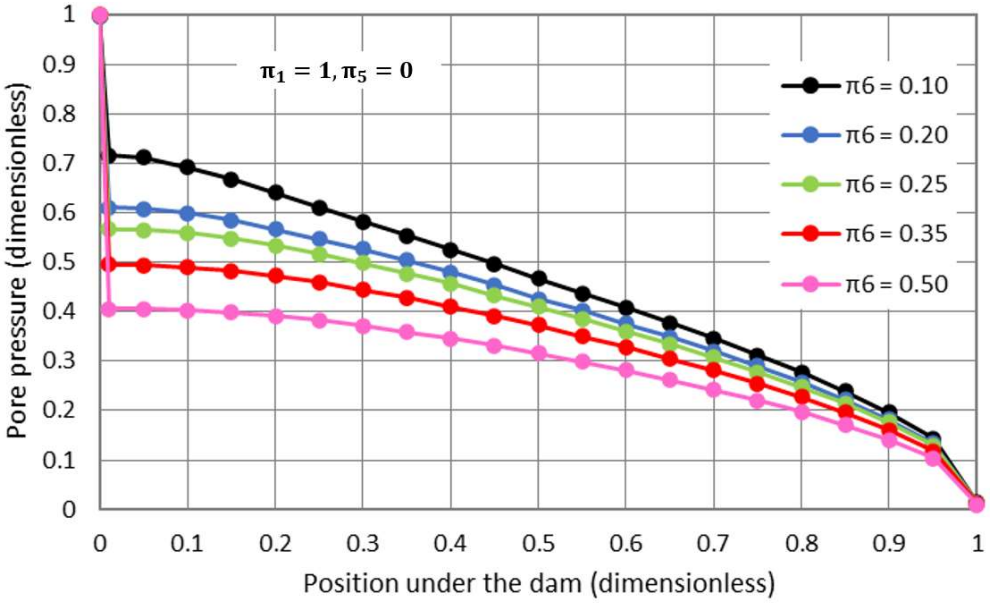

Figure 4.31. Dimensionless pore pressure distribution for $\pi_1 = 1$ and $\pi_5 = 0$

If, still for π_5=0, we studied the application point for high values of π_1, its behaviour is more complex to estimate. According to Figure 4.32 (for $\pi_1 = 10$), the pore pressure curves are different to each other along the whole dam base for each value of π_6.

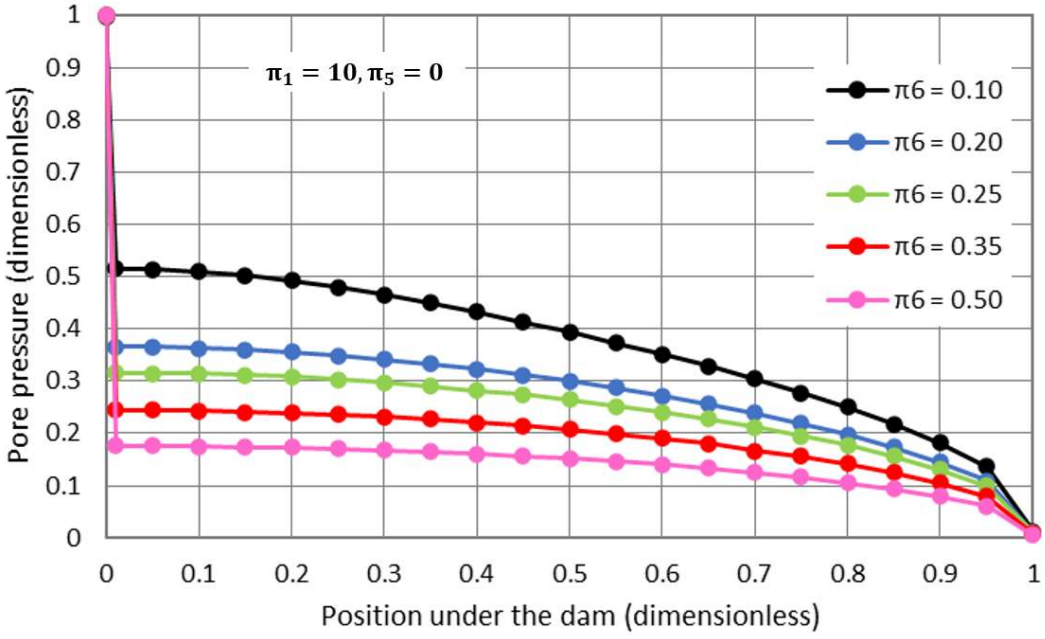

Figure 4.32. Dimensionless pore pressure distribution for $\pi_1 = 10$ and $\pi_5 = 0$

Figure 4.33 shows the behaviour of variable π_C when the sheet pile is placed in the middle of the dam base, $\pi_5 = 0.5$.

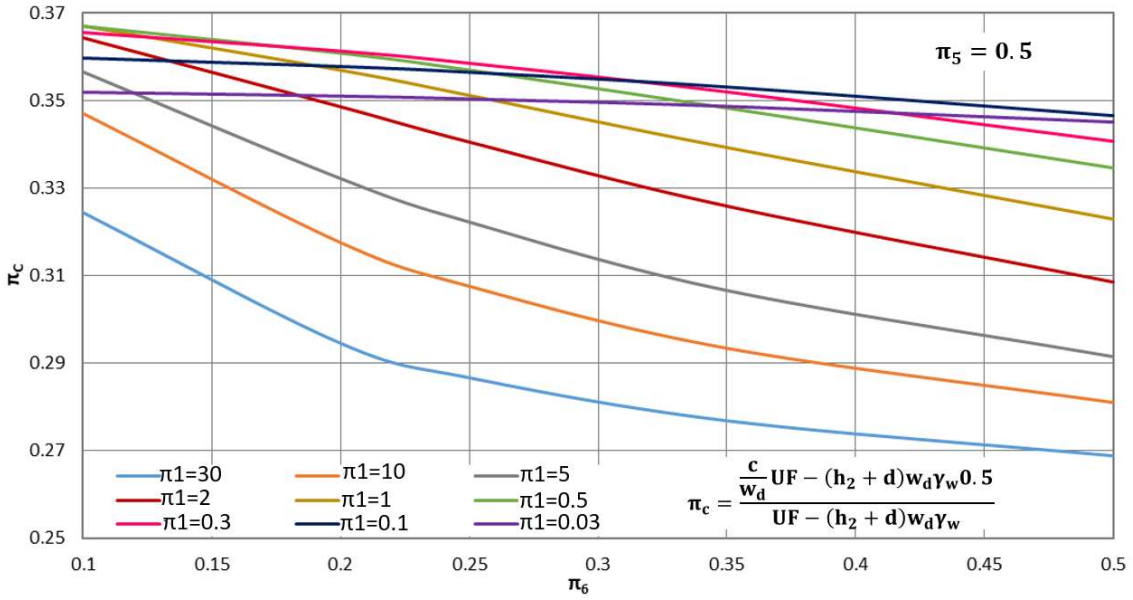

Figure 4.33. Dimensionless application point of the uplift force for $\pi_5 = 0.5$

In Figure 4.33 we observe that, in all cases, as π_6 increases, the dimensionless application point decreases. As the sheet pile length is larger, the pore pressure before it and under the dam increases, and the opposite happens on the other half of the base. In this way, the application point of the uplift force moves upstream, so its value decreases. This happens for each value of π_1. Figure 4.34 gives an example of pore pressure curves for $\pi_1 = 1$.

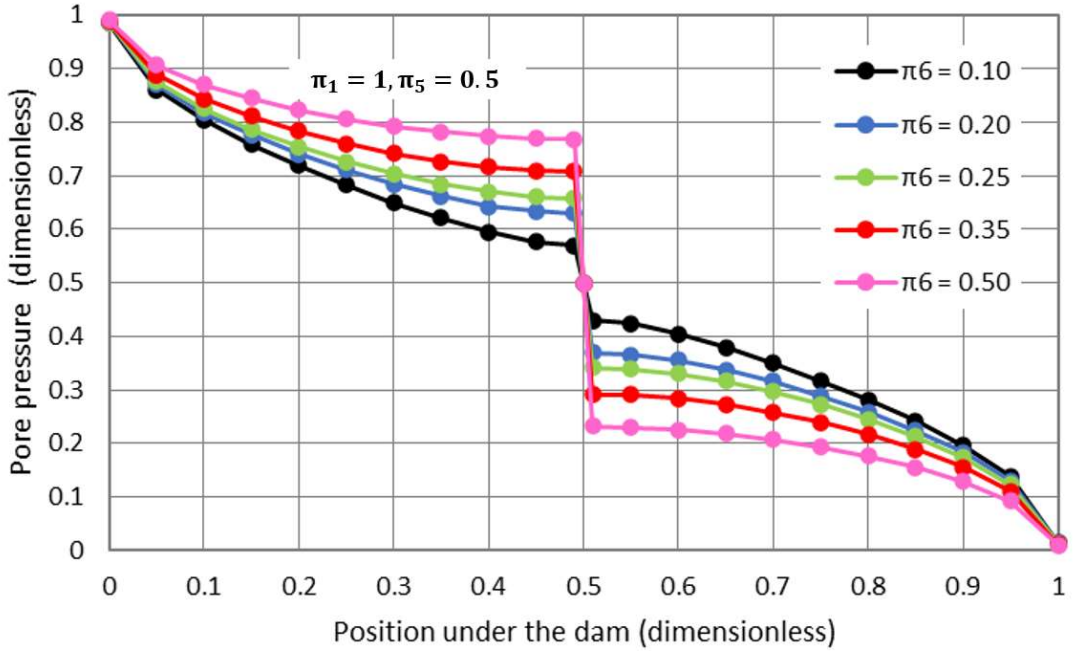

Figure 4.34. Dimensionless pore pressure distribution for $\pi_1 = 1$ and $\pi_5 = 0.5$

Considering the effect of π_1 presented in Figure 4.33, it shows a change of trend (for low values of π_6): π_C grows for $\pi_1 \leq 0.5$ and, from this point, it declines. It must be pointed out that, for low values of π_1, the pore pressure curves (for each value of π_6) are very close among them, so the application point variable hardly varies. For higher values of π_1, these curves are more separated to each other, strongly affecting the location of the application point.

Finally, Figure 4.35 is the abacus for the dimensionless application point under the dam for π_5 = 1 (sheet pile at the dam toe).

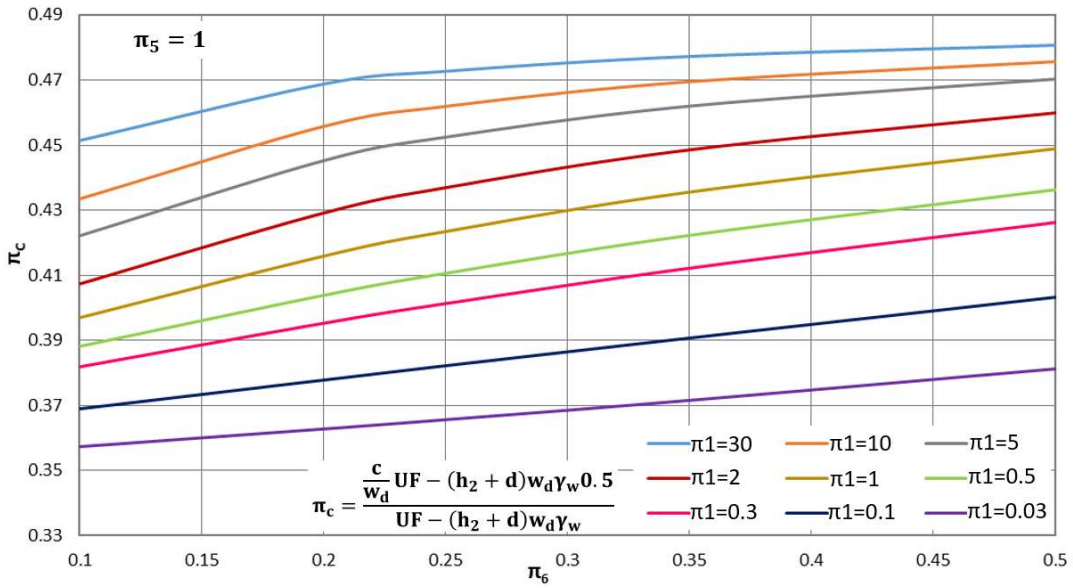

Figure 4.35. Dimensionless application point of the uplift force for π_5 = 1

In this case, the behaviour is easier to estimate: the higher the value of π_6, the higher that of π_C, since the increase of the sheet pile length leads to the increase of the pore pressure along the base. This can be observed in Figure 4.36 for a value of π_1 = 1.

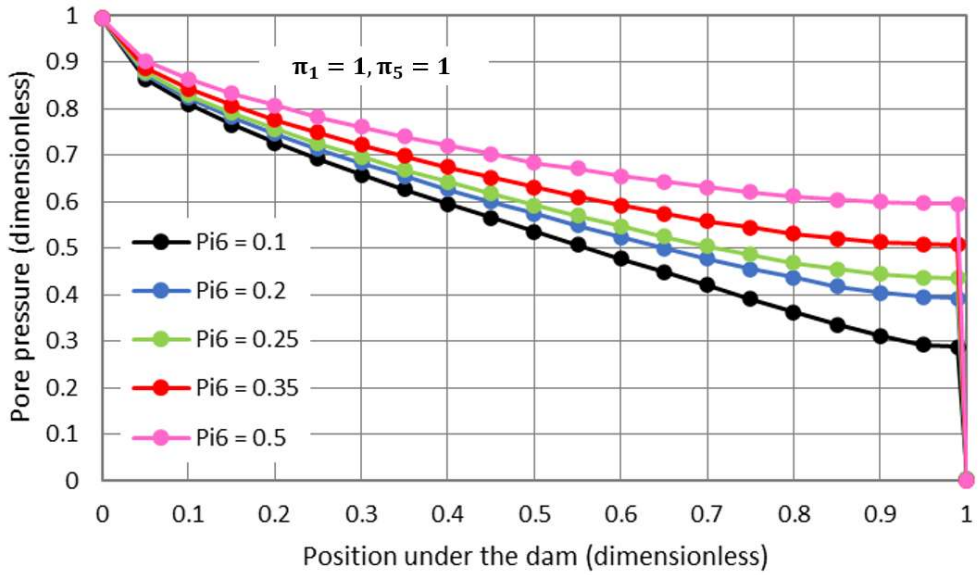

Figure 4.36. Dimensionless pore pressure distribution for π_1 = 1 and π_5 = 1

The effect of π_1 shown in Figure 4.35 is similar, since, as this variable grows, the application point moves downstream (the pore pressure is increased along the dam base) and its value is increased.

The abaci related to the dimensionless average exit gradient is shown in Figure 4.37. In this case, it has only been studied for a sheet pile located at the dam feet.

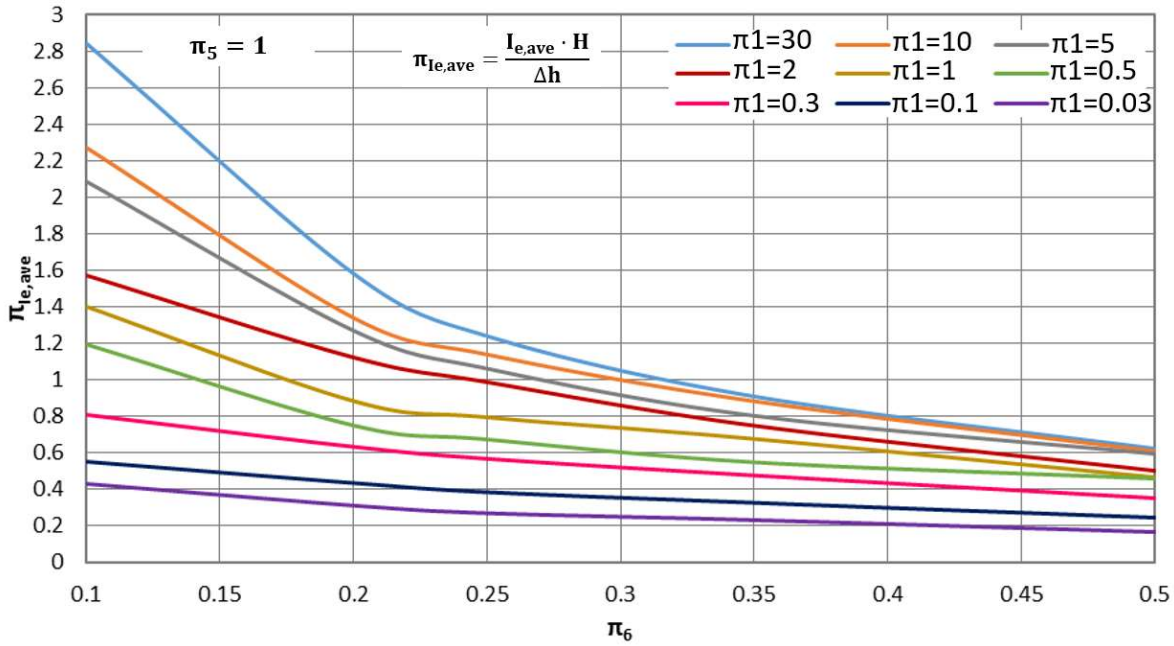

Figure 4.37. Dimensionless average exit gradient for $\pi_5 = 1$

The effect of π_1 and π_6 is similar as for the study of the dimensionless groundwater flow. In the case of π_1, the higher this variable is, the higher the potential variation along the sheet pile becomes and, therefore, a lower variation under the dam. In this way, the average exit gradient increases. Moreover, if π_6 increases, this means that the sheet pile is a longer surface where the potential variation is applied, so the value of $\pi_{Ie,ave}$ decreases.

The following variable whose abaci are presented are those of the dimensionless force on the upstream side of the sheet pile (π_{FUS}). The variable is again presented for the three sheet pile positions studied in this section ($\pi_5 = 0$, 0.5 and 1). Figure 4.38 shows the abacus for $\pi_5 = 0$, Figure 4.39 for $\pi_5 = 0.5$ and Figure 4.40 for $\pi_5 = 1$.

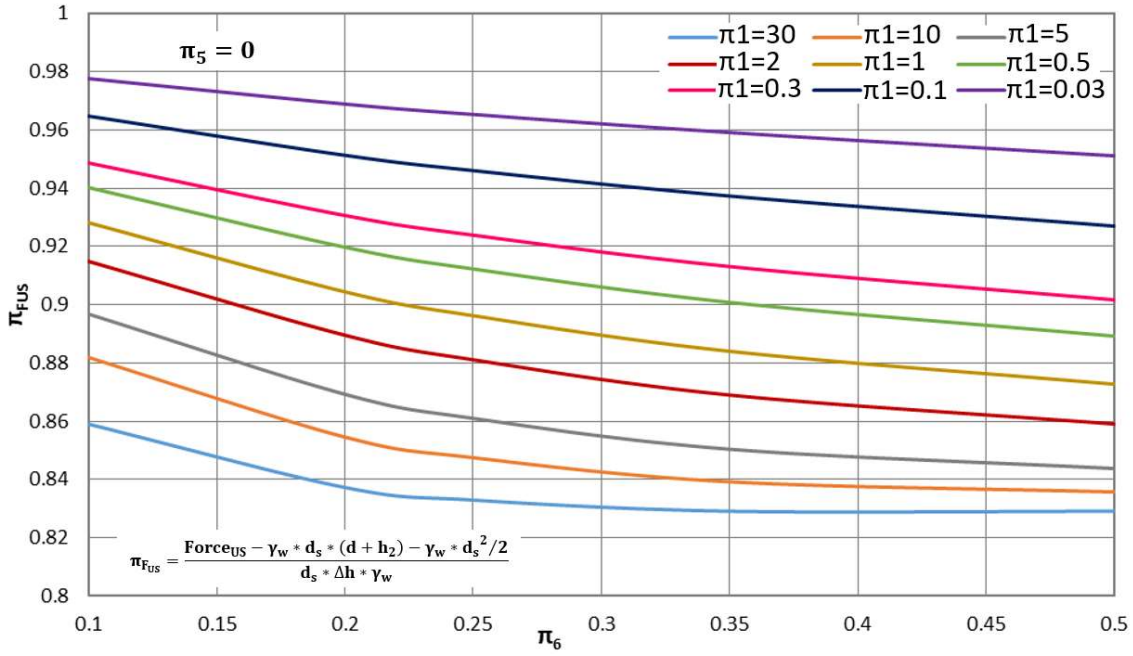

Figure 4.38. Dimensionless force on the upstream side of the sheet pile for $\pi_5 = 0$

Studying Figure 4.38, it is observed that the effect of π_1 and π_6 is similar, since in both cases, when any of them increases, π_{FUS} decreases. The effect of π_6 is because, when the sheet pile length increases, the potential variation grows, keeping constant the value on the upper end. For this reason, as it is compared with the reference value ($d_s \Delta h \gamma_w$), the dimensionless value is reduced. Referring to π_1, when the sheet pile is located at the dam heel, the water must flow through a longer vertical distance. For this, if the value of π_1 is high, the flow is hindered, and the potential variation is higher at this side of the sheet pile. This is translated into a lower value of π_{FUS}.

Figure 4.39 is the abacus of the variable π_{FUS} when the sheet pile is located at the centre of the dam base.

According to Figure 4.39, when placing the sheet pile at the centre of the dam base, the dimensionless force on the upstream side of the sheet pile increases with monomials π_1 and π_6. The effect of π_1 is similar to that for $\pi_5 = 0$; however, when obtaining the dimensionless value, due to the way it is calculated and turned into dimensionless, instead of decreasing as the monomial grows, it increases because it involves higher values of water head at the upper side of the pile.

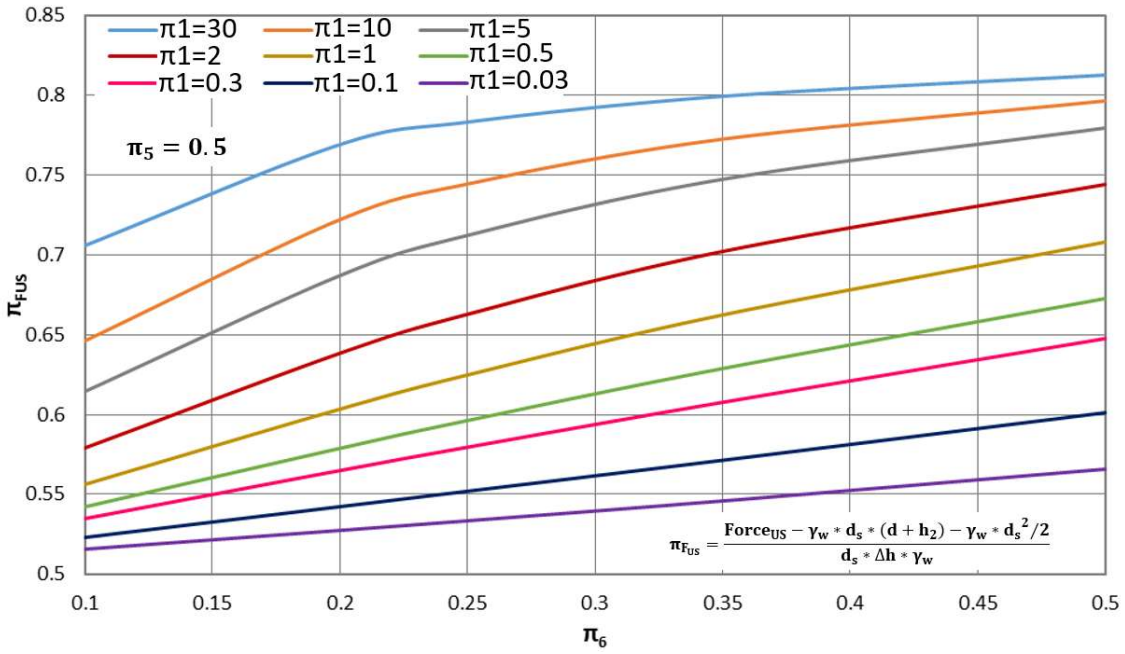

Figure 4.39. Dimensionless force on the upstream side of the sheet pile for $\pi_5 = 0.5$

Monomial π_6 affects π_{FUS} in a similar way. The increase of the sheet pile length leads to an increment of the potential variation. Moreover, since the potential value at the base of the sheet pile (of negligible thickness) always presents the average value of the upstream and downstream potentials, $\frac{h_1+h_2}{2}$, independently of its length, the potential variation increased.

Finally, Figure 4.40 shows the abacus of π_{FUS} for the scenarios in which the sheet pile is placed at the dam toe ($\pi_5 = 0$).

According to Figure 4.40, the effect of the monomials π_1 and π_6 is like that of placing the sheet pile at the centre. π_{FUS} increases with the growth of π_1 because an increase of the horizontal permeability with respect to the vertical one creates a higher water head variation along the sheet pile, which leads to larger head values involved in the force. This means an increase of the dimensionless variable.

The effect of π_6 on π_{FUS} is similar to the one of the permeability monomial since the increase of the sheet pile length means a higher water head variation, involving again larger potential values. In this way, the dimensionless force also becomes larger as π_6 grows.

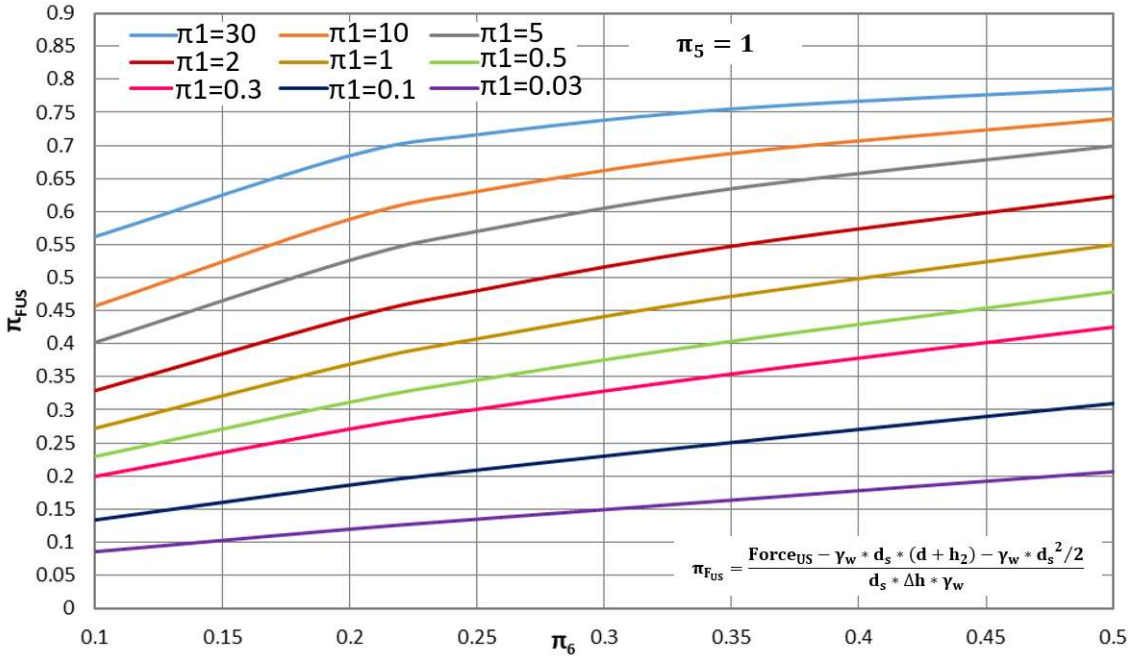

Figure 4.40. Dimensionless force on the upstream side of the sheet pile for $\pi_5 = 1$

It is interesting to focus on the universal curves of π_{FDS} as the following step, because, as shown later, variables π_{FUS} and π_{FDS} are somehow related. The first abacus presented is π_{FDS} for $\pi_5 = 0$ (Figure 4.41).

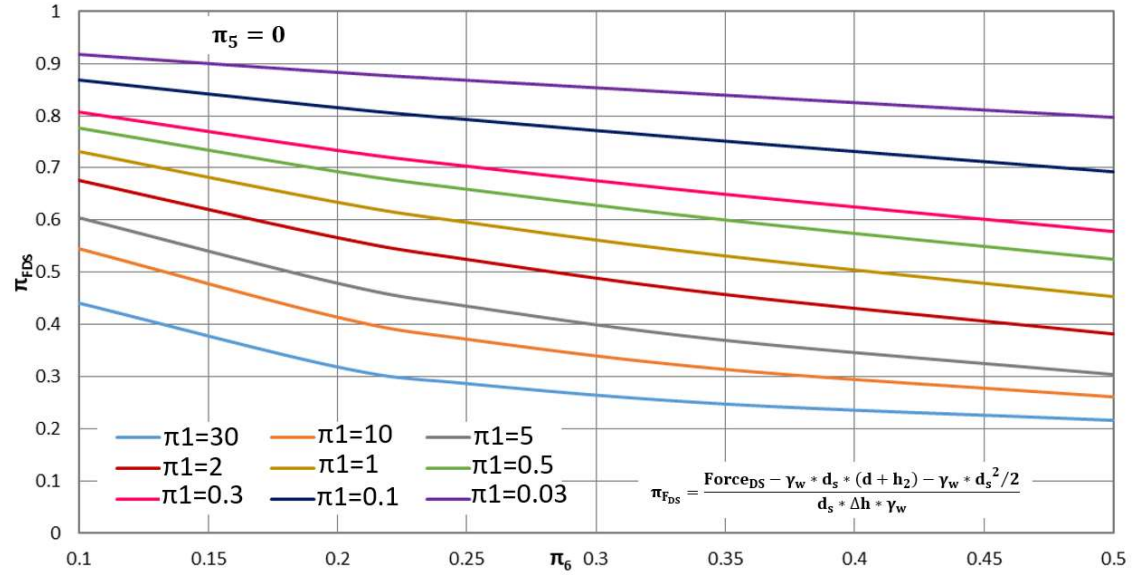

Figure 4.41. Dimensionless force on the downstream side of the sheet pile for $\pi_5 = 0$

According to Figure 4.41, the variable π_{FDS} decreases its value as π_1 and π_6 increase, since they both lead to a higher potential variation along that side of the sheet pile. However, at this side of the structure, the increase of the water head variation means lower values of the water head and, therefore, lower dimensionless force. Moreover, Figure 4.41 (π_{FDS} abacus for $\pi_5 = 0$) is

related to Figure 4.40 (π_{FUS} abacus for $\pi_5 = 1$), since both scenarios are symmetrical. The values of the two scenarios can be obtained as follows, Equation (IV-49):

$$\pi_{F_{DS}}(\pi_1, \pi_5 = 0, \pi_6) = 1 - \pi_{F_{US}}(\pi_1, \pi_5 = 1, \pi_6) \quad \text{(IV-49)}$$

The following abacus, Figure 4.42, is the set of universal curves π_{FDS} for $\pi_5 = 0.5$.

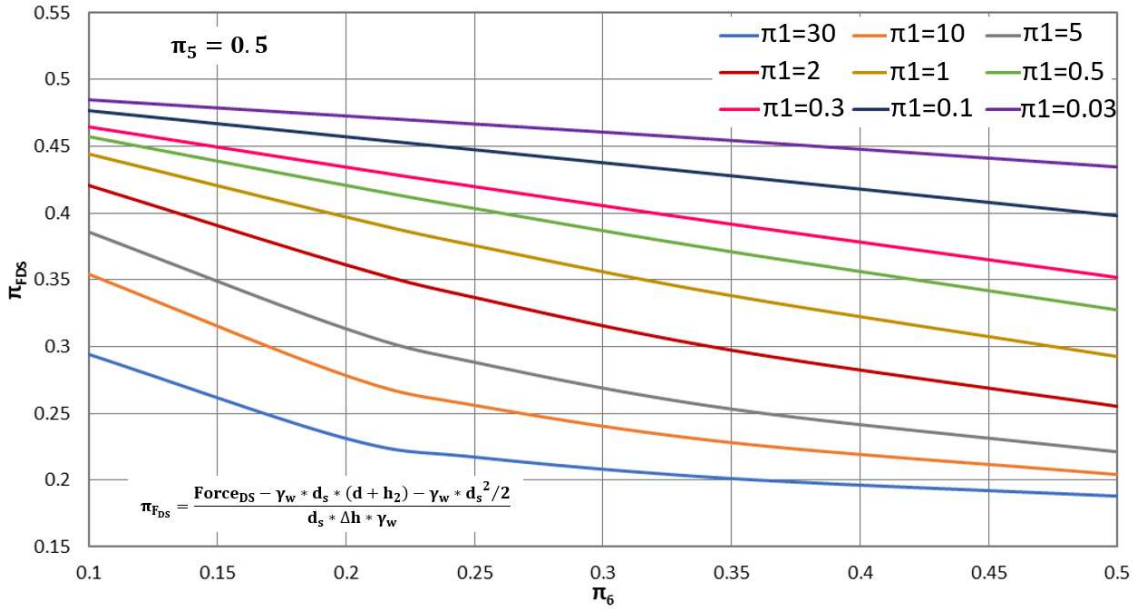

Figure 4.42. Dimensionless force on the downstream side of the sheet pile for $\pi_5 = 0.5$

As in the previous scenario, the increase of the governing monomials π_1 and π_6 leads to the decrease of the dimensionless variable π_{FDS} because similar reasons as in the last scenario: they lead to an increase of the water head variation that, at the downstream side of the pile, means lower head values.

In addition, the dimensionless values of the forces on both sides of the sheet pile are associated (since the scenario is symmetrical). This means that the values in Figure 4.42 and Figure 4.39 are related, and those of the downstream side can be obtained with those of the upstream side following Equation (IV-50).

$$\pi_{F_{DS}}(\pi_1, \pi_5 = 0.5, \pi_6) = 1 - \pi_{F_{US}}(\pi_1, \pi_5 = 0.5, \pi_6) \quad \text{(IV-50)}$$

The last abacus to show for π_{FDS} is for $\pi_5 = 1$, Figure 4.43. In this case, the monomial π_{FDS} behaves in the opposite way of that for $\pi_5 = 0$ and $\pi_5 = 0.5$, since its value is increased as π_1 and π_6 do the same. The reason why this occurs, however, is the same as in those scenarios: the water head variation grows, and it can only occur by increasing the potential values at the bottom area of the pile, which leads to an increase on the dimensionless force on the downstream side.

The abacus of π_{FDS} for $\pi_5 = 1$ is related to the one presenting a symmetrical scenario, which is π_{FUD} for $\pi_5 = 0$. The values of the two abaci are associated according to Equation (IV-51):

$$\pi_{F_{DS}}(\pi_1, \pi_5 = 1, \pi_6) = 1 - \pi_{F_{US}}(\pi_1, \pi_5 = 0, \pi_6) \quad \text{(IV-51)}$$

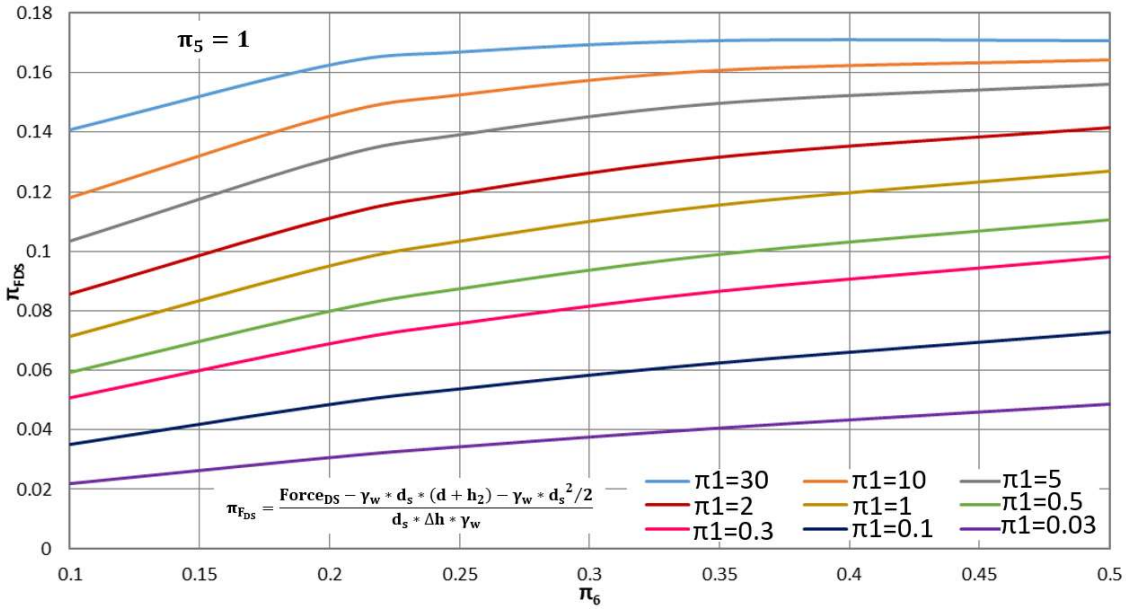

Figure 4.43. Dimensionless force on the downstream side of the sheet pile for $\pi_5 = 1$

For the application point of the force on the upstream side of the sheet pile, the first abacus is the one for $\pi_5 = 0$ (Figure 4.44).

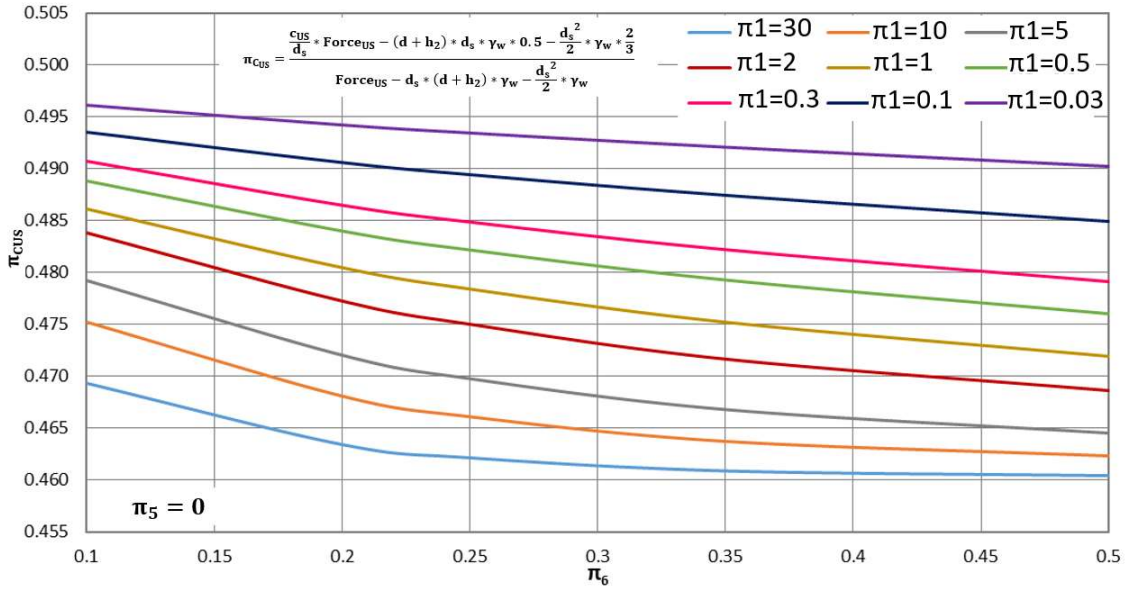

Figure 4.44. Dimensionless application point of the force on the upstream side of the sheet pile for $\pi_5 = 0$

Figure 4.44 presents the behaviour of the curves of the application point in the upstream side of the sheet pile. This variable decreases with π_1 and π_6, as happened for the dimensionless force on the upstream side for π_5=0. As the water head variation increases (inducing a reduction in the potential value at the bottom of the pile), the dimensionless application point moves upwards, so its value becomes lower. This is the case ofπ_1 and π_6: on the one hand, the effect of π_1 is due to the increase of the horizontal permeability respect to the vertical one; on the other

hand, increasing the value of π_6 means that the sheet pile is longer, and that leads to an increase of the potential variation.

The abacus of π_{CUS} for $\pi_5 = 0.5$ is shown in Figure 4.45.

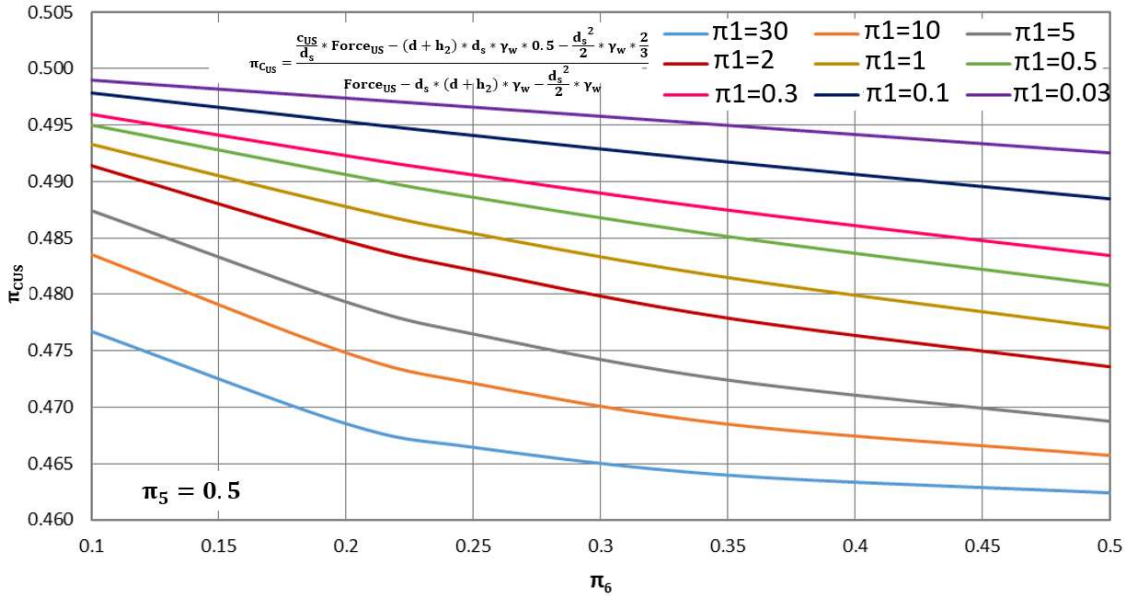

Figure 4.45. Dimensionless application point of the force on the upstream side of the sheet pile for $\pi_5 = 0.5$

The behaviour respect to π_1 and π_6 is the opposite of that of the force for the same scenarios, since in this case, as for the previous abacus, the value of π_{CUS} decreases with the increase of both monomials. However, the reasons are the same. As π_1 and π_6 become higher, the increase of the potential variation generates an increment of the hydraulic potential values in the upper area of the sheet pile. This leads to a displacement of the application point to the upper zone, so the values of π_{CFUS} become lower.

Finally, Figure 4.46 shows the universal curves of π_{CUS} for $\pi_5 = 1$.

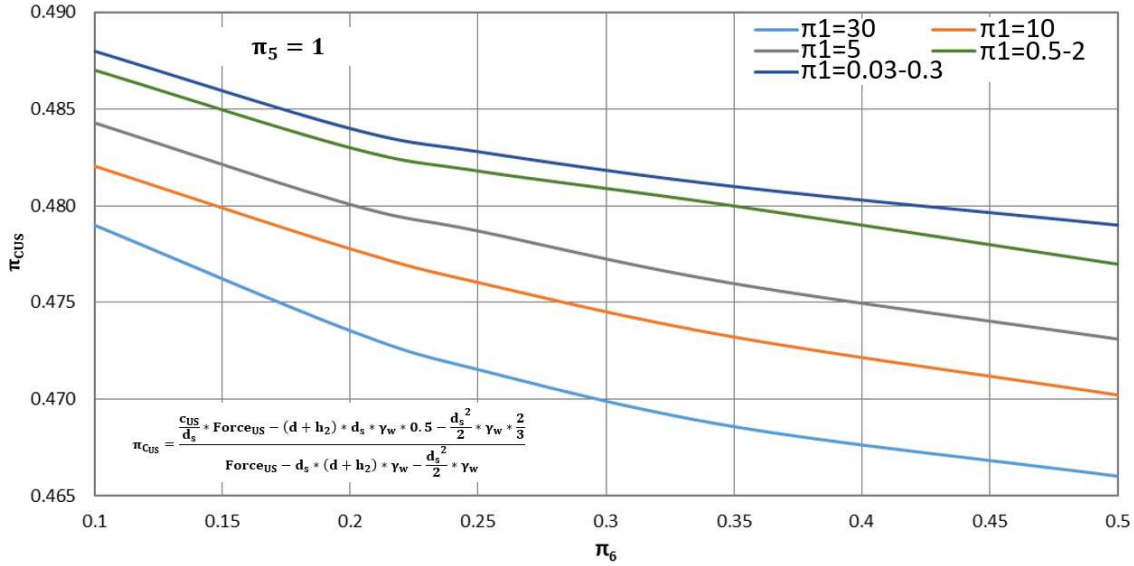

Figure 4.46. Dimensionless application point of the force on the upstream side of the sheet pile for $\pi_5 = 1$

The effect of π_1 and π_6 is the same as in the two previous configurations. Moreover, in this case, the same occurs as for the sheet pile at the centre of the dam base: the behaviour is the opposite of that of the force on that side of the sheet pile, since it decreases as π_1 and π_6. The reasons are the same as in the previous case because the increase of the potential at the upper area of the sheet pile, displacing the application point there and reducing then the value of π_{CUS}.

The last variable is the application point of the force on the downstream side of the pile. The first abacus is that for $\pi_5 = 0$ (Figure 4.47).

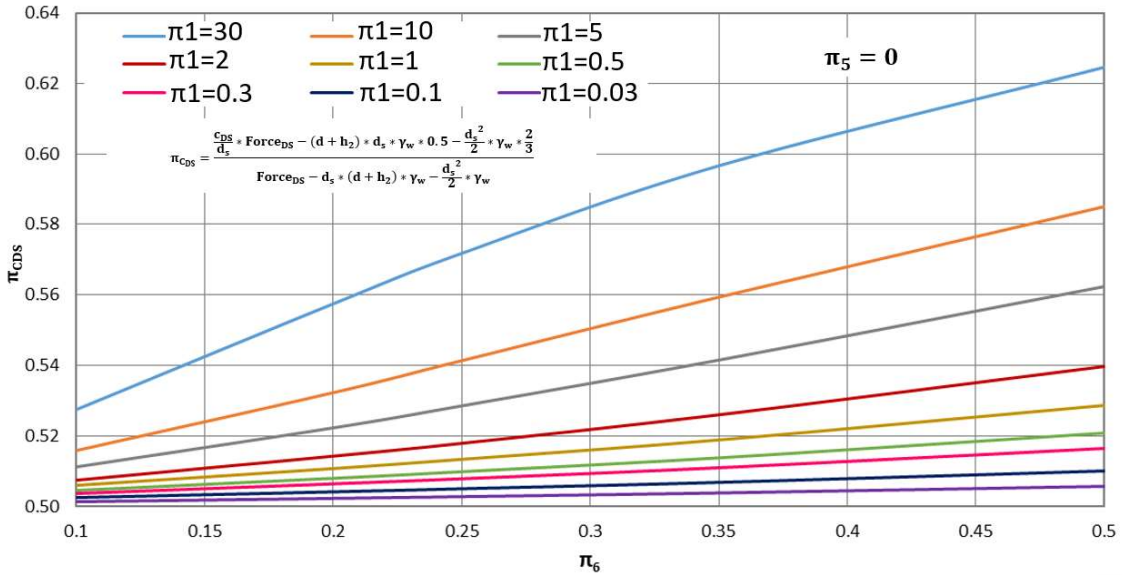

Figure 4.47. Dimensionless application point of the force on the downstream side for $\pi_5 = 0$

Figure 4.47 shows that the behaviour of π_{CDS} respect to π_1 and π_6 is the opposite of that of the dimensionless application point for the same configuration on the upstream side (π_{CFUS}) since it now grows as the two monomials increase.

As effect of an increase of π_1, there is a higher potential variation, which leads to lower values of potential on the upper side of the sheet pile. This is translated into a displacement of the application point to the lower area of the sheet pile. For this reason, the value of the dimensionless application point increases. π_6 affects this variable in a similar way, as the increase of the sheet pile lengths means that the potential values on the upper zone are lower, displacing therefore the dimensionless application point to the lower zone of the sheet pile.

Figure 4.48 presents the abacus of π_{CFDS} for $\pi_5 = 0.5$.

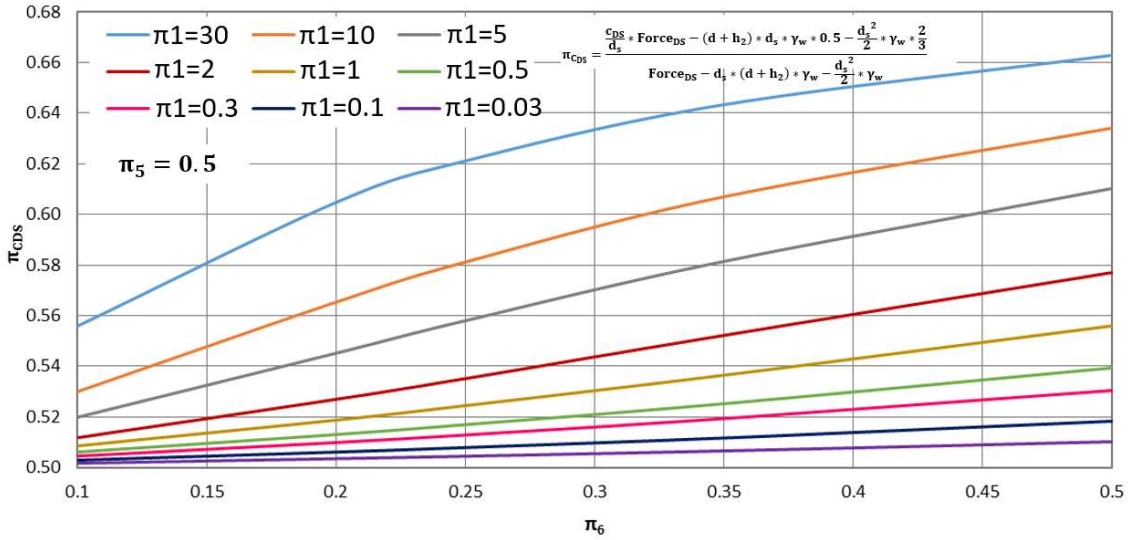

Figure 4.48. Dimensionless application point of the force on the downstream side of the sheet pile for $\pi_5 = 0.5$

When placing the sheet pile at the centre of the dam base (Figure 4.48), the effect of π_1 and π_6 on the dimensionless application point on the downstream side is the same as for the previous configuration. The reasons are similar to those mentioned in the previous case, since, either for the increase of the horizontal permeability (π_1) or the sheet pile length (π_6), there is a reduction of the hydraulic potential in the upper zone of the sheet pile, so the dimensionless application point is displaced to its lower zone.

Finally, the universal curves of π_{CDS} for $\pi_5 = 1$ are shown in Figure 4.49.

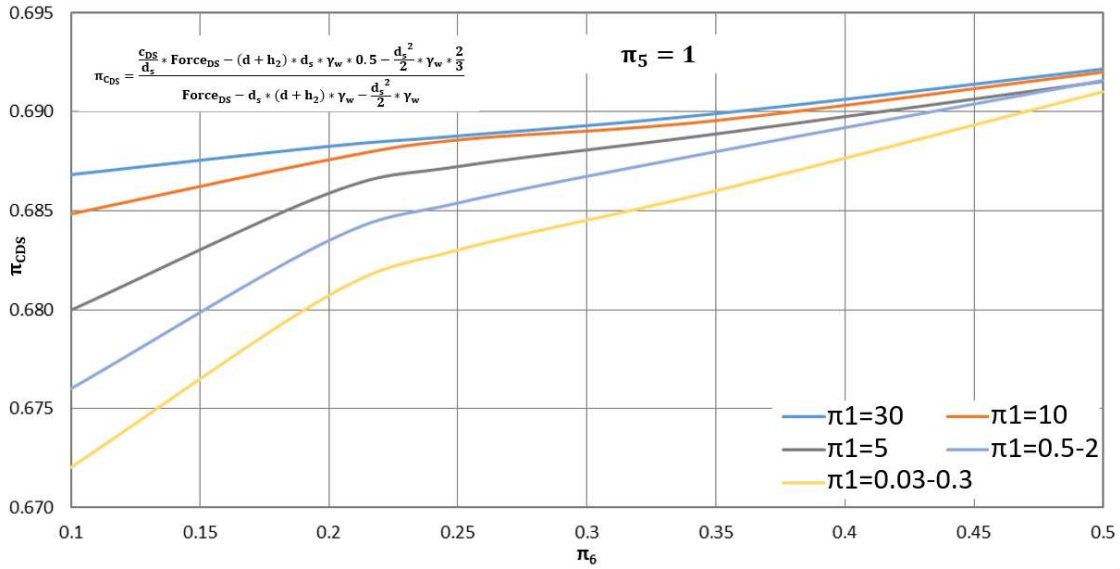

Figure 4.49. Dimensionless application point of the force on the downstream side of sheet pile for $\pi_5 = 1$

The effect of π_1 and π_6 is the same as for the previous configurations, this is, it grows with these monomials. The reason is the increase of the potential values in the lower area of the sheet pile (in the upper zone, it takes an imposed value of h_2). For this, the application point is displaced

to the lower area of the sheet pile, either for higher value of horizontal permeability or a longer sheet pile, and this means that the dimensionless application point increases its value.

IV.2.3. Flow under gravity dams in an infinite medium

IV.2.3.1 Mathematical model

Let us present the following case: a dam on the surface of the stratum with a width much smaller than the other quantities of the problem (upstream and downstream length, and stratum thickness). In fact, these quantities would be so big that they could be considered as infinite, although to run any code (including the one developed in this thesis) and obtain the results, their values must be introduced. However, from which value of these quantities can the problem be considered as infinite? Which parameters (and which range) are involved?

For this, the study must be started with the finite case, meaning this that the governing equation and boundary condition are the same as in Sections IV.2.1 and IV.2.2:

$$\kappa_x \frac{\partial^2 h}{\partial x^2} + \kappa_y \frac{\partial^2 h}{\partial y^2} = 0 \qquad \text{(IV-3)}$$

$$\frac{1}{\kappa_y}\frac{\partial^2 \Psi}{\partial x^2} + \frac{1}{\kappa_x}\frac{\partial^2 \Psi}{\partial y^2} = 0 \qquad \text{(IV-7)}$$

$h = h_{o,r}$ at boundary regions 1,2…r (first class) (IV-4)

$\left.\frac{\partial h}{\partial n}\right|_s = 0$ at boundary regions 1,2…s (second class) (IV-5)

$\Psi = \Psi_{o,p}$ at boundary regions 1,2…p (first class) (IV-8)

$\left.\frac{\partial \Psi}{\partial n}\right|_q = 0$ at boundary regions 1,2…q (second class) (IV-9)

In this scenario, the dam has no foundations. Figures 4.50 and 4.51 present the nomenclature and the boundary conditions.

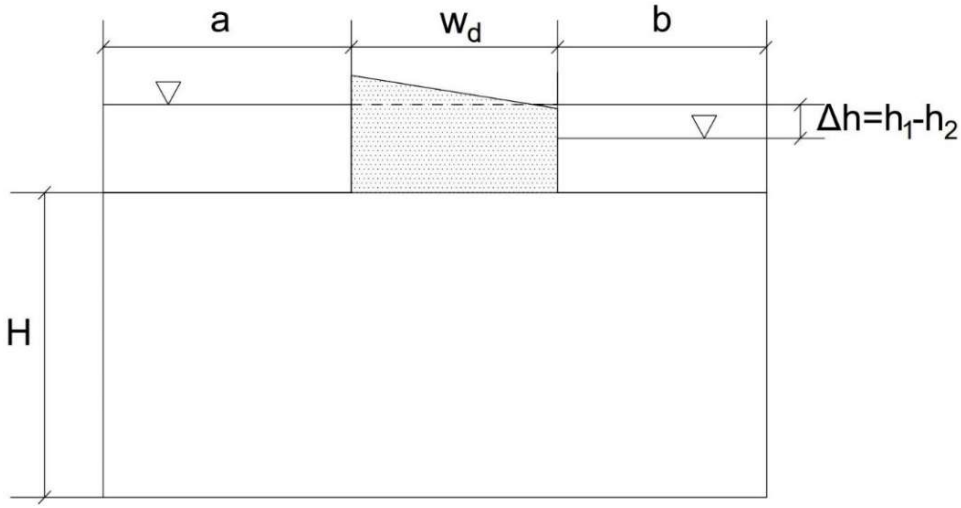

Figure 4.50. Nomenclature of the studied problem

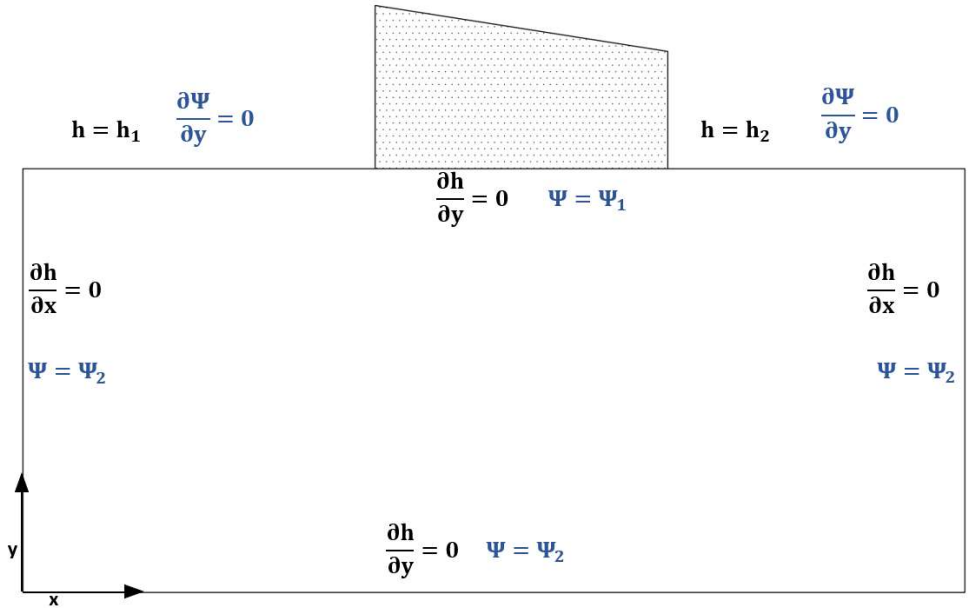

Figure 4.51. Boundary conditions of the studied problem

IV.2.3.2 Dimensionless governing equation and discriminated monomials

In order to obtain the dimensionless groups that rule the scenario studied in this section, the variables involved in the governing equation (Equation (IV-3)) are turned into dimensionless variables. However, in this case, instead of dividing the horizontal variable *x* by the dam width, since this parameter becomes negligible if considering infinite media, it is divided by the horizontal medium length upstream the dam, a. In this way, the new dimensionless variables are

$$x' = \frac{x}{a}, y' = \frac{y}{H}, h' = \frac{h}{\Delta h} \quad \text{(IV-52)}$$

and the dimensionless governing equation turns to be

$$\frac{\kappa_x}{a^2}\frac{\partial^2 h\prime}{\partial x\prime^2}+\frac{\kappa_y}{H^2}\frac{\partial^2 h\prime}{\partial y\prime^2}=0 \qquad \text{(IV-53)}$$

Then, employing Equation (IV-53) to obtain the first monomial ruling the problem leads to a different definition of π_1, which is still a permeability ratio, but in this case the aspect relation is different.

$$\pi_1=\frac{\kappa_x H^2}{\kappa_y a^2} \qquad \text{(IV-54)}$$

In order to reach an 'infinite' medium by simulations, the procedure that has been followed increasing the values of H, a and b until they reach very high values. Moreover, they have been supposed to have the same value, so they all approach 'infinite' at the same time. According to this, the three parameters are given the same value in each simulation, L (discrimination is considered in this scenario, so they keep their discriminated dimensions). This means that Equation (IV-54) can be transformed into

$$\pi_1=\frac{\kappa_x L^2}{\kappa_y L^2}=\frac{\kappa_x}{\kappa_y} \qquad \text{(IV-55)}$$

This new definition of π_1 is not dimensionless but works as it is. This fact is also considered by Muskat [1937] and Harr [2012] for the curves and abaci presented in their works, which depended on a monomial that was an aspect ratio, so it has dimensions. However, as the soil they considered was isotropic, their aspect ratios were simply degenerations of dimensionless monomials akin to the ones in Equations (IV-54) and (IV-12) where the permeability (or hydraulic conductivity) values are the same, even if they have different discriminated dimensions.

Monomial π_2, previously presented in Equation (IV-13) loses its meaning in this section, since for all the cases studied here, the length of the dam foundation is always 0. Moreover, as the stratum thickness will be increased until reaching an 'infinite' value, π_2 would lose its importance anyway.

The following group, π_3, keeps the same expression as in the previous problems studied in this chapter, which is

$$\pi_3=\frac{a}{w_d} \qquad \text{(IV-14)}$$

As π_3 increases its values, it will become negligible and will not govern the dimensionless scenario.

Finally, π_4 (= $\frac{a}{b}$) presents a constant value of 1, because a and b take the same values in every case, as happens with H. The result that is expected will be only ruled by π_1, which in this case is a simple ratio of hydraulic conductivity.

The aim of this study is to achieve the dimensionless values of groundwater flow π_Q according to the permeability ratio when the scenario can be considered as infinity. To this, new dimensionless unknown monomials related to the characteristic lengths are studied. They can be defined as those through which a significant percentage of flow runs, as they show the most relevant areas from a hydrogeological point of view. For this work, it is decided to study these lengths for values of 95% and 90% of the total flow, as these percentages involve most of the flow rate. The dimensionless groundwater flow variable presents the same formulation, Equation (IV-21), while the dimensionless characteristic length monomials are defined as presented in Equations (IV-56) to (IV-59). In order to simplify their definition, for the dimensionless lengths, the dimensional ones are divided by L instead of a and b for horizontal lengths and H for vertical lengths.

$$\pi_Q = \frac{Q}{\sqrt{\kappa_x \kappa_y}\Delta h} \tag{IV-19}$$

$$L_{x,nondim,95\%} = \frac{l_{x,95}}{L} = \pi_{L_{x,95}} \tag{IV-56}$$

$$L_{x,nondim,90\%} = \frac{l_{x,90}}{L} = \pi_{L_{x,90}} \tag{IV-57}$$

$$L_{y,nondim,95\%} = \frac{l_{y,95}}{L} = \pi_{L_{y,95}} \tag{IV-58}$$

$$L_{y,nondim,90\%} = \frac{l_{y,90}}{L} = \pi_{L_{y,90}} \tag{IV-59}$$

IV.2.3.3 Universal abaci

The values of π_3 presented go from 1 to 5000 in every case (except for π_1 = 0.01, where it goes up to 10000), also presenting the value of 200000 to check if unknown monomials get to an asymptotic value. For π_1, on the other side, values 1, 10, 100, 0.1 y 0.01 are presented. Figure 4.52 shows the results for the dimensionless groundwater flow (π_Q), Figure 4.53 for the characteristic length in vertical direction for a flow of 95 % ($\pi_{Ly,95}$), Figure 4.54 for the characteristic length in horizontal direction for a flow of 95 % ($\pi_{Lx,95}$), Figure 4.55 for the characteristic length in vertical direction for a flow of 90 % ($\pi_{Ly,90}$) and Figure 4.56 for the characteristic length in horizontal direction for a flow of 90 % ($\pi_{Lx,90}$).

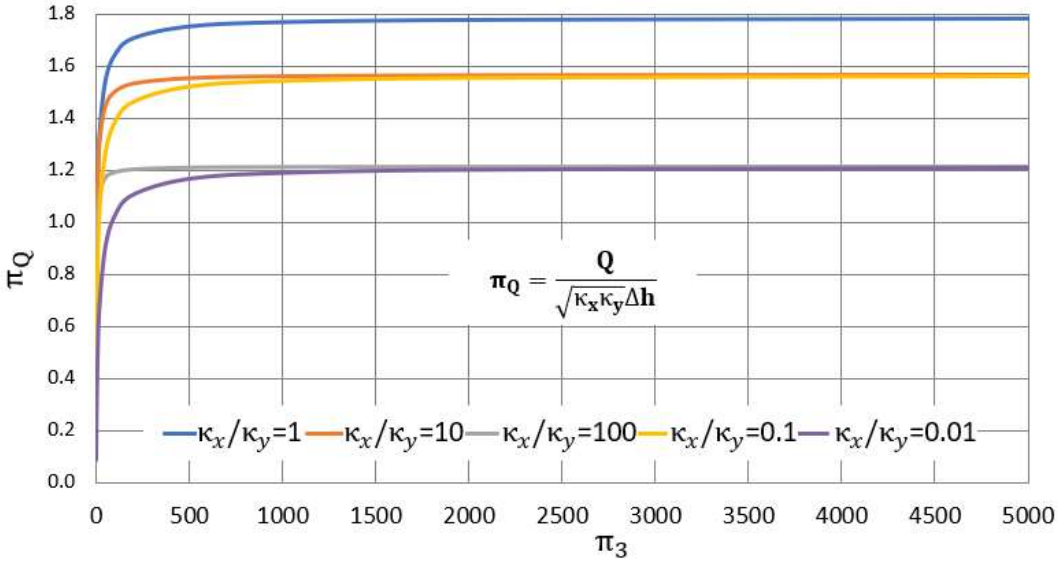

Figure 4.52. Trend of the dimensionless groundwater flow

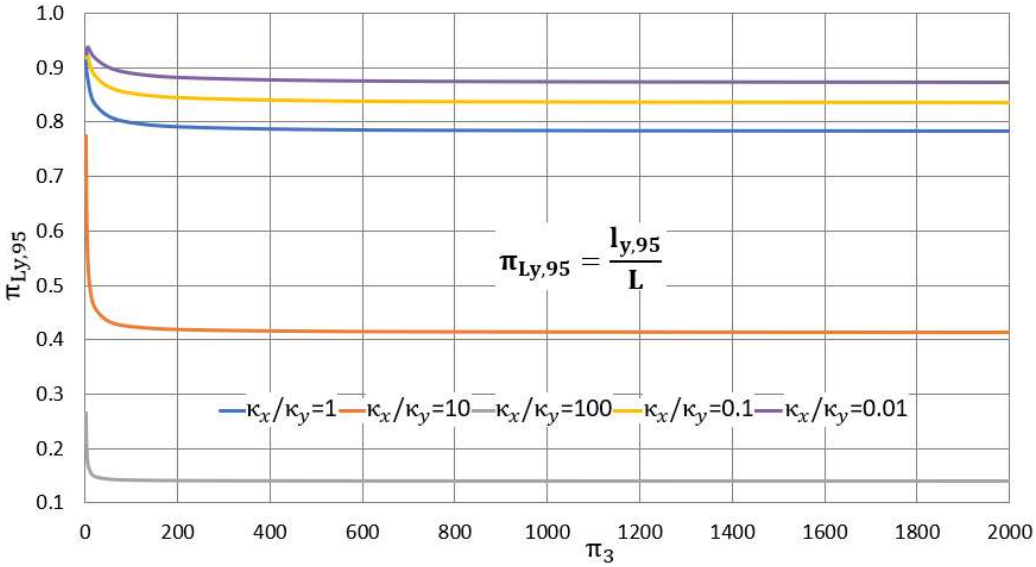

Figure 4.53. Trend of the dimensionless characteristic length in the vertical direction for 95% flow

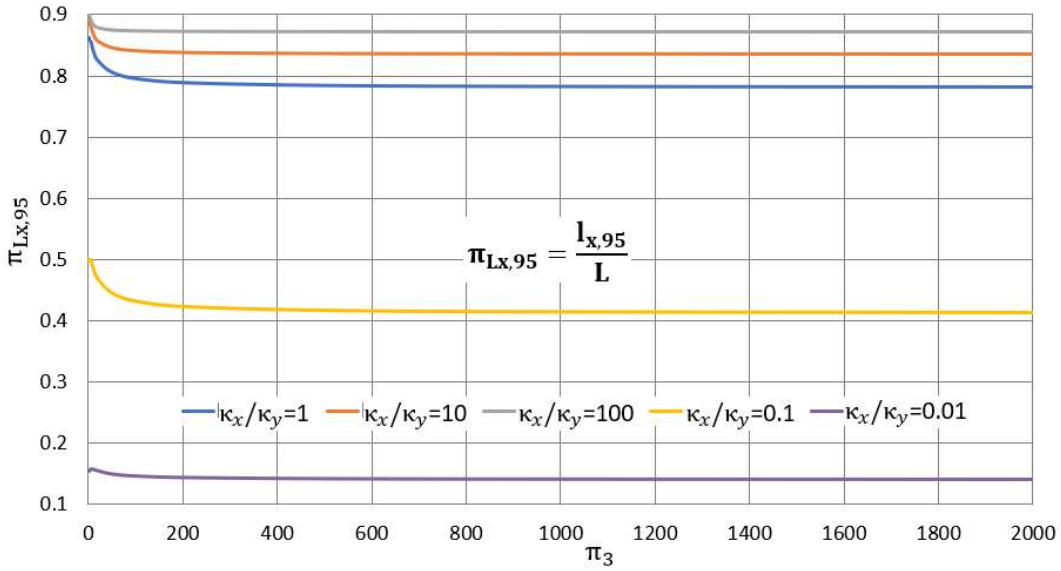

Figure 4.54. Trend of the dimensionless characteristic length in the horizontal direction for 95% flow

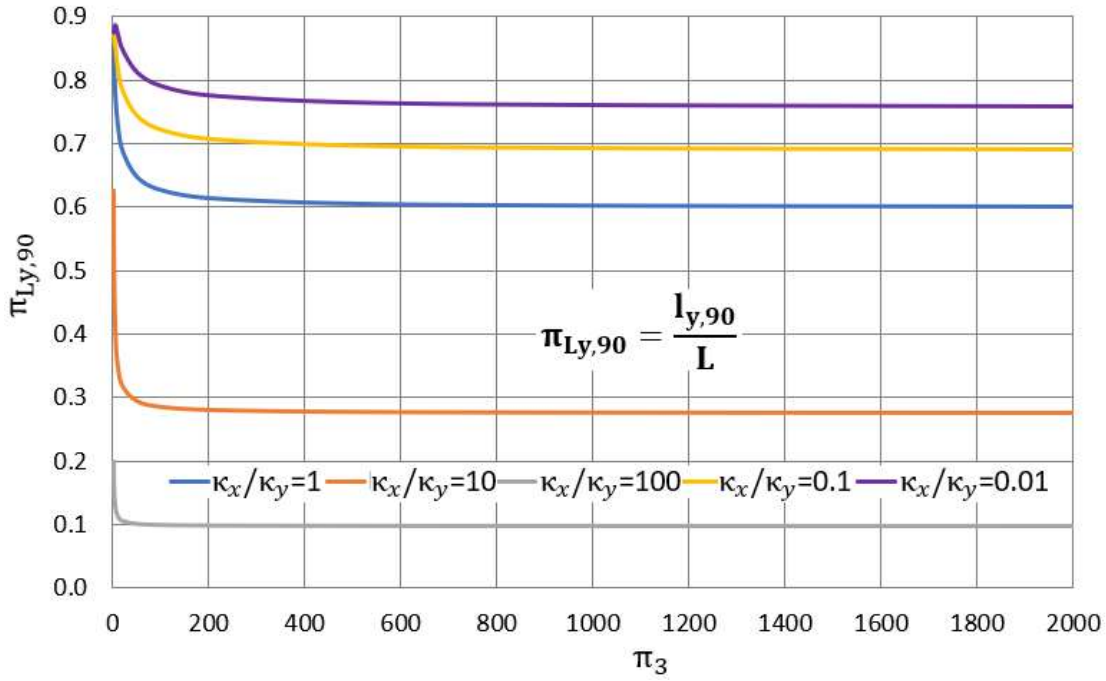

Figure 4.55. Trend of the dimensionless characteristic length in the vertical direction for 90% flow

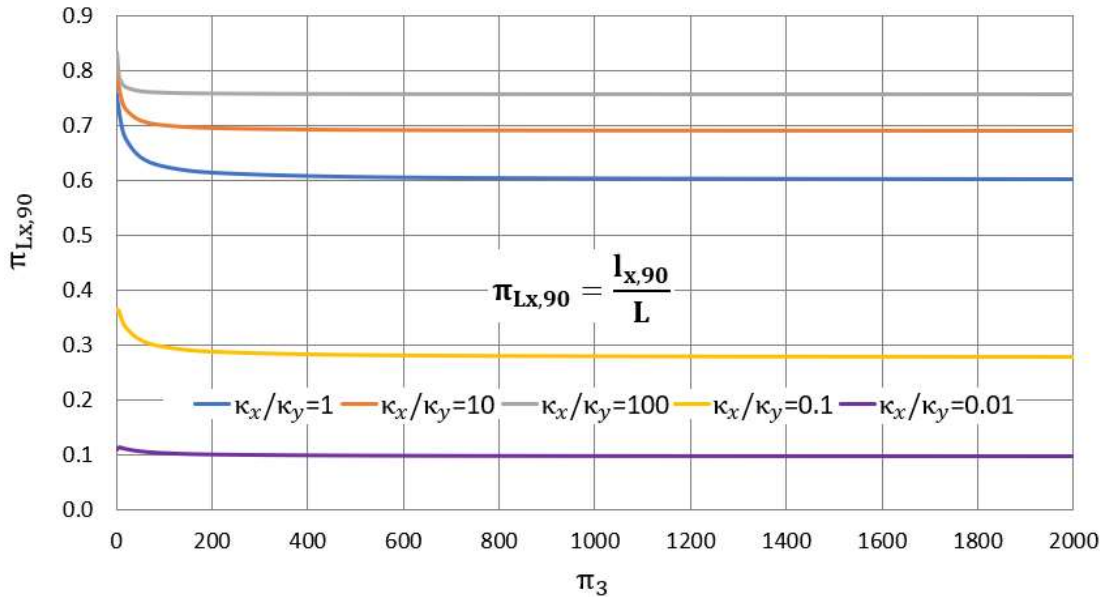

Figure 4.56. Trend of the dimensionless characteristic length in the horizontal direction for 90% flow

Two observations can be mentioned: i) the value for each of the unknown monomials studied according to monomial π_1 trends to the ones presented in Table 4.1 and ii) π_3 loses its importance when trending to an infinite value.

Table 4.1. Limit values of unknown monomials according to π_1

π_1	**0.01**	**0.1**	**1**	**10**	**100**
π_Q	1.212	1.565	1.781	1.565	1.212
π_{Ly95}	0.871	0.835	0.782	0.412	0.141
π_{Lx95}	0.141	0.412	0.782	0.835	0.871
π_{Ly90}	0.757	0.689	0.6	0.276	0.097
π_{Lx90}	0.097	0.276	0.6	0.689	0.757

As it appears in Table 4.1, π_Q takes the same value for π_1= 10 and 0.1, and the same happens for π_1= 100 and 0.01. Something similar occurs for the characteristic length. If $\pi_{Ly,95}$ for π_1=10 and $\pi_{Lx,95}$ for π_1=0.1 values are compared, it is visible that both are the same, 0.412. This can also be observed for the following combinations:

- $\pi_{Ly,90}$ for π_1=10 and $\pi_{Lx,90}$ for π_1=0.1, 0.276
- $\pi_{Lx,95}$ for π_1=10 and $\pi_{Ly,95}$ for π_1=0.1, 0.835
- $\pi_{Lx,90}$ for π_1=10 and $\pi_{Ly,90}$ for π_1=0.1, 0.689
- $\pi_{Ly,95}$ for π_1=100 and $\pi_{Lx,95}$ for π_1=0.01, 0.141
- $\pi_{Ly,90}$ for π_1=100 and $\pi_{Lx,90}$ for π_1=0.01, 0.097

- $\pi_{Lx,95}$ for π_1=100 and $\pi_{Ly,95}$ for π_1=0.01, 0.874
- $\pi_{Lx,90}$ for π_1=100 and $\pi_{Ly,90}$ for π_1=0.01, 0.757

In this way, employing the previous abaci, the user can estimate the maximum groundwater rate flow and the influence area to expect in large scenarios. This estimation is feasible whether the soil consists on isotropic or anisotropic medium.

IV.2.4 Steady flow in unconfined aquifers due to a pumping well

IV.2.4.1 Mathematical model

Unconfined aquifers present the characteristic that their upper border (phreatic level) is at atmospheric pressure. This means that, if the reference for the vertical coordinates, *z*=0, is set at the bottom of aquifer, the water head values at the phreatic level are those of the vertical coordinate at those points. Unlike confined aquifers, in which the water head value is always above its roof (even if it varies), modelling pumping wells in unconfined aquifers becomes difficult. The presence of the potential within the limits of the stratum thickness leads to the appearance of vertical flow, an effect that has been disregarded in traditional approaches to the problem.

As for any other problems of flow through porous media, Laplace equation also describes this phenomenon. Equation (IV-61) shows Darcy's law for 2-D radial media.

$$v_r = -\kappa_r \frac{\partial h}{\partial r} \text{ and } v_z = -\kappa_z \frac{\partial h}{\partial z} \quad \text{(IV-60)}$$

In addition, steady state problem and no sources or sinks are considered, the continuity equation can be expressed as in Equation (IV-61).

$$\frac{1}{r}\frac{\partial}{\partial r}(r v_r) + \frac{\partial v_z}{\partial z} = 0 \quad \text{(IV-61)}$$

Once Darcy's law is introduced in the continuity equation, Laplace expression for anisotropic soil in radial 2-D coordinates is deduced (Equation (IV-62)).

$$\kappa_r \frac{1}{r}\frac{\partial}{\partial r}\left(r\frac{\partial h}{\partial r}\right) + \kappa_z \frac{\partial^2 h}{\partial z^2} = 0 \quad \text{(IV-62)}$$

Isotropic soils can be considered too, with κ_r=κ_z=κ, so Equation (IV-62) is simplified to Equation (IV-63).

$$\frac{1}{r}\frac{\partial}{\partial r}\left(r\frac{\partial h}{\partial r}\right) + \frac{\partial^2 h}{\partial z^2} = 0 \quad \text{(IV-63)}$$

As commented previously, traditional formulation does not consider vertical flow either far from the well center or in its vicinity. If that term is removed from Equation (IV-63), the traditional expression for modelling these problems is obtained.

$$\frac{1}{r}\frac{\partial}{\partial r}\left(r\frac{\partial h}{\partial r}\right) = 0 \qquad \text{(IV-64)}$$

In order to reach Dupuit's solution [1863] as well as understand the nomenclature of the problem, Figure 4.57 shows a sketch of the scenario with the variables and parameters involved.

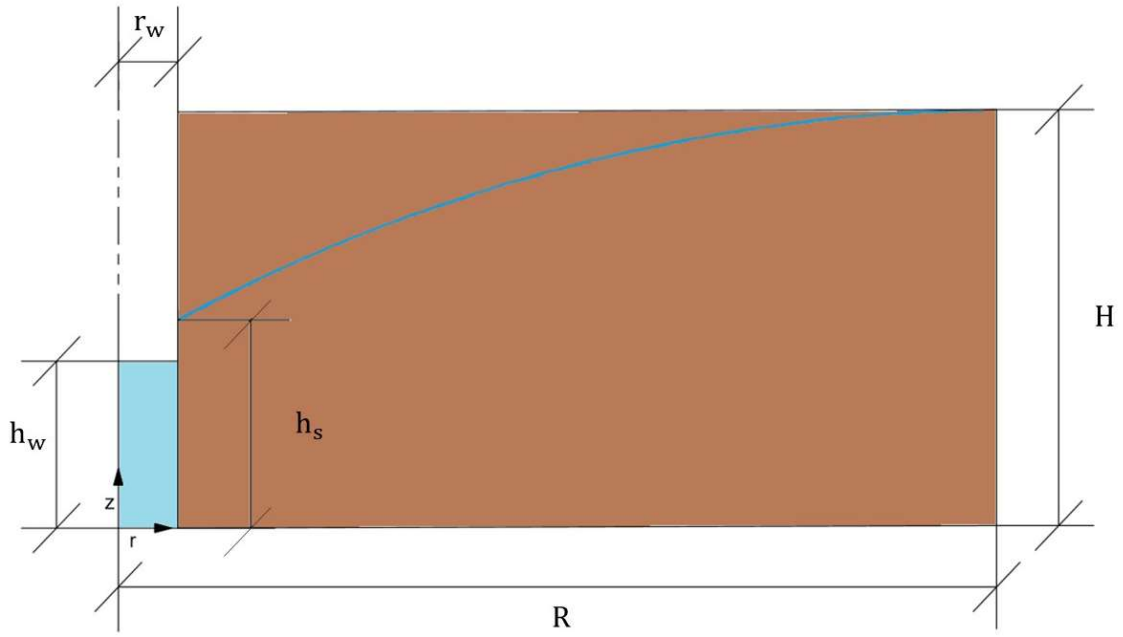

Figure 4.57. Nomenclature of the studied problem

The advantage of employing Dupuit's solution is its simplicity to obtain an analytical formulation that relates water flow and potential variation.

$r\left(\frac{\partial h}{\partial r}\right) = c_1$, according to Equation (IV-65). Moreover, Darcy's law states that $Q = 2\pi r h \kappa \frac{\partial h}{\partial r}$, so the constant value c_1 must take the value $c_1 = \frac{Q}{2\pi h \kappa}$. This leads to Equation (IV-65).

$$h\,\partial h = \frac{Q}{2\pi\kappa}\frac{\partial r}{r} \qquad \text{(IV-65)}$$

The first term of Equation (IV-64) is now integrated from h to H and the second one from r to R, thus, Dupuit's solution is obtained.

$$H^2 - h^2 = \frac{Q}{\pi\kappa}\ln\frac{R}{r} \qquad \text{(IV-66)}$$

The appearance of a second term in the governing equation that involves the vertical variation of the potential makes the mathematical resolution of the problem very complex, and the possibility of reaching an analytical solution is almost impossible without assuming other

simplifications. This is the reason why a numerical model based on the network method has been chosen to study these problems, so phenomena such as the seepage surface (h_s-h_w in Figure 4.57) can be studied.

Once the governing equation has been obtained, the boundary conditions must be set in order to complete the mathematical model. Again, as in the other problems previously studied along this chapter, two kinds of boundary conditions are needed: first class conditions (or Diritlech conditions), which are employed to model those borders with constants values of water head, and second class conditions (or Neumann conditions) correspond to impervious borders. Their expressions are shown in Equations (IV-4) and (IV-5).

$h = h_{o,r}$ at boundary regions 1,2…r (first class) (IV-4)

$\left.\frac{\partial v}{\partial n}\right|_s = 0$ at boundary regions 1,2…s (second class) (IV-5)

Unlike the problems previously studied here two different types of first -class boundary conditions have to be employed. There are borders on which the same water head values is set along it, while on others the constant value changes in each of its points. Moreover, the scenarios of flow in unconfined aquifers present two more kind of borders: free surface and seepage surface, and those are not data, but unknowns of the problem. Figure 4.58 shows the boundary conditions of the problem.

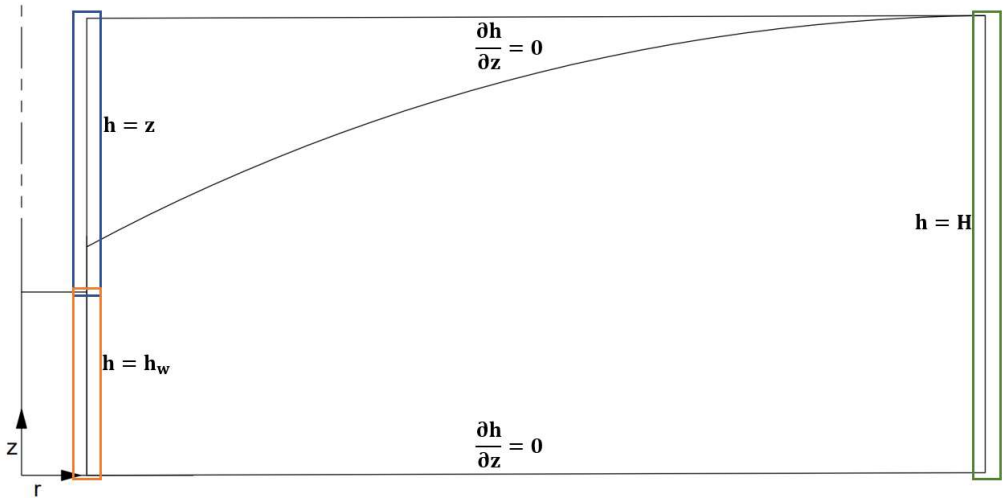

Figure 4.58. Boundary conditions of the studied problem

IV.2.4.2 Dimensionless governing equation and discriminated monomials

In scenarios of flow in unconfined aquifers due to a pumping, the parameters employed to obtain the dimensionless monomials governing the problem are the following:

R: aquifer horizontal length or radius (or if the scenario is very extent, it can be substituted by the influence radius) (m)
r_w: well radius (m)
h_1: water potential before pumping (m)
h_w: water potential in the well when it is pumping (m)
H: aquifer thickness (m)
Δh: h_1-h_w (m)

Along this thesis, H and h_1 are considered of the same value, although the first is a vertical length and the second is a water head or potential. For this reason, in some of the expressions where h_1 should appear, the parameter used is H.

These variables can be considered as references in order to obtain the discriminated dimensionless governing equation. Therefore, the references for variable r, z and h are R, h_1 and Δh are

$$r' = \frac{r}{R}; r = r'R, z' = \frac{z}{h_1}; z = z'h_1, h' = \frac{h}{\Delta h}, h = h'\Delta h \quad \text{(IV-67)}$$

from which

$$\partial r = \partial r' R;\ \partial r^2 = \partial r'^2 R^2, \partial z = \partial z' h_1;\ \partial z^2 = \partial z'^2 {h_1}^2, \partial h = \partial h' \Delta h;\ \partial^2 h = \partial^2 h' \Delta h \quad \text{(IV-68)}$$

Introducing these expressions into the governing equation (Equation (IV-63), its dimensionless form is set

$$\kappa_r \frac{1}{r'R} \frac{\partial}{R\,\partial r'} \left(r'R \frac{\Delta h\, \partial h'}{R\,\partial r'} \right) + \kappa_z \frac{\Delta h\, \partial^2 h'}{{h_1}^2\, \partial z^2} = 0 \quad \text{(IV-69)}$$

It is visible that the solution does not depend on the variation of water potential due to the pumping well. If the derivatives of r', z' and h' are assumed to be of order of magnitude unity, two dimensionless groups can be obtained

$$\pi_1 = \frac{\kappa_r {h_1}^2}{\kappa_z R^2} = \frac{\kappa_r H^2}{\kappa_z R^2} \quad \text{(IV-70)}$$

$$\pi_2 = \frac{r_w}{R} \quad \text{(IV-71)}$$

Nevertheless, the expressions for π_1 that are going to be used in this thesis are

$$\pi_1 = \sqrt{\frac{\kappa_r}{\kappa_z}} \frac{h_1}{R} \text{ or } \sqrt{\frac{\kappa_r}{\kappa_z}} \frac{H}{R} \quad \text{(IV-72)}$$

The monomial π_1 can also be expressed as $\frac{\kappa_r H^2}{\kappa_z {r_w}^2}$ or $\sqrt{\frac{\kappa_r}{\kappa_z}} \frac{H}{r_w}$, since the two horizontal lengths are related by equation (IV-72). This second way to express π_1 can be useful, as we see later in this section, where it is called π_1'. The second monomial, π_2, can also be obtained if the geometrical

conditions are studied, specifically those in the horizontal direction. Considering geometrical conditions too, in this case involving vertical ones, another discriminated monomial is deduced

$$\pi_3 = \frac{h_w}{H} \tag{IV-73}$$

The effects of the monomials on the flow depend on how they affect radial and vertical flows, since in this kind of problems water flow is predominantly radial. A high value of π_1 means that radial flow is more important than vertical one, and the opposite happens if the value is low.

Referring to π_2, it shows the behaviour of the horizontal flow. The lower the value of this monomial is, the more relevant the horizontal flow is since the vertical borders, where the hydraulic potentials are applied, are further from each other. Finally, π_3 shows the importance of vertical flow, as, if considering that the well only works pumping water out of the aquifer, low values of this group are equivalent to a higher importance of vertical flow.

Among the unknowns that can be investigated in this kind of problems, the first one is the water flow pumped out of the system, which can be transformed into a dimensionless variable if the correct reference is found. This can be obtained from different means, but it always should keep the same units of the water flow. In the next paragraph a possible reference flow Q_{ref} is deduced.

In this work, the reference flow is considered as a horizontal flow generated by the hydraulic potential change ($H-h_w$). This flow runs along the aquifer horizontal length ($R-r_w$). A general expression of the reference flow can be $Q_{ref} = v_{ref} \cdot S_{ref}$, where the reference velocity can be defined as

$$v_{ref} = \kappa_r \frac{H-h_w}{R-r_w} \tag{IV-74}$$

with discriminated units $\frac{[L_r]}{[T]}$, where $\kappa_r = \frac{[L_r]^2}{[T][L_{wc}]}$, $H \text{ and } h_w = [L_{wc}]$, and $R \text{ and } r_w = [L_r]$.

The reference cross-section (S_{ref}) is the lateral surface of a cylinder that, in order to reach dimensionless values of water flow lower than 1, presents radius R and height H: $S_{ref} = 2\pi RH$, with discriminated units $S_{ref} = [L_\alpha][L_z]$. The reason why, although parameter R has units $[L_r]$, the units of S_{ref} are $[L_\alpha][L_z]$ is that, as R is multiplied by 2π in order to obtain the horizontal length of the cylinder, the unit of the whole product is $[L_\alpha]$ (see Alhama y Madrid [2012]). In this way, the reference water flow presents the expression

$$Q_{ref} = \kappa_r \frac{H-h_w}{R-r_w} 2\pi RH \tag{IV-75}$$

This variable has the same units of the water flow obtained by the simulation, $\frac{[L_r][L_\alpha][L_z]}{[T]}$, so the monomial is dimensionless.

$$\pi_Q = \frac{Q}{\kappa_r \frac{H-h_w}{R-r_w} 2\pi RH} \quad \text{(IV-76)}$$

The second unknown variable to be studied is the seepage surface, which is the length above the well through which water also flows (alternatively, it might be defined as the length of the well wall where the water head is higher than its vertical position). The variable h_s is the whole contact surface between the well and the aquifer where the potential is higher than the position, as authors such as Hall [1955] or Simpson et al. [2003] have considered in their work.

The deduction of the dimensionless group which includes the seepage surface is simpler than that of the water flow, as it must include somehow a ratio of this variable and one of the boundary hydraulic potentials (or the difference of the two of them). After trying different options of dimensionless group for this variable, the one which leads to more understandable and accurate results is

$$\pi_{h_s} = \frac{h_s - h_w}{H} \quad \text{(IV-77)}$$

This dimensionless group includes both the initial hydraulic potential in the aquifer and the potential imposed in the well.

The last dimensionless variable that is presented here is the influence radius, R_{inf}. In this thesis, the influence radius has been defined as the radius value from which, if the aquifer is bigger, the difference between the estimate and the real groundwater flow would be less than a certain (low) percentage. Again, as in the two previous unknowns, different expressions can be deduced to obtain the dimensionless value of a variable. In this case, Equation (IV-78) shows the two possibilities for the influence radius.

$$\pi_{Rinf} = \frac{R_{inf}}{r_w} \text{ or } \frac{R_{inf}}{\sqrt{\frac{\kappa_r}{\kappa_z}} \cdot H} \quad \text{(IV-78)}$$

IV.2.4.3 Universal abaci

Four different abaci are presented in order to characterize this problem: one for the groundwater flow (Figure 4.59), another one for the seepage surface (Figure 4.60), and the last ones for the influence radius considering a difference of 10% between two consecutive iterations in which the aquifer's radius is increased a considered length (Figures 4.61 and 4.62). The last value of π_3, 0.001, is used to approach the problem of a well where the hydraulic potential is imposed to be at its bottom, and therefore, the aquifer's one, as the well is considered as fully penetrating.

After all the simulations, it was evident that the differences of π_Q according to π_1 for the same values of π_2 and π_3 were low enough to consider that the group involving hydraulic conductivities does not affect the dimensionless water flow (the highest difference is around 2.3%). This fact leads to a simplification of the abacus (Figure 4.59) as it only includes one curve for each π_2.

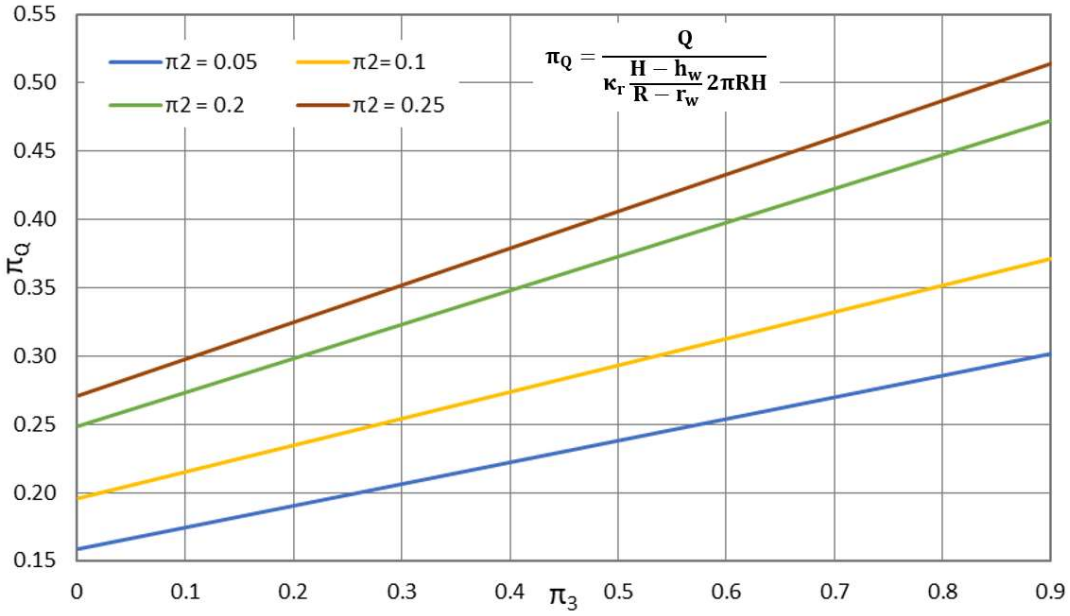

Figure 4.59. Dimensionless groundwater flow

Beyond the 'lack of effect' of π_1 monomial, it is also relevant to know how the geometrical conditions affect the problem, this is π_2 and π_3. Referring to the effect on water flow, it can differ whether the real or the dimensionless water flow is being considered. Studying the impact of π_2, it is observed that, as it increases its value (which means that the well radius is wider), the pumping capacity is also increased. These influence both real and dimensionless water flow.

π_3 affects differently the behaviour of real and dimensionless water flow. If studying the real variable, the lower the value of π_3, the higher the potential difference is, which generates more water flow. Nevertheless, when comparing this with the reference flow, Q_{ref}, as it is also incremented with the decrease of π_3, the difference between the two water flows also grows. This is translated into a reduction of π_Q.

Figure 4.60 presents the abacus for the dimensionless seepage surface, π_{hs}, and unlike the dimensionless groundwater flow, this dimensionless variable is affected by the permeability monomial, π_1.

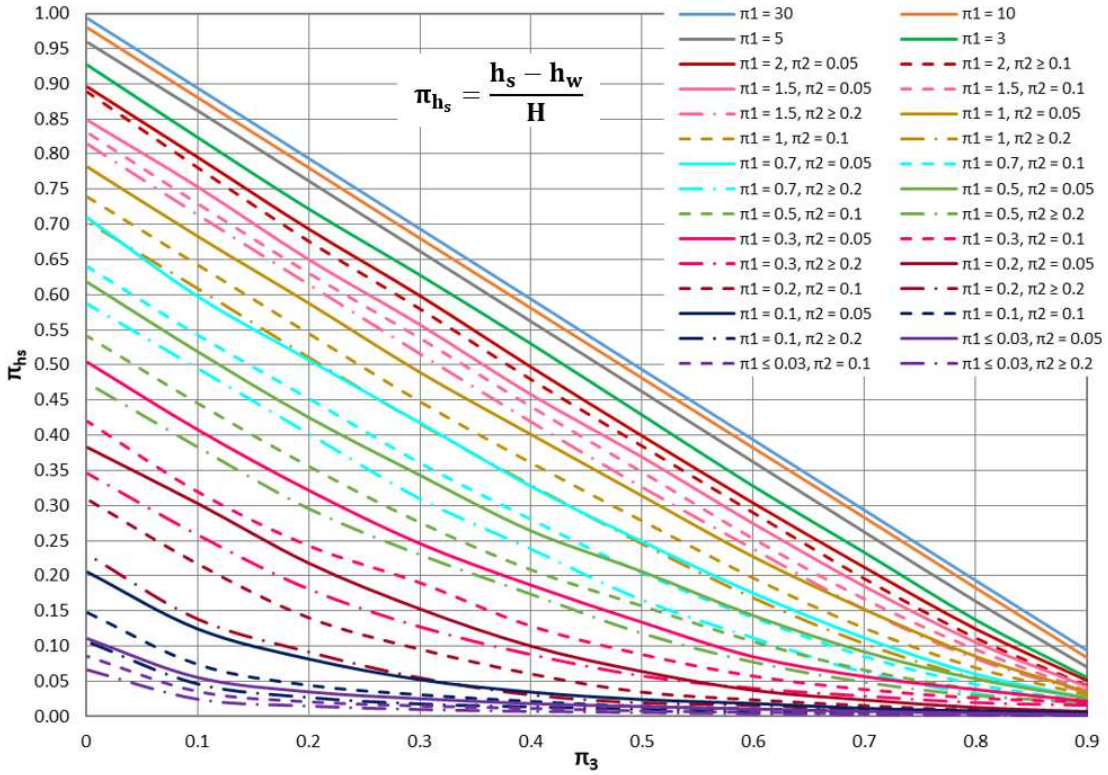

Figure 4.60. Dimensionless seepage surface

For this dimensionless variable, the effect of π_1 is somehow expected: the higher the horizontal flow is, the higher the value of the seepage surface, because it is easier for the flow to go on in the horizontal direction. The monomial π_2 has the opposite effect, as higher values of π_{hs} are obtained as π_2 decreases: low values of π_2 stimulates horizontal flow. Finally, the effect of π_3 is also expected: π_{hs} increases its value with π_3 as happens with the groundwater flow.

The last dimensionless variable studied is the influence radius considering a difference lower than 10%. For this, two abaci are presented, one for each of the possible ways to turn it into dimensionless (Equation (IV-78)), Figures 4.61 and Figure 4.62

After carrying out all the simulations it was observed that π_3 had little effect on π_{Rinf} (the difference for a certain value of π_1' is always less than 1.02%). Therefore, the only monomial affecting the influence radius is π_1'. As this group is increased, the dimensional influence radius also increases, which is shown in Figure 4.61. Changing the reference and introducing the anisotropy ratio, the trend is altered.

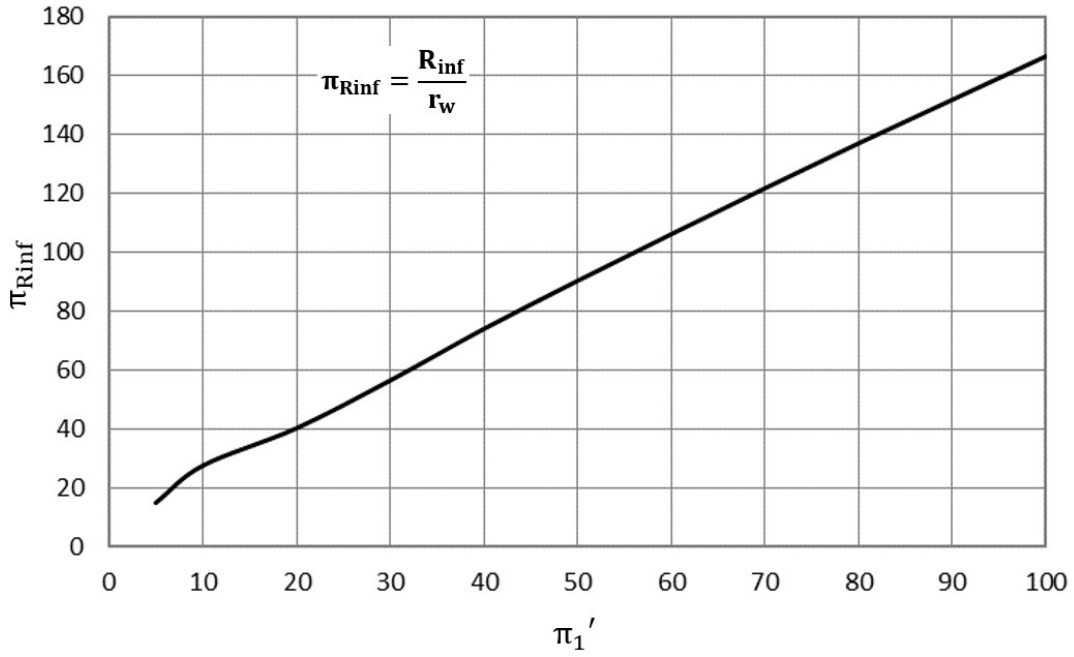

Figure 4.61. Dimensionless influence radius taking r_w as reference

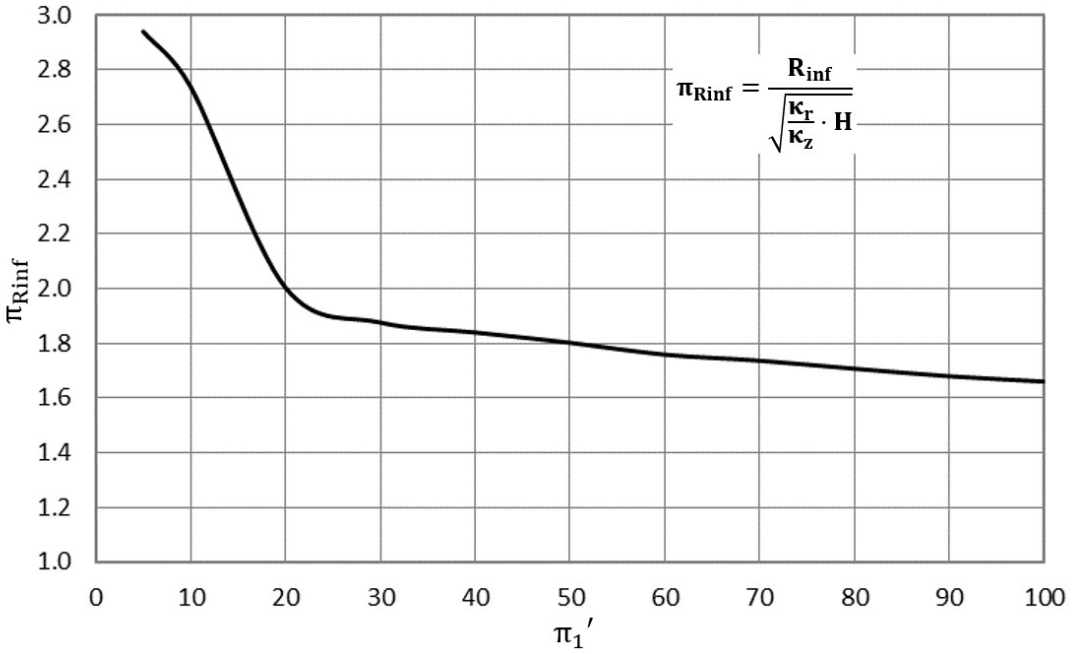

Figure 4.62. Dimensionless influence radius taking $\sqrt{\frac{\kappa_r}{\kappa_z}} \cdot H$ as reference

However, the influence radius present larger values if reducing the percentage from 10 to 1, which would probably lead to more realistic results to model a real scenario and the extension affected by the pumping well. Although this was the first idea, after carrying out the corresponding simulations, the results cannot be plotted in a universal curve or abacus, because of the high variability of results for π_3 without any trend, and the lack of continuity for each π_1'.

The maximum and minimum values of the dimensionless influence radius according to the second expression in Equation (IV-78) are shown in Table 4.2.

Table 4.2. Minimum and maximum dimensionless influence radius for a groundwater flow differences of 1%

π_1'	Min π_{Rinf}	Max π_{Rinf}
5	16.94	21.70
10	14.97	18.98
20	14.87	17.58
30	13.77	15.95
40	13.81	14.91
50	11.98	13.91
60	12.84	12.98
70	10.99	12.83
80	10.97	12.76
90	10.93	11.84
100	9.97	11.73

In this way, when modelling real scenarios, it would be a good practice to consider both value of influence radius, 10 and 1% of groundwater flow, and see the results obtained with both considerations.

Most of the empirical formulations for the calculation of the dimensional influence value present the variable time in their expressions (for example Choultse and Koussakine, presented in Castany [1971]), since reaching a steady-state scenario is not always possible. Other authors do not include time in their formulation, for example Camberfort or Kyrieleis- Sichardt, also in Castany, but in these cases only isotropic hydraulic conductivity is involved. These are empirical formulations somehow based on Dupuit's equation and, therefore, those depend on the same restrictions as this traditional expression. Finally, pumping manuals, such as that of Villanueva & Iglesias [1984], give a range of values for estimating the influence radius depending on the type of aquifer (confined, semi-confined and unconfined) as well as the type of material in the aquifer (karstic, porous or a mixture of the two previous). For an unconfined porous aquifer, the influence radius would be between 400 and 700 m, according to Villanueva & Iglesias.

Chapter VI, in which Figures 4.59 and 4.60 are used to study an inverse problem related to flow in unconfined aquifers, presents examples of how to read values of groundwater flow from the abacus in Figure 4.59.

IV.2.4.4 Verification of the dimensionless groups

In this section, the groups governing the problem of flow in unconfined aquifers due to pumping wells are verified with the dimensionless unknowns 'groundwater flow' and 'seepage surface'. In this way, we can observe the validity of the discriminated nondimensionalization technique. Similar verifications have been carried out for all the scenarios presented in this chapter but, as they have so many unknowns variables whose universal abaci are studied, the validity is only illustrated for the scenarios of flow in unconfined aquifers.

In order to verify a monomial, the process consists on designing different dimensional scenarios that can be turn into the same dimensionless problem, this is, the monomials governing the phenomenon take the same value. When the dimensionless expression of the unknown variables have been correctly obtained, then in all the designed scenarios they have the same value. If this does not occur, the definition of all the monomials must be revised so correct expressions can be found. As the scenario studied in this section has more than one governing monomial, then each monomial is verified with a different set of dimensional scenarios whose dimensionless translation only differs in the value of one monomial.

Table 4.3 shows the dimensional geometric and hydraulic parameters of the different scenario, as well as their dimensional results. Table 4.4, however, shows the same scenarios, but summarized into their dimensionless form, so the cases can be paired into the same dimensionless problem. This is, Case 1 and Case 2 can be presented as the same dimensionless scenario, and so on. Cases 1 and 2 are the base dimensionless scenario, with $\pi_1 = 1$, $\pi_2 = 0.1$ and $\pi_3 = 0.5$. In cases 3 and 4, π_1 is changed from 1 to 0.2, keeping π_2 and π_3 the same as in cases 1 and 2. Cases 5 and 6 have the same values of π_1 and π_3 as cases 1 and 2, while π_2 takes now a value of 0.25. Finally, in cases 7 and 8 the same values of π_1 and π_2 as in cases 1 and 2 are employed, and π_3 now is 0.7 instead of 0.5.

Table 4.3. Dimensional scenarios

Case	κ_r (m/s)	κ_z (m/s)	R (m)	r_w (m)	H (m)	h_w (m)	Q (m^3/s)	h_s (m)
1	0.0001	0.0001	10	1	10	5	0.0103	7.736
2	0.000225	0.0001	15	1.5	10	5	0.0231	7.736
3	0.0001	0.0001	50	5	10	5	0.0104	5.343
4	0.0001	0.000025	50	5	5	2.5	0.0260	2.672
5	0.0001	0.0001	10	2.5	10	5	0.0171	7.349
6	0.0005	0.0001	22.36	5.59	10	5	0.0854	7.349
7	0.0001	0.0001	10	1	10	7	0.0070	8.240
8	0.0003	0.0001	10	1	5.77	4.07	0.0070	4.753

Table 4.4. Dimensionless scenarios

Case	π_1	π_2	π_3	π_Q	π_{hs}
1	1	0.1	0.5	0.295	0.274
2	1	0.1	0.5	0.295	0.274
3	0.2	0.1	0.5	0.297	0.034
4	0.2	0.1	0.5	0.297	0.034
5	1	0.25	0.5	0.408	0.235
6	1	0.25	0.5	0.408	0.235
7	1	0.1	0.7	0.334	0.124
8	1	0.1	0.7	0.334	0.123

As seen in Tables 4.3 and 4.4, although the dimensional scenarios in each pair are different, when turned into dimensionless, the value of the dimensionless unknown are the same, which verifies the technique employed along this chapter. The only values that differ are those of π_{hs} in Cases 7 and 8, but this slight difference (below 1%) is due to the numerical simulation.

Moreover, it is also interesting to remark the little difference between the values of π_Q for π_1 = 1, π_2 = 0.1 and π_3 = 0.5 and for π_1 = 0.2, π_2 = 0.1 and π_3 = 0.5, which are 0.295 and 0.297 respectively. This shows what was explained previously in Figure 4.59: permeability monomial has little effect on the dimensionless groundwater flow (in this case, less than 0.7%).

The effect of the other two monomials governing the scenario, π_2 and π_3, is the one shown in Figure 4.59: if the well radius is increased, then more dimensional and dimensionless

groundwater flow is obtained, while if the well height is the modified parameter (increasing its value), then the dimensionless flow increases, although this means that the dimensional flow has been decreased.

The effect of the three monomials in the dimensionless values of the seepage surface, π_{hs} is also the one shown in Figure 4.60. The decrease of monomial π_1 leads to a lower value of the seepage surface. If π_2 monomial is the one changed, increasing its value, it also leads to a decrease of the seepage surface. Finally, increasing π_3 leads to a decrease in the seepage surface monomial.

Chapter V. Network models and the software DamSim and WaWSim

In this chapter, first an introduction to the Network Method is presented, explaining how the different devices involved in the circuits are implemented from the equivalence between the constitutive equations that define them (which rule the electric circuits) and the addends of the governing equations that define the physical problem to be simulated. The following section explains how the Network Method and the electrical analogy are applied to simulate scenarios of flow under dams with or without a sheet pile, while Section V.3 shows the same for problems of flow in unconfined aquifers with pumping wells. Afterwards, the explanation of how the boundary conditions are implemented is presented (Section V.4). Section V.5 explains how the text file needed as input information for Ngspice is structured, and the next section shows the results that can be obtained and exported to Matlab. Finally, Section V.7 presents the different windows that make up the developed software and how they work.

V.1 Network model creation process. Introduction

When simulating problems of flow through porous media in steady-state condition, whether retaining structures or wells are being considered, Laplace equation is the one that governs the process. This partial derivative equation sets the balance of flow in each elemental volume of

the domain. Writing this equation in its spatially discretized form, each one of their addends is implemented as a current that cross a branch of the network model. All the currents balance each other in a common node identified as the central node of the cell or volume element. Thus, there are as many branches as terms in the discretized equation and each branch is electrically connected between the input or output node of the cell and the central one. Each branch of the cell in the network model implements a suitable electrical device (resistor, capacitor, controlled source…), according to the mathematical expression of the addends related to the branch. The set of these devices in conjunction with their topology, or electrical connections between them through the nodes, is what we name the network model of a cell. The whole model of the scenario is completed by making ideal electrical connections between adjacent cells and adding the devices that implement the boundary conditions at the face of the required cells.

By doing all the steps mentioned above, the equivalence between the physical and electrical models is completely established thanks to the fact that the equations of both (in finite differences) are equivalent. The errors between the exact solutions and those of the electrical model are only attributable to the global number of cells in which the scenario is discretized and can be reduced with a sufficiently large value of them at the cost of increasing computation time.

In this way, in both 2-D studied scenarios, the network model of the cell contains four branches, a pair for each of the second derivative terms of the equation, i.e., two for the horizontal flow and two for the vertical one. This means that, for each direction, inflow and outflow is being modelled or implemented in a separate branch. If transient flow, a fifth branch would appear in order to simulate the storage or partial time derivative addend.

Setting the equivalence between physical and electrical variables:

electric current, J (A) ⇔ water flow, Q (m^3/s)
electric potential, v (V) ⇔ water head, h (m)

the expressions of the addends of the equations for a given cell (i,j) are

$$Q_{i,j} = f\left(h_{\text{at the nodes of the cell i,j}}\right) \quad \text{(V-1)}$$

$$J_{i,j} = f\left(V_{\text{at the nodes of the cell i,j}}\right) \quad \text{(V-2)}$$

Equations (V-1) and (V-2) are also equivalent each other. For instance, if a simple expression is obtained of an addend of the mathematical discretized model has the form

$$Q_{i,j} = \frac{m}{n}\left(h_{i,j} - h_{i-1,j}\right) \quad \text{(V-3)}$$

we can set the analogue equation (Ohm´s law)

$$I_R = \frac{V_R}{R} \tag{V-4}$$

with I_R the electrical current that cross a resistor with a voltage V_R at its ends. The value of the resistance, placed between nodes i,j and i-1,j , is given by

$$R = \frac{n}{m} \tag{V-5}$$

In the two studied scenarios the only devices that are needed to model them are resistors, as all the terms involved in their governing equation are spatial variations of water potential.

The circuit solution solved by Ngspice [2016] (a specific computer software for this purpose), provides all the unknowns of the model: i) voltages at all central and lateral nodes of the cell, ii) currents through each of the devices in each cell and iii) any other quantity related to the boundary conditions.

V.2 Flow under gravity dams with or without a sheet pile

For this geometry, whose scheme is presented in Figure 5.1 where water basically flows from left to right (x direction), the mathematical model is shown in Equations (V-6) to (V-11).

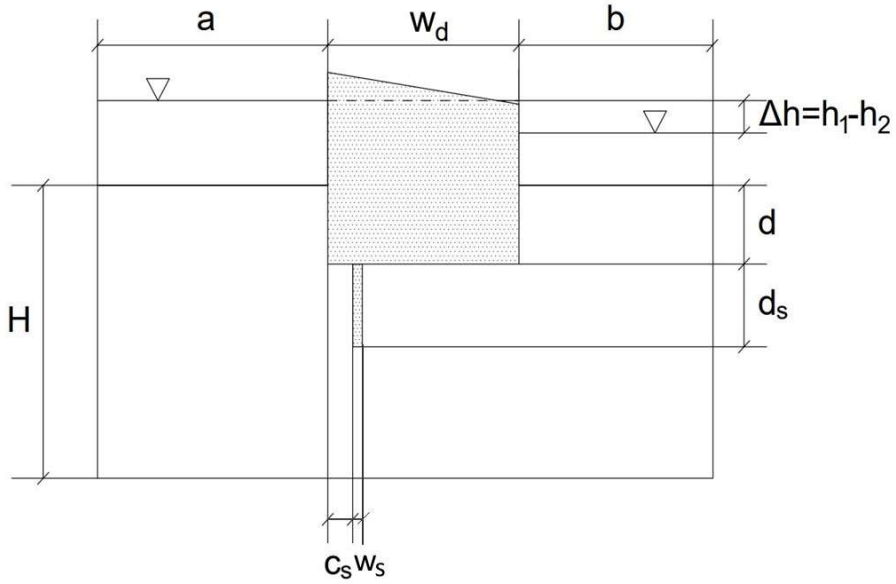

Figure 5.1. Nomenclature of dam scenarios

$$\kappa_x \frac{\partial^2 h}{\partial x^2} + \kappa_y \frac{\partial^2 h}{\partial y^2} = 0 \qquad \text{(local balance equation)} \tag{V-6}$$

$$h_{x=0-a,y=0} = h_1 \quad \text{(constant water potential upstream the dam)} \tag{V-7}$$

$$h_{x=a+w_d-a+b+w_d,y=0} = h_2 \quad \text{(constant water potential downstream the dam)} \tag{V-8}$$

$$\frac{\partial h}{\partial x_{x=0,y}} = \frac{\partial h}{\partial x_{x=a+w_d+b,y}} = \frac{\partial h}{\partial y_{x,y=H}} = 0 \quad \text{(impervious outer borders)} \tag{V-9}$$

$$\frac{\partial h}{\partial x_{x=a,y=0-d}} = \frac{\partial h}{\partial x_{x=a+w_d,y=0-d}} = \frac{\partial h}{\partial y_{x=a-a+w_d,d}} = 0 \text{ (impervious dam borders)} \tag{V-10}$$

$$\frac{\partial h}{\partial x_{x=a+c_s.y=d-d+d_s}} = \frac{\partial h}{\partial x_{x=a+c_s+w_s,y=d-d+d_s}} = \frac{\partial h}{\partial y_{x=a+c_s-a+c_s+w_s,y=d+d_s}} = 0$$

(impervious sheet pile borders) (V-11)

Figure 5.2 presents the nomenclature of the elemental volume. Although the governing equation is the one presented in Equation (V-6), as commented previously in this thesis, it comes from the combination of the continuity equation and Darcy's law

$$Q_{x,in} - Q_{x,out} + Q_{y,in} - Q_{y,out} = 0 \tag{V-12}$$

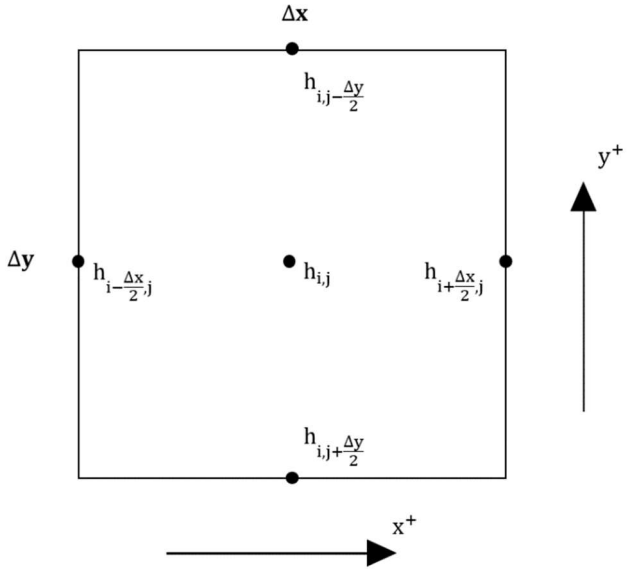

Figure 5.2. Nomenclature of the elemental volume for problems of flow under dams

The reason why it is decided to employ the continuity equation instead of Laplace's (Martínez-Moreno et al. [2020]) is the need to use a progressive reticulation in which smaller cells are closer to the retaining structure and larger ones far from it. Near the structure more information is needed as most of the main phenomena happen there while the same information is not so relevant in further zones.

In terms of velocity, continuity equation can be written as

$$v_{x,in}S_{x,in} - v_{x,out}S_{x,out} + v_{y,in}S_{y,in} - v_{y,out}S_{y,out} = 0 \tag{V-13}$$

Substituting the values of cross sections and velocities in the continuity equation

$$S_{x,out} = S_{x,in} = \Delta y, \qquad S_{y,out} = S_{y,in} = \Delta x \tag{V-14}$$

$$v_{x,in}=v_{i+\frac{\Delta x}{2},j} = -\kappa_x \frac{h_{i+\frac{\Delta x}{2},j}-h_{i,j}}{\frac{\Delta x}{2}},\ v_{x,out} = v_{i-\frac{\Delta x}{2},j} = -\kappa_x \frac{h_{i,j}-h_{i-\frac{\Delta x}{2},j}}{\frac{\Delta x}{2}},$$

$$v_{y,in} = v_{i,j+\frac{\Delta y}{2}} = -\kappa_y \frac{h_{i,j+\frac{\Delta y}{2}}-h_{i,j}}{\frac{\Delta y}{2}}, \qquad v_{y,out} = v_{i,j-\frac{\Delta x}{2}} = -\kappa_y \frac{h_{i,j}-h_{i,j-\frac{\Delta y}{2}}}{\frac{\Delta y}{2}} \tag{V-15}$$

results

$$-\frac{h_{i+\frac{\Delta x}{2},j}-h_{i,j}}{\frac{\Delta x}{2\kappa_x \Delta y}} + \frac{h_{i,j}-h_{i-\frac{\Delta x}{2},j}}{\frac{\Delta x}{2\kappa_x \Delta y}} - \frac{h_{i,j+\frac{\Delta y}{2}}-h_{i,j}}{\frac{\Delta y}{2\kappa_y \Delta x}} + \frac{h_{i,j}-h_{i,j-\frac{\Delta y}{2}}}{\frac{\Delta y}{2\kappa_y \Delta x}} = 0 \tag{V-16}$$

Other definitions for these velocities could be chosen if employing the adjacent cells (as is common in numerical applications) but all would lead to the same numerical solutions for fine grid size. Each term of equation can be assumed to be an electrical current which we call

$$j_{R_{i+\Delta x/2,j}} = \frac{h_{i,j}-h_{i+\frac{\Delta x}{2},j}}{\frac{\Delta x}{2\kappa_x \Delta y}},\ j_{R_{i-\Delta x/2,j}} = \frac{h_{i-\frac{\Delta x}{2},j}-h_{i,j}}{\frac{\Delta x}{2\kappa_x \Delta y}},$$

$$j_{R_{i,j+\Delta y/2}} = \frac{h_{i,j}-h_{i,j+\frac{\Delta y}{2}}}{\frac{\Delta y}{2\kappa_y \Delta x}},\ j_{R_{i,j-\Delta y/2}} = \frac{h_{i,j-\frac{\Delta y}{2}}-h_{i,j}}{\frac{\Delta y}{2\kappa_y \Delta x}} \tag{V-17}$$

As the current and the potential variable are proportionally dependent, the electrical component that implements each term of the equation in the network model is a resistor (Ohm's law). The four resistors are located in the elemental volume as presented in Figure 5.3. The resistance values are:

$$R_{i+\Delta x_i/2,j} = R_{i-\Delta x_i/2,j} = \frac{\Delta x_i}{2\kappa_x \Delta y_j} \qquad R_{i,j+\Delta y_j/2} = R_{i,j-\Delta y_j/2} = \frac{\Delta y_j}{2\kappa_y \Delta x_i} \tag{V-18}$$

with Δx_i and Δy_j the lengths of the rectangular cell, which can vary according to the progressive reticulation. In isotropic soils where constant reticulation is used instead of progressive one, resistors values are the same.

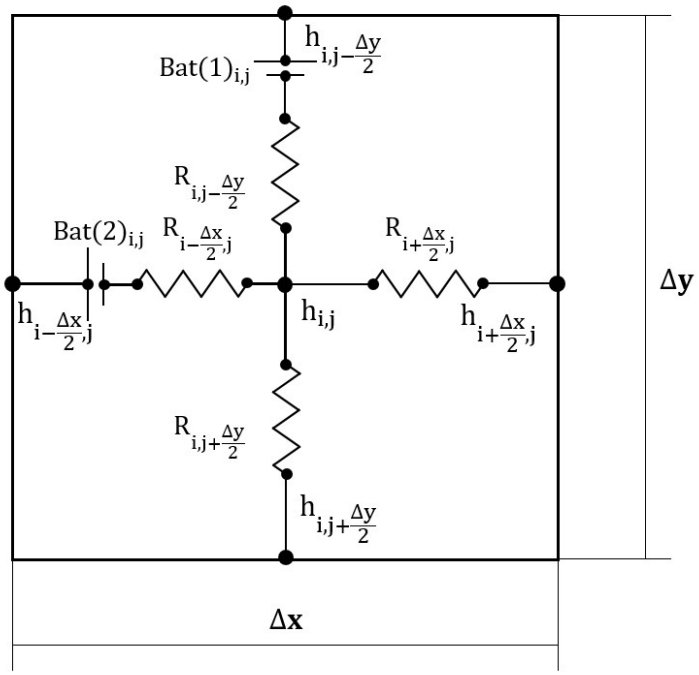

Figure 5.3. Elemental circuit for problems of flow under dams

In order to be able to know the water flow running through the elemental volume in both directions, zero voltage batteries are placed in one of the two branches of each direction. These batteries do not affect the results. Instead, they allow the code to read the value of current through them and, therefore, according to the electrical analogy, the value of the water flow.

V.3 Flow in unconfined aquifers in steady state due to a pumping well

In this problem, whose geometry is presented in Figure 5.4, the flow goes from the point of higher potential, placed at the aquifer border, to that of lower, which is imposed in the well. These scenarios are ruled by Equation (V-19) and boundary conditions Equations (V-20) to (V-23).

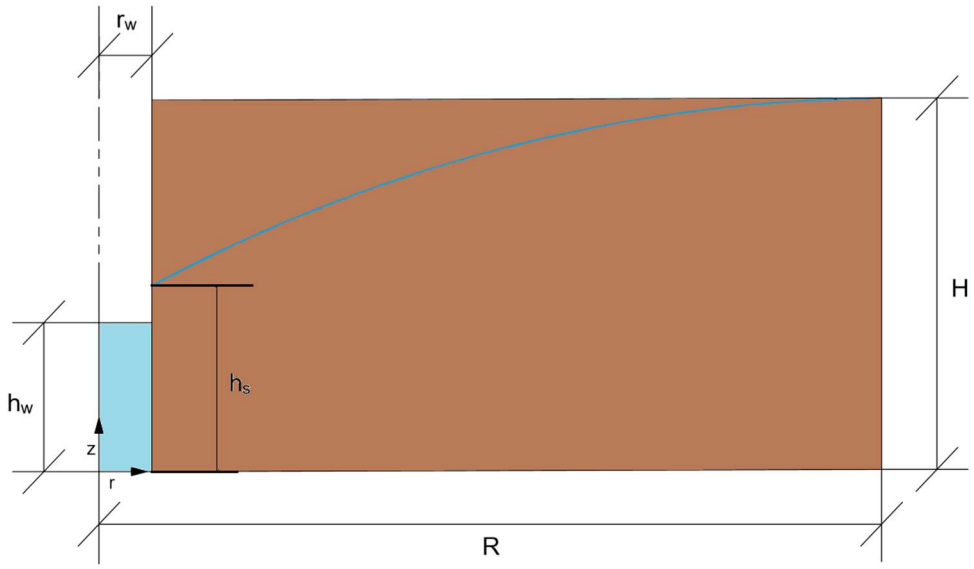

Figure 5.4. Nomenclature of scenarios of well in unconfined aquifers

$$\kappa_r \frac{1}{r}\frac{\partial}{\partial r}\left(r\frac{\partial h}{\partial r}\right) + \kappa_z \frac{\partial^2 h}{\partial z^2} = 0 \quad \text{(local balance equation)} \tag{V-19}$$

$$h_{r=R,z=0-H} = H \quad \text{(constant water potential at the aquifer border / saturated thickness)} \tag{V-20}$$

$$h_{r=r_w,z=0-h_w} = h_w \quad \text{(constant water potential at the well border / well height)} \tag{V-21}$$

$$h_{r=r_w,z=h_w-H} = z \quad \text{(constant water potential at the vertical border above the well)} \tag{V-22}$$

$$\frac{\partial h}{\partial y_{r=r_w-R,z=H}} = \frac{\partial h}{\partial y_{r=r_w-R,z=0}} = 0 \quad \text{(impervious border at the top and bottom borders of the aquifer)} \tag{V-23}$$

The nomenclature is shown in Figure 5.5. To determine the value of the resistors involved in the network model of the cell, we start from the steady-state conservation equation:

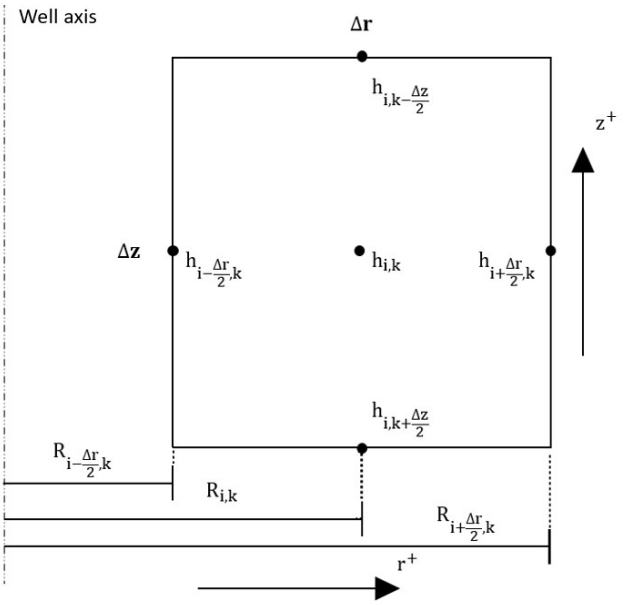

Figure 5.5. Nomenclature of the elemental volume for problems of flow in unconfined aquifers due to a pumping well

$$Q_{r,in} - Q_{r,out} + Q_{z,in} - Q_{z,out} = 0 \quad \text{(V-24)}$$

If expressing the water flow as the product of the velocity and the crossing section, the former equation can be written as

$$v_{r,in}S_{r,in} - v_{r,out}S_{r,out} + v_{z,in}S_{z,in} - v_{z,out}S_{z,out} = 0 \quad \text{(V-25)}$$

Now, using Darcy's law, this equation is transformed into

$$v_{r\,i-\frac{\Delta r_i}{2},k} = -\kappa_r \frac{h_{i,k} - h_{i-\frac{\Delta r_i}{2},k}}{\frac{\Delta r_i}{2}}, v_{r\,i+\frac{\Delta r_i}{2},k} = -\kappa_r \frac{h_{i+\frac{\Delta r_i}{2},k} - h_{i,k}}{\frac{\Delta r_i}{2}},$$

$$v_{z\,i,k-\frac{\Delta z_k}{2}} = -\kappa_z \frac{h_{i,k} - h_{i,k-\frac{\Delta z_k}{2}}}{\frac{\Delta z_k}{2}}, v_{z\,i,k+\frac{\Delta z_k}{2}} = -\kappa_z \frac{h_{i,k+\frac{\Delta z_k}{2}} - h_{i,k}}{\frac{\Delta z_k}{2}} \quad \text{(V-26)}$$

Water flows with these velocities through the corresponding cell section crossing their boundaries, whose sections are calculated with the following formulae. For the radial velocity, this section changes from input to output due to cylindrical crown form of the cell while for the vertical velocity the input and output sections are the same.

$$S_{r,out} = S_{i-\frac{\Delta r_i}{4},k} = 2\pi\left(r_{i,k} - \frac{\Delta r_i}{4}\right)\Delta z_k, S_{r,in} = S_{i+\frac{\Delta r_i}{4},k} = 2\pi\left(r_{i,k} + \frac{\Delta r_i}{4}\right)\Delta z_k,$$

$$S_{z,in} = S_{z,out} = S_{i,k+\frac{\Delta z_k}{4}} = S_{i,k-\frac{\Delta z_k}{4}} = \pi\left[\left(r_{i,k} + \frac{\Delta r_i}{2}\right)^2 - \left(r_{i,k} - \frac{\Delta r_i}{2}\right)^2\right] \quad \text{(V-27)}$$

Different definitions for the velocities can be used if considering the adjacent cells, although all of them converge to the same solution for fine grid size. Equations (V-26) and (V-27) can be introduced in (V-25), leading to (V-28).

$$-\kappa_r \frac{h_{i,k} - h_{i-\frac{\Delta r_i}{2},k}}{\frac{\Delta r_i}{2}} 2\pi\left(r_{i,k} - \frac{\Delta r_i}{4}\right)\Delta z_k + \kappa_r \frac{h_{i+\frac{\Delta r_i}{2},k} - h_{i,k}}{\frac{\Delta r_i}{2}} 2\pi\left(r_{i,k} + \frac{\Delta r_i}{4}\right)\Delta z_k - \kappa_z \frac{h_{i,k} - h_{i,k-\frac{\Delta z_k}{2}}}{\frac{\Delta z_k}{2}} \pi\left[\left(r_{i,k} + \frac{\Delta r_i}{2}\right)^2 - \left(r_{i,k} - \frac{\Delta r_i}{2}\right)^2\right] + \kappa_z \frac{h_{i,k+\frac{\Delta z_k}{2}} - h_{i,k}}{\frac{\Delta z_k}{2}} \pi\left[\left(r_{i,k} + \frac{\Delta r_i}{2}\right)^2 - \left(r_{i,k} - \frac{\Delta r_i}{2}\right)^2\right] = 0 \quad \text{(V-28)}$$

Each of the addends of the previous equation can be translated into an electrical current (j). In this way, we shall write

$$j_{Ri-\frac{\Delta r_i}{2},k} = \frac{h_{i,k} - h_{i-\frac{\Delta r_i}{2},k}}{\frac{\Delta r_i}{4\kappa_r \pi\left(r_{i,k} - \frac{\Delta r_i}{4}\right)\Delta z_k}}, j_{Ri+\frac{\Delta r_i}{2},k} = \frac{h_{i+\frac{\Delta r_i}{2},k} - h_{i,k}}{\frac{\Delta r_i}{4\kappa_r \pi\left(r_{i,k} + \frac{\Delta r_i}{4}\right)\Delta z_k}},$$

$$j_{Ri,k-\frac{\Delta z_k}{2}} = \frac{h_{i,k} - h_{i,k-\frac{\Delta z_k}{2}}}{\frac{\Delta z_k}{2\kappa_z \pi\left[\left(r_{i,k} + \frac{\Delta r_i}{2}\right)^2 - \left(r_{i,k} - \frac{\Delta r_i}{2}\right)^2\right]}}, j_{Ri,k+\frac{\Delta z_k}{2}} = \frac{h_{i,k+\frac{\Delta z_k}{2}} - h_{i,k}}{\frac{\Delta z_k}{2\kappa_z \pi\left[\left(r_{i,k} + \frac{\Delta r_i}{2}\right)^2 - \left(r_{i,k} - \frac{\Delta r_i}{2}\right)^2\right]}} \quad \text{(V-29)}$$

Using Ohm's law for each addend of the equation, the value of the resistors (which depend on the geometrical characteristics of the grid and the hydrogeological parameters of the scenario) are

$$R_{i-\frac{\Delta r_i}{2},k} = \frac{\Delta r_i}{4\kappa_r \pi\left(r_{i,k}-\frac{\Delta r_i}{4}\right)\Delta z_k}, R_{i+\frac{\Delta r_i}{2},k} = \frac{\Delta r_i}{4\kappa_r \pi\left(r_{i,k}+\frac{\Delta r_i}{4}\right)\Delta z_k},$$

$$R_{i,k-\frac{\Delta z_k}{2}} = R_{i,k+\frac{\Delta z_k}{2}} = \frac{\Delta z_k}{2\kappa_z \pi\left[\left(r_{i,k}+\frac{\Delta r_i}{2}\right)^2-\left(r_{i,k}-\frac{\Delta r_i}{2}\right)^2\right]} \quad \text{(V-30)}$$

For the two kind of problems studied along this thesis, the use of the continuity equation instead of the traditional approach represents some improvements. The most important ones are:

- It is not necessary to carry out mathematical manipulations to obtain the values of water potential and flow, as they are those of voltage and current that can be measured straight from the circuit once the simulation is done.
- Extra devices, such as current generators, are avoided, simplifying the calculations and, therefore, reducing the computational time.

However, because of the specific nature of the problems of flow in unconfined aquifers due to the presence of pumping wells, another type of devices is necessary to simulate the scenarios in a correct way. These devices are switches, which connect or disconnect the cells according to a rule that has been previously established. When a drawdown happens, the area that loses water once the circuits have been solved (that is, the area which is above the final phreatic level), presents lower values of voltage than vertical coordinates, which would mean that the pore pressure in those points is negative. As no capillary fringe is being considered, these values are not possible, so the solution to avoid it in the post-simulation calculations is disconnecting these cells. Therefore, according to the position of the elemental volume in the scenario, switches have been located in different circuit branches. Nevertheless, despite their location, all switches work as follows: if the voltage in a given node is higher or equal to its z coordinate, the switch is closed, and the current is allowed to run through that branch; conversely, if its voltage is lower, then the switch opens, and the electrical current cannot run through that branch.

The use of more or less ideal switches in the circuit computer codes currently employed broadens the possibilities of simulating this kind of models. When in the 1950s and before analogical simulators were used for modelling problems of groundwater flow in scenarios with 'free surfaces', their contours could only be reproduced cutting the electrolytical paper along a line that was approximately considered as the free surface. The chance of obtaining this contour

in an automatic and accurate way employing switches has only been successfully carried out in this thesis, as far as we know.

To conclude the structure of the circuit in which each elemental volume is transformed, other extra elements are introduced, although these do not affect the results. On the contrary, they are used to obtain valuable information from the circuits that could not be given in any other way. Although voltage values can be measured from any node of the simulated circuits without any specific device, this does not occur when current values are needed. For this reason, batteries of null voltage are placed in those branches in which electrical current values (and therefore water flow) have to be achieved. Figures 5.6 to 5.11 show the network models of the different elemental volumes that have been employed in this scenario.

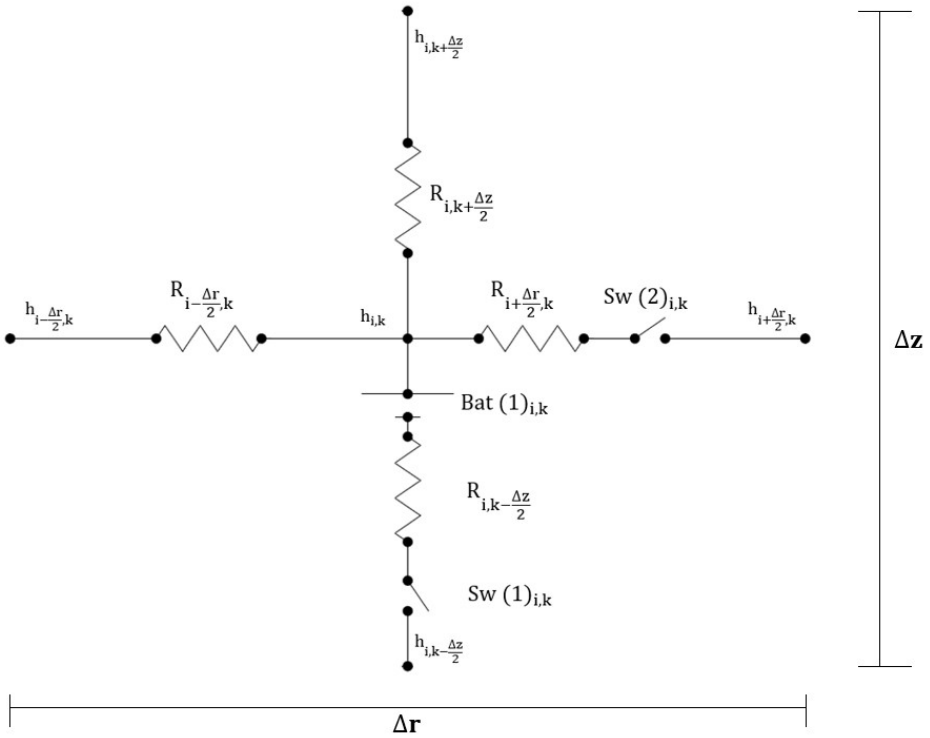

Figure 5.6. Scheme of a typical cell (central area of the scenario)

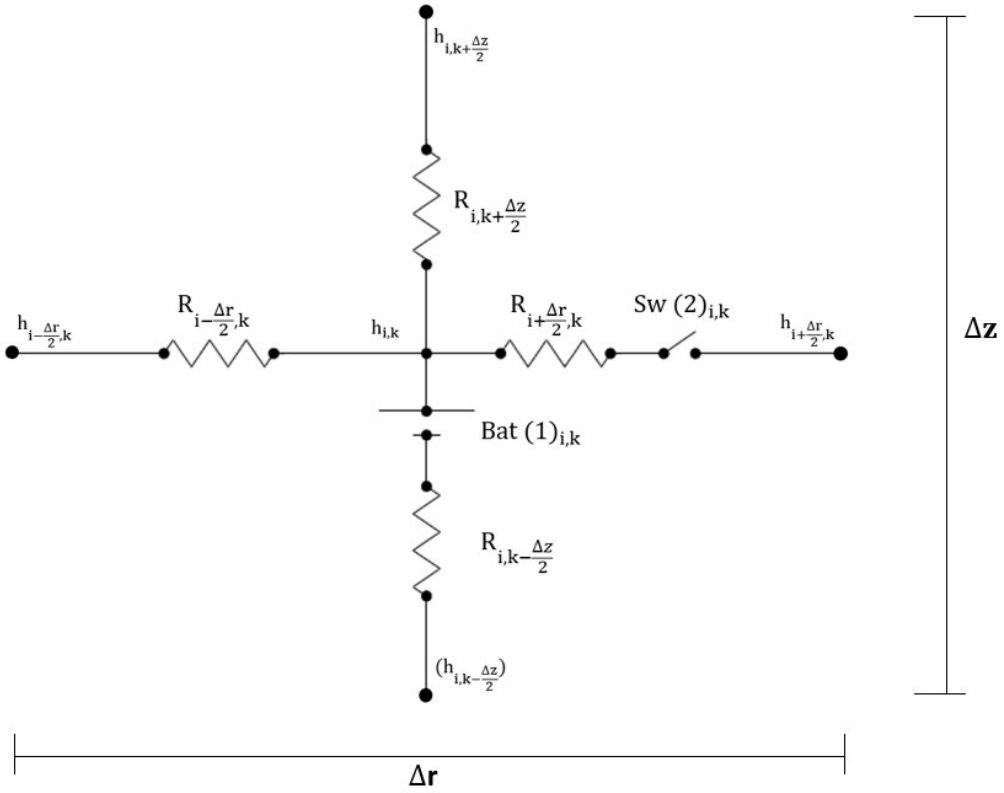

Figure 5.7. Scheme of a typical cell (central area bottom border)

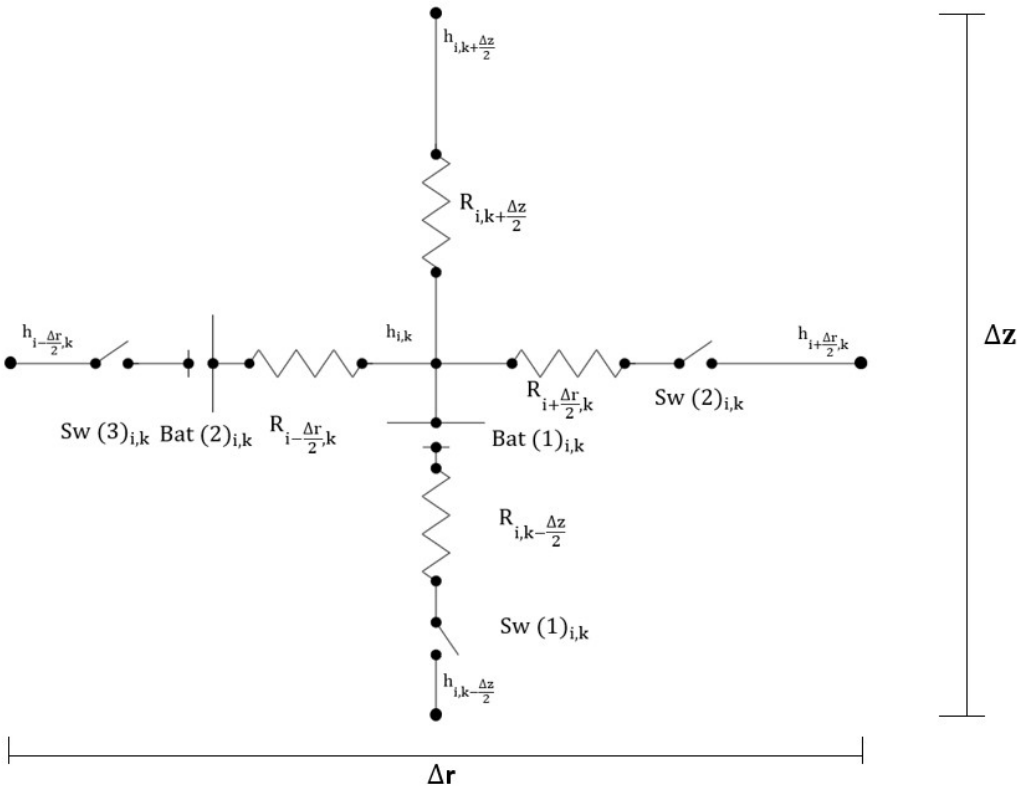

Figure 5.8. Scheme of a typical cell (well border)

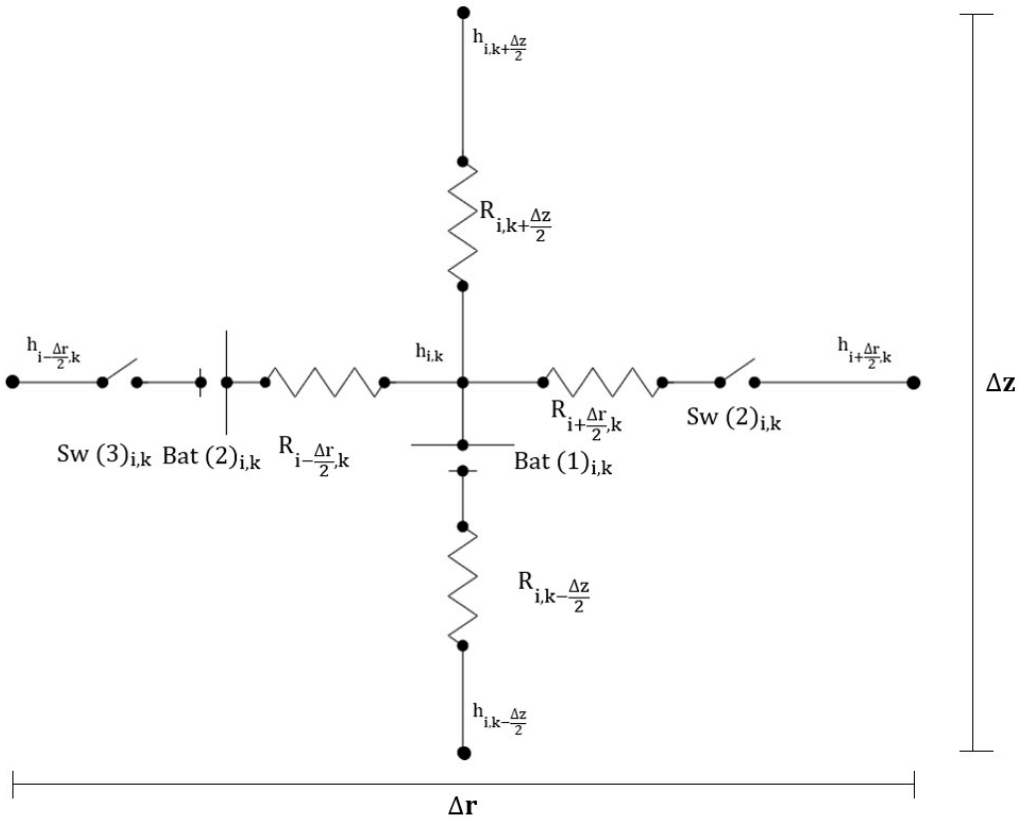

Figure 5.9. Scheme of the well border- bottom border cell

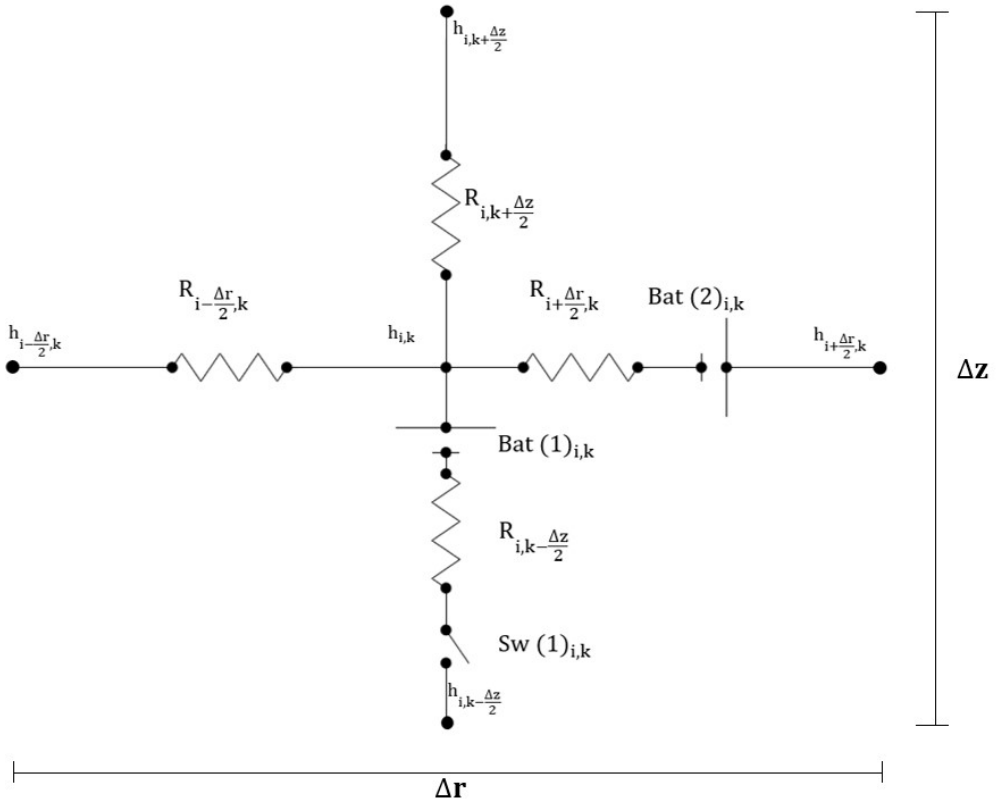

Figure 5.10. Scheme of a typical cell (aquifer vertical border)

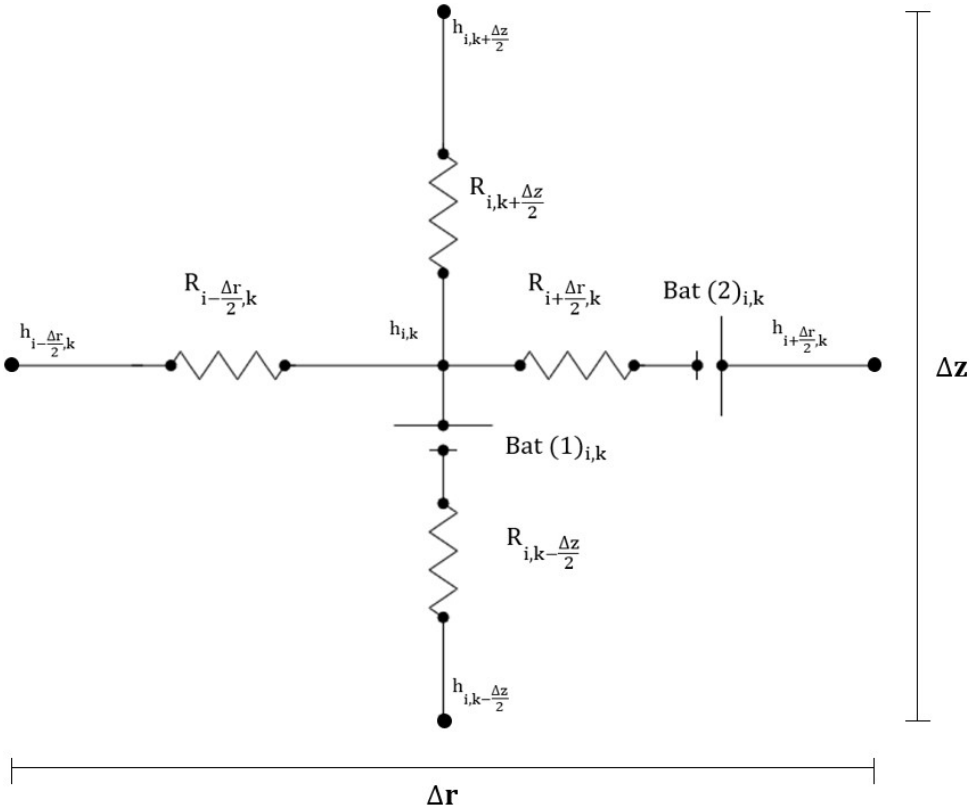

Figure 5.11. Scheme of the cell aquifer vertical border-bottom border

Figures 5.6 to 5.11 show the three different kind of switch behaviours that are employed in the designed code:

- Switch 1 (Sw (1)). This device controls the vertical branch closer to the floor border. For an i,k cell, it keeps closed as long as the voltage in the central node of the cell which is right below it (i,k-1) is higher than its vertical position, $z_{i,k-1}$. This means that the voltage in this lower cell is higher than its position, so it is saturated and water flow can be developed. Nevertheless, when the voltage in the central node of this lower cell is not as high as the vertical position, then the studied cell is considered as dry and water cannot run downwards, which is simulated by opening the switch. As the cells that form the bottom border do not have any other elemental volumes below them, switches are not placed in their vertical lower branches.
- Switch 2 (Sw (2)). It governs the horizontal branch closer to the aquifer border. Considering an i,k cell, this switch is closed when the voltage at the central node of the cell on its right (i+1,k) is higher than its vertical position. According to this, the cell is being simulated as saturated, allowing horizontal flow. If the voltage in this adjacent cell presents a value that is lower than its vertical position, this cell is considered as dry, which is simulated with an open switch, and then no horizontal flow can occur. Those

cells defining the aquifer border do not present this switch, as no elemental volumes are modelled on their right.

- Switch 3 (Sw (3)). This one is only employed in those cells modelling the well border. It is close when the voltage value in the central node of cell i,k is higher than its vertical position, and it is open when the contrary happens. This mechanism is needed in order to correctly simulate the seepage surface.

In any case, despite the three types of switch are governed by different nodes, they behave in a similar way, and, for this reason, the same structure is used to control them (Figure 5.12):

(i) The switch measures the voltage value in an auxiliary node placed outside the principal circuit. A non-linear dependent voltage source is connected to this auxiliary node, as well as a resistor with a resistance value of one (in this way, according to Ohm's law, the current has the same value as the voltage). Both the source and the resistor are connected to ground node, closing the circuit.

(ii) A value must be given to the non-linear dependent voltage source. In this case, is the ratio of the values controlling the switch: the voltage and the vertical position of the node in which the comparison is being done.

(iii) When the ratio is higher than one, the voltage is then higher than the vertical position of the studied node. The switch must be close according to this, allowing the current to flow. If this ratio is lower than one, the voltage value is lower than the vertical position (negative pore pressure), so the switch is open in order to avoid the flowing current.

(iv) A hysteresis value is considered as a mean to set the precision of the switch measure. The lower this value is, the more precise the transition from open to close is (and vice versa).

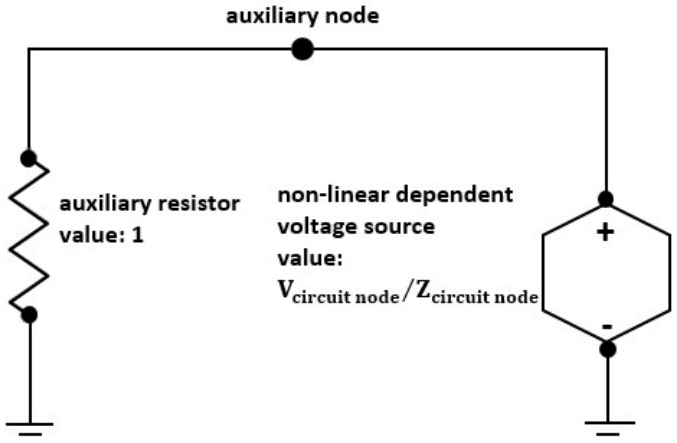

Figure 5.12. Auxiliary circuit for controlling switches

V.4 Boundary conditions

Two different kind of boundary conditions are used: constant water potential values and impervious borders. For flow under gravity dams, these conditions can be written as:

$$h_{\text{upstream dam}} = h_1; h_{\text{downstream dam}} = h_2 \quad \text{(first class of Dirichlet condition)} \quad \text{(V-31)}$$

$$\frac{\partial h}{\partial n}_{\text{impervious outer borders}} = \frac{\partial h}{\partial n}_{\text{impervious structure borders}} = 0$$

$$\text{(second class or Neumann condition)} \quad \text{(V-32)}$$

In the study of flow in unconfined aquifers, although the same kinds of boundary condition are set, these are not located in the same place and do not present the same values.

$$h_{\text{aquifer border}} = H;\ h_{\text{well border}} = h_w;\ h_{\text{border above well}} = z$$

$$\text{(first class or Dirichlet condition)} \quad \text{(V-33)}$$

$$\frac{\partial h}{\partial z}_{\text{upper impervious border}} = \frac{\partial h}{\partial z}_{\text{lower impervious border}} = 0$$

$$\text{(second class or Neumann condition)} \quad \text{(V-34)}$$

There is an extra border in these problems, however, that cannot be modelled before carrying out the simulations. This is the phreatic level, which must be considered as an unknown of the problem, since it appears when those points of null pore pressure (h=z) are connected. Depending on the boundary condition that is being modelled, different electrical devices are used.

First class boundary conditions, this is, imposing a specific value to a node (usually the central node of the border cell), is simulated by connecting this node to a battery that provides a voltage of that value. This does not vary whether the value is the same along the whole boundary or each cell must have a different one. The device can be given the correct value employing the code.

In this way, on the one hand, providing the constant potential values in the upstream and downstream horizontal borders of the dam problems is as easy as connecting all the cells along those borders to batteries with values h_1 and h_2 respectively. On the other hand, the well border must be divided into two different zones. One zone in which, as happened in the first problem, all cells are connected to batteries of the same voltage value, which would be the well height. Another zone where the border cells are connected to a battery whose voltage value is the vertical position of its central node, which is the border above the well. Figure 5.13 shows the

boundary conditions of an arbitrary problem of flow under dams, while Figure 5.14 does the same for problems of flow in unconfined aquifers due to pumping wells.

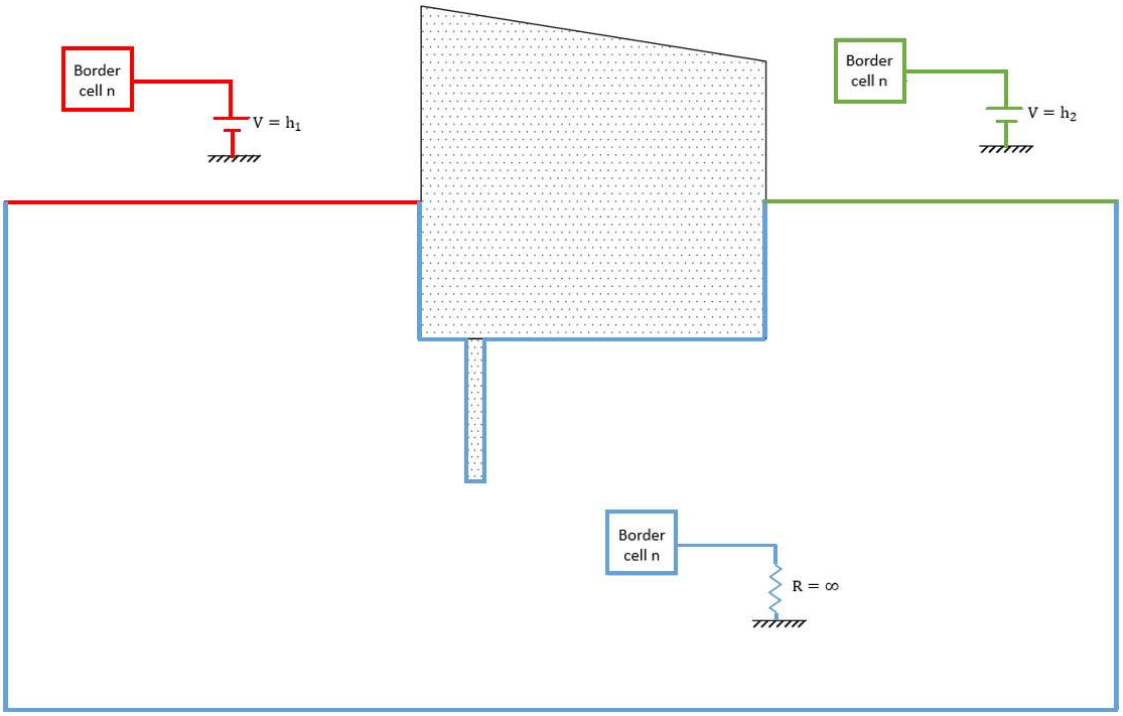

Figure 5.13. Devices for the boundary conditions in problems of flow under dams

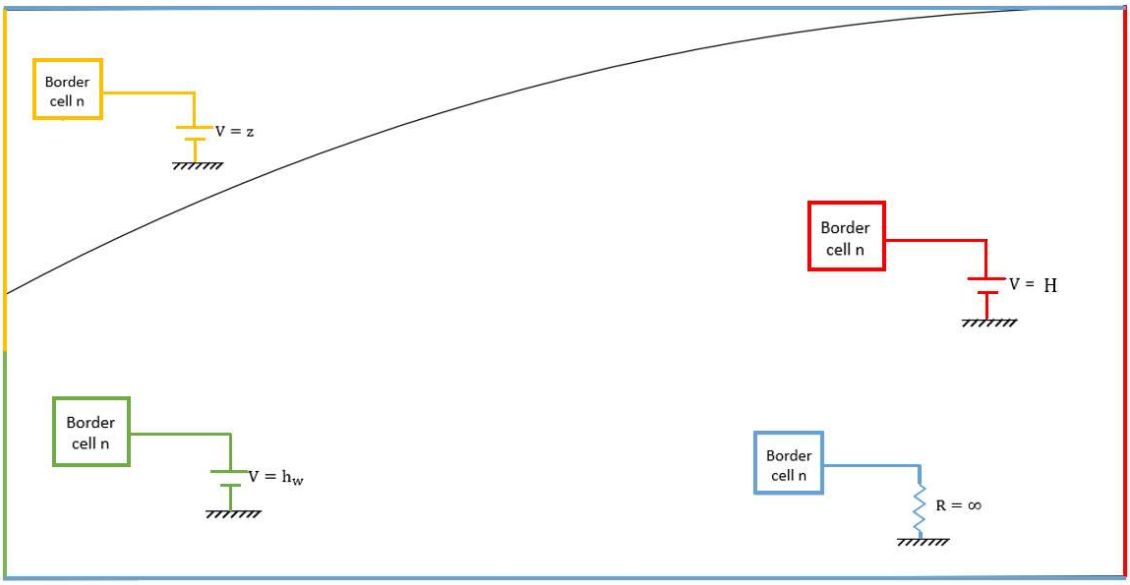

Figure 5.14. Devices for the boundary conditions in problems of flow in unconfined aquifers due to a pumping well

V.5 Structure of the model text file

The corresponding file is generated following the rules of Ngspice software. It can be organized in different sections according to the information that is introduced or the process or calculation

that is carried out. The first section of the file shows the name and parameters that must be introduced in order to simulate the chosen scenarios. Section 2 presents the structure of the cells that are used to model the problem, while Section 3 stablished the boundary conditions of the scenario. Finally, Section 4 is a list of the required variables, which are the raw data for calculating the sought results. The text file finishes with an 'end' sentence. Figures 5.15 to 5.18 are an example of the different sections in which the file is organized.

```
**** SECTION 1. Name, definition, problem data and list of the parameters of the problem
**
**DamSim
**Parameters
**Definition of the circuit
**List pf the parameters of the problem
```

Figure 5.15. Section 1 in a Ngspice file generated by DamSim

```
****SECTION 2. List of components in each cell
**
**Cell #1
RdX1Y1 dX1Y1 cX1Y1 50.2395
VflujouX1Y1 cX1Y1 cX1Y1u 0
RuX1Y1 cX1Y1u dX1Y0 50.2395
VflujolX1Y1 cX1Y1 cX1Y1l 0
RlX1Y1 rX0Y1 cX1Y1l 49761666.6667
RrX1Y1 cX1Y1 rX1Y1 49761666.6667
...
...
**Cell #N
RdX281Y27 dX281Y27 cX281Y27 9899.5211
VflujouX281Y27 cX281Y27 cX281Y27u 0
RuX281Y27 cX281Y27u dX281Y26 9899.5211
VflujolX281Y27 cX281Y27 cX281Y27l 0
RlX281Y27 rX280Y27 cX281Y27l 252537.47
RrX281Y27 cX281Y27 rX281Y27 252537.47
```

Figure 5.16. Example of the structure of two cells in Section 2

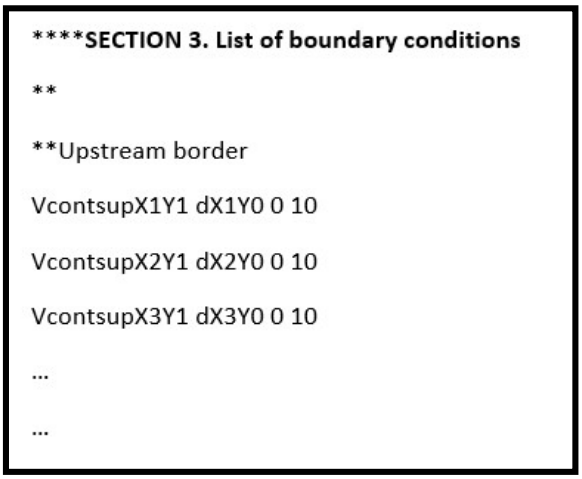

Figure 5.17. Example of part of the list of boundary conditions

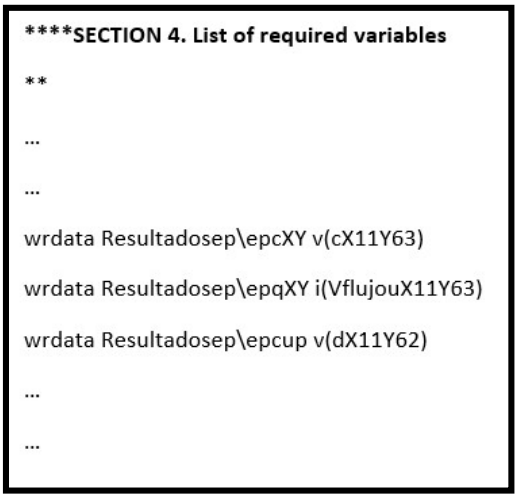

Figure 5.18. Example of part of the list of the required variables

In order to automatically elaborate the text file, we have developed a couple of Matlab codes (one for each kind of scenarios that have been studied along this thesis) for the following tasks:

i) windows for introducing the geometrical and hydrogeological parameters of the scenario,
ii) automatic generation of nodes and devices,
iii) elaboration of the complete text file for the network model,
iv) 'start' routine and simulation model in Ngspice,
v) graphical and numerical results in Matlab.

One of them, DamSim, simulates problems of flow through porous media under gravity dams. These structures may present a foundation or not, and there is also the option to locate a sheet pile under it. Moreover, the modelled soil can be isotropic or anisotropic, in order to reflect the conductivity of the media in a realistic way.

The code is able to obtain the groundwater flow, pore pressure distribution or average exit gradient. In addition, the flow net is the main graphical solution, where isopotential lines and streamlines are shown, helping to understand the behaviour of the flow.

The second software , WaWSim, simulates flow in unconfined aquifers due to a pumping well and has also been developed employing Matlab and Ngspice. In this case, the numerical solutions are groundwater flow and seepage surface, and the graphical result is also a flow net, although this also presents iso-pressure lines.

V.6 Data post-processing and result obtaining

After printing the results in text files with Ngspice (.data extension), Matlab closes the software and imports the voltage and current values. Following some rules and programming the necessary routines, the raw data are organized in arrays and matrixes. Finally, we can calculate the numerical and plot the graphical results.

Depending on the scenario being simulated, the final solutions would vary, although all the calculations employ the values of water head (and sometimes those of water flow) in the nodes of the cells in which the scenario has been discretized. In this way, the common results are water flow and flow net, while in scenarios of flow under dams other results are also pore pressure distribution under the dam (which can be summarized as the uplift force and its application point) and the average exit gradient. Furthermore, if there is a sheet pile at the dam base, then other solutions are the pore pressure distribution along the sheet pile in its upstream and downstream side (these again can be summarized as a force and its application point). Finally, scenarios of flow in unconfined aquifers due to a pumping well, apart from the water flow and the flow net, seepage surface is another result.

V.7 DamSim and WaWSim

These two software use Ngspice (free software for solving electric circuits) as their computational code, and Matlab as the tool to program files, communication interface and result presentation. With simple graphic interfaces, the user can introduce the geometric and physical soil properties, the initial water head variation and the reticulation of the scenario. Once the calculation is finished, any of the two software allows knowing different results, either numerical or graphical.

For DamSim, Figure 5.19 shows the nomenclature for the scenarios of flow under gravity dams. If no sheet pile is considered, then those parameters related to it (length d_s and position under the base c_s) take a value of 0, while if there is not a foundation, the value of its length (d) must also be 0. On the other hand, Figure 5.20 presents the nomenclature for WawSim.

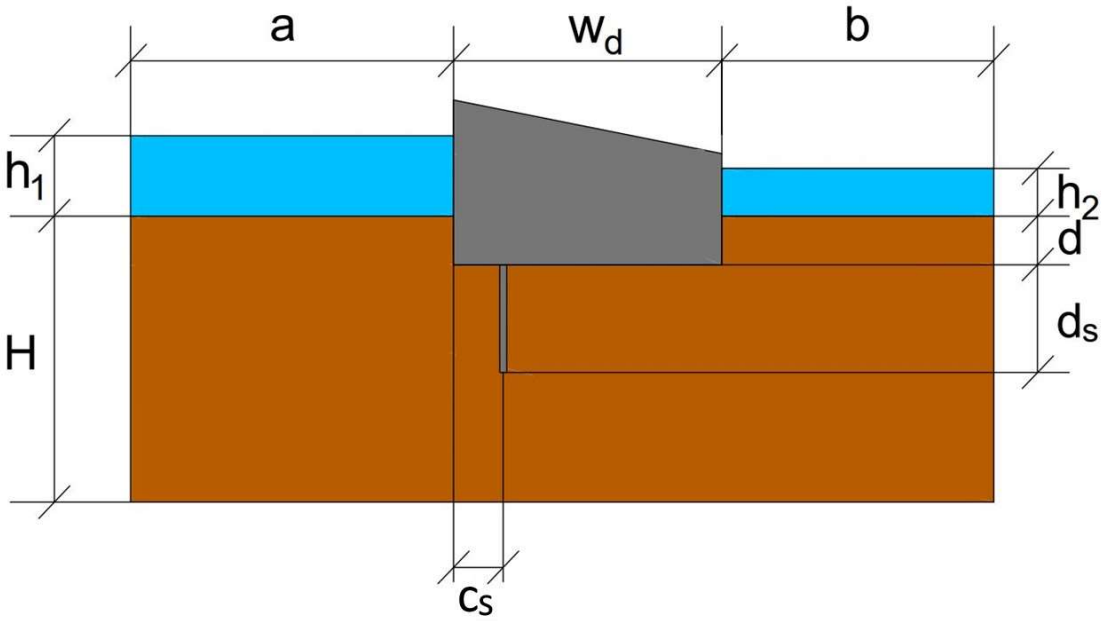

Figure 5.19. Nomenclature for DamSim

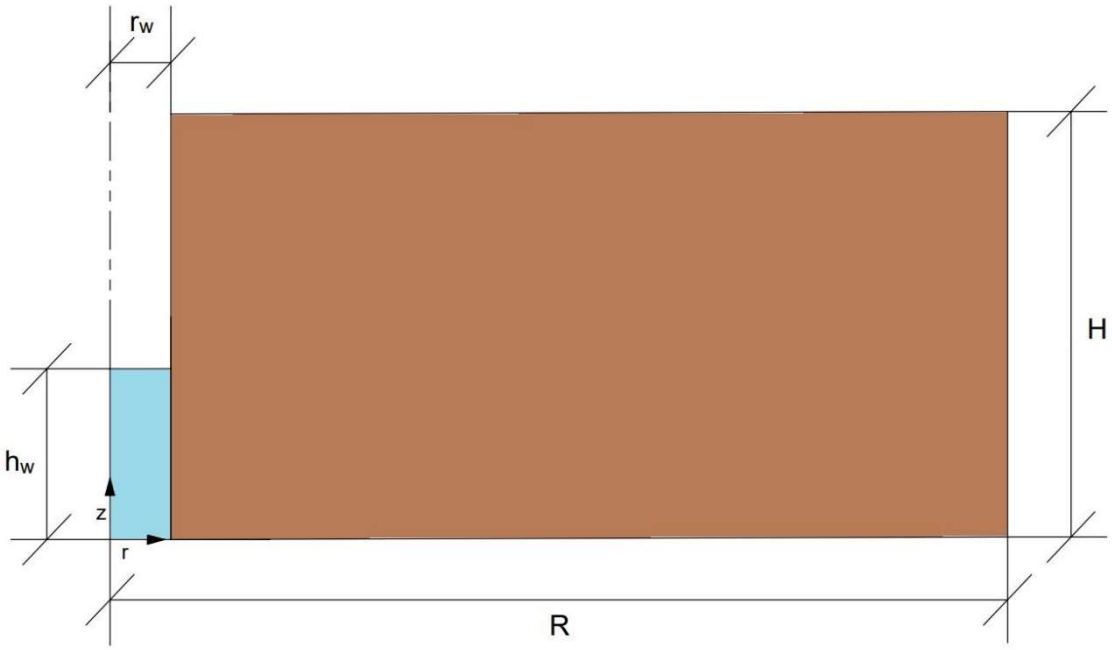

Figure 5.20. Nomenclature for WaWSim

The software organization and structure have been designed so the user has a useful tool that can be employed in a simple way.

V.7.1 Data introduction

The first step in both software is to introduce the data to model the chosen scenario (input information). In both codes, these parameters are entered using a window in which geometric and hydrogeological parameters must be written. In DamSim, input window varies depending on the scenario we intend to simulate (Figure 5.21, initial interface where the user chooses the scenario to simulate, no sheet piles or one sheet pile), since the parameters that define the position and length of the sheet pile must not appear if it is not going to be simulated. Moreover, in this window the number of cells for each of the lengths is also introduced. There is a 'Verification' push button, so the code can check if all these data are coherent, as well as a 'Simulation' push button to start running the simulation. Figures 5.22 and 5.23 show the window for the data input when no sheet piles is modelled and when one is located under the dam, respectively.

Figure 5.21. Initial window of DamSim

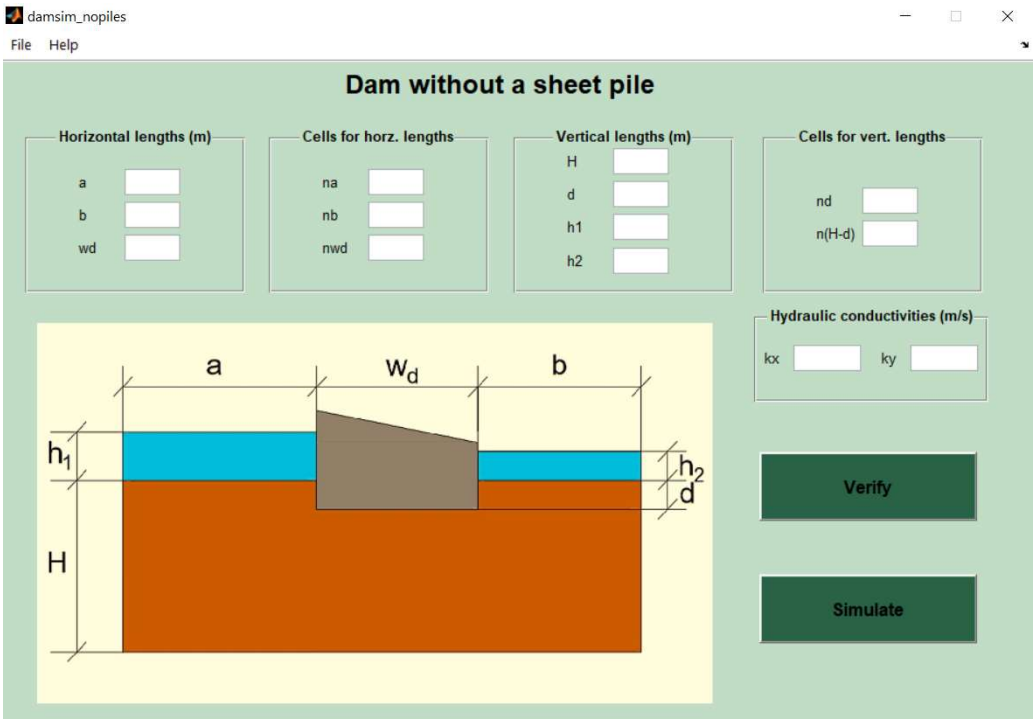

Figure 5.22. Data input window for scenarios of flow under dam without a sheet pile

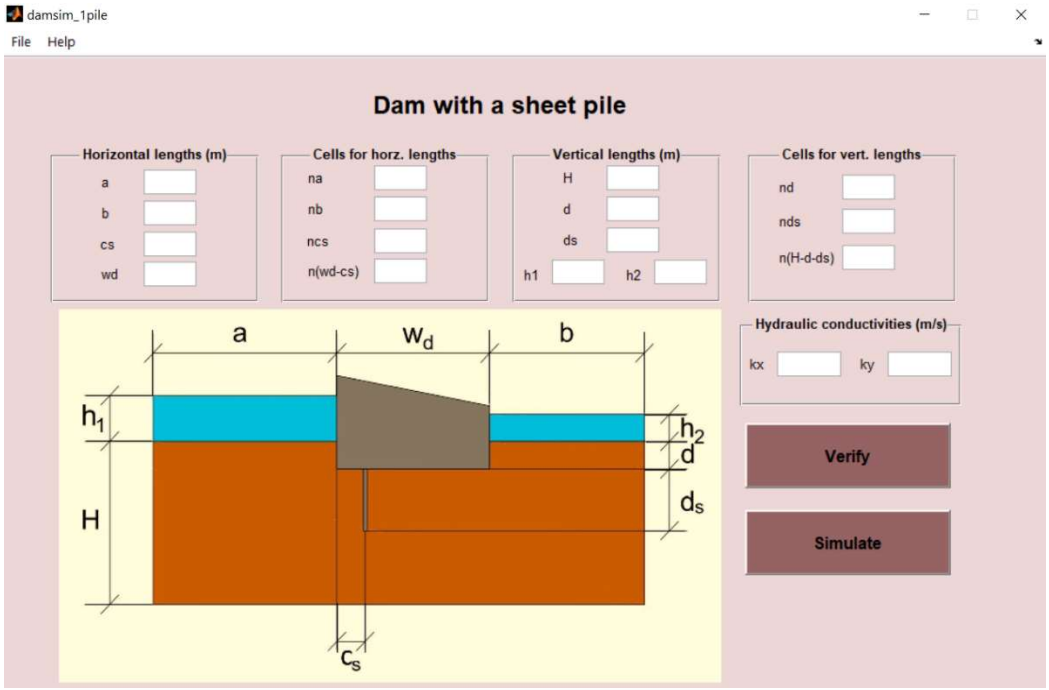

Figure 5.23. Data input window for scenarios of flow under dams with a sheet pile

In the input windows, some error banners or messages are programmed in order to ensure that data are correct values (for example, letters or negative values cannot be written, most variables cannot be given a value of zero, and the number of cells cannot be a decimal value). Moreover, once all data have been written, the 'Verification' button must be pressed, and then the whole scenario is checked to see if all data are compatible. For instance, the value of the water head

upstream the dam must be higher than that downstream, the vertical length of the whole impervious structure (d or $d+d_s$) must be lower than the stratum thickness, and the position of the pile under the dam cannot take a larger value than that of the dam width. In addition, a different error appears when the user has chosen to simulate a scenario of flow under a dam with a sheet pile but then they give a value of zero to d_s, indicating that a sheet pile is not modelled. In this case, the error message explains that the software should be restarted, and the user should choose the option of 'dam without a sheet pile'. Finally, the 'Verify' button gives the user information about the type of soil that the user has introduced. If both values of hydraulic conductivity are the same, a message appears explaining that the soil is isotropic, while if both values are different but the vertical conductivity is higher than the horizontal conductivity, then another message is shown, although in this case it explains that it is an uncommon fact.

Once the simulation has been carried out, a second window appears where the user can choose which graphical and numerical solutions are wanted to be shown (output information). Figure 5.24 shows this 'Result' window for the scenario of dam without a sheet pile, as it is very similar to that of the scenario of flow under dams with a sheet pile.

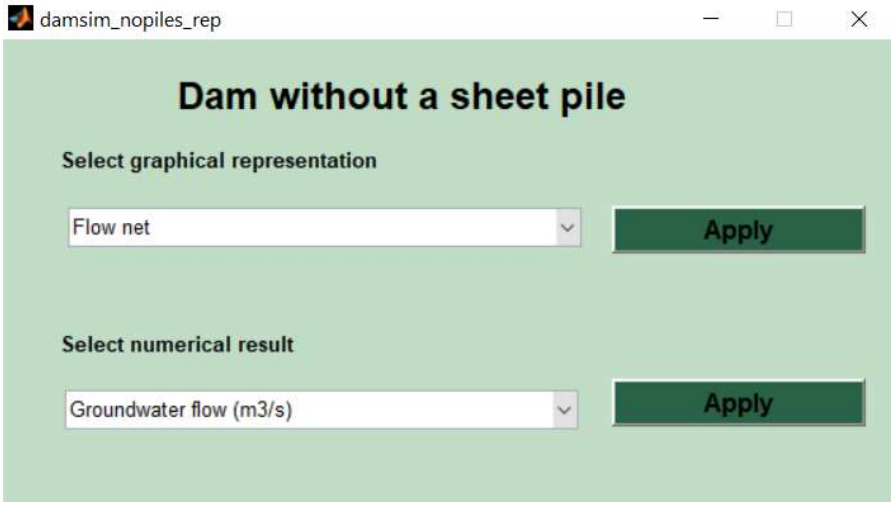

Figure 5.24. Example of result window

V.7.2 Numerical simulations. Post-process results

Ngspice, has been chosen because it leads to almost exact solutions and whose errors are only due to the chosen reticulation. Solutions are obtained with low computation times. The text file for the model, elaborated with Matlab, is designed following the network method. These text files (.cir extension) are sent to Ngspice for their simulation. The typical file is the one that has

been displayed in Figures 5.15 to 5.18 since it is based on the same codes. The solutions for all the chosen variables are the raw data and they are printed in text files, and when this task is finished, Matlab closes Ngspice and import the output files. In this way, all these data can be arranged into arrays and matrixes for mathematical calculations and graphical representations.

The different windows that correspond to the software WaWSim are not shown in this dissertation, since the objective with this second code is also to introduce the model for transient flow in unconfined aquifers due to a pumping well. However, it would probably have a similar appearance.

V.7.3 Graphical solutions

Depending on the chosen software different graphical outputs are expected and can be chosen by the user. For any of the chosen scenarios that can be simulated with the two software, a flow net can be displayed if the user demands it.

DamSim also elaborates pore pressure distribution graphics since the problems that this code simulates have impervious structures where the pore pressure is applied. If no sheet pile is considered, there is only one output graphic solution apart from the flow net, which shows the pore pressure distribution under the dam base. On the other hand, if a sheet pile must be modelled, a third graphic can be displayed, one where the pore pressure distribution along the sheet pile is shown for both sides of it (upstream and downstream).

Examples of a flow net, pore pressure distribution under the dam and pore pressure distributions along the sheet pile are shown in Figures 5.25, 5.26 and 5.27 respectively.

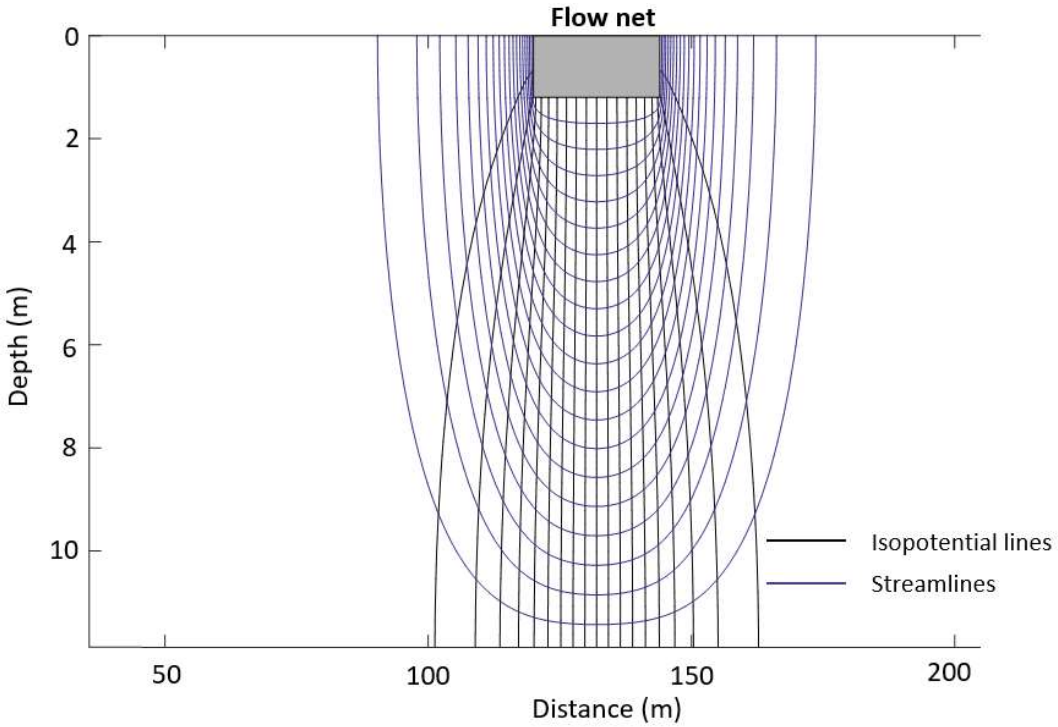

Figure 5.25. Example of flow net graphic for a scenario of flow under dam without a sheet pile (1V:10H)

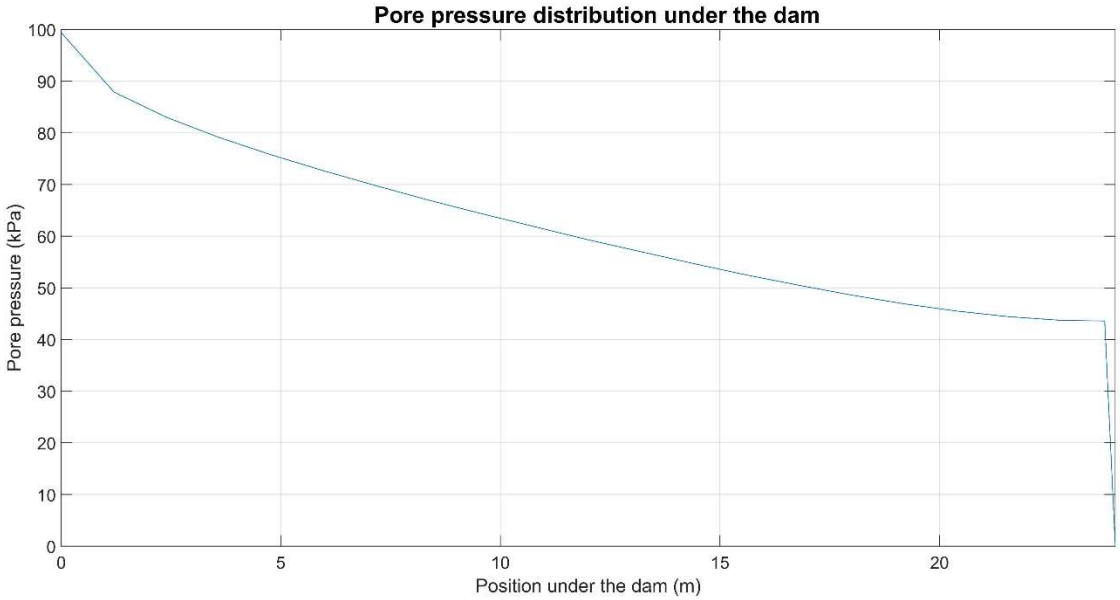

Figure 5.26. Example of pore pressure distribution in problems of flow under dam with a sheet pile

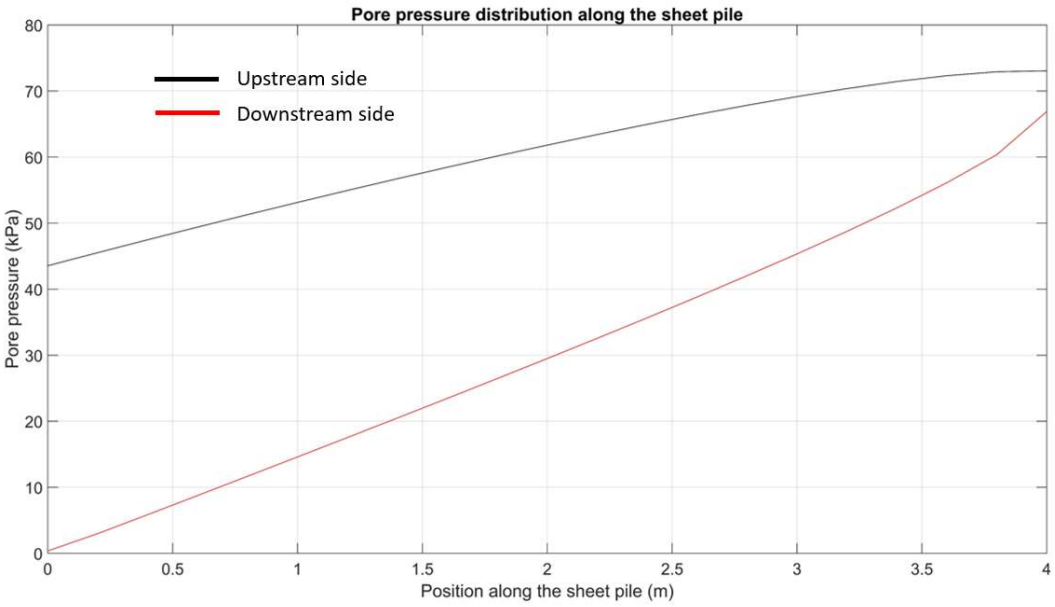

Figure 5.27. Example of pore pressure distributions along the sheet pile in problems of flow under dam with a sheet pile

Chapter VI. An application of inverse problem: a protocol to obtain hydraulic properties in unconfined aquifers with pumping well

Employing the protocol of inverse problem we determine the horizontal and vertical hydraulic conductivities from direct measures of pumping flow rate and seepage surface. Section VI.1 is an introduction to the inverse problem, while Sections VI.2 and VI.3 present two alternative methods for solving this problem. Finally, Section VI.4 shows as an application in which the influence of errors in the value of water flow and seepage measures on the solutions of hydraulic conductivities is studied.

VI. 1 Introduction of the inverse problem

Once we have characterized the problem of flow through porous media corresponding to unconfined aquifers where water is abstracted from a pumping well, a universal solution for the variables of interest, that is, water flow (Q) and seepage surface (h_s) has been stablished. Both are function of the problem parameters: aquifer radius (R), well radius (r_w), initial saturated thickness and hydraulic conductivities in the horizontal (κ_r) and vertical (κ_z) direction. In the inverse problem, Q and h_s are data, which are obtained from experimental measures affected by the error inherent to the measure instruments, and κ_r and κ_z become the unknowns. The

inverse problem can be approached either by a classical way, from successive numerical simulations, or by the use of the universal curves from Chapter IV.

VI.2 Inverse problem with the network method

We start this study with the solution of the inverse problem in a classical way, (Beck et al. [1985], Zueco & Alhama [2005, 2006, 2007]), employing as numerical tool the code developed in this thesis (WaWSim).

After carrying out numerous simulations for obtaining the universal curves in Chapter IV, we could see that horizontal hydraulic conductivity essentially determines the value of groundwater flow. Significant changes in the vertical conductivity lead to variations of around 2% in the pumping flow value. This verification simplifies the inverse problem, since it allows calculating first the radial (horizontal) hydraulic conductivity from the water flow value, and once this conductivity has been estimated, we can then approximately determine the vertical hydraulic conductivity that leads (by iterations) to the empirical seepage surface value. The inverse problem requires a large number of numerical simulations for which a protocol must be stablished to change the estimate parameters until the results converge to an acceptable approximation. These simulations are organized in two groups: the first for the calculation of the horizontal conductivity, and the second for the vertical conductivity.

The first group of iterations consists of a non-defined number of loops in which the real water flow is compared to that obtained from the simulations. In each iteration, the value of the horizontal hydraulic conductivity is changed. The estimated horizontal conductivity is considered as accurate enough if the deviation for the water flow variable, Equation (VI-1), presents a value between 0.01 and -0.01,

$$\Gamma_Q = \frac{Q_{real} - Q_{sim}}{Q_{real}} \qquad \text{(VI-1)}$$

Before starting the iterations, we must assign an initial value for the radial hydraulic conductivity, which is estimated according to the knowledge we have about the soil (its geological nature, porosity, grain size, etc), from previous experience, field or laboratory test, or employing ground engineering manuals. If doing so, the compilation time would be reduced, since the number of iterations is lower as the initial value is closer to the real one. In any case, the code always leads to a solution (always the same one), independently of the initial value of the radial hydraulic conductivity. Moreover, most engineering manuals provide estimations of

isotropic hydraulic conductivities, which may also lead to longer compilation time if those values are introduced for horizontal and vertical conductivities.

In the first loop, the changes of κ_r in each iteration are calculated as $\frac{\kappa_{r,initial}}{10}$ or $\frac{\kappa_{r,initial}}{10^1}$. If the conductivity of the simulation is lower than the real (or expected), the deviation value would be higher than zero, and the opposite would happen if the simulation conductivity is higher than the real value. When the deviation is higher than zero, the calculated increment would be added to the last calculated conductivity, and it would be subtracted if it is lower. The current loop finishes one of the following cases happens:

a) Deviation is positive in the second last iteration and negative in the last, but in none of the iterations their value is between 0.01 and -0.01.
b) Deviation is negative in the second last iteration and positive in the last, but in none of the iterations their value is between 0.01 and -0.01.
c) Deviation is between 0.01 and -0.01 in the last iteration.

In case c) there will not be a following loop, and the solution of κ_r is the value from the last iteration. The inverse problem for κ_r would be solved.

If cases a) or b) happen, a second loop begins using the second last radial conductivity from the previous loop. If case a) happens, an increment is added, which in the second loop takes a value of $\frac{\kappa_{r,initial}}{100}$ or $\frac{\kappa_{r,initial}}{10^2}$; if case b) occurs, then the increment is subtracted. The second loop works in the same way as the first, and if the deviation, Γ_Q does not reach a value between 0.01 and -0.01, a third loop begins, where $\frac{\kappa_{r,initial}}{1000}$ or $\frac{\kappa_{r,initial}}{10^3}$; looping process will continue until the deviation takes the sought value. In each loop, the value of the increment is calculated as $\frac{\kappa_{r,initial}}{10^n}$, where n is the number of the loop that is in progress. Figure 6.1 shows the flowchart for this first part of the protocol for the inverse problem.

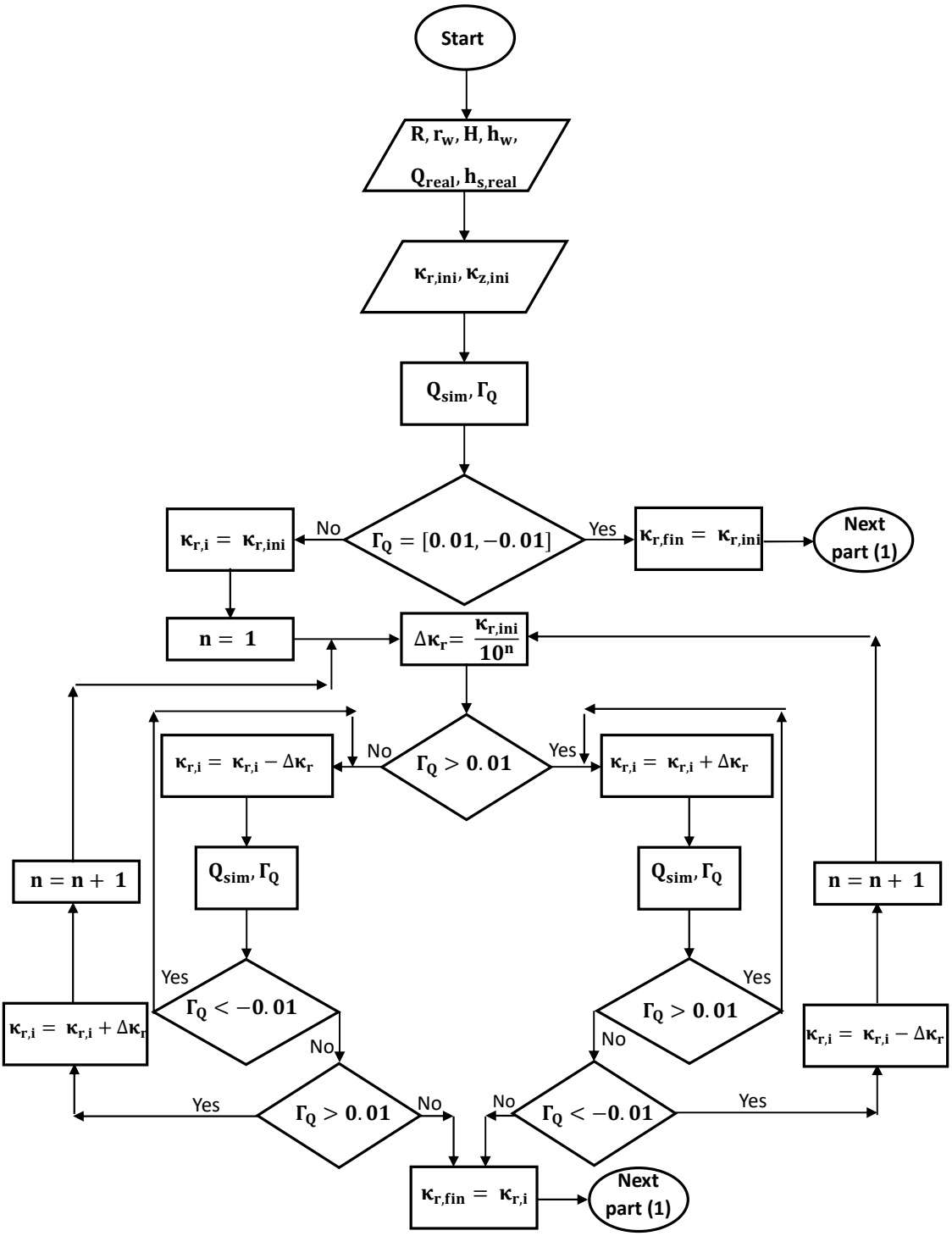

Figure 6.1. Flow chart for the first part of the protocol (calculation of κ_r)

Once the horizontal hydraulic conductivity has been estimated, the protocol starts the second group of simulations for calculating the vertical conductivity. In this case, the number of loops is also undetermined and in each simulation the deviation for the seepage variable, Γ_{hs}, is calculated as

$$\Gamma_{hs} = \frac{h_{s,real} - h_{s,sim}}{h_{s,real}} \quad \text{(VI-2)}$$

Due to the sensitivity of the problem for the variable of seepage surface and how it is related to the vertical hydraulic conductivity, the range of values of the deviation for which the simulation is accepted is more accurate: now it must be between 0.001 and -0.001. As for the study of the radial conductivity, we must assign an initial value to the vertical hydraulic conductivity. We can adopt the same initial value as for κ_r or, alternatively, one of the following options can be chosen: i) $\kappa_{z,\,initial}$ takes the value of $\kappa_{r,\,final}$, so the soil is initially considered as isotropic; ii) $\kappa_{z,\,initial}$ takes a fraction of $\kappa_{r,\,initial}$ or $\kappa_{r,\,final}$ (for example, a fifth or a tenth), since the vertical conductivity is commonly lower than the horizontal one; or iii) $\kappa_{z,\,initial}$ is directly introduced by the user, although it can also meet some of the previous criteria.

The seepage surface behaves different than the water flow. In order to increase the seepage surface, the vertical hydraulic conductivity must be decreased, so in each iteration the radial flow becomes more important. The contrary happens if the seepage surface must be reduced in the following iteration.

In the first loop for calculating κ_z, if the deviation is higher than zero, which means that the simulated seepage surface is lower than the real value, the vertical hydraulic conductivity is decreased subtracting the increment $\frac{\kappa_{z,initial}}{10} = \frac{\kappa_{z,initial}}{10^1}$. The opposite occurs when the deviation takes a value lower than zero. As happened in the calculation of the horizontal conductivity, the loop finishes with one of the following ends:

a) Deviation is positive in the second last iteration and negative in the last iteration, but in none of the iterations their value is between 0.001 and -0.001.
b) Deviation is negative in the second last iteration and positive in the last iteration, but in none of the iterations their value is between 0.001 and -0.001.
c) Deviation takes a value between 0.001 and -0.001 in the last iteration.

In case c) this loop would be the last one, and the solution of κ_z is the value calculated in the last iteration. If cases a) or b) occur, the following loop begins, starting with the conductivity value of the second last iteration in the previous loop. If case a) happens, a second loop starts, and the increment that now is subtracted takes a value of $\frac{\kappa_{z,initial}}{100} = \frac{\kappa_{z,inital}}{10^2}$. The opposite occurs in case b). The second loop finishes as the first one, and there would be the required number of loops for finding a value of the vertical hydraulic conductivity that leads to an error value in the chosen range. In each loop, the value of the increment would be $\frac{\kappa_{z,inital}}{10^n}$, where n is the number of the loop that is ongoing. Figure 6.2 shows the flow chart for the second part of the protocol.

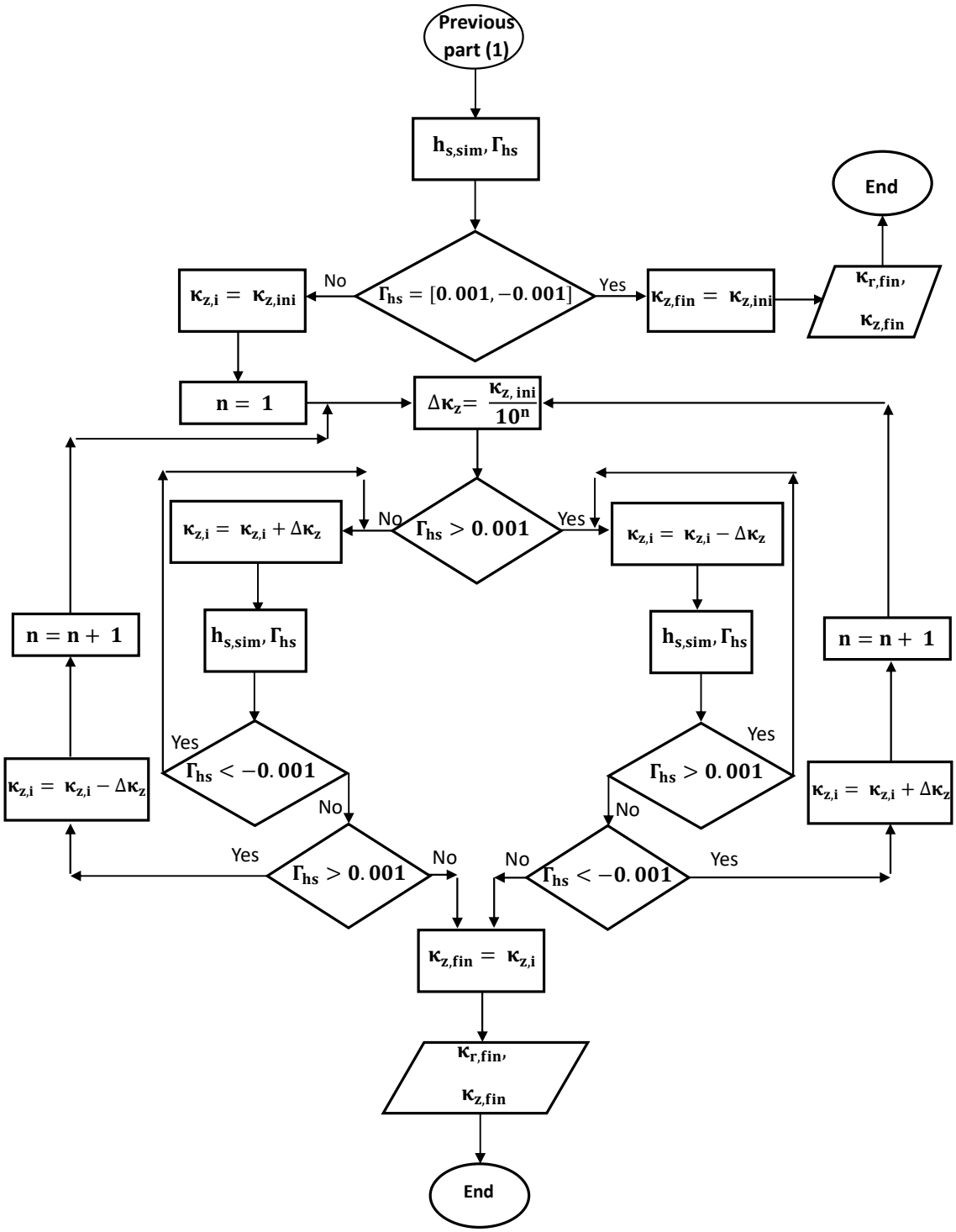

Figure 6.2. Flow chart for the second part of the protocol (calculation of κ_z)

Due to the complexity of the problem, convergence is not always possible for all the discretization, since there is a correlation between the values of the simulated conductivities and the reticulation that leads to a solution. In addition, the designed code shows an error based on the difference between the values of seepage surface calculated by water head and by pressure. When employing the water head, we look for the point of the well wall where this variable takes the same value as the vertical position. On the other hand, when measuring the

seepage surface using the pore pressure, we would look for the point of 0 kPa. As following these two methodologies can lead to wrong values of seepage surface, the code looks for the point of 0.1 kPa pressure value. Of course, the seepage surface value calculated with this method is lower than the real, but when the code calculates correctly this variable by the values of the water head, the seepage surfaces obtained with the two methodologies are very close (with difference around 5 %). If the difference is higher than 10%, the code shows an error and finishes although a solution has not been reached.

It is also possible, in problems of high values of vertical hydraulic conductivity and/or low seepage surface values, that these two variables cannot be related in an accurate way, so estimated value of the vertical conductivity must be considered as an approximation.

VI.3 Inverse problem with the universal abaci

Studying the inverse problem with the dimensionless curves is simpler, since we can benefit from numerous simulations previously carried out to plot these curves (Section IV-2.4). In this way, obtaining the sought parameters is more direct, since the fact of separating the calculation of the two conductivities simplifies the problem.

The monomials governing the direct problem (Section IV-2.4) cluster both kind of parameters of the problem (geometric and hydrogeological). These are:

$$\pi_1 = \sqrt{\frac{\kappa_r}{\kappa_z}}\frac{H}{R} \quad \text{(IV-72)}$$

$$\pi_2 = \frac{r_w}{R} \quad \text{(IV-71)}$$

$$\pi_3 = \frac{h_w}{H} \quad \text{(IV-73)}$$

The unknown monomials were also obtained in Section IV-2.4:

$$\pi_Q = \frac{Q}{\kappa_r \frac{H-h_w}{R-r_w} 2\pi RH} \quad \text{(IV-77)}$$

$$\pi_{h_s} = \frac{h_s - h_w}{H} \quad \text{(IV-78)}$$

If we use the same then the data monomials or the monomials governing the scenario are π_2, π_3 and π_{hs}, while the monomials with unknown variables are π_1 and π_Q. Since the abacus where the water flow monomial with the data groups (Figure 4.59) shows that π_1 does not affect it, we can

obtain π_Q from π_2 and π_3. From the obtained value, we can estimate the value for the radial hydraulic conductivity, κ_r.

Once the horizontal conductivity has been obtained (with a deviation lower than 2%, according to the results obtained when plotting Figure 4.59), we look for the vertical hydraulic conductivity value from the dimensionless abacus for the seepage surface (4.60). In this case, for each value of π_1 there is a set of four curves at maximum (one for each value of π_2 that has been simulated, if some or all of them cannot be summarized in one due to their similarity). Each of these curves relates π_{hs} and π_3. In this way, although the value of π_1 is still unknown, as we do know those of π_2, π_3 and π_{hs}, we can find the point of the abacus that corresponds to the sought value of π_1. Since we already know the value of κ_r, the only unknown involved in the definition of π_1 is the vertical hydraulic conductivity, κ_z.

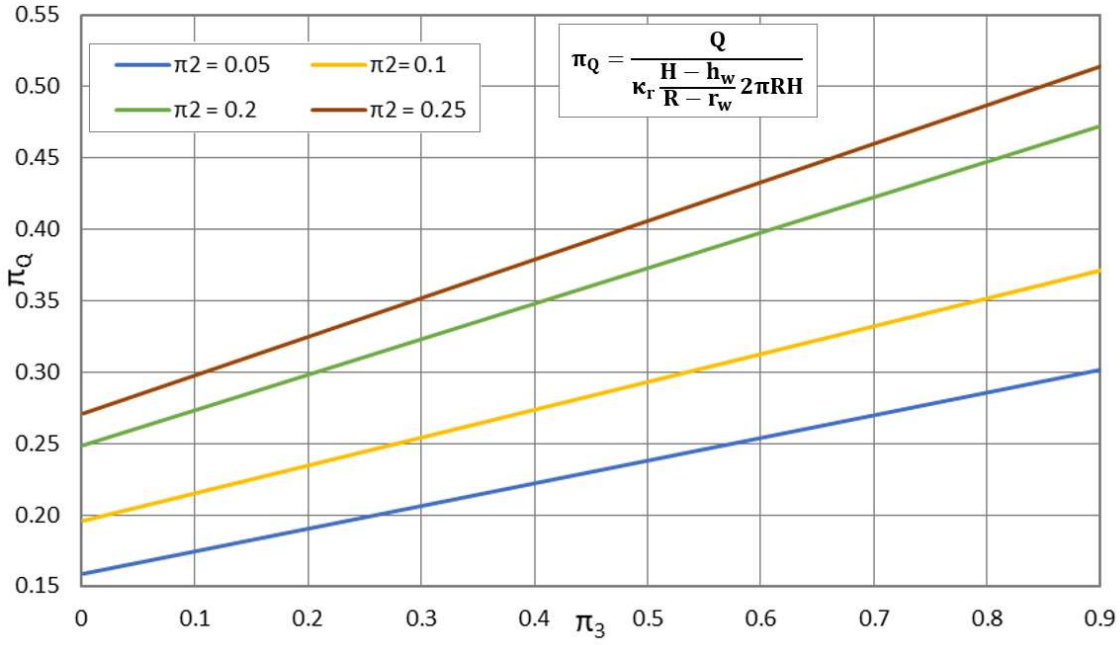

Figure 4.59. Dimensionless groundwater flow

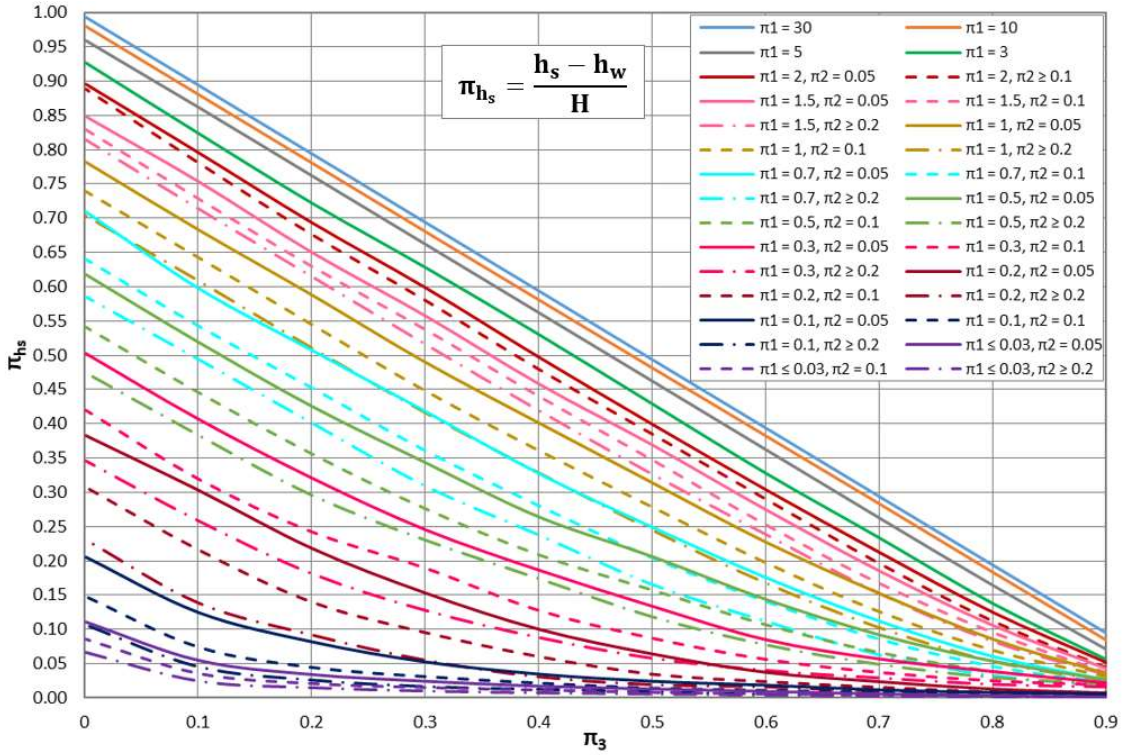

Figure 4.60. Dimensionless seepage surface

Therefore, the inverse problem is solved with two simple steps and easy mathematical calculations.

VI.4 Inverse problem application

As an example, the scenario that is going to be employed for the verification has the following data (see Figure 4.57):

H = 10 m
h_w = 5 m
R = 10 m
r_w = 1m
Q = 0.002308 m^3/s
h_s = 8.471 m
κ_r = 0.0000225 m/s
κ_z = 0.00001 m/s

The value of the hydraulic conductivities indicates that the soil of the aquifer can be defined as a coarse sand. Moreover, its anisotropy degree is not very high ($\frac{\kappa_r}{\kappa_z} = 2.25$), as this ratio can actually present value of 100 in average soils, or even larger (Custodio & Llamas [1976]). If we consider an anisotropy degree range between 1 and 100, the ratio $\frac{H}{R}$ takes then a value between 0.001 and 30 when applying monomial π_1 shown in Figure 4.60. The value of 30 seems quite

unlikely to occur, but as the conductivity ratio can take higher values than those in the chosen range, these high values of π_1 were simulated.

VI.4.1 Application employing the dimensionless curves

Supposing that we do not know the values of the hydraulic conductivity, the monomials we can calculate are:

$$\pi_2 = \frac{r_w}{R} = \frac{1}{10} = 0.1 \quad \text{(VI-3)}$$

$$\pi_3 = \frac{h_w}{H} = \frac{5}{10} = 0.5 \quad \text{(VI-4)}$$

$$\pi_{hs} = \frac{h_s - h_w}{H} = \frac{8.471-5}{10} = 0.347 \quad \text{(VI-5)}$$

From π_2 and π_3, employing the abacus in Figure 4.59 we see that the value of the monomial π_Q is 0.295. From Equation IV-77 we can calculate κ_r as follows:

$$\kappa_r = \frac{Q}{\pi_Q \frac{H-h_w}{R-r_w} 2\pi HR} = \frac{0.002308}{0.295 \cdot \frac{10-5}{10-1} \cdot 2\pi \cdot 10 \cdot 10} = 0.0000224\ m/s \quad \text{(VI-6)}$$

Once we know this value, we can calculate the error percentage, as show in Equation (VI-7).

$$\frac{\kappa_{r,real} - \kappa_{r,cal}}{\kappa_{r,real}} 100\% = \frac{0.0000225 - 0.0000224}{0.0000225} \cdot 100\% = 0.44\% \quad \text{(VI-7)}$$

Knowing the value of κ_r allows us to calculate κ_z from the abacus in Figure 4.60, since employing it and the values of π_{hs}, π_2 and π_3 we see that monomial π_1 takes a value of 1.5. From this, we calculate κ_z in the following way:

$$\kappa_z = \frac{\kappa_r}{{\pi_1}^2} \frac{H^2}{R^2} = \frac{0.0000224}{1.5^2} \frac{10^2}{10^2} = 0.00000996\ m/s \quad \text{(VI-8)}$$

The error for this variable can be calculated according to Equation (VI-9).

$$\frac{\kappa_{z,real} - \kappa_{z,cal}}{\kappa_{z,real}} 100\% = \frac{0.0000 \quad .00000996}{0.00001} \cdot 100\% = 0.4\% \quad \text{(VI-9)}$$

We observe that, in both cases, the error is much lower than 1%, which shows the reliability of the methodology.

Next, a brief study of the effect of possible measure errors may have on the resolution of the problem is carried out. For this, a statistical random error is applied to the real values of Q and h_s, ξ (±0.5, 1, 1.5 and 2%), which leads to a set of experimental values, Q_ξ and $h_{s,\xi}$. From these measures we calculate the deviation associated to each of the chosen ξ. These results are shown

in Figures 6.3 (with statistic errors of the same mathematical sign) and 6.4 (with statistic errors of the opposite mathematical sign), and Tables 6.1 and 6.2 (as happened in Figures 6.3 and 6.4).

Table 6.1. Maximum errors of κ_r and κ_z as a function of ξ (dimensionless curves). Same sign

Error ξ (%)	$\kappa_r \cdot 10^{-5}$ (m/s)	Max Error κ_r (%)	$\kappa_z \cdot 10^{-5}$ (m/s)	Max Error κ_z (%)
0	2.24	0.44	0.996	0.40
0.5	2.23/2.25	0.89	1.060/1.000	6.05
1	2.22/2.26	1.33	1.100/0.910	9.94
1.5	2.21/2.28	1.78	1.150/0.860	15.04
2	2.20/2.29	2.22	1.190/0.820	19.47

Table 6.2. Maximum errors of κ_r and κ_z as a function of ξ (dimensionless curves). Different sign

Error ξ (%)	$\kappa_r \cdot 10^{-5}$ (m/s)	Max Error κ_r (%)	$\kappa_z \cdot 10^{-5}$ (m/s)	Max Error κ_z (%)
0	2.24	0.44	0.996	0.40
0.5	2.23/2.25	0.89	1.07/0.99	7.02
1	2.22/2.26	1.33	1.12/0.89	11.92
1.5	2.21/2.28	1.78	1.19/0.84	18.69
2	2.20/2.29	2.22	1.24/0.78	24.36

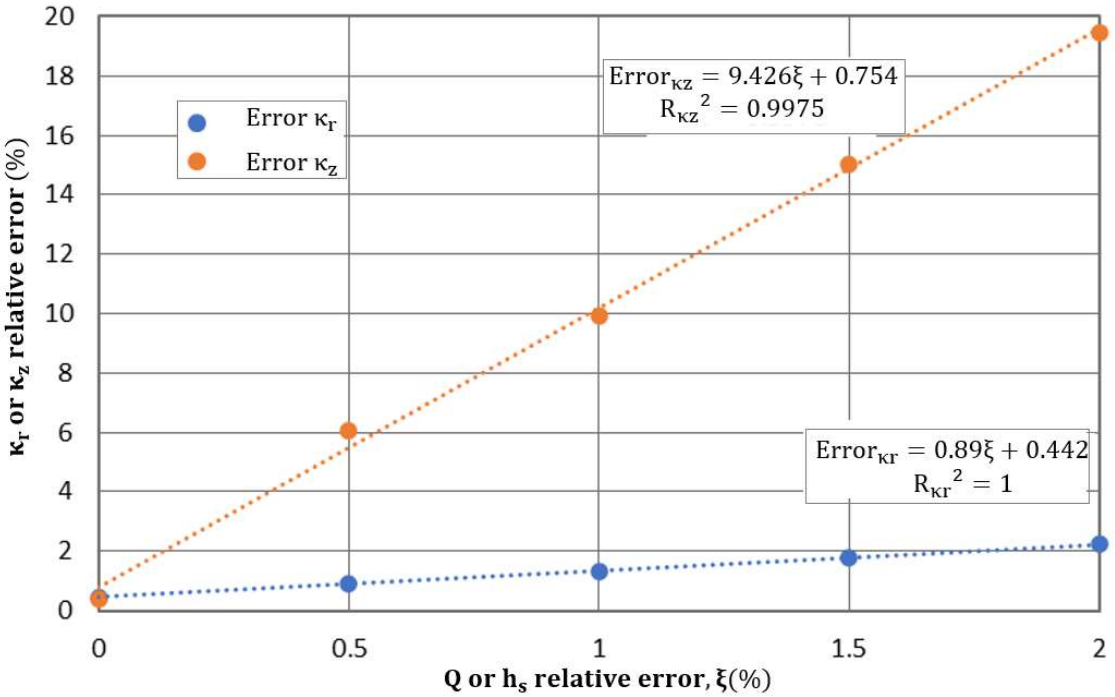

Figure 6.3. Maximum deviation of κ_r and κ_z as a function of ξ (dimensionless curves). Same sign

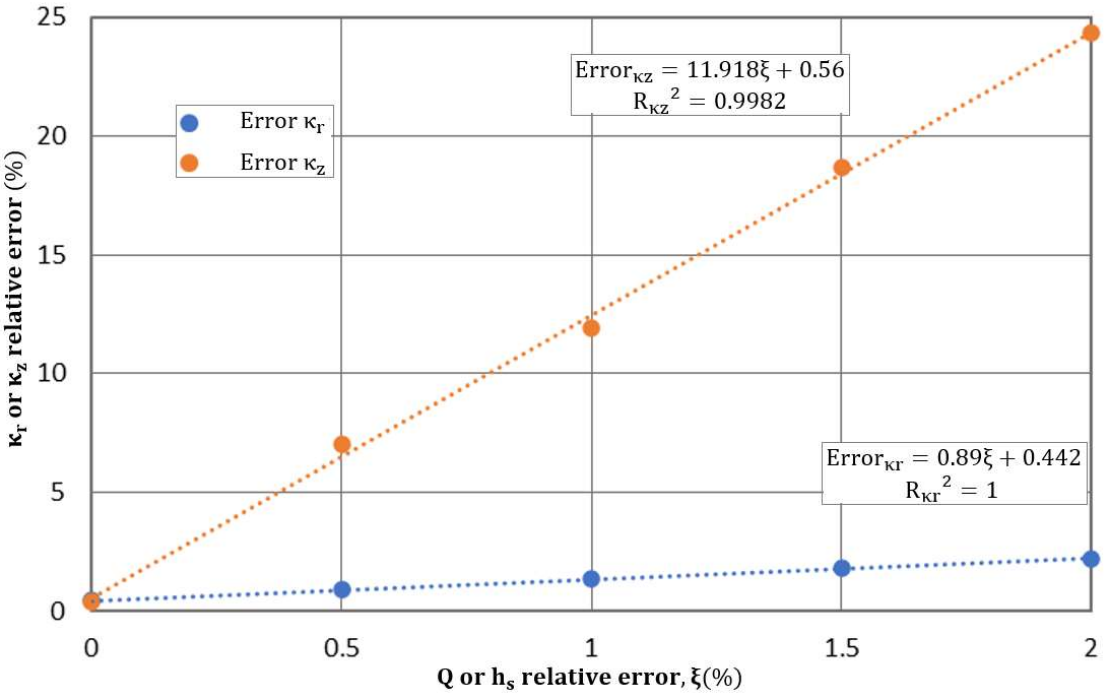

Figure 6.4. Maximum deviation of κ_r and κ_z as a function of ξ (dimensionless curves). Different sign

We can see how, for statistic random errors up to 2%, the deviation in the estimation of the vertical hydraulic conductivity can reach values between 20 and 25%, while for the horizontal conductivity, this is reduced to 2%. The high deviation for the vertical conductivity is due to, essentially, the error affecting the horizontal conductivity and to the seepage surface. For this reason, in Tables 6.1 and 6.2 apart from the errors, we also show the values of the conductivities, so we can appreciate the difference with the real value.

VI.4.2 Application employing WaWSim

In this case, before starting the simulations, initial values of the conductivities for the modelled aquifer have been chosen from a manual. According to Custodio & Llamas [1976], a coarse sand usually presents a hydraulic conductivity between 0.005 and 0.00001 m/s. These are for an isotropic soil, but since the flow is predominantly radial, we consider this range for the horizontal component. Finally, a value of κ_r of 0.0001 m/s is selected and the initial vertical conductivity is 0.00005 m/s.

When studying the error, we have to consider that, apart from the deviation due to the inverse problem itself (as shown in VI.4.1 with the dimensionless curves), the protocol requires an error range to end with the simulations and come up with a solution. Therefore, we can expect a larger deviation due to the statistic error.

Firstly, the hydraulic conductivities are calculated introducing the real values of Q and h_s, which are 0.002308 m^3/s and 8.471 m respectively. Once the simulations have been carried out, the following results are obtained:

κ_r = 0.0000224 m/s
κ_z = 0.0000096m/s

The deviations for each of the parameters calculated with the inverse problem are obtained according to Equation (VI-10) and (VI-11).

$$\frac{\kappa_{r,real}-\kappa_{r,sim}}{\kappa_{r,real}}100\% = \frac{0.0000225-0.0000224}{0.0000225}\cdot 100\% = 0.44\% \quad \text{(VI-10)}$$

$$\frac{\kappa_{z,real}-\kappa_{z,sim}}{\kappa_{z,real}}100\% = \frac{0.00001-0.0000096}{0.00001}\cdot 100\% = 3.75\% \quad \text{(VI-11)}$$

We see, studying these results, that the accuracy for the calculation of the horizontal hydraulic conductivity is similar employing the code or the dimensionless curves, while for the vertical conductivity, the deviation is higher with the code (3.75%) because it combines the deviation of the horizontal conductivity and the error in the protocol (deviation range between 0.001 and -0.001).

Once we know the deviations of the inverse problem, a statistic error is applied to the measured variables, Q and h_s, and we can see how this affects to the hydraulic conductivities, in the same way it was done in section VI.4.1. The results of the conductivities and the deviations are shown in Tables 6.3 and 6.4, while the errors are also presented in Figures 6.5 and 6.6.

Table 6.3. Maximum errors of κ_r and κ_z as a function of ξ (numerical simulation). Same sign

Error ξ (%)	$\kappa_r \cdot 10^{-5}$ (m/s)	Max Error κ_r (%)	$\kappa_z \cdot 10^{-5}$ (m/s)	Max Error κ_z (%)
0	2.24	0.44	0.96	3.75
0.5	2.25/2.23	0.88	0.87/1.00	12.99
1	2.26/2.20	2.22	0.86/0.99	14.45
1.5	2.27/2.20	2.22	0.80/1.08	20.00
2	2.30/2.20	2.22	0.77/1.15	22.73

Table 6.4. Maximum errors of κ_r and κ_z as a function of ξ (numerical simulation). Different sign

Error ξ (%)	$\kappa_r \cdot 10^{-5}$ (m/s)	Max Error κ_r (%)	$\kappa_z \cdot 10^{-5}$ (m/s)	Max Error κ_z (%)
0	2.24	0.44	0.96	3.75
0.5	2.25/2.23	0.88	0.87/1.00	13.11
1	2.26/2.20	2.22	0.85/1.02	15.00
1.5	2.27/2.20	2.22	0.80/1.15	20.00
2	2.30/2.20	2.22	0.73/1.20	26.58

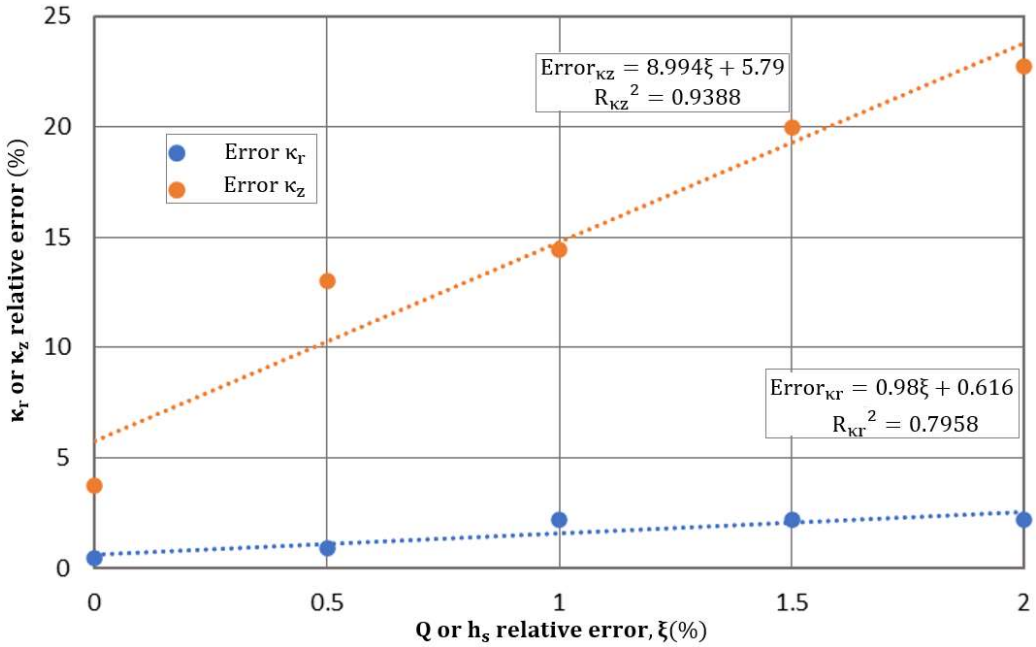

Figure 6.5. Maximum deviation of κ_r and κ_z as a function of ξ (numerical simulation). Same sign

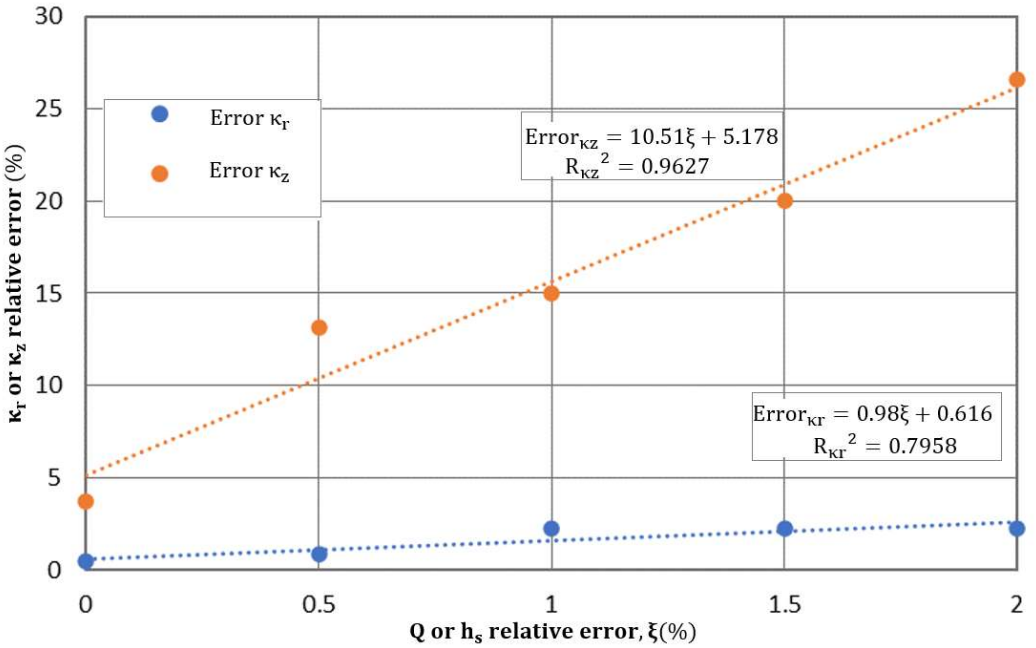

Figure 6.6. Maximum deviation of κ_r and κ_z as a function of ξ (numerical simulation). Different sign

It can be observed that, while the horizontal hydraulic conductivity reaches a maximum error value of 2.22% (as happened with the dimensionless curves), the vertical conductivity presents a deviation between 23 and 26%, being these values quite similar to those obtained with the dimensionless abaci (20 and 25%). The error graphics in Figures 6.5 and 6.6 can be modified for the horizontal hydraulic conductivity κ_r, in order to separate the section of constant slope (statistic random error ξ between 0 and ± 1) and that of null slope (ξ between ± 1 and 2). This modification and its new trend lines are presented in Figures 6.7 and 6.8.

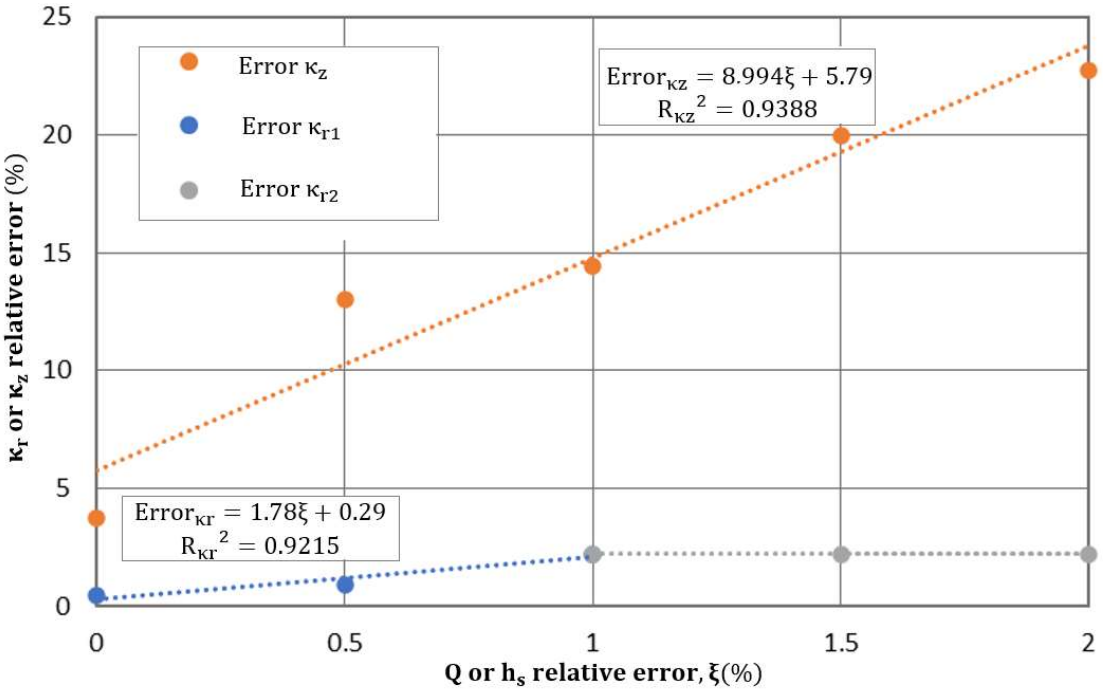

Figure 6.7. Modification of Figure 6.5

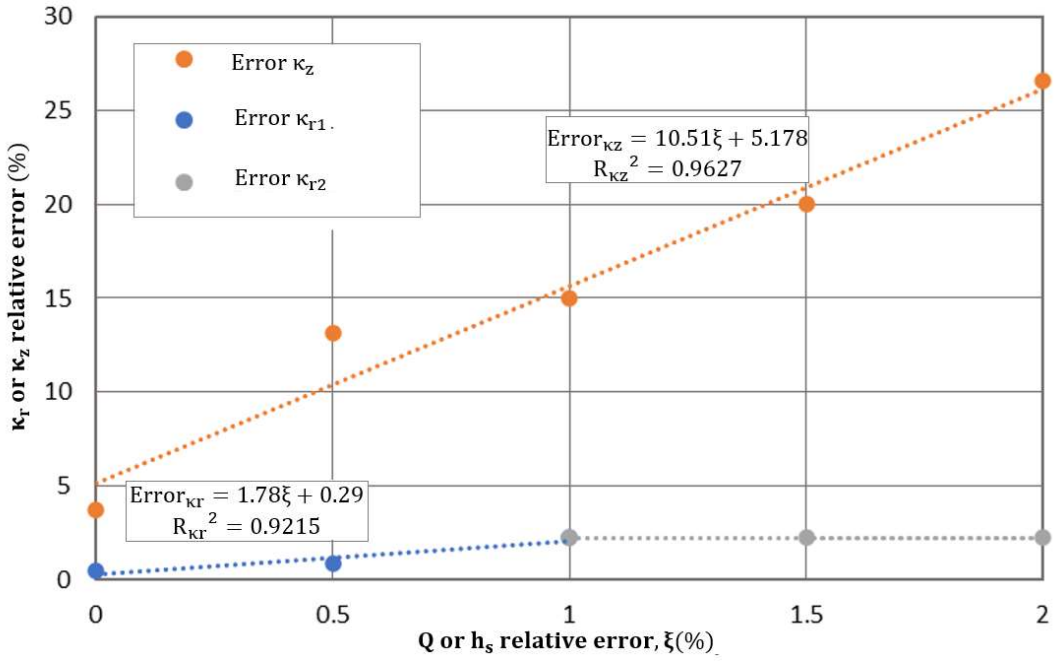

Figure 6.8. Modification of Figure 6.6

In light of these results, we can conclude that the horizontal hydraulic conductivity can be accurately estimated, even for statistics errors of 2%. Moreover, deviations are similar whether applying dimensionless curves or the protocol based on the network method. For the calculation of the vertical conductivity, the application of a statistic error of 0% presents a deviation of 0.4% with the curves and 3.75% with WaWSim, while the maximum deviation is around 25% for the maximum statistic error with both methodologies. This makes sense, since for the design of

protocol the validity range for the deviation, Γ_{hs}, was set between 0.001 and -0.001 because considering the same values as for the case of the groundwater flow variable (which were ten times larger), we did not get a satisfactory solution. In this way, we can see the need of accurately measuring the seepage surface if we want to obtain a precise vertical hydraulic conductivity.

Chapter VII. Simulation of scenarios

In this chapter we present some simplified applications of each of the three scenarios to illustrate the potential versatility of the models developed in this thesis and explained in Chapter V. In the first example (Section VII.1), flow under a gravity dam without a sheet pile, two graphics are shown: flow net and pore pressure distribution under the dam. The variables studied in this case, which are groundwater flow, average exit gradient, uplift force under the dam and its application point are also depicted. Moreover, pore pressure distributions for different configurations are verified by comparing them to dimensionless pore pressure values that can be found in reference manuals.

For the second scenario, flow under a gravity dam with a sheet pile at the dam toe (Section VII.2), three graphics are displayed: flow net, pore pressure distribution under the dam and pore pressure distribution along both sides of the sheet pile. The interest variables are also presented: groundwater flow, average exit gradient, uplift force and its application point and forces on both sides of the sheet pile and their application points. For this second example, the variable compared to values from reference manuals for different configurations is groundwater flow.

The third example illustrates an unconfined aquifer with a pumping well (Section VII.3), for which the flow net and the iso-pressure lines are also presented, and the studied variables are groundwater flow and seepage surface, both provided by the code. For these scenarios, the seepage surface values are compared to those found in references.

VII. 1 Scenarios of flow under gravity dams without a sheet pile

In order to exemplify this scenario, an anisotropic soil has been chosen. The geometrical parameters for the example are shown in Figure 7.1.

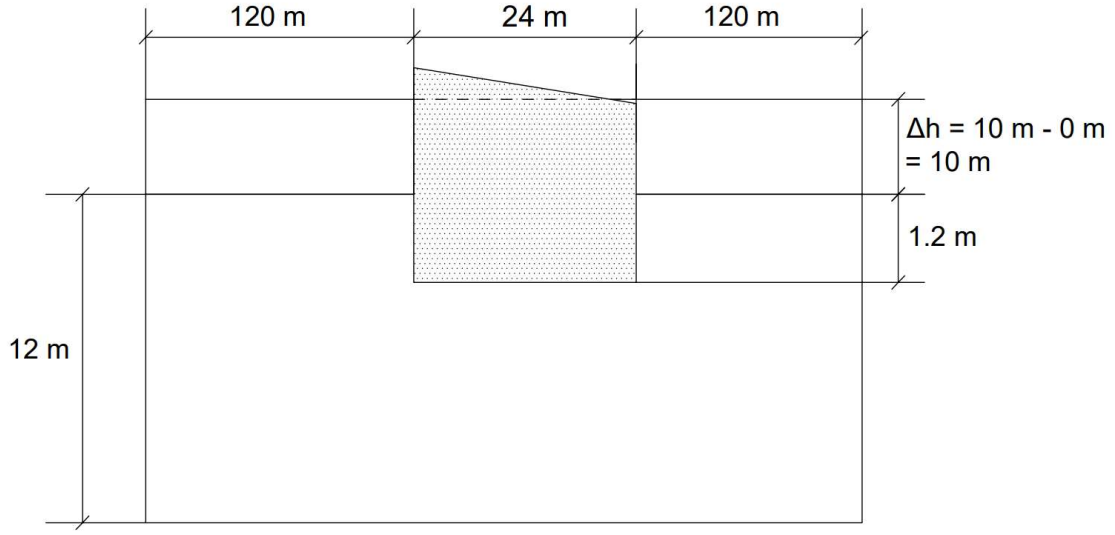

Figure 7.1. Geometric data for the scenario of flow under dams without a sheet pile

It is a dam with foundation in a soil which conductivities are κ_x = 0.0001 m/s y κ_y = 0.00005 m/s. From the data simulated by Ngspice, we can determine the variables of interest: groundwater flow (Q), uplift force under the dam (UF), application point of UF (C), and average exit gradient after the dam ($I_{e,ave}$). The results are summarized in Table 7.1. The application point is measured from the dam heel. In addition, the numerical simulation of this scenario leads to the flow net presented in Figure 7.2, while the pore pressure distribution is shown in Figure 7.3.

Table 7.1. Summary of numerical results for the scenario of flow under gravity dams without a sheet pile

Variable	Value
Groundwater flow, Q (m^3/s)	0.000258
Uplift force, UF (kN)	1487.44
Application point, C (m)	9.82
Average exit gradient, $I_{e,ave}$ (dimensionless)	0.64

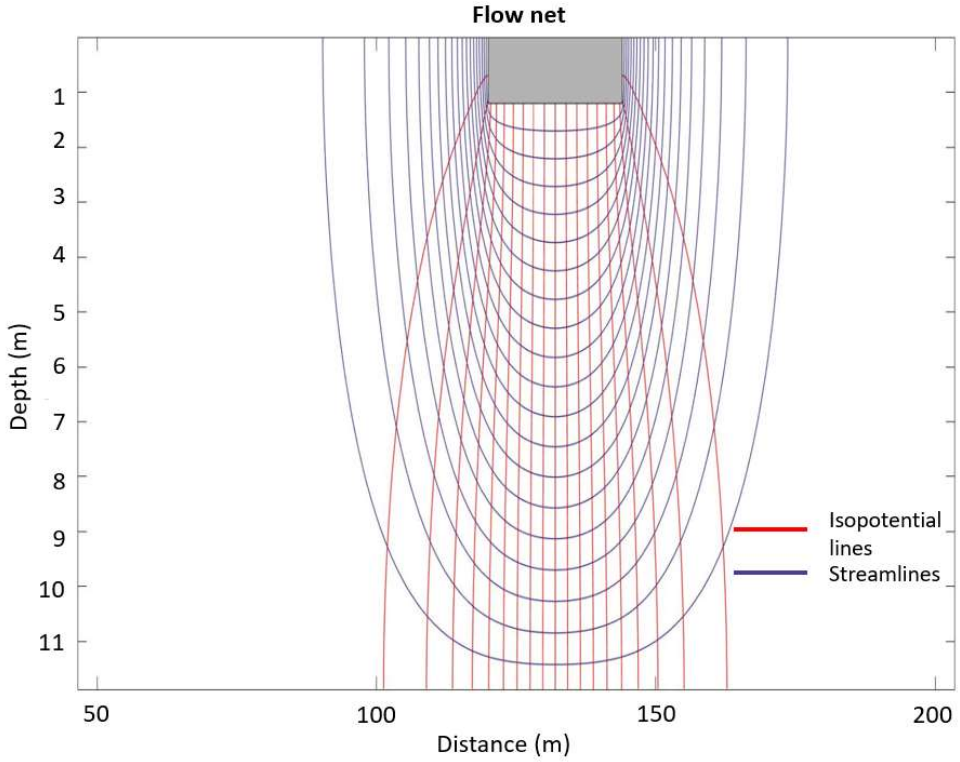

Figure 7.1. Flow net for the scenario of flow under gravity dams without a sheet pile (1V:10H)

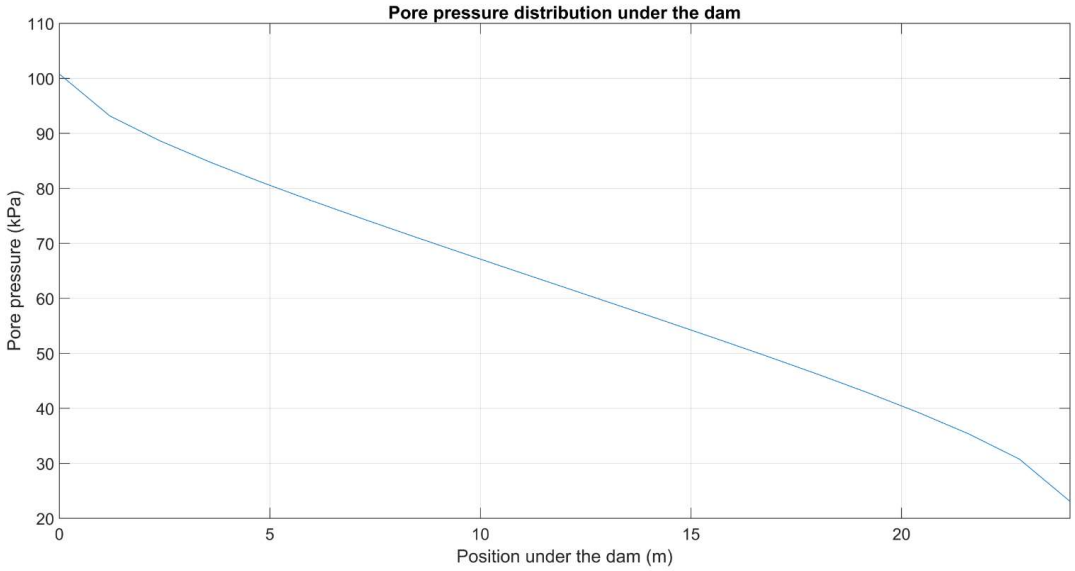

Figure 7.2. Pore pressure distribution for the scenario of flow under gravity dams without a sheet pile

In order to show the versatility and effectiveness of the network models, deduced in this thesis employing the Network Simulation Method, we have compared its solutions with those presented by Harr [2012] for some isotropic scenarios. Pore pressure values have been turned into dimensionless and plotted together with those from Harr's text in order to quantify the deviations. Figure 7.4 is the graphic with the comparisons while Table 7.2 shows the absolute

and relative deviations, where p' is the dimensionless pore pressure value and x' the dimensionless position under the dam.

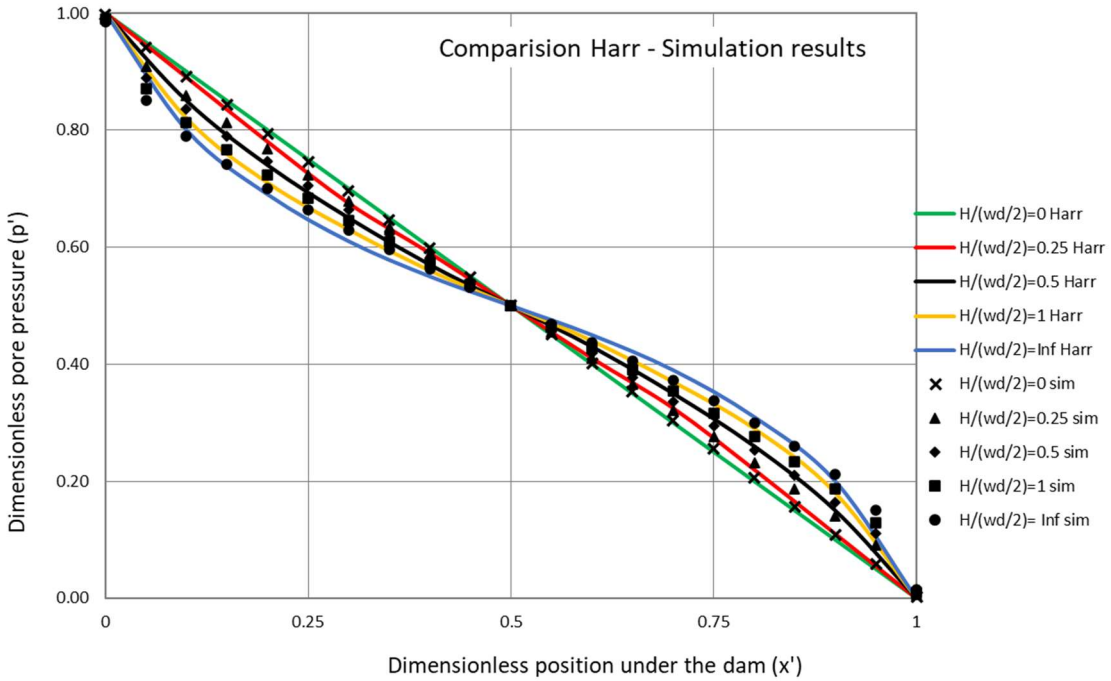

Figure 7.3. Comparison between Harr and simulated results

Table 7.2. Results and comparison from Harr and simulations (pore pressure distribution)

$H/(w_d/2)$	x'		0.1	0.2	0.3	0.4	0.5	0.6	0.7	0.8	0.9
0	p'	Harr	0.90	0.80	0.70	0.60	0.50	0.40	0.30	0.20	0.10
		Sim	0.89	0.79	0.70	0.60	0.50	0.40	0.30	0.21	0.11
	Abs. error		0.01	0.01	0.00	0.00	0.00	0.00	0.00	0.01	0.01
	Rel. error (%)		1.12	1.27	0.00	0.00	0.00	0.00	0.00	4.76	9.09
0.25	p'	Harr	0.88	0.78	0.68	0.59	0.50	0.41	0.32	0.22	0.12
		Sim	0.86	0.77	0.68	0.59	0.50	0.41	0.32	0.23	0.14
	Abs. error		0.02	0.01	0.00	0.00	0.00	0.00	0.00	0.01	0.02
	Rel. error (%)		2.33	1.30	0.00	0.00	0.00	0.00	0.00	4.35	14.29
0.5	p'	Harr	0.85	0.74	0.65	0.57	0.50	0.43	0.35	0.26	0.15
		Sim	0.83	0.75	0.66	0.58	0.50	0.42	0.34	0.25	0.17
	Abs. error		0.02	0.01	0.01	0.01	0.00	0.01	0.01	0.01	0.02
	Rel. error (%)		2.41	1.33	1.52	1.72	0.00	2.38	2.94	4.00	11.76
1	p'	Harr	0.82	0.71	0.63	0.56	0.50	0.44	0.37	0.29	0.18
		Sim	0.81	0.72	0.65	0.57	0.50	0.43	0.35	0.28	0.19
	Abs. error		0.01	0.01	0.02	0.01	0.00	0.01	0.02	0.01	0.01
	Rel. error (%)		1.23	1.39	3.08	1.75	0.00	2.33	5.71	3.57	5.26
Inf	p'	Harr	0.80	0.69	0.62	0.55	0.50	0.45	0.38	0.31	0.20
		Sim	0.79	0.70	0.63	0.56	0.50	0.44	0.37	0.30	0.21
	Abs. error		0.01	0.01	0.01	0.01	0.00	0.01	0.01	0.01	0.01
	Rel. error (%)		1.27	1.43	1.59	1.79	0.00	2.27	2.70	3.33	4.76

The deviations between the values from the literature and those simulated in this thesis are somehow expected and partially justified by the fact that Harr considered that the upstream and downstream horizontal lengths of the domain are infinite, a condition that cannot be expressly applied in the simulations. However, very large horizontal lengths in both sides of the domain have been adopted so that the border effects are as low as possible (all isopotential lines appear under the structure). The same happens for the scenario in which $\frac{H}{w_d/2}$ is infinite. The relative difference between the theoretical and the simulated value is below 10%, except for some cases of x'=0.9, where it is not larger than 15%. However, this relative difference that seems high is basically caused because two small values are compared. The absolute deviations are not different to other points of the same distribution which are located closer to the dam heel.

Another result that we can verify with this example is the fact that equal dimensionless scenarios (with the same monomials) always lead to equivalent flow nets or solution patterns. Since the monomials that summarize the example are $\pi_1 = 0.5$, $\pi_2 = 0.1$, $\pi_3 = 5$ y $\pi_4 = 1$, we simulate a new scenario whose vertical parameters (stratum thickness, foundation depth and vertical hydraulic conductivity) are kept constant, but the horizontal parameters are modified, maintaining the value of the dimensionless monomials. The data for the second simulation are a = b = 240 m, w_d = 48 m y κ_x = 0.0004 m/s. The flow net presented in Figure 7.5 is practically identical to that shown in Figure 7.2, although the horizontal lengths have been changed. As we wanted to prove, we would have the same dimensionless flow net.

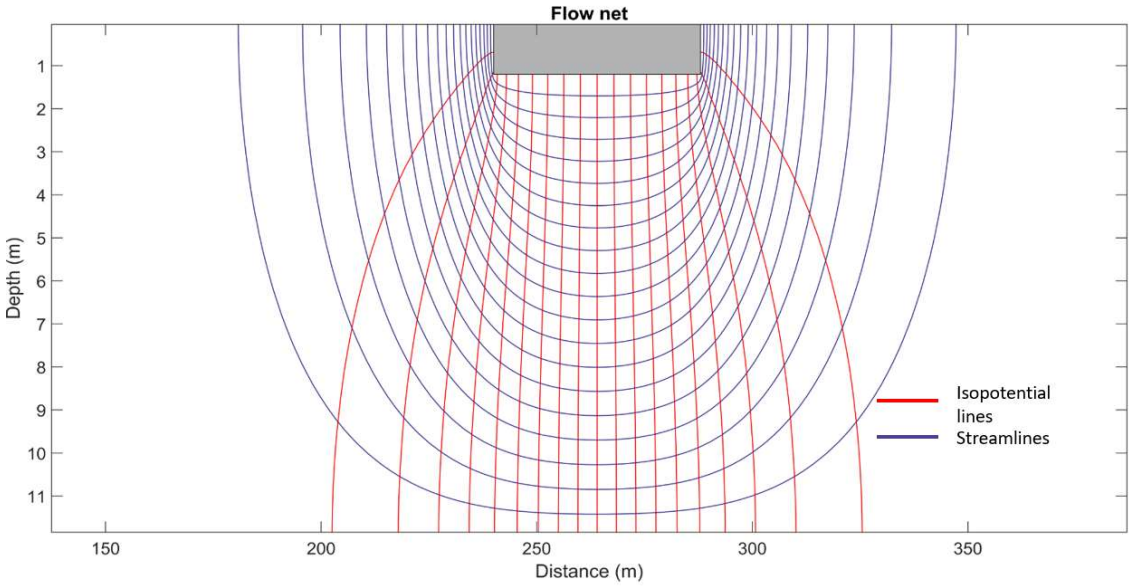

Figure 7.4. Flow net for an equivalent scenario of flow under dams without a sheet pile (1V:10H)

In order to deepen in this comparison of scenarios, we study two points of the flow net, showing that, although they have different dimensional position, they are found in the same dimensionless location and, therefore, have the same hydraulic potential value. These results appear in Table 7.3.

Table 7.3. Comparisons of points from the two simulations

Point	Dimensionless results	Dimensional results
1	x' = 0.385, y' = 0.83, h' = 0.95	x= 101.63 m, y = 10 m, h = 9.5 m
		x = 203.25 m, y = 10 m, h = 9.5 m
2	x' = 0.565, y' = 0.67, h' = 0.15	x = 149.25 m, y = 8 m, h = 1.5 m
		x = 298.5 m, y = 8 m, h = 1.5 m

VII. 2 Scenarios of flow under gravity dams with a sheet pile

In this example an anisotropic medium and a dam without foundation is considered. The geometrical parameters for this example are shown in Figure 7.6.

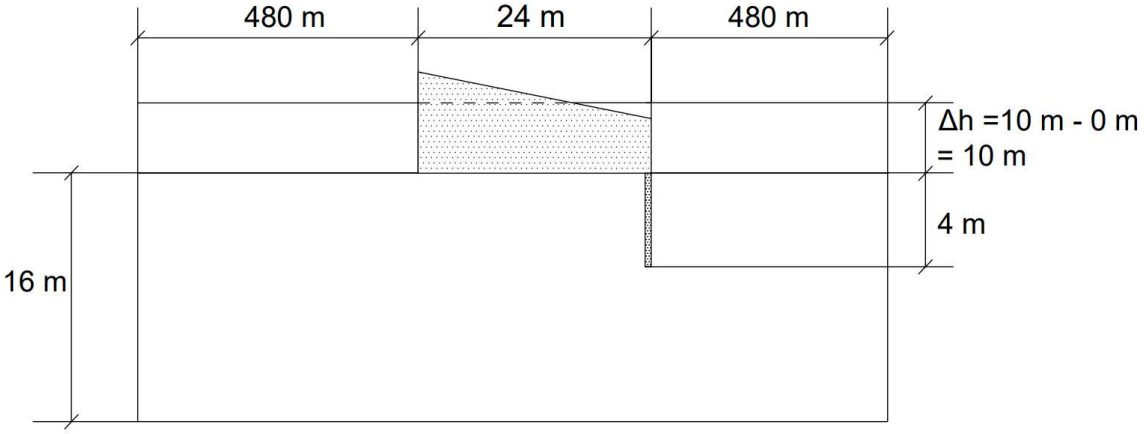

Figure 7.6. Geometric data for the scenario of flow under dams with a sheet pile

The hydraulic conductivity of the soil is κ_x = 0.00009 m/s for horizontal and y κ_y = 0.00004 m/s for the vertical. Once the simulation and the calculations are carried out, the code leads to the following graphical solutions: flow net (Figure 7.7), pore pressure distribution under the dam (Figure 7.8) and pore pressure distribution along both sides of the sheet pile (Figure 7.9).

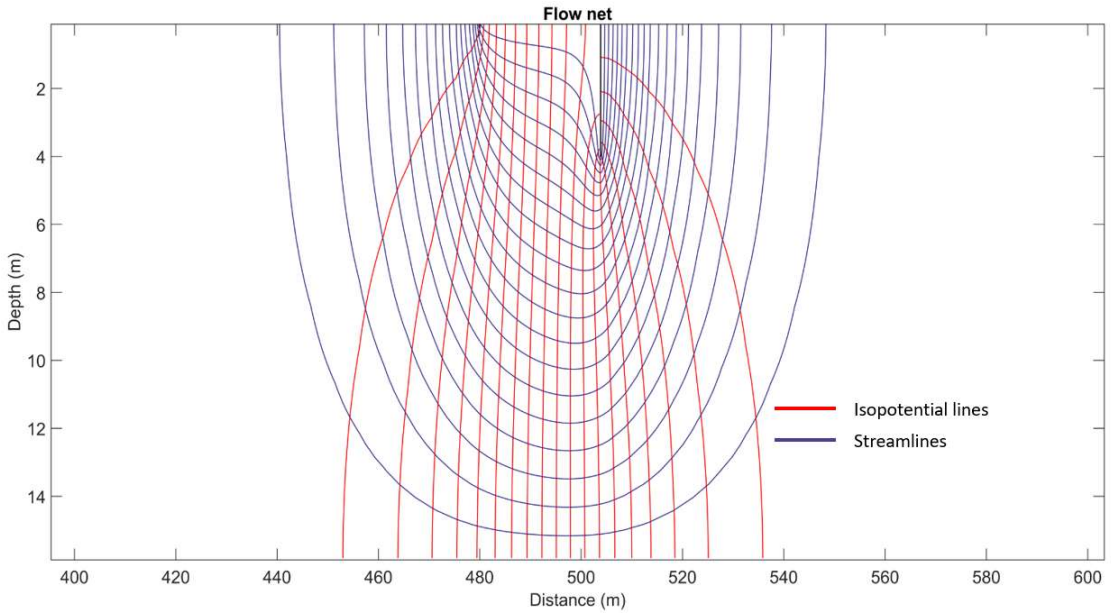

Figure 7.7. Flow net for the scenario of flow under gravity dams with a sheet pile (3V:20H)

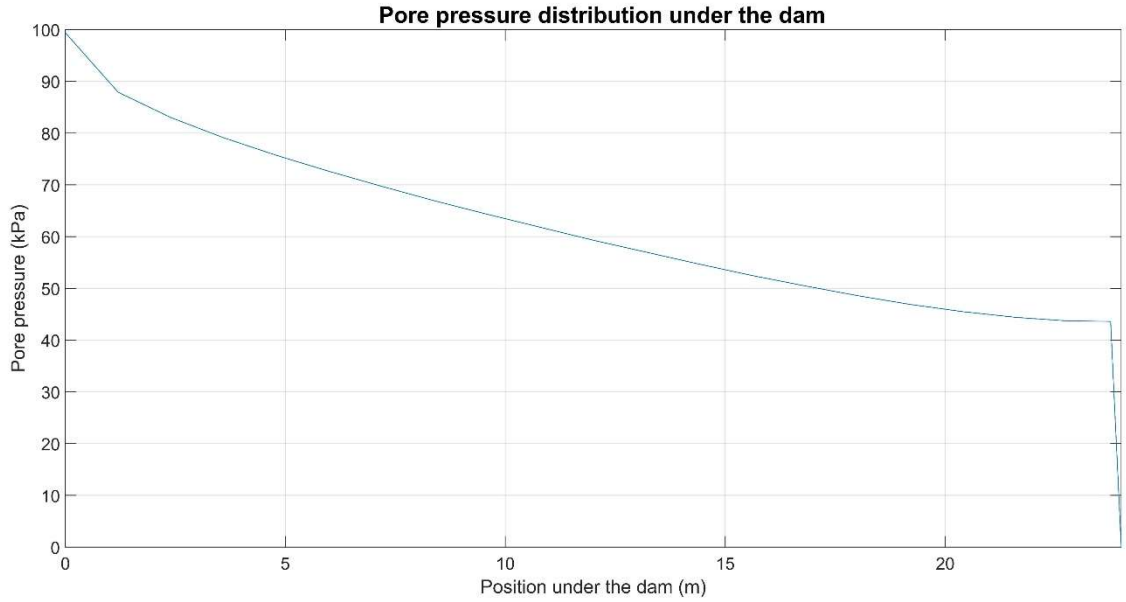

Figure 7.8. Pore pressure distribution for the scenario of flow under gravity dams with a sheet pile

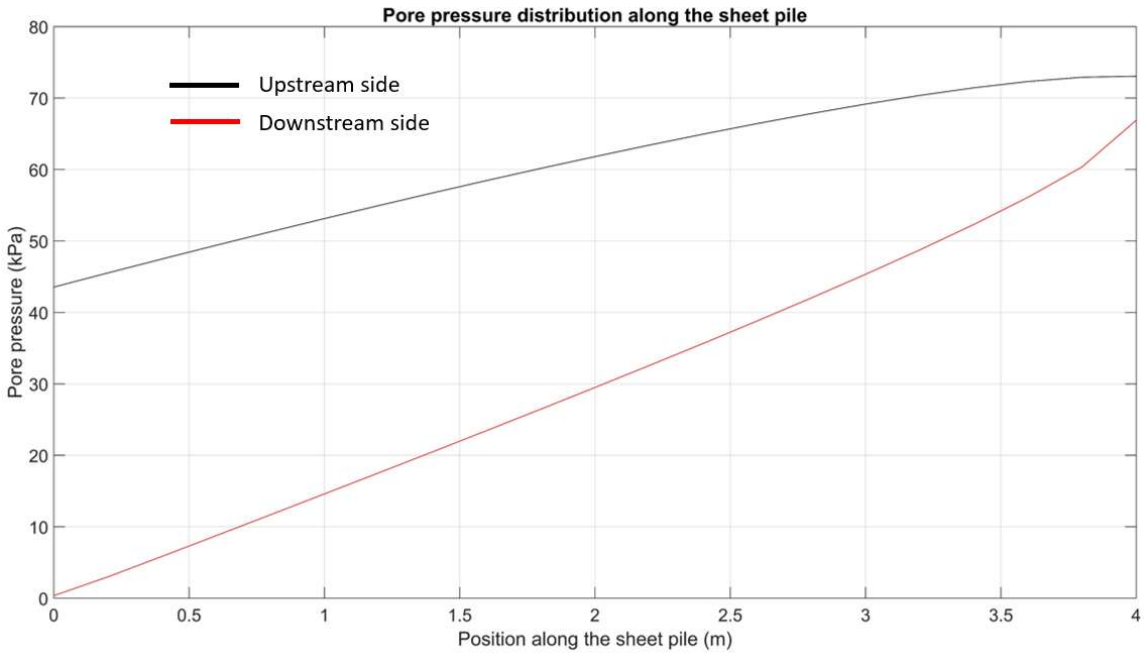

Figure 7.9. Pore pressure distribution along the sheet pile (upstream side and downstream side)

Moreover, from the solutions that Matlab imports from Ngspice we can mathematically calculate (with enough accuracy for not excessively large meshes) the most interest numerical variables: groundwater flow (Q), uplift force under the dam (UF), application point of UF (C), average exit gradient ($I_{e,ave}$), force on the upstream side of the sheet pile (F_{US}), application point of F_{US} (C_{US}), force on the downstream side of the sheet pile (F_{DS})and application point of F_{DS} (C_{US}). The application points of the forces on the sheet pile are measured from its upper border. These results are shown in Table 7.4.

Table 7.4. Summary of numerical results for the scenario of flow under gravity dams with a sheet pile

Variable	Value
Groundwater flow, Q (m^3/s)	0.000271
Uplift force, UF (kN)	1456.56
Application point, C (m)	10.16
Average exit gradient, $I_{e,ave}$ (dimensionless)	0.50
Force on the upstream side of the sheet pile, F_{US} (kN)	243.21
Application point of F_{US}, C_{US} (m)	2.17
Force on the downstream side of the sheet pile, F_{DS} (kN)	121.39
Application point of F_{DS} (m)	2.69

In order to verify again the accuracy of the model by comparing its results to analytical solutions found in literature (dimensionless curves in Harr [2012]), we have compared values of groundwater flow in isotropic scenarios with a sheet pile located in the centre of the dam base. As far as we know, there are not universal solutions for anisotropic scenarios. The length of the sheet pile is 30% of the simulated stratum. The results and deviations between the theoretical and simulated results are shown in Table 7.5.

Table 7.5. Results and comparison from Harr and simulations (groundwater flow)

w_d/H	Q_{Harr}	Q_{sim} (m^3/s) $\cdot 10^{-4}$	Q_{sim}	Abs. error	Error (%)
0*	0.66	6.69	0.67	0.01	1.36
0.25	0.59	5.92	0.59	0.00	0.33
0.5	0.48	4.75	0.48	0.00	1.04
0.75	0.39	3.89	0.39	0.00	0.26
1	0.33	3.27	0.33	0.00	0.91
1.25	0.28	2.82	0.28	0.00	0.71
1.5	0.25	2.47	0.25	0.00	1.20

The symbol * in Table 7.5 means that, as that ratio value cannot be simulated, a scenario that tends to that ratio has been chosen. Moreover, from the table we can conclude that the numerical solution is very close to that presented in Harr's text (errors lower than 1.5%). These differences can appear because of the chosen reticulation and the fact that we cannot simulate scenarios that are infinite in the horizontal direction, which is what Harr supposed.

VII. 3 Scenarios of flow in unconfined aquifers due to a pumping well

In order to show the versatility of the developed code, an anisotropic domain in radial coordinates is presented. Its geometrical parameters are those in Figure 7.10.

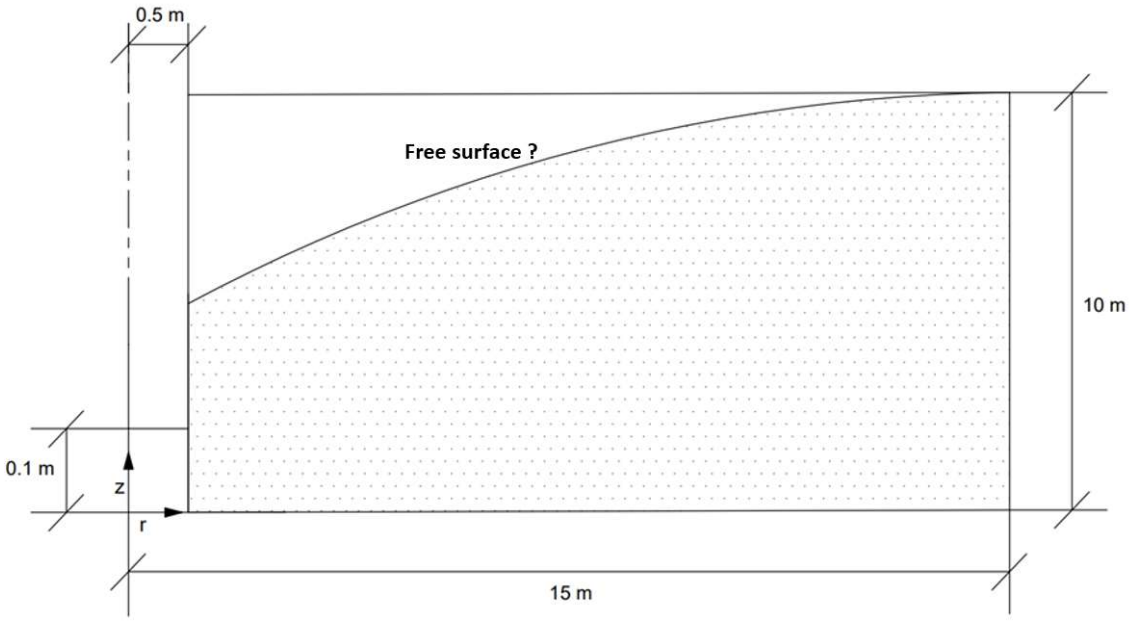

Figure 7.10. Geometric data for the scenario of flow in unconfined aquifers due to a pumping well

The hydraulic conductivities for the scenario are κ_r = 0.00008 m/s y κ_z = 0.00004 m/s. The graphical solution, common to the previous examples, is a flow net (where the iso-potential lines and the streamlines are shown, Figure 7.11), although, in this case, it is complemented with iso-pressure lines. Employing the last iso-pressure lines, we can somehow approximate to the limit known as free surface. Due to the behaviour of the software, where the switches allow not considering those zones where the hydraulic potential is lower to its position, we cannot know the streamline which corresponds to the 100% flow (or, equivalently, the free surface line for problems in which the capillary flow is not studied). For this reason, we try to give an approximate limit with the iso-pressure line of 1 kPa.

The variables that can be calculated from the solutions provided by Ngspice are abstracted volume of water (Q) and the seepage surface (h_s). For the simulated scenario, the values for these variables are shown in Table 7.6.

Table 7.6. Summary of numerical results for the scenario of flow in unconfined aquifers due to a pumping well

Variable	Value
Pumped groundwater flow, Q (m^3/s)	0.00741
Seepage surface (h_s)	7.82

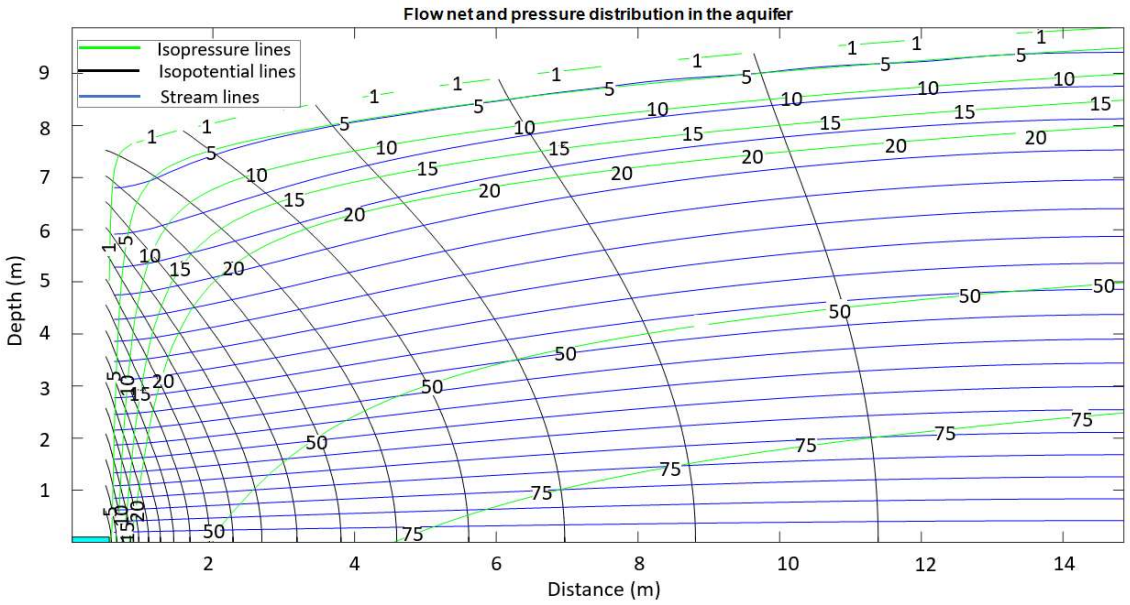

Figure 7.11. Flow net and pore pressure distribution for the scenario of flow in unconfined aquifers due to a pumping well

Again, with the aim of verifying the model, we have simulated some of the scenarios presented by Hall [1955], who obtained the seepage surface with experimental tests. The set of tests that has been chosen is that named by Hall as 'A', since these were 'ideally' carried out (the sand samples were saturated before performing the tests, constant temperature, etc). Seepage surface values obtained by Hall and those calculated with the code are shown in Table 7.7, together with the absolute and relative deviations.

Table 7.7. Results and comparison from Hall tests and simulations (seepage surface)

Test	$h_{s,\ Hall}$ (m)	$h_{s,\ sim}$ (m)	Abs. error	Rel. error (%)
A-1	1.107	1.107	0.000	0.000
A-2	1.043	1.057	0.014	1.342
A-3	0.945	0.945	0.000	0.000
A-4	0.902	0.902	0.000	0.000
A-5	0.864	0.864	0.000	0.000
A-6	0.848	0.852	0.004	0.472
A-7	0.833	0.818	0.015	1.801
A-8	0.833	0.821	0.012	1.441

Table 7.7 shows that errors are quite low, in every case lower than 2% and in many of them lower than 1%, which demonstrate the reliability of our model.

Chapter VIII. Contributions and conclusions

In this PhD thesis three problems of flow through porous media in the field of Ground Engineering have been studied: flow under gravity dams without a sheet pile, flow under gravity dam with a sheet pile and flow in unconfined aquifers due to pumping wells. For this, two different approaches have been employed. On the one hand, a protocol based on the discriminated nondimensionalization technique has been followed to deduce the dimensionless monomials that rule the processes. On the other hand, specific numerical models have been developed using the network method to carry out the numerical simulations. These simulations have allowed verifying the dimensionless groups and depicting the universal curves that present the relation among the monomials. In addition, as consequence of this research, the following results have been obtained: software for the simulation of the scenarios, a protocol based on the inverse problem for estimating the hydraulic properties, and a deep study of the dimensional character of permeability and hydraulic conductivity.

The most important contributions of the three approached problems are the following:

i) Flow under gravity dams without a sheet pile at its base

Employing the discriminated nondimensionalization technique, four monomials were obtained involving geometrical and hydrogeological parameters of the scenario. The monomial with highest influence on the unknown variables, and therefore called π_1, is the ratio of the hydraulic conductivities affected by an aspect factor, and it was derived from the nondimensionalization of the governing equation. The other three dimensionless groups are simply defined as discriminated ratios of lengths in the same direction.

The unknown dimensionless variables studied in this problems were groundwater flow, pore pressure distribution under the dam (which can also be presented as an uplift force and its application point) and average exit gradient. From numerical simulations, twenty-one abaci have been depicted, each of them involving 7-9 curves.

If comparing these results to those previously shown in reference manuals, the main advance of this thesis is the consideration of anisotropy. In this way, since most of the soils on which dams are built have larger values of hydraulic conductivity in the horizontal than in the vertical direction, the use of the curves presented would lead to more realistic results. Furthermore, the use of the discriminated nondimensionalization technique has also led to the correct expression of the most important monomial, π_1, in which the aspect factor affecting the conductivity ratio involves the square values of the employed lengths.

To simplify the graphical representation of the unknown variables, the value of last monomial, π_4, which is the ratio of the upstream and downstream length and gives information about the symmetry of the scenario, is always 1. For each of the unknown dimensionless variables, abaci reflect how they are affected by the data groups. Apart from the relation presented with the curves, two main aspect can be highlighted:

- Although data monomials change the behaviour of the dimensionless curves of the pore pressure distribution, the dimensionless uplift force always presents a value of 0.5.The dimensionless application point is the variable that shows the effect of the groups governing the scenario.
- Not only has the anisotropy of the soil affected the definition of the governing group, π_1, but also the area in which the average exit gradient has been calculated.

ii) Flow under gravity dams with a sheet pile at its base

In this case, two new discriminated monomials appear, one involving the position of the sheet pile at the dam base and another that is the ratio of the pile length and the stratum thickness. Variables of this scenario are also highly affected by π_1, and, in order to study the effects of the new data monomials, these, together with π_1 are the chosen monomials depicted in the abaci: the dam has no foundation ($\pi_2 = 0$), and the horizontal upstream and downstream lengths are very large ($\pi_3 = 20$ and $\pi_4 = 1$).

Apart from those dimensionless unknowns studied for scenarios without a sheet pile, new unknowns have appeared in this case because of the pile located under the dam: forces on both sides of the sheet pile caused by the pore pressure and their application point. Therefore,

seventeen abaci have been plotted, having each of them nine curves that relate the unknown variables with the data monomials.

As occurred with the scenario without a sheet pile, the main difference between the results obtained in this thesis and those in manuals is that isotropic and anisotropic soils can be characterized employing the curves presented in this document, leading to more accurate results. Monomial π_1 has the same expression in both scenarios, so the same advantages and comments have also been applied in this second problem.

Important behaviours can be noted in this problem:

- As regard dimensionless groundwater flow, it presents the same values when the sheet pile is placed at symmetrical points at the dam base (for example, dam heel and toe), having a maximum when the pile is located at the centre of the dam base.
- Focusing on the uplift force, its behaviour is also related to the symmetrical position of the pile, since values of the variables when the pile is at the dam toe are symmetrical to those for a pile at the heel respect to a horizontal axis of a value of 0.5.
- Studying the uplift force in scenarios of a sheet pile at the centre of the dam base, it was observed that it presents the same value as scenarios of dam without a sheet pile, not being affected by any of the other monomials involved.
- The dimensionless results of the forces on both sides of the sheet pile are also influenced by symmetry when locating the pile. In this case, the relation is more complex to find:
    - The value of the force on the upstream side of the pile when it is placed at the heel is related to that of the force on the downstream side of the pile when it is placed at the toe.
    - The force of the upstream side of the pile when located at the toe is related to that of the force on the downstream side of the pile when located at the heel.
    - When the pile is at the centre, the forces on both sides are related.

iii) Flow in unconfined aquifers due to pumping wells

The use of the discriminated nondimensionalization technique in this scenario has led to three discriminated groups that rule the problem: again, one involving a ratio of conductivities affected by an aspect factor, and two which simply relate lengths in the same direction. The dimensionless unknowns studied in the scenario are groundwater flow, seepage surface and influence radius, and they are presented in abaci with different number of curves each of them:

groundwater flow abacus has four curves, seepage surface thirty, and there is one curve in each of the abaci for influence radius.

Apart from the consideration of soil anisotropy, there are more differences between the approach of the scenario in this thesis and more traditional ones: not only is radial flow considered, but also vertical one; therefore, the values of the seepage surface can be accurately calculated. Different aspects should be noted from this scenario:

- Conductivity monomial, also named π_1, has so little effect on the dimensionless groundwater flow (differences of around 2%) that it has not been necessary to depict one curve for each value of π_1.
- In a similar way, when calculating the dimensionless values of the influence radius, it was not affected by π_3, which is the ratio of the water potential at the well and the initial value of the aquifer. This has simplified the graphical representation of the variable.
- If keeping all parameters constant but the vertical hydraulic conductivity, as this parameter decreases, the value of the seepage surface increases because radial flow becomes more important.

As commented before in this chapter and throughout the thesis, the basic structure of two tools based on the Network Method have been developed for obtaining the points of the corresponding abaci: DamSim, a software for simulating flow under dams with and without a sheet pile (in registration process), and the software WaWSim for problems of flow in unconfined aquifers due to a pumping well (in development process because transient state will be also included in the final version). Both software present numerical and graphical solutions, such as groundwater flow or flow net, in a window environment. These software program are free, versatile and easy-to-use tools accessible to all scientific community.

In connection to the discussion of permeability and hydraulic conductivity, their dimensional character has been demonstrated to be ambiguous and imprecise from the point of view of their physical meaning. It is an issue on which the agreement has not been reached in literature. For this aim, a research line that applies the concept of dimensional discrimination to the physical properties involved in permeability (grain size, tortuosity, connectivity, etc) has been followed. The same protocol has been employed to successfully assign accurate dimension to the hydraulic conductivity and to discriminate these dimensions (according to their direction) when studying anisotropic media. This result was confirmed by the proposed procedure of discriminated nondimensionalization of the governing equation, expressed in terms of any of the common potential variables (pressure, hydraulic potential or water head, etc). The results

go beyond those that would be derived employing classical techniques for obtaining dimensionless groups and, in fact, have allowed characterizing anisotropic scenarios in an accurate way for all the studied problems. In this way, if traditional dimensions of hydraulic conductivity were $[\kappa]=LT^{-1}$, after this research, and using x direction as an example to employ discriminated dimensions, $[\kappa_x]=L_x^2T^{-1}L_{wc}^{-1}$, with L_{wc} the dimension of water potential variable. Introducing discrimination and the dimension of the potential variable in the dimensional basis has led to the monomials that relate conductivities in anisotropic scenarios.

Finally, as regards the inverse problem of flow in unconfined aquifers due to a pumping well, employing WaWSim and the universal abaci of the scenario, protocols have been designed to calculate radial and vertical conductivities. The expected deviation has been calculated with an application following both methodologies. Moreover, the effect of possible deviations (measure errors) of field parameters, groundwater flow and seepage surface, in the conductivity values is presented.

In future research, aspects that have not been studied in this thesis can be approached. Since dam scenarios have only been characterized and modelled with and without a sheet pile, a possible investigation line might deal with the location two or more sheet piles under the dam. Furthermore, it would also be interesting to obtain abaci for overall resulting force on sheet pile(s) and application point, which is a more summarized way to present the dimensionless values. Considering pumping wells in unconfined aquifers, this work has only focused on steady-state scenarios with a single, fully-penetrating well, so possible advances in this topic could be transient-state problems and partial penetrating structures, in order to develop universal solutions and inverse problems. Another phenomenon that might be considered in future investigations is rewetting. These tasks, addressed with more sophisticated models, would also allow the research of flow through earth dams.

Reference list

Åberg, B. (1992 a). Void Ratio of Noncohesive Soils and Similar Materials. *Journal of Geotechnical Engineering, 118*(9), 1315-1334. https://doi.org/10.1061/(ASCE)0733-9410(1992)118:9(1315)

Åberg, B. (1992 b). Hydraulic Conductivity of Noncohesive Soils. *Journal of Geotechnical Engineering, 118*(9), 1335-1347. https://doi.org/10.1061/(ASCE)0733-9410(1992)118:9(1335)

Alarcón García, M. (2001). *Transporte de Calor en Sistemas con Aletas. Coeficientes de Rendimiento y Red de Transferencia*. Ph. D. Thesis. Universidad Politécnica de Cartagena.

Alarcón, M., Alhama, F., & González-Fernández, C. F. (2002). Transient Conduction in a Fin-Wall Assembly with Harmonic Excitation--Network Thermal Admittance. *Heat Transfer Engineering*, *23*(2), 31-43. https://doi.org/10.1080/01457630252800412

Alhama, F., & Zueco, J. (2007). Application of a Lumped Model to Solids with Linearly Temperature-Dependent Thermal Conductivity. *Applied Mathematical Modelling*, *31* (2), 302-310. https://doi.org/10.1016/j.apm.2005.11.015

Alhama, F., & Madrid, C.N. (2012). *Análisis Dimensional Discriminado en Mecánica de Fluidos y Transferencia de Calor.* Reverté, Barcelona.

Alhama, F., & Madrid, C. N. (2007). Discriminated dimensional analysis versus classical dimensional analysis and applications to heat transfer and fluid dynamics. *Chinese Journal of Chemical Engineering, 15*(5), 626-631.

Alhama, I., Alhama, F., & Meca, A. S. (2012). The Network Method for A Fast and Reliable Solution of Ordinary Differential Equations: Applications to Non-Linear Oscillators. *Computers & Electrical Engineering*, *38*(6), 1524-1533. https://doi.org/10.1016/j.compeleceng.2012.05.008

Anderson, D. G. (1940). *Void Volume and Flow Resistance of Beds of Particles*. PhD Dissertation. Columbia University.

Anwar Bég, O., Zueco, J., & Takhar, H.S. (2009). Unsteady Magnetohydrodynamic Hartmann Couette Flow and Heat Transfer in a Darcian Channel with Hall Current, Ion Slip, Viscous and Joule Heating Effects: Network Numerical Solutions. *Communications in Nonlinear Science and Numerical Simulation*, *14*(4), 1082-1097. https://doi.org/10.1016/j.cnsns.2008.03.015

Arenas, A. (1970). *Análisis Dimensional en la Mecánica de Fluidos y Transmisión de Calor*. Ph. D. Thesis, Universidad de Madrid.

Ayvaz, M.T., & Karahan, H. (2008). A Simulation/Optimization Model for the Identification of Unknown Groundwater Well Locations and Pumping Rates. *Journal of Hydrology 357,*76-92. https://doi.org/10.1016/j.jhydrol.2008.05.003

Azizi, F. (1999). *Applied Analyses in Geotechnics*. CRC Press.

Babbitt, H. E., & Caldwell, D. H. (1948). *The Free Surface around, and Interference between, Gravity Wells*. University of Illinois at Urbana Champaign, College of Engineering. Engineering Experiment Station.

Baker, W. E., & Shortt, D. J. (1990). Integrated Electrical/Thermal Component Modeling. *Proceedings of the 25th Intersociety Energy Conversion Engineering Conference, 2*, 78-83. https://doi.org/10.1109/IECEC.1990.716550

Bakis, R., & Tuncan, A. (2011). An Investigation of Heavy Metal and Migration through Groundwater from the Landfill Area of Eskisehir in Turkey. *Environmental Monitoring and Assessment 176,* 87–98. doi:10.1007/s10661-010-1568-3

Barlow, P.M., & Leake, S.A. (2012). Streamflow Depletion by Wells—Understanding and Managing the Effects of Groundwater Pumping on Streamflow. *U.S. Geological Survey Circular 1376.*

Baughn, J. W., & Rossi, M. (1992). Two-Dimensional Transient Heat Conduction Analysis Using Spreadsheets. *Heat Transfer Engineering*, *13*(2), 71-79. https://doi.org/10.1080/01457639208939775

Beck, J. V., Blackwell, B., & Clair Jr, C. R. S. (1985). *Inverse Heat Conduction: Ill-Posed Problems*. Wiley-Interscience, New York.

Beckwith, C. W., Baird, A. J., & Heathwaite, A. L. (2003 a). Anisotropy and Depth-Related Heterogeneity of Hydraulic Conductivity in a Bog Peat. I: Laboratory Measurements. *Hydrological Processes, 17*(1), 89-101. https://doi.org/10.1002/hyp.1116

Bejan, A. (1995). Theory of Heat Transfer-Irreversible Power Plants—II. The Optimal Allocation of Heat Exchange Equipment. *International Journal of Heat and Mass Transfer*, *38*(3), 433-444. https://doi.org/10.1016/0017-9310(94)00184-W

Bejan, A., & Krauss, A.D. (2003). *Heat Transfer Handbook*, New Jersey: John Wiley & Sons.

Bello, V. G. (1991). Electrical Models of Mechanical Units Widen Simulator's Scope. *Electronics Design News, 36*(7), 139-144.

Benavent, A., Castro, E., & Gallego, A. (2010). Evaluation of Low-Cycle Fatigue Damage in RC Exterior Beam-Column Subassemblages by Acoustic Emission. *Construction and Building Materials*, *24*(10), 1830-1842. https://doi.org/10.1016/j.conbuildmat.2010.04.021

Bonilla, C. F. (1965). Fundamentals of Heat Transfer. *Nuclear Science and Engineering*, *21*(4), 586-587. https://doi.org/10.13182/NSE65-A18809

Bose, N. K. (1929). *Punjab lrrigation & Search Memoirs*, vol. 2. India.

Bose, N. K. (1930). *Punjab Engineering Congress*, 140. India.

Boulton, N. S. (1951). The Flow Pattern Near a Gravity Well in a Uniform Water-Bearing Medium. *Journal of The Institution of Civil Engineers*, *36*(10), 534-550.

Bradfield, K. N. E., Hooker, S. G., & Southwell, R. V. (1937). Conformal Transformation with the Aid of an Electrical Tank. *Proceedings of the Royal Society of London. Series A-Mathematical and Physical Sciences*, *159*(898), 315-346. https://doi.org/10.1098/rspa.1937.0075

Bridgman, P. W. (1931). *Dimensional Analysis*. New Haven: Yale University Press. https://doi.org/10.1002/bimj.19640060310

Buckingham, E. (1914). On Physically Similar Systems; Illustrations of the Use of Dimensional Equations. *Physical Review*, *4*(4), 345. https://doi.org/10.1103/PhysRev.4.345

Cánovas, M., Alhama, I., Trigueros, E., & Alhama, F. (2015). Numerical Simulation of Nusselt-Rayleigh Correlation in Bènard Cells. A Solution Based on the Network Simulation Method. *International Journal of Numerical Methods for Heat & Fluid Flow*, *25*(5), 986-997. https://doi.org/10.1108/HFF-09-2014-0282

Cánovas, M., Alhama, I., Trigueros, E., & Alhama, F. (2016). A Review of Classical Dimensionless Numbers for the Yusa Problem Based on Discriminated Non-Dimensionalization of the Governing Equations. *Hydrological Processes*, *30*(22), 4101-4112. https://doi.org/10.1002/hyp.10878

Capobianchi, M., & Aziz, A. (2012). A Scale Analysis for Natural Convective Flows over Vertical Surfaces. *International Journal of Thermal Sciences, 54*, 82-88. https://doi.org/10.1016/j.ijthermalsci.2011.11.009

Carman, P. C. (1939). Permeability of Saturated Sands, Soils and Clays. *The Journal of Agricultural Science, 29*(2), 262-273. https://doi.org/10.1017/S0021859600051789

Carman, P.C. (1938). The Determination of the Specific Surface of Powders. *Journal of the Society of Chemical Industry Transactions, 57,* 225.

Carrier III, W. D. (2003). Goodbye, Hazen; Hello, Kozeny-Carman. *Journal of Geotechnical and Geoenvironmental Engineering*, *129*(11), 1054-1056. https://doi.org/10.1061/(ASCE)1090-0241(2003)129:11(1054)

Carslaw, H. S. (1921). *Introduction to the Mathematical Theory of the Conduction of Heat in Solids*. MacMilland and Co, London.

Casagrande, A. (1940). Seepage through Dams. Contributions to Soil Mechanics, 1925-1940. *Boston Society of Civil Engineers, Boston*.

Castany, G. (1971). *Tratado Práctico de las Aguas*. Barcelona. Omega.

Castro E. (2005). *Simulación de Ondas Elásticas en Vigas Mediante el Método de Redes y Detección de Daño Mediante la Transformada Wavelet*. Ph. D. Thesis. Universidad de Granada.

Castro, E., García-Hernández, M. T., & Gallego, A. (2005). Transversal Waves in Beams Via the Network Simulation Method. *Journal of Sound and Vibration*, *283*(3-5), 997-1013. https://doi.org/10.1016/j.jsv.2004.05.026

CEN (European Committee for Standardization) (2004). Eurocode-7 Geotechnical design - Part 1: General rules. Eurocode-7, Brussels, Belgium: CEN.

Childs, E. C., Collis-George, N., & Holmes, J. W. (1957). Permeability Measurements in the Field as an Assessment of Anisotropy and Structure Development. *Journal of Soil Science, 8* (1), 27-41. https://doi.org/10.1111/j.1365-2389.1957.tb01865.x

CONCRELIFE (2019): Alhama I. & Sánchez, J.F., *Software for the calculation of the service life of reinforced concrete structures in marine environments,* NAR: 25/09/19, ©Universidad Politécnica de Cartagena.

CODENS-13 (2014): Alhama, F., Alhama, I., Sánchez, J.F.& Morales, J.L., *Coupled Ordinary Differential Equations by Network Simulation*, NAR: 16/01/2014, ©Universidad Politécnica de Cartagena.

Conesa, M., Pérez, J. S., Alhama, I., & Alhama, F. (2016). On the Nondimensionalization of Coupled, Nonlinear Ordinary Differential Equations. *Nonlinear Dynamics*, *84*(1), 91-105. https://doi.org/10.1080/00986440802115655

Custodio, E., & Llamas, M. R. (1976). *Hidrología Subterránea* (Vol. 1). Barcelona. Omega.

DamSim (2021): Martínez-Moreno, E., García-Ros, G., Alhama, I & Alhama F.J., *Software for Simulation of Flow under Dams with and without a sheet pile* (in registration process), © Universidad Politécnica de Cartagena

Darcy, H. P. G. (1856). *Les Fontaines Publiques de la Ville de Dijon. Exposition et Application des Principes à Suivre et des Formules à Employer dans les Questions de Distribution d'Eau, etc.* V. Dalamont.

Davies, M G (1979). A Thermal Circuit for Radiant Exchange. *Building and Environment, 14*(1), 43-46. https://doi.org/10.1016/0360-1323(79)90027-1

Davies, M G (1994). Longwave Radiant Exchange between Rooms. *Building and Environment, 29*(1), 97-98. https://doi.org/10.1016/0360-1323(94)90057-4

Davies, R. J., Almond, S., Ward, R. S., Jackson, R. B., Adams, C., Worrall, F., ... & Whitehead, M. A. (2014). Oil and Gas Wells and their Integrity: Implications for Shale and Unconventional Resource Exploitation. *Marine and Petroleum Geology*, *56*, 239-254. https://doi.org/10.1016/j.marpetgeo.2014.03.001

de Cazenove, E. (1961). Rabattement d'une Nappe á Surface Libre Exploitée par Puits ou Tranchées. *La Houille Blanche*, (3), 252-265.

De Glee, G., J. (1930). *Over Groundwaterstormingen bij Wateronttrekking door middle von Putten* (Doctoral Thesis). Delft.

Del Cerro Velázquez, F. (2009). *Desarrollo de un Programa de Conducción de Calor, Usando Analogía Eléctrica, mediante el Lenguaje C# y el Módulo de Cálculo Pspice. Aplicaciones Lineales y No Lineales En Diferentes Geometrías*. Ph. D. Thesis. Universidad de Murcia.

Duffin, R. J., & Knowles, G. (1984). A Passive Wall Design to Minimize Building Temperature Swings. *Solar Energy*, *33*(3-4), 337-342. https://doi.org/10.1016/0038-092X(84)90163-4

Dupuit, J. É. J. (1863). *Études Théoriques et Pratiques sur le Mouvement des Eaux dans les Canaux Découverts et à Travers les Terrains Perméables: avec des Considérations Relatives au Régime des Grandes Eaux, au Débouché à leur Donner, et à la Marche des Alluvions dans les Rivières à Fond Mobile*. Dunod.

EDUCONSOL (2018): Alhama, I. & García-Ros, G., *Educational Consolidation*, NAR: 20/03/2018, © Universidad Politécnica de Cartagena.

Ehrenberger, R. (1928). Versuche uber die Ergiebigheit von Brunnen und Bestim-Mung der Durchlassigkeit des Sandes. *Zeitschrift des Osterreicher Ingenieur und Architektunvereins, Heft* 11/12, Austria (in German).

EPSNET_10 (2011): Morales J.L., Moreno J.A. & Alhama F., *Elasticity Problems Simulation Network*, NAR: 08/2011, © 2011 Universidad Politécnica de Cartagena.

FAHET (2010): Alhama I., Soto Meca A. & Alhama F., *Flow and Heat Transport Simulator*, NAR: 08/2011©, Universidad Politécnica de Cartagena.

Fancher, G. H., Lewis, J. A., & Barnes, K. B. (1933). Some Physical Characteristics of Oil Sands. [Porosity, Permeability, and Screen Analysis]. *Penn. State Coll., Mineral Ind. Expt. Sta., Bull., 12.*

FATSIM-A (2010): Alhama I., Soto Meca A. & Alhama F., *Fluid Flow and Solute Transport Simulator*, NAR: 08/2010 ©, Universidad Politécnica de Cartagena.

Fourier, J. B. J. (1822). *Théorie Analytique de la Chaleur*, Chez Firmin Didot, Paris. (2ª ed., París, Gauthiers-Villars, 1888). https://doi.org/10.1017/CBO9780511693229

García-Ros, G. (2016). *Caracterización Adimensional y Simulación Numérica de Procesos Lineales y No Lineales de Consolidación de Suelos*. Ph. D. Thesis. Universidad Politécnica de Cartagena. https://doi.org/10.31428/10317/5937

García-Ros, G., Alhama, I., & Alhama, F. (2019 a). Dimensionless Characterization of the Non-Linear Soil Consolidation Problem of Davis and Raymond. Extended Models and Universal Curves. *Applied Mathematics and Nonlinear Sciences*, *4*(1), 61-78. https://doi.org/10.2478/AMNS.2019.1.00008

García-Ros, G., Alhama, I., & Cánovas, M. (2018). Powerful Software to Simulate Soil Consolidation Problems with Prefabricated Vertical Drains. *Water*, *10*(3), 242-251. https://doi.org/10.3390/w10030242

García-Ros, G., Alhama, I., & Morales, J. L. (2019 b). Numerical Simulation of Nonlinear Consolidation Problems by Models Based on the Network Method. *Applied Mathematical Modelling*, *69*, 604-620. https://doi.org/10.1016/j.apm.2019.01.003

Gibbings, J. C. (2011). *Dimensional Analysis*. Springer Science & Business Media.

González de Vallejo, L.I. (2002). *Ingeniería Geológica.* Pearson.

González-Fernández, C. F., Alhama, F., López Sánchez, J. F., & Horno, J. (1998). Application of the Network Method to Heat Conduction Processes with Polynomial and Potential-Exponentially Varying Thermal Properties. *Numerical Heat Transfer, Part A Applications*, *33*(5), 549-559. https://doi.org/10.1080/10407789808913954

González-Fernández, C. F., García-Hernández, M. T., & Horno, J. (1995). Computer Simulation of a Square Scheme with Reversible and Irreversible Charge Transfer by the Network Method. *Journal of Electroanalytical Chemistry*, *395*(1-2), 39-44. https://doi.org/10.1016/0022-0728(95)04147-G

Gray, W. A. (1968). *The Packing of Solid Particles* (No. 631.43). Chapman & Hall, London.

Hall, H. P. (1955). An Investigation of Steady Flow toward a Gravity Well. *La Houille Blanche*, (1), 8-35.

Hamill, D. C. (1993). Learning about Chaotic Circuits With SPICE. *IEEE Transactions on Education*, *36*(1), 28-35. https://doi.org/10.1109/13.204812

Hantush, M. S. (1964). Hydraulics of Wells. *Advances in Hydroscience, 1*, 281-432.

Harr, M. E. (2012). *Groundwater and Seepag*e. Courier Corporation.

Harza, L. F. (1935). Uplift and Seepage under Dams on Sand. *Transaction of the American Society of Civil Engineers*, *100*, 1352-1406. https://doi.org/10.1061/TACEAT.0004642

Hazen, A. (1892). Some Physical Properties of Sands and Gravels, with Special Reference to their Use in Filtration. *24th Annual Rep., Massachusetts State Board of Health*, Pub. Doc. No. 34, 539–556.

Helle-Shaw, H. S. (1899). Stream-Line Motion of a Viscous Film*. 68º Meeting Butish As for the advancements of Science*.

Herdan, G. (1960). *Small Particle Statistics*, 2nd revised ed. Butterworths, London.

Herranz, A. & Arenas, A. (2005). *Análisis Dimensional y sus Aplicaciones.* Diego Marin. Murcia.

Horno Montijano, J. (2002). *Network Simulation Method*. Research Signpost.

Horno, J., González-Caballero, F., Hayas, A., & González-Fernández, C. F. (1990). The Effect of Previous Convective Flux on the Nonstationary Diffusion through Membranes. Network Simulation. *Journal of Membrane Science*, *48*(1), 67-77. https://doi.org/10.1016/S0376-7388(00)80796-6

Huntley, H. E. (1952). *Dimensional Analysis*. Dover publications.

Jacob, C., E. (1963). Determining the Permeability of Water-Table Aquifers. *Methods of Determining Permeability, Transmissibility and Drawdown.* U.S. Geological Survey Water Supply.

Juárez Badillo, E. & Rico Rodríguez, A. (2010*). Mecánica de Suelos, Tomo 3.* Limusa Ed. México.

Karplus, W. J. (1958). *Analog Simulation: Solution of Field Problems*. McGraw-Hill.

Kayan, C. F. (1945). Temperature Distribution in Complex Wall Structures by Geometrical Electrical Analogue. *Journal of the American Society of Refrigerating Engineers, 45*, 113-117.

Khosla, A. N., Bose, N. K., & Taylor, E. M. (1954). *Design of Weirs on Permeable Foundations*. Central Board of Irrigation, New Delhi.

Kozeny, J. (1927). Ueber kapillare Leitung des Wassers im Boden.*Wien, Akad. Wiss.,136*(2a), 271.

Kreith, F., & Bohn, M. S. (1993). *Principles of Heat Transfer*. St. Paul: West Publishing Company. https://doi.org/10.1115/1.2887901

Lambe, T. W., & Whitman, R. V. (2005). *Soil Mechanics*. Linusa.

Landau, H. G. (1957). A Simple Procedure for Improved Accuracy in The Resistor-Network Solution of Laplace's and Poisson's Equation. *Journal of Applied Mechanics*, *79*, 93-97.

Lindquist, E. (1933). On the Flow of Water through Porous Soil. *Premier Congrès des Grands Barrages*, *Stockholm, 5*, 81-101.

Loudon, A. G. (1952). The Computation of Permeability from Simple Soil Tests. *Geotechnique, 3*(4), 165-183. https://doi.org/10.1680/geot.1952.3.4.165

Luna-Abad, J. P., Alhama, F., & Campo, A. (2010). Optimization of Longitudinal Rectangular Fins through the Concept of Relative Inverse Admittance. *Heat Transfer Engineering*, *31*(5), 395-401. https://doi.org/10.1080/01457630903375228

Luna-Abad, J. P., Alhama, F., & Campo, A. (2017). The Use of Relative Inverse Thermal Admittance for the Characterization and Optimization of Fin-Wall Assemblies. *Thermal Science*, *21*(1 Part A), 151-160. https://doi.org/10.2298/TSCI130507138L

Luna-Abad, J.P. (2010). *Caracterización, Optimización y Diseño de Algunos Tipos De Aletas A Través Del Concepto De Admitancia Térmica Inversa Relativa*. Ph. D. Thesis. Universidad Politécnica de Cartagena.

Macneal, R. H. (1953). An Asymmetrical Finite Difference Network. *Quarterly of Applied Mathematics*, *11*(3), 295-310. https://doi.org/10.1090/qam/99978

Madrid, C. N., & Alhama, F. (2005). Discriminated Dimensional Analysis of the Energy Equation: Application to Laminar Forced Convection Along a Flat Plate. *International Journal of Thermal Sciences*, *44*(4), 333-341. https://doi.org/10.1016/j.ijthermalsci.2004.11.008

Madrid, C. N., & Alhama, F. (2006). Discrimination: A Fundamental and Necessary Extension of Classical Dimensional Analysis Theory. *International Communications in Heat and Mass Transfer*, *33*(3), 287-294. https://doi.org/10.1016/j.icheatmasstransfer.2005.11.002

Madrid, C. N., & Alhama, F. (2008). Study of the Laminar Natural Convection Problem along an Isothermal Vertical Plate Based on Discriminated Dimensional Analysis. *Chemical Engineering Communications, 195*(12), 1524-1537. https://doi.org/10.1080/00986440802115655

Manteca Jr, I. A., Meca, A. S., & Alhama, F. (2012). Mathematical Characterization of Scenarios of Fluid Flow and Solute Transport in Porous Media by Discriminated Nondimensionalization. *International Journal of Engineering Science*, *50*(1), 1-9. https://doi.org/10.1016/j.ijengsci.2011.07.004

Manteca, I. A., Alcaraz, M., Trigueros, E., & Alhama, F. (2014). Dimensionless Characterization of Salt Intrusion Benchmark Scenarios in Anisotropic Media. *Applied Mathematics and Computation*, *247*, 1173-1182. https://doi.org/10.1016/j.amc.2014.09.033

Manteca, I. A., García-Ros, G., & López, F. A. (2018). Universal Solution for the Characteristic Time and the Degree of Settlement in Nonlinear Soil Consolidation Scenarios. A Deduction Based on Nondimensionalization. *Communications in Nonlinear Science and Numerical Simulation*, *57*, 186-201. https://doi.org/10.1016/j.cnsns.2017.09.007

Marín García, F. (2013). *Aplicación del Método de Redes a la Solución de Problemas de Fricción Seca: Superficies Suaves a Escala Atómica y Superficies a Escala Macroscópica.* Ph. D. Thesis. Universidad Politécnica de Cartagena. https://doi.org/ 10.31428/10317/4017

Marín, F., Alhama, F., & Moreno, J. A. (2012). Modelling of Stick-Slip Behaviour with Different Hypotheses on Friction Forces. *International Journal of Engineering Science*, *60*, 13-24. https://doi.org/10.1016/j.ijengsci.2012.06.002

Martínez-Moreno, E., Garcia-Ros, G., & Alhama, I. (2020). A different approach to the network method: continuity equation in flow through porous media under retaining structures*. Engineering Computations*, *37* (9), 3269-3291. http://dx.doi.org/10.1108/EC-10-2019-0493

Martynenko, O.G., & Khramtsov, P.P. (2005). *Free-Convective Heat Transfer*. Berlin: Springer.

Massuel, S., Amichi, F., Ameur, F., …, & Hammani, A. (2017). Considering Groundwater Use to Improve the Assessment of Groundwater Pumping for Irrigation in North Africa. *Hydrogeology Journal 25*, 1565–1577 doi: 10.1007/s10040-017-1573-5

Mateo-Lázaro, J., Sánchez-Navarro, J. Á., García-Gil, A., Edo-Romero, V., & Castillo-Mateo, J. (2016). Modelling and Layout of Drainage-Levee Devices in River Sections. *Engineering Geology*, *214*, 11-19. https://doi.org/10.1016/j.enggeo.2016.09.011

Matlab. Version 8.5.1. (2015). Natick, Massachusetts: The MathWorks Inc.

Mavis, F. T., & Wilsey, E. F. (1936). *A Study of the Permeability of Sand*. University of Iowa.

Moore, A. D. (1936). The Hydrocal. *Industrial and Engineering Chemistry, 28*(6), 704-708.

Morales Guerrero, J. L. (2012). *Solución Numérica de Problemas de Elasticidad Bidimensional, Basados en la Formulación Directa de Navier o en Funciones Potenciales, Mediante el Método de Redes. El Programa Epsnet_10*. Ph. D. Thesis. Universidad Politécnica de Cartagena. https://doi.org/10.31428/10317/2451

Morales, J. L., Moreno, J. A., & Alhama, F. (2012 a). Application of the Network Method to Simulate Elastostatic Problems Defined by Potential Functions. Applications to Axisymmetrical Hollow Bodies. *International Journal of Computer Mathematics, 89*(13-14), 1781–1793. https://doi.org/10.1080/00207160.2012.663910

Morales, J. L., Moreno, J. A., & Alhama, F. (2012 b). New Additional Conditions for the Numerical Uniqueness of the Boussinesq and Timpe Solutions of Elasticity Problems. *International Journal of Computer Mathematics*, *89*(13-14), 1794-1807. https://doi.org/10.1080/00207160.2012.667088

Moya, A. A. (2011). Influence of DC Electric Current on the Electrochemical Impedance of Ion-Exchange Membrane Systems. *Electrochimica Acta*, *56*(8), 3015-3022. https://doi.org/10.1016/j.electacta.2010.12.103

Muskat, M. (1937). *The Flow of Homogenous Fluids through Porous Media*. Ann Arbor, Mich: J.W. Edwards.

Muskat, M. (1946). *The Flow of Homogeneous Fluids through Porous Media* (No. 532.5 M88).

Nagel, L. W. (1975). *SPICE2: A Computer Program to Simulate Semiconductor Circuits*. University of California, Electronics Res. Lab., ERL-M520, Berkeley, California.

Ngspice. (2016). Open Source Mixed Mode, Mixed Level Circuit Simulator (based on Bekeley's Spice3f5). http://ngspice.sourceforge.net/

Nield, D. A., & Bejan, A. (2006). *Convection in Porous Media* Vol. 3. New York: Springer. https://doi.org/10.1007/978-3-319-49562-0

Odong, J. (2007). Evaluation of Empirical Formulae for Determination of Hydraulic Conductivity Based on Grain-Size Analysis. *Journal of American Science, 3*(3), 54-60.

Oppenheim, A. K. (1956). Radiation Analysis by the Network Method. *Transactions of the American Society of Mechanical Engineers*, *78*, 725-735.

OXIPSIS-12 (2013): Sánchez J.F., Alhama F. & Moreno, J.A*., Oxidation Processes Simulation Software*, NAR: 08/2013 ©, Universidad Politécnica de Cartagena.

Palacios, J. F. (1955). *Análisis dimensional*. Espasa-Calpe, Madrid.

Palacios, J. F. (1964). *Dimensional Analysis*. MacMillan & Co. Ltd. New York. St Martin's Press.

Paschkis, V., & Baker, H. D. (1942). A Method for Determining Unsteady-State Heat Transfer by Means of an Electrical Analogy. *Transactions of the American Society of Mechanical Engineers*, *64*(2), 105-112.

Paschkis, V., & Heisler, M. P. (1946). The Accuracy of Lumping in an Electric Circuit Representing Heat Flow in Cylindrical and Spherical Bodies. *Journal of Applied Physics*, *17*(4), 246-254. https://doi.org/10.1063/1.1707711

Pavlovsky, N. N. (1933). Motion of Water under Dams*. Trans. 1st Congress on Large Dams*. Vol 4. Stockholm.

Perez, J. S., Conesa, M., & Alhama, I. (2016). Solving Ordinary Differential Equations by Electrical Analogy: A Multidisciplinary Teaching Tool. *European Journal of Physics*, *37*(6), 065703. http://doi.org/10.1088/0143-0807/37/6/065703

Potter, M.C. & Wiggert, D C. (1997*). Mechanics of Fluids, 2nd ed*. Prentice Hall. New Jersey.

Prieto, J. I., Fano, J., Diaz, R., & González, M. A. (1994). Application of Discriminated Dimensional Analysis to the Kinematic Stirling Engine. *Proceedings of the Institution of Mechanical Engineers, Part C: Journal of Mechanical Engineering Science, 208*(5), 347-353. https://doi.org/10.1243%2FPIME_PROC_1994_208_137_02

PROCCA-09 (2005): Alhama F. & Del Cerro Velázquez F., *Code for Heat Conduction*, NAR: 08/2005, © Universidad Politécnica de Cartagena.

PRODASIM (2005): Gómez Lopera S., Alhama F & del Cerro Velázquez F*., Code for the Design of Simple Fins,* NAR: 08/2005, © Universidad Politécnica de Cartagena.

Rel'tov, B. F. (1936). Study of Seepage in Spatial Problems by Electrical Analogues. *Transactions of. 2d Congress on Large Dams. Washington*, *5.*

Robertson, R. H., & Emödi, B. S. (1943). Rugosity of Granular Solids. *Nature, 152*(3862), 539-540. https://doi.org/10.1038/152539a0

Runge, C. (1952). *Enc. Math. Wiss*., (5,1). London.

Sánchez Pérez, J. F., Moreno, J. A., & Alhama, F. (2015). Numerical Simulation of High-Temperature Oxidation of Lubricants Using the Network Method. *Chemical Engineering Communications*, *202*(7), 982-991. https://doi.org/10.1080/00986445.2014.896345

Sánchez Pérez, J.F. (2013). *Solución Numérica de Problemas de Oxidación mediante el Método de Simulación por Redes*. Ph. D. Thesis. Universidad Politécnica de Cartagena. https://doi.org/10.31428/10317/3395

Sánchez, J. F., Alhama, F., & Moreno, J. A. (2012). An Efficient and Reliable Model Based on Network Method to Simulate CO2 Corrosion with Protective Iron Carbonate Films. *Computers and Chemical Engineering*, *39*, 57-64. https://doi.org/10.1016/j.compchemeng.2011.11.011 (2013)

Sánchez-Pérez, J. F., Alhama, F., Moreno, J. A., & Cánovas, M. (2019). Study of Main Parameters Affecting Pitting Corrosion in a Basic Medium Using the Network Method. *Results in Physics*, *12*, 1015-1025. https://doi.org/10.1016/j.rinp.2018.12.066

Sanchez-Perez, J.F., & Alhama, I. (2020). Universal Curves for the Solution of Chlorides Penetration in Reinforced Concrete, Water-Saturated Structures with Bound Chloride. *Communications in Nonlinear Science and Numerical Simulation, 84, 105201.* https://doi.org/10.1016/j.cnsns.2020.105201

Sanchez-Perez, J.F., Conesa, M., Alhama, I., & Canovas, M. (2020). Study of Lotka-Volterra Biological or Chemical Oscillator Problem Using the Normalization Technique: Prediction of Time and Concentrations. *Mathematics, 8*(8), 1324. https://doi.org/10.3390/math8081324

Schafferank, F. (1917). Über die Standicherheit Durchlaessiger Geschuetteter Dämme. *Allge, Eauzeitung*.

Scheidegger, A.E. (1974). *The Physics of Flow through Porous Media*. University of Toronto Press, Toronto.

Scott, R. F. (1963). *Principles of Soil Mechanics*. Adison Wesley Publishing Co. Massachusetts.

Seco-Nicolás, M., Alarcón, M.L., & Alhama, F. (2018). Thermal Behaviour of Fluid within Pipes Based on Discriminated Dimensional Analysis. An Improved Approach to Universal Curves. *Applied Thermal Engineering, 131,* 54-69. https://doi.org/10.1016/j.applthermaleng.2017.11.091

Selim, M. A. (1947). Uplift Pressure in and beneath Dams: A Symposium: Dams on Porous Media. *Transactions of the American Society of Civil Engineers*, *112*(1), 488-505.

Shin, C. (2017). Tortuosity Correction of Kozeny's Hydraulic Diameter of a Porous Medium. *Physics of Fluids, 29*(2), 023104. https://doi.org/10.1063/1.4976550

SICOMED_3D (2017): García-Ros, G Alhama, I. and Sánchez Pérez, J. F., *Simulation of Consolidation with Strip Drains,* NAR: 08/03/2017, © Universidad Politécnica de Cartagena.

Simpson, M. J., Clement, T. P., & Gallop, T. A. (2003). Laboratory and Numerical Investigation of Flow and Transport near a Seepage-Face Boundary. *Groundwater*, *41*(5), 690-700. https://doi.org/10.1111/j.1745-6584.2003.tb02407.x

Slichter, C.S. (1899). Theoretical Investigation of the Motion of Groundwater. *US Geol. Survey 19th Ann. Rept.*, 2, 295–384.

Sonin, A.A. (1992). *The Physical Basis of Dimensional Analysis*. Cambridge, MA: Department of Mechanical Engineering, MIT.

Soto A., Alhama F., & González-Fernández C.F. (2007 a). Density-Driven Flow and Solute Transport Problems. A 2-D Numerical Model Based on The Network Simulation Method*. Computer Physics Communications*, *177*(9), 720-728. https://doi.org/10.1016/j.cpc.2007.06.008

Soto Meca, A., Alhama, F.,.& González-Fernández, C.F. (2007 b). An Efficient Model for Solving Density Driven Groundwater Flow Problems Based on the Network Simulation Method*. Journal of Hydrology*, *339* (1-2), 39-53. https://doi.org/10.1016/j.jhydrol.2007.03.003

Soto, A. (2007). *Simulación Numérica de Procesos de Intrusión Salina en Acuíferos mediante el Método de Simulación por Redes.* Ph. D. Thesis. Universidad Politécnica de Cartagena.

Stallman, R. W. (1963). *Electric Analog of Three-Dimensional Flow to Wells and its Application to Unconfined Aquifers* (No. 1536-H). USGPO.

Szirtes, T. (2007). *Applied Dimensional Analysis and Modeling*. Butterworth-Heinemann.

Taylor, D. W. (1948). *Fundamentals of Soil Mechanics.* Wiley Int. Ed., New York

Terzaghi, K. (1925). Principles of Soil -Mechanics: III — Determination of Permeability of Clay. *Engineering News Records, 95*(21), 832–836.

Theis, C. V. (1935). The Relation between the Lowering of the Piezometric Surface and the Rate and Duration of Discharge of a Well Using Ground-Water Storage. *Eos, Transactions American Geophysical Union, 16*(2), 519-524. https://doi.org/10.1029/TR016i002p00519

Thiem, G. (1906). *Hydrologische Methoden*. Gebhardt, Leipzig.

Van Iterson, F. F. (1916 and 1917). Eenige Theoretische Beschouwinger over Kwel (Some theoretical considerations about seepage). *Der ingenieur.*

Villanueva, M, & Iglesias, A. (1984). *Pozos y acuíferos. Técnicas de evaluación mediante ensayos de bombeo*. Instituto Geológico y Minero Español. Madrid.

Vreedenburgh, C. G. F. (1936). On the Steady Flow of Water Percolating through Soils with Homogeneous-Anisotropic Permeability. In *Proceedings of the International Conference on Soil Mechanics and Foundation Engineering, (1)*.

Vreedenburgh, C. G. J., & Stevens, O. (1936). Electric Investigation of Underground Water Flow Nets. In *Proceedings of the International Conference on Soil Mechanics and Foundation Engineering, (1)*.

Weaver, W. (1932). Uplift Pressure on Dams. *Studies in Applied Mathematics*, *11*(1-4), 114-145. https://doi.org/10.1002/sapm1932111114

Williams, W. (1892). XXVII. On the Relation of the Dimensions of Physical Quantities to Directions in Space. *The London, Edinburgh, and Dublin Philosophical Magazine and Journal of Science, 34(*208), 234-271. https://doi.org/10.1080/14786449208620315

Wise, M. E. (1952). Dense Random Packing of Unequal Spheres. *Philips Research Reports 7*, 321-343.

Wyckoff, R. D., & Reed, D. W. (1935). Electrical Conduction Models for the Solution of Water Seepage Problems. *Physics*, *6*(12), 395-401. https://doi.org/10.1063/1.1745283

Wyllie, M. R. J., & Rose, W. D. (1950). Application of the Kozeny Equation to Consolidated Porous Media. *Nature, 165*(4207), 972–972. doi:10.1038/165972a0

Zimparov, V.D., & Petkov, V.M. (2009). Application of Discriminated Analysis to Low Reynolds Number Swirl Flows in Circular Tubes with Twisted-Tape Inserts. Pressure Drop Correlations. *International Review of Chemical Engineering, 1* (4), 346-356.

Zueco, Harza, J., & Alhama F. (2007). Simultaneous Inverse Determination of Temperature-Dependent Thermo-Physical Properties in Fluids Using the Network Simulation Method. *International Journal of Heat and Mass Transfer*, *50(*15-16), 3234-3243. https://doi.org/10.1016/j.ijheatmasstransfer.2007.01.004

Zueco, J., Alhama F., & González-Fernández C.F. (2005). Inverse Problem of Estimating Time-Dependent Heat Transfer Coefficient with the Network Simulation Method. *Communications in Numerical Methods in Engineering*, *21*(1), 39-48. https://doi.org/10.1002/cnm.726

Zueco Jordán, J. (2003). *Solución de Problemas Inversos en Conducción de Calor Mediante el Método de Simulación por Redes.* Ph. D. Thesis, Universidad Politécnica de Cartagena. https://doi.org/10.31428/10317/794

Zueco, J., & Alhama, F. (2005). Estimation of the Thermal Properties in Alloys as an Inverse Problem. *Revista de Metalurgia, 41*(3), 227-232.

Zueco, J., & Alhama, F. (2006). Inverse Estimation of Temperature Dependent Emissivity of Solid Metals. *Journal of Quantitative Spectroscopy and Radiative Transfer, 101*(1), 73-86. https://doi.org/10.1016/j.jqsrt.2005.11.005

Zueco, J., Alhama, F., & González-Fernández, C. F. (2006). Inverse Determination of Temperature Dependent Thermal Conductivity Using Network Simulation Method. *Journal of Materials Processing Technology*, *174*(1-3), 137-144. https://doi.org/10.1016/j.jmatprotec.2005.03.031